Partitioning and Diffusion of Macromolecules in Charged Gels

by

Erin M. Johnson

B.S., Chemical Engineering
University of California at Davis
(1990)

M.S., Chemical Engineering Practice
Massachusetts Institute of Technology
(1992)

Submitted to the
Department of Chemical Engineering
in partial fulfillment of the degree of
DOCTOR OF PHILOSOPHY

at the
MASSACHUSETTS INSTITUTE OF TECHNOLOGY
September 1995

Signature of Author: _____
Department of Chemical Engineering
July 7, 1995

Certified by: _____
William M. Deen
Professor, Department of Chemical Engineering
Thesis Supervisor

Accepted by: _____
Robert Cohen
Chairman, Department Committee for Graduate Students

Partitioning and Diffusion of Macromolecules in Charged Gels

Submitted to the Department of Chemical Engineering
on July 7, 1995 in partial fulfillment of the
requirements for the Degree of
Doctor of Philosophy in Chemical Engineering

ABSTRACT

The macromolecular partition and diffusion coefficients are equally important in describing diffusion through gel membranes. The goals of this thesis were to determine what effects electrostatic, hydrodynamic and steric interactions have on the partitioning and diffusion of macromolecules in agarose gels. To accomplish this measurements of the partitioning and diffusivity of proteins and Ficolls were made in charged and uncharged agarose gels and theoretical predictions were developed for the effects of electrostatic interactions on the partitioning of charged spherical macromolecules in random fiber arrays.

The effects of electrostatic interactions on the diffusion and equilibrium partitioning of fluorescein-labeled proteins in charged gels were examined using fluorescence recovery after photobleaching (FRAP) and gel chromatography, respectively. Measurements were made with bovine serum albumin (BSA), ovalbumin, and lactalbumin in SP-Sepharose (6% sulfated agarose), in phosphate buffers at pH 7 and ionic strengths ranging from 0.01 to 1.0 M. Diffusivities in individual gel beads (D) and in the adjacent bulk solution (D_∞) were determined from the spatial Fourier transform of the digitized two-dimensional fluorescence recovery images. Equilibrium partition coefficients (Φ) were measured by recirculating protein solutions through a gel chromatography column until equilibrium was reached, and using a mass balance. Diffusion in the gel beads was hindered noticeably, with $D/D_\infty = 0.4 - 0.5$ in each case. There were no effects of ionic strength on BSA diffusivities, but with the smaller proteins (ovalbumin and lactalbumin) D_∞ increased slightly and D decreased at the lowest ionic strength. In contrast to the modest changes in diffusivity, there were marked effects of ionic strength on the partition coefficients of these proteins. We conclude that for diffusion of globular proteins through gel membranes of like charge, electrostatic effects on the effective diffusivity ($D_{eff} = \Phi D$) are likely to result primarily from variations in Φ, with only small contributions from the intramembrane diffusivity.

A theory has also been developed to predict the effects of electrostatic interactions on the equilibrium partition coefficient (Φ) of spherical macromolecules in gels, the gels being modeled as random arrays of fibers. The partitioning theory derived by Ogston (Trans. Faraday Soc. 54: 1754-1757, 1958) for neutral macromolecules and fibers was extended by using a Boltzmann factor, containing an electrostatic free energy, to modify the probability of fitting a sphere in a space between fibers. This approach, which is limited to dilute solutions of macromolecules, is approximate in that the only electrostatic interactions considered are those between the sphere and the nearest fiber. The electrostatic free energy was calculated from finite-element solutions to the linearized Poisson-Boltzmann equation for a sphere interacting with a long cylinder, both with specified surface charge densities. Free energies calculated for many combinations of sphere radius, fiber radius, separation distance, Debye length, and the surface charge densities of the sphere and fiber are presented as a correlation involving the various dimensionless parameters. When the

sphere and fiber have like charges, Φ decreases with increases in the sphere size, the volume fraction of fibers, the Debye length, and either surface charge density; results are presented to illustrate each of these effects. Predictions from the theory are in good agreement with recent measurements of Φ for proteins in moderately charged gels.

To characterize the microstructure of the agarose gel a new technique was developed to measure the hydraulic permeability of reinforced gel membranes, allowing calculation of the Darcy permeability (κ) of the gel. The method was applied to agarose with concentrations ranging from 2.0-7.3%. To create membranes which would be thin enough to yield easily measured filtration rates at modest applied pressures, yet be able to withstand handling, gels were cast on woven polyester meshes. The resulting membranes had thicknesses of 70-100 μm and a fractional open area of 0.32. To correct for the presence of the mesh, finite-element solutions were obtained for the pressure field in the three-dimensional region occupied by the gel. For the particular meshes employed here, the hydraulic permeability of the reinforced membrane was calculated to be 0.47-0.55 times that for a layer of pure gel, the exact value depending on the thickness of the composite membrane. The principal determinant of κ was the agarose concentration, but there was a secondary effect of applied pressure. The Darcy permeability extrapolated to zero applied pressure (κ_0) varied from 616 nm^2 for 2.0% agarose to 22 nm^2 for 7.3% agarose. At a given gel concentration, the value for κ_0 was as much as twice the value for κ measured at the maximum pressure difference of 20 kPa. The method used should be adaptable to a variety of other gel materials.

The diffusivities of uncharged macromolecules in gels (D) are typically lower than in free solution (D_∞), due to a combination of hydrodynamic and steric factors. To examine these factors, we measured D and D_∞ for dilute solutions of several fluorescein-labeled macromolecules, using an image-based fluorescence recovery after photobleaching (FRAP) technique. Test macromolecules with Stokes-Einstein radii (r_s) of 2.1-6.2 nm, including three globular proteins (bovine serum albumin, ovalbumin, lactalbumin) and four narrow fractions of Ficoll, were studied in agarose gels with agarose volume fractions (ϕ) of 0.038-0.073. The gels were characterized by measuring the hydraulic permeability of supported agarose membranes, allowing calculation of the Darcy permeability (κ) for each gel sample. The diffusivity ratio D/D_∞, which varied from 0.20 to 0.63, decreased with increases in r_s or ϕ. Thus, as expected, diffusional hindrances were most severe for large macromolecules and/or relatively concentrated gels. According to a recently proposed theory for hindered diffusion through fibrous media, the diffusivity ratio is given by the product of a hydrodynamic factor (F) and a steric factor (S). The functional form is $D/D_\infty = F(r_s/\kappa^{1/2})\, S(f)$, where $f = [(r_s + r_f)/r_f]^2\phi$ and r_f is the fiber radius. Values of D/D_∞ calculated from this effective medium theory, without use of adjustable parameters, were in much better agreement with the measured values than were predictions based on other approaches.

Thesis Advisor: William M. Deen
Professor, Department of Chemical Engineering

Acknowledgements

The years spent here at MIT have truly been a remarkable experience and I wish to thank all who have made this such a pleasant experience. First of all, I would like to thank my thesis advisor, Professor Bill Deen. His guidance and perspective have been invaluable. Thanks are also due to my thesis committee members, Professors Daniel Blankschtein, Alan Grodzinsky (Department of Electrical Engineering and Computer Science), Alan Hatton, and Rakesh Jain (Harvard Medical School). Their enthusiasm has been infectious.

Thanks to the Biotechnology Process Engineering Center for providing funding in the form of a National Institutes of Health Traineeship.

My work would not have been possible without the assistance of Dr. David Berk and Professor Rakesh Jain. Their generosity was gratifying and I appreciate all the time and effort that they spent on our collaboration.

Thanks to all my lab mates both past and present who made my experience so enjoyable, Jennifer Smith, Nikola Juhaz, Jim Oliver, Claudia Drumond, Randy Lewis, Aurelie Edwards, Glen Bolton, Scott Johnston, Manish Keshive, Jeff White and Pat Gwynne. Special appreciation goes to Jennifer Majernik and Julie Rahman who devoted much time and effort to their research projects.

Thanks to Grace Colon. Her vitality and enthusiasm have been wonderful.

Thanks go to Christine and Tom Moore, for friendship, support and many fun excursions.

I would also like to express my gratitude to Debbie and Bill Diercks for the great times that we shared here in Boston.

Thanks to my whole family who supported me from afar. Mom and Dad have been truely inspirational. Bobbie and Coleman for their unwavering love and support. Sunny and Naim for some of the best conversations. Patrick for his wonderful outlook on life. Karen and Matt for sharing their puppies with me as well as some truely great times. Kim and Tim for their enthusiasm and optimism.

My deepest appreciation goes to my husband, Mark. His love and support thoughout the past five years have been invaluable. His perspective and perception have contributed enormously to both the development of this thesis and to my happiness.

Contents

List of Figures

List of Tables

Chapter 1

1. Background

1.1 Introduction

Hydrogels are cross-linked polymers that have a high water content (up to 98% water). These gels have recently been found to have numerous applications in biomedical engineering and biotechnology. Therapeutic devices such as contact lenses, breast implants, and drug delivery capsules are composed of gels (Peppas, 1987). One strategy for developing implants for organ replacement is to encapsulate cells in gels which do not significantly interfere with the transport of nutrients or desired products (e.g., insulin from pancreatic islets) (Lacy et al., 1991). Due to their high water content, hydrogels provide an ideal matrix for cell growth and are commonly used to propagate bacteria and mammalian cells. Gels are also used to separate macromolecules in size-exclusion and ion-exchange chromatography and in electrophoresis.

Several important body tissues have characteristics which are remarkably similar to hydrogels, for example connective tissue, vascular and epithelial basement membranes, and vitreous humor. The glomerular basement membrane (GBM) is a particularly interesting body tissue because it is one of the primary structures responsible for the filtration of blood in the kidney. High molecular weight proteins and cells are retained in the blood stream while large volumes of plasma and small molecules are allowed to pass through the GBM to be processed into urine. The GBM consists of collagen IV associated with proteoglycans and other extracellular components to form a fibrous gel-like structure.

Robinson and Walton (1987) have suggested that the GBM can be accurately modeled as a random fiber matrix gel. In addition to restricting the transport of proteins based upon size, the glomerular capillary wall exhibits significant charge selectivity, which has been attributed in large part to the presence of fixed negative charges in the GBM (Kanwar & Venkatachalam, 1992). There are several diseases which can affect the microstructure of the GBM by changing the membrane thickness or by loss of net charge and thus will alter the protein filtration properties (Drumond and Deen, 1994). A better understanding of the filtration properties of proteins and exogenous polymers across the GBM in the normal and abnormal kidney could be obtained with theories for the partitioning and diffusion of charged macromolecules through charged gels.

Chromatography media, which are widely utilized for purifying proteins consist largely of highly porous hydrogels. Traditionally, gel chromatography has been used to separate macromolecules based upon size (size-exclusion chromatography) and upon charge (ion exchange chromatography). A key characteristic and likewise a key drawback of ion exchange chromatography is that the gel and the solute must have opposite charge signs. That is either the gel or the solute must be negatively charged while the other is positive. Recently there has been interest in using chromatography to separate solutes having similar size and charge sign and but having differing charge *densities* (Dubin et al., 1993). This has been termed ion exclusion chromatography. However, such separations are very difficult to develop empirically due to the fact that multiple physical phenomena need to be carefully balanced to exploit differing charge densities. In fact, a rigorous theory is needed which would be able to use the known physical parameters, such as solute radius, gel volume fraction and charge densities on the solute and gel matrix, in order to effectively develop such a separation technique.

1.2 Overview of Transport through Gels

Hydrogels are composed of macromolecules that are cross-linked, either physically or chemically, to form a highly hydrated polymer network. The volume occupied by the polymer fibers is usually between 2 - 10% of the total volume, the rest being filled with water. Due to the high water content of hydrogels there can be large voids between polymer fibers through which other macromolecules, such as proteins, may permeate. The characteristic spacing between the gel fibers can be as small as the radius of the gel fiber, r_f, and as large as $50r_f$. Measurements of the permeability of the gel to water have been used in determining this characteristic spacing. A review of the permeability measurements in gels is given in section 1.5.3 and a complete discussion is presented in Chapter 4.

With most chemically cross-linked polymer gels, the gel fibers are flexible and mobile, allowing them to respond to environmental changes. In particular, electrostatic interactions between polymer fibers can cause a cross-linked gel, such as polyacrylic acid, to either expand or shrink with changing buffer pH and ionic strength. Such expansions and contractions change the microstructure of the gel and the volume fraction occupied by the polymer and often complicate determinations of the partition and diffusion coefficients. One particular gel, agarose, is unique in that it does not expand or contract with changing buffer conditions. This is due to the very rigid fibers that make up agarose gels. Because agarose is physically cross-linked and the fibers are composed of several individual agarose chains, there is relatively little mobility or flexibility. One particular advantage of using a rigid gel such as agarose in studies of electrostatic interactions is the elimination of variations in the volume fraction occupied by the fibers. With this particular gel, the effects of electrostatic interactions on the transport coefficients can be isolated from the effects of expansion and contraction of the polyelectrolyte gel. A review of the physical characteristics of agarose is given in section 1.6.

When macromolecules partition into uncharged gel matrices the concentration inside the gel is lower than in the bulk solution. This is primarily due to steric effects. That is,

there is a certain volume that is occupied by the gel fibers and hence, is inaccessible to the solute. This is discussed in more detail in section 1.3. When the gel and solute are charged, electrostatic interactions will also affect the partition coefficient. Repulsion between the macromolecule and the gel will decrease the partitioning while attraction will increase the partitioning. As a result of the use of the partition coefficient in gel chromatography experiments there has been substantial interest in measuring the partition coefficient in neutral gels (see section 1.5.1) and in developing theoretical predictions (for a review see section 1.3). While there has been more recent interest in measuring the partition coefficient into charged gels (for a review see section 1.5.1), there has been no available theory to predict the effects of electrostatic interactions on the partitioning.

Rates of diffusion are also strongly affected by the gel matrix. That is, the diffusivity of the macromolecules through gel matrices is restricted when compared to the diffusion in bulk solution. There are two components in this reduction; a frictional resistance and tortuosity. In the diffusion of macromolecules in well defined pores, the frictional resistance (hydrodynamic effects) have been found to be instrumental in predicting the reduction in mobility (for a complete review see Deen, 1987). In gels, the surfaces are less well defined than in a pore and it is difficult to know precisely where the gel fibers are for any given diffusing macromolecule. In addition, hydrodynamic effects are very long range and predictions or calculations for the diffusivity require the use of a many proximate fibers (Phillips et al., 1989;1990). The second reason for the reduction in the diffusivity is a tortuosity effect. Because the trajectory of a macromolecule through the gel matrix is not straight there is an increase in path length that will contribute to the reduction in the apparent diffusivity. The pertinent theoretical models for the diffusivity are reviewed in section 1.4, while a review of previous measurements of the diffusivity are discussed in section 1.5.2.

When considering the flux of a solute across a charged gel membrane, both the partition coefficient and the diffusion coefficient are important. The steady state flux across a one-dimensional gel slab, N, is given by

$$N = \frac{\Phi\ D}{L}(C_1 - C_0) \qquad (1)$$

where Φ is the equilibrium partition coefficient (which is defined as the concentration inside the gel (base upon the total volume) divided by the concentration in the bulk solution at equilibrium), D is the intramembrane diffusivity, L is the thickness of the gel slab, C_1 and C_0 are the upstream and downstream concentrations in the external solution. From equation 1, it is apparent that both Φ and D are necessary in describing the transport across gels. In many experiments using gel membranes researchers report the measured coefficient as D_{eff} ($=\Phi$ D) and often refer to this as the "diffusivity". In this thesis, the term diffusivity is restricted to D (the intramembrane diffusivity) or D_∞ (the diffusivity of the solute in bulk solution).

This thesis is concerned with determining what effects electrostatic, hydrodynamic and steric interactions have on the equilibrium partition coefficient and the diffusion coefficient of macromolecules in charged gels and with developing models to predict the coefficients from the molecular structure of the gel and the permeating solutes. To accomplish this we first determined the partitioning and diffusion of three proteins in a highly sulfated agarose gel at various ionic strengths. The techniques used and the results of the experiments are presented in Chapter 2. To model the partition coefficient of macromolecules in charged gels, Ogston's (1958) partitioning model (for the partitioning of neutral spheres into random fiber arrays) was extended to include electrostatic interactions as discussed in Chapter 3. One important parameter useful in characterizing the gel microstructure is the water permeability. These results along with a novel technique for

measuring permeability are presented in Chapter 4. After ascertaining that the effects of electrostatic interactions were minimal on the diffusion coefficient (discussed in Chapter 2), experiments were performed in neutral agarose for a range of macromolecular sizes and gel concentrations to determine the effects of hydrodynamic and steric interactions on the diffusivity. The diffusion experiments and an effective medium model for predicting the diffusivity from independantly measurable parameters is presented and evaluated in Chapter 5.

1.3 Equilibrium Partitioning Theory

In order to develop any theory for the partitioning of macromolecules into porous media, an accurate description of the microstructure is required. In describing the microstructure of porous media two types of models have been used, the cylindrical pore models and the random fiber matrix models. While there are specific types of porous media in which an array of cylindrical pores accurately describes the microstructure, such as the Nuclepore track-etched polycarbonate membranes, this model does not appear to characterize gel-like structures due to the lack of a specific pore radius for the gel. A better model of the gel structure is that of a random fiber array wherein the microstructure of the gel is that of an array of cylindrical fibers randomly placed and randomly aligned. In fact, the Ogston partition coefficient model based upon the random fiber array presented in section 1.3.1, works very well for the partitioning of proteins in gels as discussed in section 1.5.1. For charged random arrays and consequently charged gels there has been no corresponding partitioning theory. While there has been some work done on predicting the effects of electrostatic interactions on the partitioning of polyelectrolytes into charged pores as discussed in section 1.3.2., this is not directly applicable to charged gels.

1.3.1 Uncharged Gels

Ogston (1958) was the first to develop an expression for the available space within a uniform random suspension of fibers and to predict a partition coefficient for a dilute solution of spheres. For long fibers, the partition coefficient (the equilibrium solute concentration in the gel relative to that in bulk solution) is given by

$$\Phi = \exp\left(-\phi \left(1 + \frac{r_s}{r_f} \right)^2 \right) \qquad (2)$$

where ϕ is the volume fraction occupied by the fibers, r_f is the radius of the fibers, and r_s is the hydrodynamic radius of the spherical probe. This partition coefficient is based upon the total gel volume, including the volume occupied by the fibers. More recently, Fanti and Glandt (1990) used a density-functional theory to independently verify the Ogston expression and to predict the partition coefficient of concentrated spheres in a random array of fibers. A more detailed description of the development of the Ogston partition coefficient is given in section 3.2.1. and a comparison of the Ogston model to experimental data is discussed in section 1.5.1.

1.3.2 Charged Pores

Smith and Deen (1980;1983) predicted the partition coefficient of a spherical polyion inside a charged pore by solving the linearized Poisson-Boltzmann equation for a solid sphere with either a constant surface potential or a constant surface charge density and for a porous sphere with a constant volumetric charge density. Johnson et al. (1989) experimentally

measured the hindered diffusivity of charged micelles through charged Nuclepore membranes. They found excellent agreement between their data and the theoretical predictions of Smith and Deen.

Lin and Deen (1992) calculated the partition coefficient of a linear polyelectrolyte inside a well defined cylindrical pore. Diffusion experiments using polystyrene sulfonate in track-etched polycarbonate membranes were compared to the theoretical predictions for the partition coefficient in conjunction with hydrodynamic models for the resistance of a sphere in a neutral pore (Brenner and Gaydos, 1977). Lin and Deen concluded that the charge effects seen in the diffusion experiments were governed primarily by partitioning. This suggests that the effects of charge on the effective diffusivity ($D_{eff} = \Phi D$) in gels might also parallel the effects of charge on the partition coefficient.

1.4 Theory for Diffusion through Gels

To date, predictions for the diffusivity of macromolecules through gels have been relatively unsuccessful. The reasons for the difficulty in developing a theory lie in the complexity of the hydrodynamic interactions between a mobile macromolecule and its surrounding environment. There has been substantial effort placed in predicting the diffusivity of spheres in straight cylindrical pores (as reviewed by Deen, 1987), but because the hydrodynamic interactions are very sensitive to alterations in the microstructure it seems unlikely that extensions of this particular model to fibrous structures will give accurate predictions. However, these theories yield insight into the nature and complexity of hydrodynamic interactions. Due to the difficulty in predicting the hydrodynamic interactions, arguments have been made which attempt to erroneously minimize their importance. The most well known and widely used model which does not include hydrodynamic interactions was developed by Ogston et al. (1973) and is based upon the stochastic jump probability of a sphere which is reviewed in section 1.4.1. While this

model has not been especially successful in predicting diffusivities, as reviewed in section 1.5.2, Ogston's model had been the *only* model available for many years. More recently, there have been efforts to use an effective medium approach to calculating the hydrodynamic interactions. As reviewed in section 1.4.2, Phillips et al.(1989;1990) suggests that the Brinkman equation can be used to approximate the frictional resistance a sphere would encounter when diffusing through a porous medium. This has been more promising than the Ogston diffusion model primarily because it attempts to take into account hydrodynamic interactions which are known to be instrumental in describing the reduction in diffusivity a sphere experiences when diffusing through a cylindrical pore.

1.4.1 Ogston Diffusion Model

Ogston et al. (1973) used the random fiber matrix model that was developed for the partition coefficient theory to predict the reduction in diffusivity of a sphere through a gel network. Their expression for the hindered diffusivity was based upon a stochastic jump through the spaces of a randomly oriented fiber network without considering hydrodynamic interactions. Assuming that any jump that would result in a collision with a fiber would not occur, Ogston formulated the probability of completing a jump. By assuming that the frequency of jumps inside the gel phase was the same as in the bulk solution, Ogston et al., used the jump probability to formulate an expression for the hindered diffusivity.

$$\frac{D}{D_\infty} = \exp\left(-\phi^{1/2}\frac{r_s}{r_f}\right) \qquad (3)$$

where D is the intramembrane diffusivity, D_∞ is the free solution diffusion coefficient, ϕ is the volume fraction of fibers, r_s is the radius of the spherical solute and r_f is the radius of the gel fiber.

This model does not include hydrodynamic interactions, which have been found to be instrumental in describing the resistance to the solute mobility in cylindrical pores. As discussed further in section 1.5.1, Ogston's stochastic jump model for the hindered diffusivity has had only limited success in describing existing experimental data and in fact tends to overpredict the diffusion coefficient.

1.4.2 Effective Medium Model

Phillips et al. (1989;1990) were the first to include hydrodynamic interactions in calculating the hindered diffusivity of a sphere in a fiber array. Their detailed hydrodynamic calculations were limited to solid spheres moving through beds of parallel fibers. They showed that if the hindrance is not too extreme, an effective medium approach that made use of Brinkman's equation could approximate the resistance encountered by the spherical solute.

$$F = \left[1 + \left(\frac{r_s^2}{\kappa}\right)^{1/2} + \frac{1}{3}\left(\frac{r_s^2}{\kappa}\right)\right]^{-1} \qquad (4)$$

where F ($\cong D/D_\infty$) is the reduction in mobility of the sphere in the porous medium and κ is the Darcy permeability. While this method has yet to be experimentally evaluated for gels, this is appealing in that the only two structural parameters necessary to describe the hydrodynamic interactions are the size of the macromolecule and the permeability of the gel

phase. While there has been relatively few measurements of the Darcy permeability of gels (as will be discussed in section 1.5.3), Jackson and James (1986) have compiled a list of permeabilities of fibrous media and reviewed theoretical predictions for κ based on hydrodynamic calculations for various arrangements of cylindrical fibers. They concluded that κ for random, three dimensional arrays of fibers could be reasonably predicted by

$$\frac{\kappa}{r_f^2} = -\frac{3}{20\phi}(\ln \phi + 0.931) \qquad (5)$$

where r_f is the fiber radius and ϕ is the volume fraction of fibers. Using equation 5 predictions for the diffusivity using equation 4 can be made from the physical characteristics of the solute and gel, r_s, r_f and ϕ. Because of the discrepancy (up to an order of magnitude) between the Jackson and James correlation (equation 5) and their reported permeability mesurments for a wide range of fibrous media, a complete evaluation of the Brinkman equation (equation 4) requires the use of the exact Darcy permeability.

1.5 Previous Experimental Studies

1.5.1 Partition Coefficient

1.5.1.1 Neutral Gels and the Ogston Partition Coefficient

Several researchers have determined the partition coefficients for a variety of proteins and for Ficoll in agarose hydrogels (Moussaoui et al., 1992; Boyer and Hsu, 1992; Laurent, 1967). A comparison of Ogston's partition expression (equation 2) to available

experimental data is given in Figure 1.1. As discussed in section 1.6, an average fiber radius of 1.9 nm was used in this analysis and the proteins and their sizes are shown in Table 1.1. The comparison between the predicted and experimental values is good indicating that the random fiber matrix model can be used to describe the microstructure of the uncharged gel phase. There is also extensive experimental work for the partition coefficient of proteins in cross-linked dextran gels (Sephadex) (Laurent and Killander, 1964). Laurent and Killander provided a summary of the results obtained by the other authors and compared the results along with their own experiments to Ogston's partitioning theory. There was some uncertainty in the determination of the volume fraction of fibers, ϕ, of the Sephadex. The clearest value for ϕ was measured by Laurent and Killander for Sephadex-200. A reanalysis of their experimental data for the partitioning of proteins on Sephadex-200 is shown in Figure 1.2 along with the Ogston partition coefficient expression (equation 2) using a volume fraction of fibers, $\phi = 0.076$. This was calculated using a water regain value of dried dextran of 19.9 grams H_2O / gram dextran and a partial specific volume of dextran of 0.61 (Laurent and Killander, 1964). While the comparison is favorable, the value used for the dextran fiber radius, 0.8 nm[1] was also determined from a curve fit to Ogston's expression. Since the actual value for the dextran radius from molecular structure should be in the range of 0.2-0.3 nm (Laurent and Killander, 1964), there is some question about the use of Ogston's random fiber matrix model for gels consisting of flexible fibers, such as dextran gels. Water molecules bound to the surface of the dextran fiber may have also created an effective fiber radius bigger than the molecular structure of dextran. Further work done on the molecular configuration of dextran is needed before conclusions can be made.

---

[1] The value cited by Laurent and Killander, 1963 was 0.7 nm for the curve fit to Ogston's expression. Our reanalysis of the curve fit gave a slightly different value of 0.8 nm.

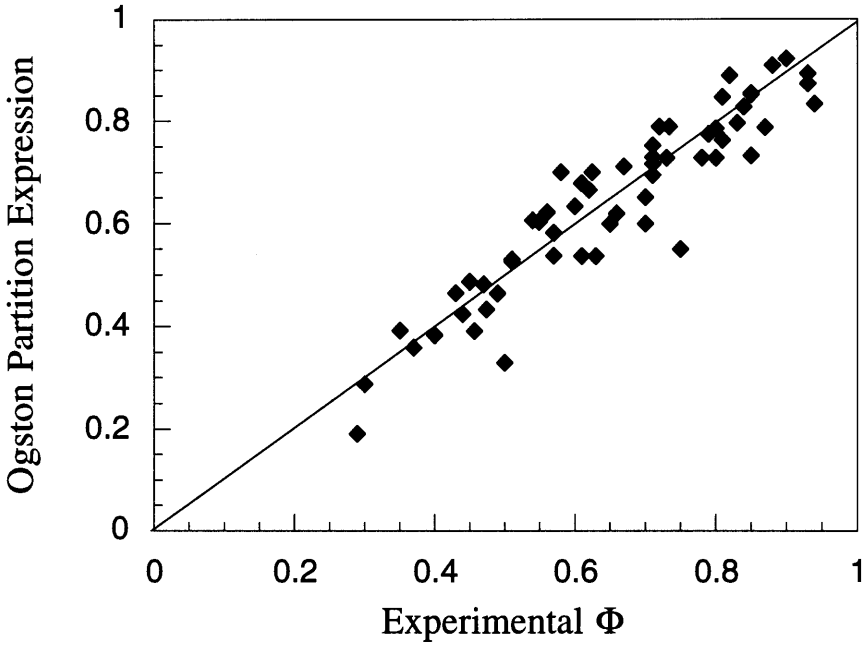

Figure 1.1 Comparison of the Ogston partition coefficient expression (equation 2) with experimental data for the partitioning of proteins and ficolls in agarose with concentrations ranging from 2-8%. References and values for data are given in Table 1.1

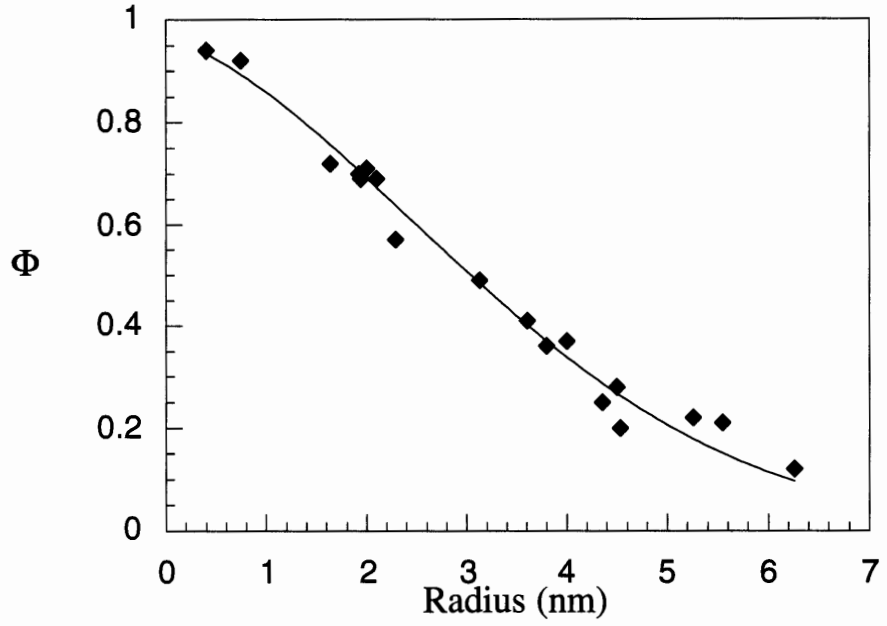

Figure 1.2 Comparison of the Ogston partition coefficient expression (equation 2) for proteins in Sephadex-200 (cross-linked dextran). The value for the radius of the dextran fiber was determined using a curve fit of equation 2 which yielded a value of 0.8 nm. Data was from Laurent and Killander, 1964.

Table 1.1 Literature values for the partition coefficients of proteins and ficoll in agarose.

Protein	Gel %	r_s (nm)	Experimental Φ	Ogston (eq. 2) Φ	Reference
Ribonuclease	0.02	1.92	0.9	0.922	1
Chymotrypsinogen A	0.02	2.24	0.88	0.909	1
Ovalbumin	0.02	2.73	0.82	0.888	1
BSA	0.02	3.6	0.81	0.846	1
Aldolase	0.02	4.9	0.79	0.774	1
Thyroglobulin	0.02	8.5	0.75	0.549	1
Ribonuclease	0.04	1.92	0.85	0.851	1
Chymotrypsinogen A	0.04	2.24	0.84	0.827	1
Ovalbumin	0.04	2.73	0.72	0.789	1
BSA	0.04	3.6	0.71	0.715	1
Aldolase	0.04	4.9	0.7	0.599	1
Thyroglobulin	0.04	8.1	0.5	0.330	1
Ribonuclease	0.06	1.92	0.8	0.785	1
Chymotrypsinogen A	0.06	2.24	0.71	0.752	1
Ovalbumin	0.06	2.73	0.58	0.700	1
BSA	0.06	3.6	0.54	0.605	1
Aldolase	0.06	4.9	0.49	0.464	1
Thyroglobulin	0.06	8.1	0.29	0.190	1
Myoglobin	0.06	1.89	0.734	0.788	2
ß-lactoglobulin	0.06	2.74	0.625	0.699	2
Ovalbumin	0.06	2.93	0.61	0.679	2
Albumin	0.06	3.59	0.55	0.606	2
Hexokinase	0.06	3.62	0.549	0.603	2
Catalase	0.06	5.21	0.474	0.432	2
Immunoglobin G	0.06	5.62	0.457	0.391	2
Ficoll	0.02	5.6	0.85	0.732	3
Ficoll	0.02	4.68	0.87	0.787	3
Ficoll	0.02	3.84	0.94	0.833	3
Ficoll	0.02	3.05	0.93	0.873	3
Ficoll	0.02	2.64	0.93	0.892	3
Ficoll	0.04	5.6	0.63	0.536	3
Ficoll	0.04	4.9	0.65	0.599	3
Ficoll	0.04	4.68	0.66	0.619	3
Ficoll	0.04	4.32	0.7	0.651	3
Ficoll	0.04	3.84	0.71	0.694	3
Ficoll	0.04	3.45	0.78	0.728	3
Ficoll	0.04	3.05	0.81	0.762	3
Ficoll	0.04	2.64	0.83	0.796	3
Ficoll	0.04	1.88	0.85	0.854	3
Ficoll	0.04	5.6	0.57	0.536	3
Ficoll	0.04	3.45	0.73	0.728	3
Ficoll	0.04	5.6	0.61	0.536	3
Ficoll	0.04	3.45	0.8	0.728	3
Ficoll	0.06	5.6	0.35	0.393	3

Ficoll	0.06	4.9	0.43	0.464	3
Ficoll	0.06	4.68	0.45	0.487	3
Ficoll	0.06	4.32	0.51	0.526	3
Ficoll	0.06	3.45	0.56	0.621	3
Ficoll	0.06	3.05	0.62	0.665	3
Ficoll	0.06	2.64	0.67	0.710	3
Ficoll	0.08	5.6	0.3	0.287	3
Ficoll	0.08	4.9	0.37	0.359	3
Ficoll	0.08	4.68	0.4	0.383	3
Ficoll	0.08	4.32	0.44	0.424	3
Ficoll	0.08	3.84	0.47	0.482	3
Ficoll	0.08	3.45	0.51	0.530	3
Ficoll	0.08	3.05	0.57	0.581	3
Ficoll	0.08	2.64	0.6	0.633	3
Ficoll	0.08	1.88	0.71	0.729	3

[1]Moussaoui et al. (1992); [2]Boyer and Hsu (1992); [3]Laurent (1967)

1.5.1.2 Partitioning in Charged Gels

There is more limited work on studying the effects of charge on the partitioning of proteins in agarose gels. Crone (1974) quantified the effects of charge and ionic strength on the partition coefficient of four proteins eluting on a Sepharose 4B chromatography column. Dubin and Principi (1989) and Edwards and Dubin (1993) also determined the effects of ionic strength for protein partitioning in agarose gels. In all three cases the partition coefficient was found to decrease substantially with decreasing ionic strength indicating that indeed the partition coefficient can be affected by charge interactions. Experimental results for the partitioning of proteins in sulfated agarose gel are presented in section 2.4.1 and a more complete discussion of predictions for the partitioning in charged gels found in section 3.5.

1.5.2 Diffusion Coefficient

1.5.2.1 Diffusion of Neutral Solutes in Gels

Several methods have been used in measuring the hindered diffusivity of proteins in agarose; FRAP (fluorescence recovery after photobleaching) (Moussaoui et al., 1992), dispersion in chromatography columns (Boyer and Hsu, 1992) and quasi-elastic light scattering (Sellen, 1985). For all macromolecules the diffusivity inside the gel is substantially reduced when compared to their diffusivities in free solution. A comparison between the experimental reduced diffusion coefficient (D/D_∞) and the theoretical models, Ogston diffusion model and the effective medium model using the Brinkman equation (see section 1.4) are shown in Figure 1.3 and the parameters used in the predictions are given in Table 1.2. While both models tend to over predict the diffusivity, the Brinkman equation (equation 4) using the Jackson and James correlation (equation 5) appears to more closely predict the diffusivity than the Ogston diffusivity (equation 3). It may be fortuitous that the Brinkman equation (equation 4) compares more favorably with the experimental data because of the uncertainties in the Darcy permeability for agarose. To fully evaluate this model, measurements for the Darcy permeability are needed (and are presented in Chapter 4) as well as an evaluation of the significance of the tortuosity of the gel matrix and its possible contribution to the reduction of the diffusivity. A full discussion of this is given in Chapter 5.

Of the three experimental methods listed above, both the dispersion in chromatography columns and quasi-elastic light scattering have difficulty in obtaining accurate measurements for the diffusion coefficient. The dispersion in a chromatography column is highly dependent upon the packing of the gel beads. In addition the value measured using the dispersion is the effective diffusivity, D_{eff}, which is the product of ΦD and so another measurement for Φ must be made with possible experimental errors before the diffusivity, D, is obtained. Sellen (1985) reported that when using QELS to measure the transport of BSA in dextran gels it was sometimes difficult to differentiate between the fluctuations of the BSA and the dextran fibrils. Since the agarose fibers are substantially

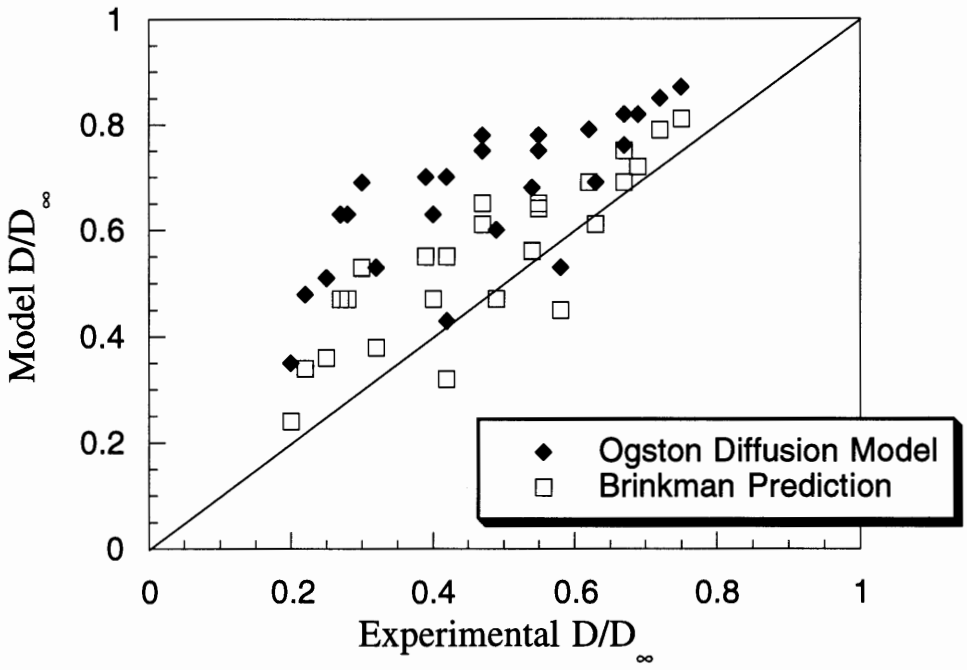

Figure 1.3 Comparison of the Brinkman expression (equation 4) and the Ogston diffusion model (equation 3) to experimental data for the diffusivity of proteins in agarose gels. Both models tend to overpredict the diffusivity. Experimental data, parameters used in the two diffusion predictions and references are given in Table 1.2.

more rigid than dextran fibers, this should not affect measurements in agarose gels. However, it is difficult to use this system on any other gel system in which the fibers fluctuate at rates similar to the diffusion rates of the permeating solute. For measuring diffusivities using FRAP, care must be used in interpreting the diffusion profiles inside of gel media. As discussed later in section 2.3.3 if the gel scatters light, the fluorescence signal is distorted and errors in the diffusivity are produced.

Table 1.2 Literature values for the diffusivity of proteins in agarose.

Protein	Gel Conc.	r_s (nm)	Experimental D/D_∞	Ogston (eq. 3) D/D_∞	Darcy Permeability (eq. 5) κ (nm^2)	Brinkman (eq. 4) D/D_∞	Ref.
Ribonuclease	0.02	1.92	0.75	0.87	80.71	0.81	1
Chymotrypsinogen A	0.02	2.24	0.72	0.85	80.71	0.79	1
Ovalbumin	0.02	2.73	0.67	0.82	80.71	0.75	1
BSA	0.02	3.6	0.67	0.76	80.71	0.69	1
Aldolase	0.02	4.9	0.63	0.69	80.71	0.61	1
Thyroglobulin	0.02	8.5	0.58	0.53	80.71	0.45	1
Ribonuclease	0.04	1.92	0.69	0.82	30.97	0.72	1
Chymotrypsinogen A	0.04	2.24	0.62	0.79	30.97	0.69	1
Ovalbumin	0.04	2.73	0.55	0.75	30.97	0.64	1
BSA	0.04	3.6	0.54	0.68	30.97	0.56	1
Aldolase	0.04	4.9	0.49	0.60	30.97	0.47	1
Thyroglobulin	0.04	8.1	0.42	0.43	30.97	0.32	1
Ribonuclease	0.06	1.92	0.55	0.78	16.99	0.65	1
Chymotrypsinogen A	0.06	2.24	0.47	0.75	16.99	0.61	1
Ovalbumin	0.06	2.73	0.39	0.70	16.99	0.55	1
BSA	0.06	3.6	0.40	0.63	16.99	0.47	1
Aldolase	0.06	4.9	0.32	0.53	16.99	0.38	1
Thyroglobulin	0.06	8.1	0.20	0.35	16.99	0.24	1
Myoglobin	0.06	1.89	0.47	0.78	16.99	0.65	2
ß-lactoglobulin	0.06	2.74	0.42	0.70	16.99	0.55	2
Ovalbumin	0.06	2.93	0.30	0.69	16.99	0.53	2
Albumin	0.06	3.59	0.28	0.63	16.99	0.47	2
Hexokinase	0.06	3.62	0.27	0.63	16.99	0.47	2
Catalase	0.06	5.21	0.25	0.51	16.99	0.36	2
Immunoglobin G	0.06	5.62	0.22	0.48	16.99	0.34	2

[1]Moussaoui et al.(1992); [2] Boyer and Hsu (1992)

1.5.2.2 Diffusion of Charged Macromolecules in Polyelectrolytes

While we are unaware of any previous diffusivity measurements of charged macromolecules in charged gels, there are experimental measurements for the diffusivity of charged solutes in polyelectrolytes. Diffusion studies using charged probes in semi-dilute polymer solutions indicate that the effect of ionic strength on D may not be negligible. In tracer diffusion studies of bovine serum albumin (BSA) in DNA solutions (Wattenbarger et al., 1992) it was found that, upon increasing the DNA concentration from 0 to 30 mg/mL, the diffusivity of BSA in a 0.01 M NaCl solution decreased more than in a 0.1 M NaCl solution. At 30 mg/mL DNA, the tracer diffusion coefficient of BSA in 0.01 M NaCl was about 20% lower than in 0.1 M NaCl. Studies of the diffusion of polystyrene latex spheres in polyacrylic acid solutions (Phillies et al., 1987; 1989) also showed that a decrease in ionic strength lowered the diffusion coefficient. Whether any of these results are applicable to gels of relatively fixed structure (e.g., charged agarose) is unclear.

1.5.3 Darcy Permeabilities

The permeability of water through gels is an important parameter in characterizing the microstructure. As previously discussed in section 1.4.2, the Darcy permeability is useful in predicting diffusion coefficients in random fiber arrays. The permeability through porous media is modeled using Darcy's law (equation 6)

$$v = \frac{\kappa}{\mu}\nabla P \qquad (6)$$

where v is the velocity of the fluid, μ is the fluid viscosity, ΔP is the pressure drop across the membrane and κ is the Darcy permeability. As noted previously in section 1.4.2, the

correlation (equation 5) given by Jackson and James (1986) can be used to predict κ from the volume fraction of fibers, ϕ, and the fiber radius, r_f, for random fiber arrays with an uncertainty of about one order of magnitude.

There have been relatively few measurements of the water permeability through gels and we are unaware of any previous measurements for the permeability of agarose. Because the water permeability is so small for all the gels, most of the experiments have been done in special chambers that are designed to either handle high pressures or measure very low velocities. The permeability of the gels that have been measured; polyacrylamide (White, 1960; Weiss and Silberberg, 1976; Tokita and Tanaka, 1991), agar (Pallman and Devel, 1945), and gelatin (Pallman and Devel, 1945; Signer and Egli, 1950) are given in Table 1.1 along with the thickness and pressure drops used for the experiments. In examining the values cited for polyacrylamide there appears to be little agreement on the Darcy permeability with the values varying by two orders of magnitude for the same concentration of gel. While it is unclear exactly why there is such a discrepancy between the reported values it is clear that obtaining accurate values of the Darcy permeability may be difficult. An interesting observation that Weiss and Silberberg (1976) make is that when the cross-linker concentration is increased the permeabilility of the polyacrylamide increases at constant polyacrylamide concentration. This would indicate that the microstructure is becoming more open and that there are larger passage ways through the polymer matrix. This is somewhat counterintuitive because Weiss and Silberberg (1976) first assumed that the increase in cross-linker concentration would tighten the pores and reduce the volume fraction of fibers. In fact they concluded from the permeablity measurements that perhaps the cross-links were occuring non-homogeneously. Consequently, the localization of the cross-linkers would produce a gel with localized concentrations of polymer fibers. Thus it is possible that the Darcy permeability can be used to probe the homogeneity of the gel microstructure as well as the characteristic spacing of the fiber network. The work on measuring the permeability of Pallman and Devel (1945) is questionable considering the

extremely large values of Darcy permeabilities. Considering the large descrepancy between their reported values and the other researchers, it must be considered that perhaps there was an error either in the experimental system or in the reporting of the permeability values. A novel method for measuring permeabilities in ultrathin gel membranes that can be used at low pressures and high velocities is described in section 4.2. and a complete discussion of agarose gel permeabilities is given section 4.4.

Table 1.3 Literature values for the Darcy permeabilities of gels.

Gel	Conc. wt/v%	Cross - linker w/w%	Volume Fraction ϕ	Thickness mm	ΔP kPa	κ nm^2	Ref.
Polyacrylamide	5	1	0.035	1.9	2 - 6	3.33	1
	8	2	0.056	1.9	2 - 6	0.67	1
Polyacrylamide	4	4	0.028			329	2
	4	8	0.028			1131	2
	7	2	0.049			165	2
	7	4	0.049			206	2
	7	6	0.049			236	2
	10	2	0.070			47	2
	10	4	0.070			53	2
	10	6	0.070			88	2
	10	8	0.070			317	2
	12	2	0.084			21	2
	12	4	0.084			31	2
	12	6	0.084			40	2
	12	8	0.084			125	2
	16	2	0.112			7	2
	16	4	0.112			10	2
Polyacrylamide	5		0.035	0.79	41 - 200	0.44	3
	8		0.054	0.79	41 - 200	0.31	3
	10		0.070	0.79	41 - 200	0.21	3
	15		0.105	0.79	41 - 200	0.16	3
	20		0.140	0.79	41 - 200	0.10	3
	25		0.175	0.79	41 - 200	0.04	3
	30		0.210	0.79	41 - 200	0.05	3
	35		0.245	0.79	41 - 200	0.02	3
Agar	2			40	9.8	20,000	4
	4			40	9.8	50,000	4
	8			40	9.8	440,000	4

Gelatin	8	40	9.8	200,000	4
Gelatin	1.29			61.2	5
	2.59			17.5	5
	5.18			5.3	5
	10.36			1.4	5

[1]Tokita and Tanaka, 1991 [2]Weiss and Silberberg, 1976; 1977 [3]White,1960
[4]Pallman and Devel, 1945 [5]Signer and Egli, 1950

1.6 Physical Characteristics of Agarose Gels

Agarose is a naturally occurring polysaccharide derived from seaweed. Unlike most chemically cross-linked gels, agarose is formed by a reversible physical cross-link. At high temperatures (generally above 80 °C depending on the agarose type) the agarose fibers are soluble in water. As the temperature of the solution decreases, the agarose fibers join to first form α-helical chains (Arnott et al., 1974). These chains can form larger fibers by bundling together. The gelation is usually complete by the time the solution reaches 40°C. There is a significant thermal hysteresis in the heating and cooling of the agarose gel network.

Because the agarose fibers consist of multiple chains, the gel network is very rigid. When sulfated there is little swelling or shrinking associated with changes in the ionic strength of the buffer. In chemically cross-linked gels, the fibers are typically formed by a single chain that has both flexibility and mobility. When charged, the repulsion between the single chains can cause the gel to swell substantially. This is not observed in agarose gels. Because the charged agarose gels do not swell, the spaces inside the gel remain constant over a wide range of ionic strength.

Because the gels are formed by a random physical linkage between multiple chains, the agarose fiber radius used in any analysis is necessarily an average. To characterize the fiber radii, researchers have used several techniques, including light scattering (Obrink, 1968), SAXS (Djabourov et al., 1989) and electron microscopy (Spencer, 1982;

Amsterdam et al., 1975; Waki et al., 1982; Whytock and Finch, 1991). The electron microscopy techniques give a range of fiber radii of 1 - 20 nm, but do not quantify the distribution of fiber sizes. Results from light scattering indicate that the average fiber radius is between 1.5 and 2.0 nm, while the SAXS results give a bimodal distribution of 87% fibers with 1.5 nm radius and 13% with 4.5 nm radius, yielding an average radius of 1.9 nm. The SAXS result is consistent with the values given using light scattering.

The agarose fibril is a helix with internally bound water (Arnott et al., 1974), so that the volume fraction of fibers cannot be obtained directly from the agarose concentration and the dry density. For this structure Arnott and co-workers determined that the hydrated chain density is 1.4 g/mL. With a dry agarose density, ρ_a, of 1.64 g/mL (Laurent, 1967) and a water density of 1.0 g/mL, the mass fraction of agarose in the fiber, ω_a, is 0.625. Denoting the mass concentration of agarose as C_a, the volume fraction of fibers in the gel can be determined by

$$\phi = \frac{C_a}{\rho_a \omega_a} \tag{7}$$

Using equation 7, the volume fraction of fibers in a 6% (by weight) agarose gel is ϕ = 0.059. Thus, coincidentally, the volume fraction of fibers is almost identical to the weight fraction of agarose.

The primary backbone of agarose consists of 1,3-linked β-D-galactopyranose and 1,4-linked 3,6-anhydro-α-L-glactopyranose (FMC, 1988). However, there are various groups that are substituted onto the agarose chain, half-ester sulfate groups, pyruvic acid ketal and methyl esters. The sulfate groups and the pyruvic acid ketal groups can confer charge onto the agarose chain. While the methyl esters are not charged, their content can

affect the thickness of the agarose fibrils and the gelling temperature (FMC,1988). Because the sources of agarose are so variable so is each batch of polymer. All agarose contains ester sulfate and it is generally reported as a % sulfate content. Generally, the percent sulfate is less than 0.35 %. On very pure batches the percent sulfate can be lower than 0.1% (Sigma, 1992). Pyruvate, which is present as a ketal condensed across the 4,6-position of some of the D-galactose residues, occurs in varying amounts in most batches, but the exact content is rarely reported. One property that is routinely reported is the EEO, which refers to the electro-osmosis of the agarose. The EEO value is calculated from

$$EEO \equiv -m_r = \frac{OD}{OD + OA} \qquad (8)$$

where OD refers to the migration distance of neutral dextran in electroosmotic flow and OA is the migration distance of albumin. Because the albumin is negatively charged, the albumin will move toward the positively charged electrode. The counter-ions for the slightly negatively charged agarose are positive and thus move toward the negatively charged electrode. This movement of positively charged ions sets up an electro osmotic flow that will sweep the neutral dextran toward the negatively charged electrode. The exact conditions for this measurement (i.e. the ionic strength, pH of the buffer solution, size of the dextrans or gel concentration) are not reported by FMC. However, FMC (1988) does show that there is a linear relationship between the value EEO that they report for each agarose batch and the total amount of charge (sulfate groups and pyruvate groups). At an EEO of 0.1, FMC (1988) indicates that the total charge on the agarose is ~4.5 meq/100 grams of agarose while at an EEO of 0.4 the total charge on agarose is ~ 18 meq/100 grams. Assuming that the fiber radius is 1.9 nm and the hydrated density of agarose is 1.4 g/mL then for an EEO = 0.1, the surface charge density would be -0.006 C/m^2. For an EEO = 0.4 the corresponding surface charge density would be -0.023 C/m^2. The charge on

gelled agarose can also be determined from titration as done by Dubin (1994) for Superose 12 (a beaded 12% agarose gel, chemically crosslinked to give a very rigid structure), who reported that the surface charge density of agarose is -0.011 C/m^2.

To determine the typical spacing inside an agarose gel, an analysis using the distribution of spaces in a random fiber matrix was used. Ogston (1958) derived a probability density function for the distance H from an arbitrary point to the surface of the nearest fiber in a random array. The result may be expressed as

$$g(H) = \frac{2\phi\left(H + r_f\right)}{r_f^2} \exp\left(\frac{-\phi\left(H + r_f\right)^2}{r_f^2}\right) \qquad \textbf{(9)}$$

We computed the average distance to the closest fiber, <H> using

$$\langle H \rangle = \frac{\int_0^\infty H\, g(H)\, dH}{\int_0^\infty g(H)\, dH} \qquad \textbf{(10)}$$

With $\phi = 0.059$ and $r_f = 1.9$ nm, the average distance to the closest fiber is 5.4 nm. The average fiber spacing was estimated as 2<H>, or 11 nm.

Chapter 2

2. Electrostatic Effects on the Transport Coefficients in SP-Sepharose

2.1 Introduction

Diffusive transport of macromolecules through gels is important in various chromatographic and membrane separation processes. For diffusion across any type of membrane, the driving force is usually expressed in terms of concentrations in the external solutions, so that the effective transmembrane diffusivity (D_{eff}) is given by

$$D_{eff} = \Phi D \qquad (11)$$

where Φ is the partition coefficient (the ratio of the intramembrane to the external concentration at equilibrium) and D is the diffusivity within the membrane phase. Accordingly, for a macromolecule in a gel membrane D_{eff} tends to be lower than the free solution diffusivity (D_∞) for two reasons. First, hydrodynamic interactions between the macromolecular solute and the fibers that compose the gel medium reduce the mobility of the solute, making D lower than D_∞. Second, Φ is ordinarily less than unity due to steric and/or electrostatic interactions.

For uncharged gels there is considerable experimental information on the partition coefficients of proteins and other macromolecules as previously discussed in section 1.5.1 Diffusivities within gels have received somewhat less attention, but available results clearly demonstrate that in neutral gels the macromolecular diffusivity is significantly reduced (see section 1.5.2). With regard to theory, Ogston (1958) derived a relationship to predict Φ for uncharged, spherical macromolecule within a randomly oriented array of cylindrical fibers,

$$\Phi = \exp\left[-\phi\left(1+\frac{r_s}{r_f}\right)^2\right] \qquad (12)$$

where ϕ is the volume fraction of fibers, r_s is the radius of the sphere, and r_f is the radius of the fibers as previously discussed in section 1.3.1. This expression, which is limited to very dilute solutions, agrees well with reported values for Φ of proteins and Ficoll in neutral agarose gels (see section 1.5.1). To describe the reduced diffusivity of a spherical molecule within a random fiber matrix, Ogston et al. (1973) proposed a stochastic jump model, which leads to the expression

$$\frac{D}{D_\infty} = \exp\left[-\phi^{1/2}\frac{r_s}{r_f}\right] \qquad (13)$$

Equation 13, which has been used with some success to obtain semi-empirical correlations of diffusion data in gels (Ogston et al., 1973), does not consider hydrodynamic interactions between the mobile solute and the fibers as previously discussed in section 1.4.1. Phillips et al. (1989;1990) suggested that hydrodynamic interactions might be approximated using

an effective medium approach, based on Brinkman's equation. As previously cited in section 1.4.2 the result was

$$\frac{D}{D_\infty} = \left[1 + \left(\frac{r_s^2}{\kappa}\right)^{1/2} + \frac{1}{3}\left(\frac{r_s^2}{\kappa}\right)\right]^{-1} \qquad \textbf{(14)}$$

where κ is the Darcy permeability of the fibrous medium.

Relatively little information is available on the partitioning or diffusion of charged macromolecules in charged gels. The effects of charge on D_{eff} for micelles (Johnson et al., 1989) and linear polyelectrolytes (Lin and Deen, 1992) in track-etch membranes with straight, cylindrical pores have been explained fully by theoretical predictions of the effects on Φ, suggesting that for macromolecules in such pores there is little or no effect of charge on D. The extent to which this might also be true for macromolecules in charged gels is unknown. As outlined in section 1.5.2 diffusion studies using charged probes in semi-dilute polymer solutions indicate that the effect of ionic strength on D may not be negligible. In tracer diffusion studies of bovine serum albumin (BSA) in DNA solutions (Wattenbarger et al., 1992) it was found that, upon increasing the DNA concentration from 0 to 30 mg/mL, the diffusivity of BSA in a 0.01 M NaCl solution decreased more than in a 0.1 M NaCl solution. At 30 mg/mL DNA, the tracer diffusion coefficient of BSA in 0.01 M NaCl was about 20% lower than in 0.1 M NaCl. Studies of the diffusion of polystyrene latex spheres in polyacrylic acid solutions (Phillies et al., 1987; 1989) also showed that a decrease in ionic strength lowered the diffusion coefficient. Whether any of these results are applicable to gels of relatively fixed structure (e.g., charged agarose) is unclear.

The purpose of this experimental work presented here is to assess the relative importance of charge interactions for Φ and D, by measuring the effects of ionic strength on the partition and diffusion coefficients of selected proteins in a gel of like charge. We chose three commonly used globular proteins (BSA, ovalbumin, and lactalbumin), whose

physical properties are fairly well characterized in the literature. Sulfated agarose gel was employed, primarily because it is a rigid polysaccharide which does not swell or shrink when exposed to changes in ionic strength, so that the volume fraction of fibers remains constant. In addition, the acidity of the sulfate groups ensures that the amount of charge on the gel is essentially independent of pH.

2.2 Materials

2.2.1 SP-Sepharose Characterization

SP-Sepharose Big Beads®, a 6% sulfated agarose gel, was obtained from Pharmacia (Piscataway, NJ). The diameters of the hydrated gel beads ranged between 100 μm and 300 μm. The charge on the SP-Sepharose was 0.23 meq/mL packed bed, as determined by titration by Pharmacia. Using the void and total volumes of the packed bed, the volume fraction of fibers, and an agarose fiber radius of 1.9 nm (see section 1.6), the surface charge density was 0.42 C/m^2. The gel beads were washed and suspended in 0.01 M sodium phosphate buffer, pH 7.1.

2.2.2 Protein Characterization

Three fluorescein-labeled proteins, bovine serum albumin (MW 68,000), ovalbumin (MW 45,000), and lactalbumin (MW 14,200) were obtained from Molecular Probes (Eugene, OR). Aqueous samples were prepared by dissolving the fluorescent proteins (4 mg/mL) in 0.01 M sodium phosphate buffer, pH 7.1. The ionic strength was increased where desired by adding either 0.10 or 1.00 M potassium chloride, yielding final ionic strengths (including the phosphate buffer) of 0.11 or 1.01 M. Size-exclusion chromatography of each sample showed that there was no detectable free fluorescein present. The net charge of each protein was calculated by using published titration curves for the unlabeled protein,

and adjusting for the contribution of the carboxyl group on the fluorescein. The average number of fluorescein groups per protein molecule was reported by Molecular Probes to be 5.3, 2.3, and 1.3 for BSA, ovalbumin, and lactalbumin, respectively, and the pK_a of the fluorescein carboxyl was taken to be 6.5 (Haugland, 1992). The size and charge characteristics of the proteins are summarized in Table 2.1. The Stokes-Einstein radii in Table 2.1 are based on the free solution diffusivities measured in the present study, as discussed in section 2.4.2.

Table 2.1 Protein characteristics

Protein	Stokes Radius (nm)	Isoelectric Point (pI)	Native Protein Charge	Fluorescein Charge	Net Protein Charge
BSA - fluorescein (Lot # 6531-1)	3.8	4.9*	-33§	-4.1	-37
Ovalbumin - fluorescein (Lot # 6521-1)	3.1	4.7*	-17‖	-1.8	-19
Lactalbumin - fluorescein (Lot # 6511-1)	2.3	5.1‡	-8‡	-1.0	-9

*Righetti and Caravaggio, 1976
‡Shukla, 1973
§Tanford et al., 1955
‖Overbeek, 1950

2.3 Methods

2.3.1 Partition Coefficient using Chromatography Column

Equilibrium partition coefficients were measured using a C-10/20 chromatography column (Pharmacia, Piscataway, NJ) containing approximately 12 mL of SP-Sepharose Big Beads®. The column had a sample applicator at the inlet and was connected to a peristaltic pump; the applicator and tubing volumes were 3.0 and 0.1 mL, respectively. A sample of

volume V_i = 3.0 mL with an initial concentration C_i of ~ 0.25 mg/mL of fluorescent protein was loaded on the column, and the eluent was recirculated at 0.5 mL/min. After the whole system had equilibrated (2 hr), the final protein concentration C_f was measured in a 1 mL sample withdrawn from the sample applicator. Protein concentrations were determined by measuring the absorbance of the sample using a Shimadzu (Columbia, MD) UV-Vis spectrophotometer at 488 nm. A calibration curve for determining the final concentration was made by making dilutions of the initial sample. Preliminary experiments performed by recirculating the eluent through a flow cell in the UV spectrophotometer confirmed that equilibration was reached within 90 min. The void volume (V_0, the total liquid volume outside the gel beads, including the flow loop) was determined similarly by recirculating fractionated blue dextran (MW 2 x 10^6). The blue dextran was fractionated to eliminate any small residual dextrans that might penetrate into the agarose beads. A small disposable 10 mL gravity feed column packed with SP-Sepharose was used to purify blue dextran. The equilibrium partition coefficient was calculated using an overall mass balance, as

$$\Phi = \frac{C_i V_i - C_f V_f}{(V_t - V_o) C_f} \qquad (18)$$

where V_t = 15.1 mL is the total volume (V_0 plus bead volume).

2.3.2 Diffusion Coefficient using Fluorescence Recovery After Photobleaching

Samples for diffusion measurements were prepared by combining the gel bead suspension, the fluorescent protein, and potassium chloride to a final protein concentration of 1 mg/mL, and allowing the suspension to equilibrate. The suspension was then drawn into 300 μm rectangular glass microslide chambers (Vitro Dynamics, Rockaway, NJ), using a syringe

attached to the microslide by silicon tubing. The ends of the microslide were blocked with a sealing compound (Hemato-seal, Fisher, Pittsburgh, PA).

2.3.2.1 Fluorescence Recovery After Photobleaching

Diffusion coefficients were determined by an image-based fluorescence recovery after photobleaching (FRAP) technique. A schematic of the apparatus is shown in Figure 2.1. The reliability of the method for measurements of diffusion in thick, light-scattering media was established by Berk et al. (1993). The sample was placed on the stage of an upright microscope (Universal, Zeiss; Thornwood, NY) equipped for epi-fluorescence. The excitation filter (485 ±11 nm, band-pass), dichroic mirror (505 nm), and barrier filter (530 nm, long-pass) are designed for fluorescein observation. By means of a beam splitting mirror, epi-illumination was provided by both a conventional mercury arc lamp (100 W lamp, Osram, Munich; with stable power supply and convection-cooled housing, models 68806 and 60000, Oriel Corp., Stratford, CT) and by an argon laser (model 2020, Spectra Physics, Mountain View, CA). The laser operated in the TEM00 mode (i.e. the intensity obeyed a radially symmetric Gaussian profile). The beam was directed through the microscope epi-illumination port to the back focal plane of the objective. With the 20x, NA 0.4 objective used for these experiments, the laser spot radius within the sample (the Gaussian radius of the attenuated beam projected onto a 50 μm thick layer of FITC (fluorescein isothiocyanate) solution) was ~20 μm. The microscope image was projected directly to an intensified CCD camera (model 2400; Hamamatsu, Japan). Fluorescence images were digitized directly (DT-2851 image processing board; Data Translation, Marlboro, MA; in an IBM PC-AT computer, Boca Raton, FL) and stored at a rate of 5 images per second. Only the central portion (100 x 125 pixels) of the full 512 x 480 pixel image was stored for analysis. An electronic shutter in the laser light path and another directly before the camera allowed automated computer control of the laser exposure time

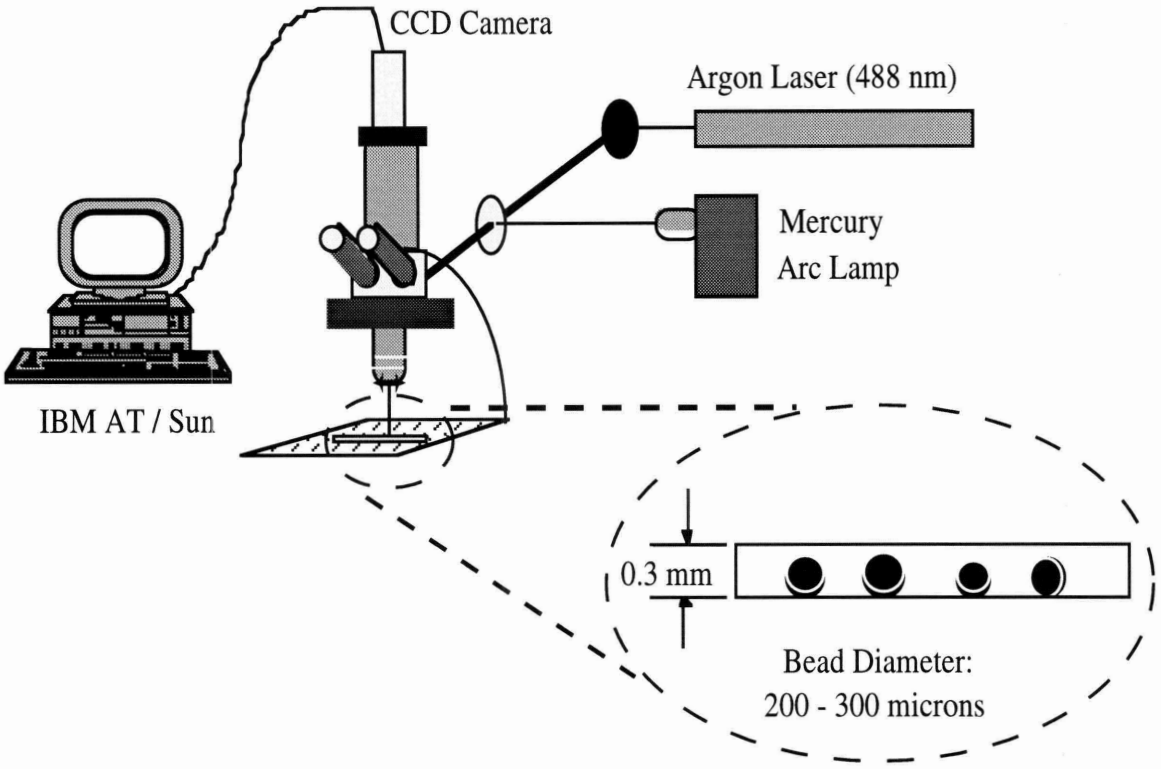

Figure 2.1 Schematic of apparatus used for fluorescence recovery after photobleaching (FRAP) to measure diffusivity coefficients

and image collection sequence. The spatial sampling rates (vertical and horizontal distances between pixels, 0.917 and 1.13 μm, respectively) were calculated from an image of a stage micrometer. The error on the distances between pixels was estimated to be less than 5%.

For each protein at each ionic strength, diffusion measurements were made with five separate gel beads. For any given agarose bead, seven measurements each were made of D and D_∞. For the gel diffusivity (D) measurements, the bead was positioned so that its center was in the focal plane and directly in the laser path. To measure D_∞ the slide was moved laterally so that no beads appeared in the image. After a brief exposure to laser illumination (30 ms) the sample was observed under conventional epi-fluorescence illumination and the digitized fluorescence images were stored for later analysis. The fluorescence intensity in a region of the image far (≥ 200 μm) from the laser spot was also monitored, to detect the occurrence of photobleaching by the conventional light source; this additional bleaching was in the range of 0 to 2% of the total intensity over a 30 seconds monitoring period. To allow for complete recovery of the bleached areas, the gel diffusion measurements were alternated with the free solution diffusivity measurements. The room temperature was recorded (23 - 29°C) and all diffusion coefficients were corrected to 20°C using the Stokes-Einstein relation and an interpolation of the viscosity of water given by the CRC handbook (Weast and Astle, 1980).

2.3.2.2 Fourier Transform Analysis of Diffusion Data

The data analysis of the diffusion data is based upon a Fourier transform of the fluorescent images recorded over the length of the experiment. This section describes the Fourier transform method and its application to the of the two dimensional diffusion equation

$$\frac{\partial C}{\partial t} = D\left(\frac{\partial^2 C}{\partial x^2} + \frac{\partial^2 C}{\partial y^2}\right) \tag{19}$$

where C is the concentration of the probe, t is time, D is the diffusivity and x and y are the spatial coordinates of the system. The Fourier representation of the concentration profile is given by

$$C(t,x,y) = \sum_{u=-\infty}^{\infty} \sum_{v=-\infty}^{\infty} A(u,v,t)\exp(2\pi i\, uf_o\, x)\exp(2\pi i\, vf_o\, y) \tag{20}$$

where f_o is a characteristic frequency (see equation 24), u and v are wavenumbers, and A(u,v,t) are the Fourier coefficients. By substituting the Fourier representation of the concentration into the diffusion equation, non-dimensionalizing the spatial coordinates with the characteristic frequency, and defining a new variable, q

$$q^2 = u^2 + v^2 \tag{21}$$

we get an ordinary differential equation for the Fourier coefficients, now a function of the wavenumber, q, and time, t.

$$\frac{\partial A(q,t)}{\partial t} + D(2\pi q)^2 A(q,t) = 0 \tag{22}$$

Solving equation 19 leads to

$$A(q,t) = A(q,0)\exp\left(-D(2\pi q)^2 t\right) \tag{23}$$

To determine the diffusivity, D, the Fourier coefficients, A(q,t), at each time need to be determined. The diffusion coefficient can be calculated for each separate frequency.

For a digitized image, a discrete Fourier transform is used. Because the pixel dimensions have a finite size (i.e., they are an average of concentrations over the ~ 1 μm distance) the Fourier concentration profile must be truncated for frequencies higher than the Nyquist critical frequency, f_c, which is given by

$$f_c \equiv \frac{1}{2\Delta} \tag{24}$$

where Δ is the distance between the pixels. In our case, the pixel distance for the 20X objective is approximately 1 μm, so the maximum frequency is ~ 0.5 $(\mu m)^{-1}$. There is a slight difference in Δ between the x and y directions. In addition, only multiples of the critical frequency can be used in the Fourier representation of the concentration profile. For a two dimensional digitized image of N x N pixels, the continuous image function, i(x,y) is approximated by

$$i(x,y) \approx i(x_j, y_k) \quad x_j = j\Delta \text{ and } y_k = k\Delta$$
$$j = 0,1,2,...,\text{N}-1 \quad k = 0,1,2,...,\text{N}-1 \tag{25}$$

Because of the limited number of data points we can only find Fourier transform coefficients for N discrete frequencies in the x and y directions, respectively. The frequencies are

$$f_u = \frac{u}{N\Delta} \quad u = -\frac{N}{2},...,\frac{N}{2}$$
$$f_v = \frac{v}{N\Delta} \quad v = -\frac{N}{2},...,\frac{N}{2} \tag{26}$$

The Fourier coefficients are defined by

$$A(f_j, f_k, t) = \int_{-\infty}^{\infty}\int_{-\infty}^{\infty} C(x,y,t)\exp(2\pi i\, f_j x)\exp(2\pi i\, f_k y)\, dx\, dy \tag{27}$$

which is approximately equal to

$$A(f_u, f_v, t) \approx \sum_{j=0}^{N-1}\sum_{k=0}^{N-1} C(j,k,t)\exp(2\pi i\, f_u x_j)\exp(2\pi i\, f_v y_k)\Delta^2$$
$$= \Delta^2 \sum_{j=0}^{N-1}\sum_{k=0}^{N-1} C(j,k,t)\exp\left(\frac{2\pi i}{N}(uj+vk)\right) \quad \textbf{(28)}$$

We can also define a dimensionless Fourier transform coefficient to be

$$A(u,v,t) = A(q,t) = \sum_{j=0}^{N-1}\sum_{k=0}^{N-1} C(j,k,t)\exp\left(\frac{2\pi i}{N}(ju+kv)\right)$$
$$A(f_u, f_v, t) = \Delta^2 A(q,t) \quad \textbf{(29)}$$

where C(j,k,t) is the concentration profile as a function of the pixel index j and k, and of time, t. To solve for the two dimensional Fourier coefficients, we need to define a constant W,

$$W = \exp\left(\frac{2\pi i}{N}\right) \quad \textbf{(30)}$$

and put the double summation in matrix form

$$\mathbf{A(u,v,t) = W^{uj+vk} c(j,k,t)} \quad \textbf{(31)}$$

An illustration of this for j=0,3 and u = 0,3 holding k and v constant is

$$
\begin{aligned}
A(0,v,t) &= W^{vk}\left[C(0,k,t)+C(1,k,t)+C(2,k,t)+C(3,k,t)\right] \\
A(1,v,t) &= W^{vk}C(0,k,t)+W^{1+vk}C(1,k,t)+W^{2+vk}C(2,k,t)+W^{3+vk}C(3,k,t) \\
A(2,v,t) &= W^{vk}C(0,k,t)+W^{2+vk}C(1,k,t)+W^{4+vk}C(2,k,t)+W^{6+vk}C(3,k,t) \\
A(3,v,t) &= W^{vk}C(0,k,t)+W^{3+vk}C(1,k,t)+W^{6+vk}C(2,k,t)+W^{9+vk}C(3,k,t)
\end{aligned} \qquad (32)
$$

Instead of solving the above equation directly (it would take too long), the FFT algorithm expands the matrix, W^{uj+kv}. Numerical Recipes (Press, 1992) gives a more complete explanation about the mechanics of this algorithm.

2.3.2.3 Padding and Windowing of the Discrete Fluorescence Image.

In this image-based fluorescence recovery technique, the diffusion coefficient is calculated from the decay of Fourier coefficients in successive images. This approach is advantageous for two reasons: first, it reduces sensitivity to out-of-focus light because the resultant image distortion affects only the relative magnitude of each Fourier coefficient but not the rate of its decay; and second, solution of the diffusion equation is simplified in Fourier space. However, one potential source of artifact is the use of a discrete Fourier transform to approximate the true transform. In particular, the truncation of the finite image gives rise to spurious high frequency components (leakage or Gibb's phenomenon) that are unrelated to the actual image and therefore interfere with the diffusion fit. We employed two strategies to overcome this problem: padding and windowing.

A discrete Fourier transform actually represents an infinitely repeating two-dimensional array of the image. Figure 2.2(a) shows a one-dimensional illustration of this feature: a discontinuity may exist at the boundary between image elements. Ideally, the

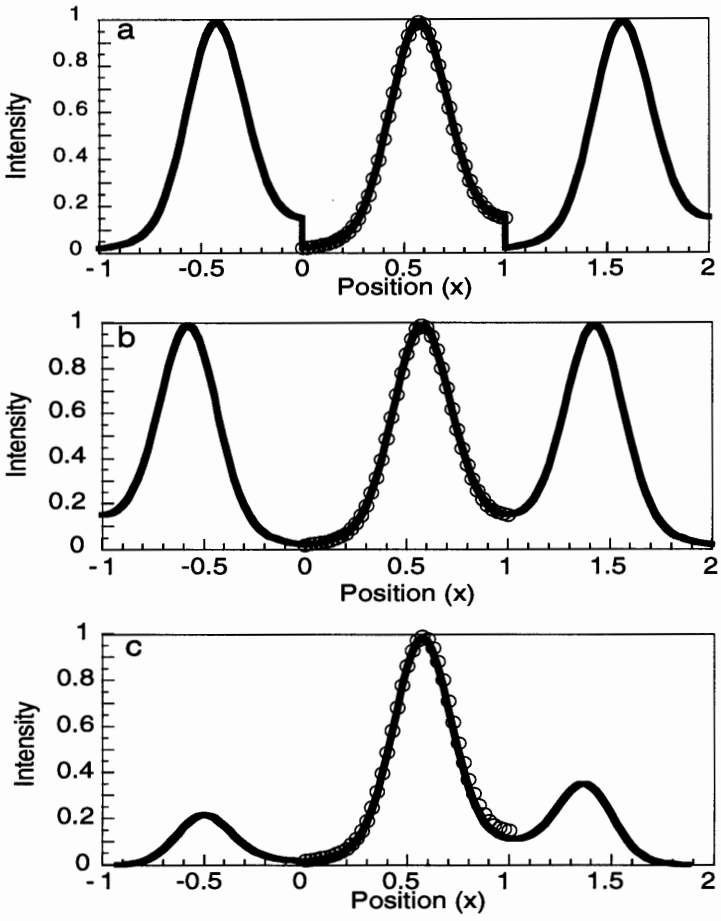

Figure 2.2 Illustration in one dimension of the padding and windowing algorithm for calculation of discrete Fourier transform (DFT) coefficients. The circles represent digitized image data corresponding to a photobleached spot (the original unbleached image minus the post-bleach image). Position (x) is scaled by the length of the data window. (a) The DFT of the data over the range x=0-1 represents the infinite waveform shown by the line. The discontinuities at x=0 and x=1 cause spurious Fourier coefficients at high frequencies. (b) The data are reflected about the axes x=0 and x=1 doubling the period to x=-0.5 to 1.5. The infinite waveform corresponding to the new DFT is now continuous. (c) A windowing function smoothly attenuates the borders with minimal distortion to the spot intensity profile.

intensity of a processed image should smoothly approach zero at the periphery, because it is a differential image (pre-bleach minus post-bleach), but in practice there are spatial and temporal fluctuations in lamp intensity, detector gain, and out-of-focus fluorescence signal. To reduce this edge discontinuity effect, the image was multiplied by a 2-dimensional hanning function (Brigham, 1974). This windowing function smoothly attenuates the image borders to zero.

It is important for the validity of the windowing approach that the size of the photobleached spot be less than the size of the image. In these experiments, the spot diameter was approximately 50 μm, compared to an image size of 115 x 115 μm. To further minimize the distortion of the spot intensity profile, the image was padded prior to the windowing step in order to produce a larger effective image size. At each edge of the image, a new border was added; this border was a symmetric reflection of the original image, as illustrated in Figure 2.2(b). The resulting padded image was twice the size of the original image, but the infinite waveform described by the discrete Fourier transform of the image is similar to one produce without padding, except that the padded waveform had no discontinuities. The discrete Fourier transform of the padded image is no less accurate a representation of the true image; the advantage of this procedure is that the padded image can be windowed with less distortion of the spot at the center of the image.

When we pad the window and double the number of pixels from N to 2N we introduce an extra frequency without adding any new information. This makes now both the zero frequency and the 1st frequency in each direction give erroneous information on the diffusional decay. When we discuss q, which is a function of both u and v, q is not valid for either u or v being equal to either 0 or 1. Which mean that the first four q values cannot be used in the diffusion calculation.

2.3.2.4 Application of Fourier Transform Analysis to 3-D Gel Bead

The actual bead system is not two dimensional as the above 2-D Fourier transform analysis would imply. There are two issues that needs to be directly addressed before using the aforementioned analysis. The first concern is that the two-dimensional image is recording the recovery of the free solution and the solution inside the gel bead. The second issue relates to using this technique in gel media that can scatter light.

Assuming that we bleach a straight column through the fluorescent material both inside and above the gel bead, any two dimensional digitized image would record the recovery of both the solute inside the gel bead and the free solution above. By using the theory of image formation, Berk et al. (1993) showed that for our system that if the free solution is 100 μm above or below the focal plane then a Gaussian spot would be out of focus enough to appear uniform. Since there is no spatial variation in the image at this distance from the focal plane, there would be no contribution to the decay in the Fourier coefficients. This out of focus light would contribute to the zero order Fourier coefficient but since this does not decay it is not used for determining the diffusion coefficient. Consequently we chose to use gel beads that were at least 240 μm in diameter, so that when we focused on the center plane of the gel bead the free solution above the spot would be at least 100 μm above the focal plane.

Another interesting issue in measuring the diffusivity is the distortion of the fluorescent signal when passing through light scattering media. As Berk et al. (1993) discuss, a major advantage of the Fourier transform method is that it can reliably measure diffusivities in thick gel media. The image recorded by the CCD camera is a convolution of the true concentration and the point spread function. The point spread function (PSF) is the distortion of a point source of light due to aberrations in the microscope lens, light adsorption and scattering properties of the sample. The Fourier transform of the point spread function is termed the optical transfer function (OTF). Since the point spread function (and thus the optical transfer function) is only dependent upon position and not

time, the Fourier transform of the image, $I(u,v,t)$ can be related to the Fourier transform of the concentration, $C(u,v,t)$ by

$$I(u,v,t) = C(u,v,t)\ OTF(u,v) \qquad (33)$$

This implies that the ratio of images is exactly equal to a ratio of concentrations

$$\frac{I}{I_o} = \frac{C}{C_0} \qquad (34)$$

By measuring the decay of the spatial Fourier transform of the ratio of images, the diffusion coefficient can be calculated without determining the optical transfer function of the microscope, and without determining the true concentration distribution in the sample.

2.3.2.5 Analysis of FRAP data

The diffusion coefficient was determined by a spatial frequency analysis of successive images (Berk et al., 1993; Tsay and Jacobson, 1991). Each post-bleach image was first subtracted from the initial pre-bleach image, then subjected to a two-dimensional discrete Fourier transform. In order to reduce the high-frequency components due to truncation of the image (Gibbs phenomenon), we employed an image padding and windowing algorithm as described in section 2.3.2.3. The processed image array was then subjected to a discrete Fourier transform (two-dimensional fast Fourier transform subroutine; IMSL, Houston, TX) to obtain an array of complex Fourier coefficients, which were converted into magnitudes, I(j,k). Discrete spatial frequencies, u and v, were then calculated from the

indices j and k. The diffusion coefficient, D, was calculated from the decay of each Fourier coefficient in successive images:

$$\frac{I(u,v,t)}{I_0} = \beta + (1-\beta)\exp\left(-4\pi^2 q^2 Dt\right) \qquad (35)$$

where q is the magnitude of the frequency ($q^2 = u^2+v^2$), β is a parameter which accounts for incomplete recovery of the fluorescence (see below), and $I_0 \equiv I(u,v,0)$. The decay of the coefficients corresponding to the lowest four frequencies was meaningless because of the padding and windowing process, but the next 20 to 30 components were observed to decay at approximately the same frequency-scaled rate. An initial estimate of D was obtained by the simultaneous fitting of several Fourier coefficients to equation 35 by a nonlinear least-squares method. For a fit of N Fourier components to the diffusional decay, there are N+2 independent parameters: the diffusion coefficient, D, the recovery parameter, β, and N separate initial values, I_0. In order to maximize signal-to-noise ratio and temporal resolution, we chose the five lowest usable frequency components, because they had the greatest magnitude and decayed at the slowest rate. The estimate of D was refined by re-plotting these components in the form

$$f(t) = -\ln\left[\frac{\frac{I}{I_o} - \beta}{1-\beta}\right] = 4\pi^2 q^2 Dt \qquad (36)$$

and performing a linear fit with I_0 and β fixed. Linear regression of f(t) versus t was restricted to early times, such that $f(t) \leq 1$.

Figure 2.3 illustrates typical results from an analysis of a single photobleaching recovery for diffusion in free solution and within a gel bead. The diffusion coefficients in free solution and in the gel phase calculated from the decay of individual Fourier components are shown in Figure 2.4. The absence of a strong dependence of D on spatial frequency indicates that the method indeed measured diffusion within the bead and not within the free solution. If the fluorescence recovery was influenced by diffusion outside the bead volume, the lower frequency components, which contain more of the out-of-focus signal, would decay at a faster scaled rate and give higher diffusivity values. For each fit of an individual component, the standard error of the diffusion coefficient was typically 5 to 10%, although some components could not be fit (standard error greater than 50%). When five or more components were combined for a global fit, as shown in Figure 2.3, the standard error of the estimate was only 1 to 2% and the correlation coefficient r^2 was at least 97%.

The parameter β introduced in equation 35 is equivalent in principle to the fraction of the total protein which is immobile. Its values typically were between -3 and +8% for the free solution measurements and between 8 and 15% for the diffusion measurements in the gel beads. The results obtained for free solution, where no adsorption could be present, indicate that small non-zero values are without physical significance, and evidently arise from signal processing difficulties. Because the signal-to-noise ratio was lower in the gel media (the gel tended to scatter some of the light), the somewhat larger values of β probably do not reflect actual adsorption of protein on the gel beads. This was confirmed by substituting the final post-bleach image in place of the pre-bleach image and repeating the analysis. This would have the effect of removing any residual spot due to an immobile fraction. The differential images should therefore decay entirely. The diffusion coefficients and β values determined in this fashion were virtually the same as those

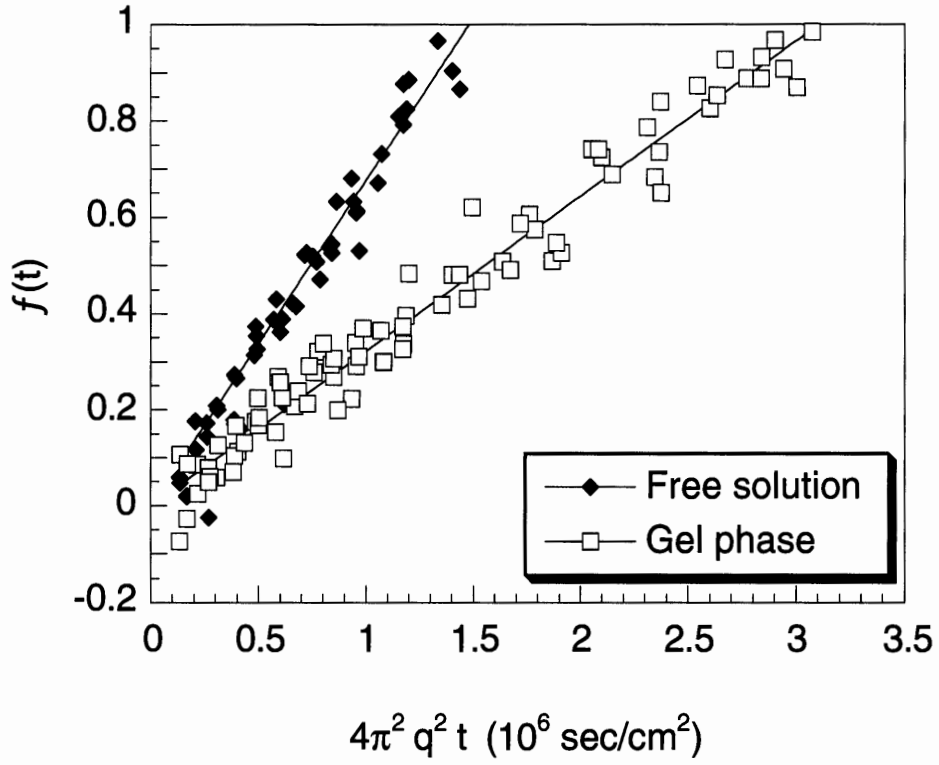

Figure 2.3 Calculation of the diffusion coefficient in a gel bead from one photobleaching recovery sequence, for BSA at an ionic strength of 1M. The temperature was 28.7 °C. The diffusion coefficient was calculated for each Fourier component for the free solution (◆) and for the gel phase (□), and overall diffusion coefficients were calculated by a global fit to equation 36 incorporating several components (—).

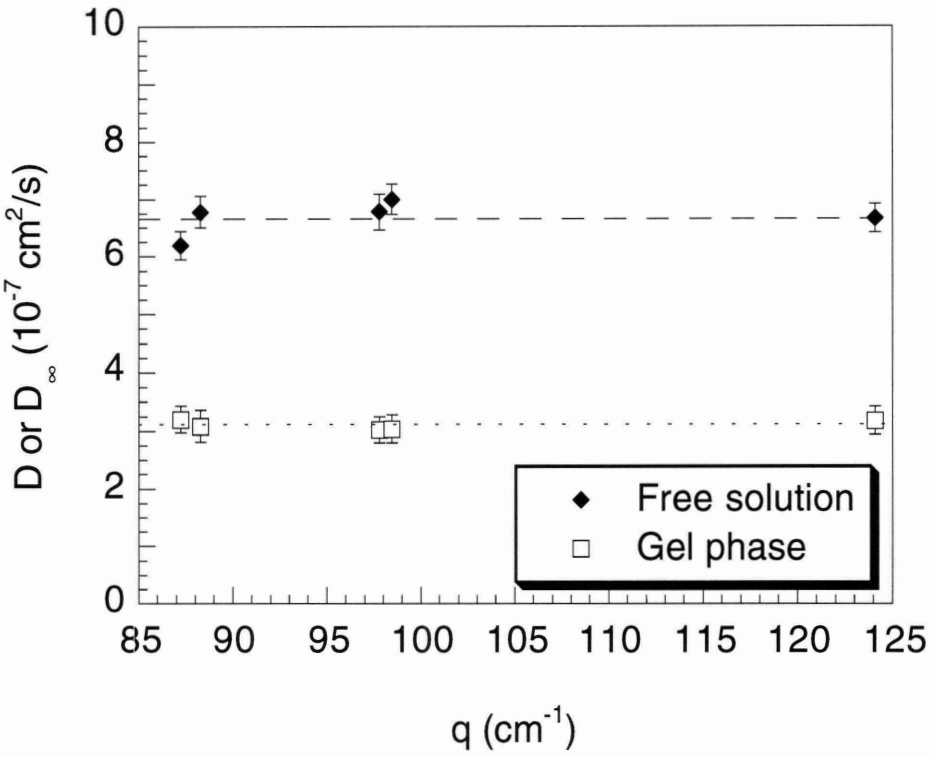

Figure 2.4 Calculation of the diffusion coefficient at differing values of the spatial frequency. The individual diffusivity values at higher spatial frequencies are not significantly lower than the overall value. This is evidence that the overall value is a valid measure of diffusion within the bead and that the method is not sensitive to photobleaching in the surrounding free solution. Diffusivity measurements were at the same conditions given in Figure 2.3.

calculated by the original method. We conclude that the true immobile fraction was less than 1%.

2.3.3 Statistical Calculations

For both the diffusion and partition coefficients, statistical differences as a function of ionic strength were assessed using an analysis of variance (ANOVA). In addition, the protein diffusivities for the three ionic strengths were compared using Tukey's method of multiple comparisons (Larson and Marx, 1986). Differences at the 95% confidence level were judged to be significant. Uncertainties in the diffusion and partition coefficients are reported as standard deviations.

2.3.4 Partition Coefficient using Microfluorescence

In normal fluorescent solutions, the concentration is directly proportional to the measured intensity. Since we were interested in measuring the partition coefficient of fluorescently labeled proteins, we wanted to utilize this phenomenon. To this end we explored a technique whereby we could measure the intensity of the protein solution both inside and outside the bead and by using a simple ratio calculate the partition coefficient. As discussed in section 2.3.4.1, the partition coefficient could not be determined directly from the ratio of the fluorescence intensity to that in the free solution. This could be due to the distortion of the fluorescence signal in the gel phase or from light scattering from the external solution that contributes constructively to the fluorescence signal. In an attempt to determine how much of the fluorescence signal from the external solution contributes to the measured fluorescence from inside the gel bead, a dual wavelength experiment was also proposed and is discussed in section 2.3.4.2. To determine the contribution of the external solution to the light measured inside the gel bead the fluorescence from a rhodamine B - dextran (2

million Da) was measured. At this molecular weight the dextran does not penetrate into the gel and any signal dectected inside the gel bead is due to the external solution. Because the filters on the microscope can be readily changed the fluorescence intensity from each fluorophore can be measured directly without interference for the gel bead of interest. By then looking at the fluorescence intensity of a fluorescein labeled protein both inside the gel and outside and subtracting off the light contribution from the external solution (as measured using the dextran) the partition coefficient can be determined. But as discussed in section 2.3.4.2, while there was a significant portion of light being constructively scattered into the gel from the external solution, the dual wavelength method could not give accurate values for the partitioning.

2.3.4.1 Partition Coefficient Measurement Using Direct Intensity

If the fluorescence is directly proportional to the concentration both inside the gel bead and in the external solution it should be possible to use a ratio of intensities to determine the partition coefficient. For any gel bead in solution there will be some free solution above the bead that will contribute to the fluorescence signal. To account for this free solution contribution it would be necessary to know the size of the gel bead and the height of the microslide so that this contribution could be subtracted out. The most accurate method of determining both the size and the fluorescence signal from the gel bead would be to measure a line of fluorescence intensity across the bead and into the free solution. By doing this the bead size could be determined from the point where the fluorescence intensity starts to decrease. In addition there would be multiple points throughout the linescan that can be used to calculate the partition coefficient. Using the equipment setup for the diffusion experiments described above in section 2.3.2, a line scan of the fluorescence intensity could be made across a SP-Sepharose bead. A schematic of the system is shown in Figure 2.1. Because the illumination of the lamp is non-uniform across the field of view

and can fluctuate with time, two linescans were needed. As shown in Figure 2.5 the first scan (a reference linescan) was made across a uniform sample of dextran-fluorescein (2 million Da) while the second scan was made across a gel bead. Because of the variations in the lamp intensity it is necessary to use the exact same pixels in the linescan for the reference and for the gel bead. To accomplish this the center of the gel bead was moved into the exact field of view where the reference linescan was taken. Because the dextran has such a high molecular weight it will not penetrate into the gel bead and should yield a partition coefficient of zero. A typical set of linescans is shown in Figure 2.5 where the fluorescence in arbitrary units is plotted versus the pixel number. To obtain a more accurate picture of the fluorescence intensity, the linescan with the bead was normalized with the reference linescan and a plot of the normalized intensity averaged for five sets of linescans is given in Figure 2.6. If the intensity measurements were directly proportional to the concentration inside the bead then we could determine the partition coefficient using the physical parameters of the microslide setup, the height of the microslide and the diameter of the gel bead. The intensity of each pixel, I, would be

$$I = HE - BE + \Phi EB \qquad (37)$$

where H is the height of the microslide, E is the excitation of the fluorophore per unit height, B is the secant distance of the bead at that pixel point, and Φ is the partition coefficient. Using the external solution as a reference (where B = 0) then we can determine the partition coefficient from

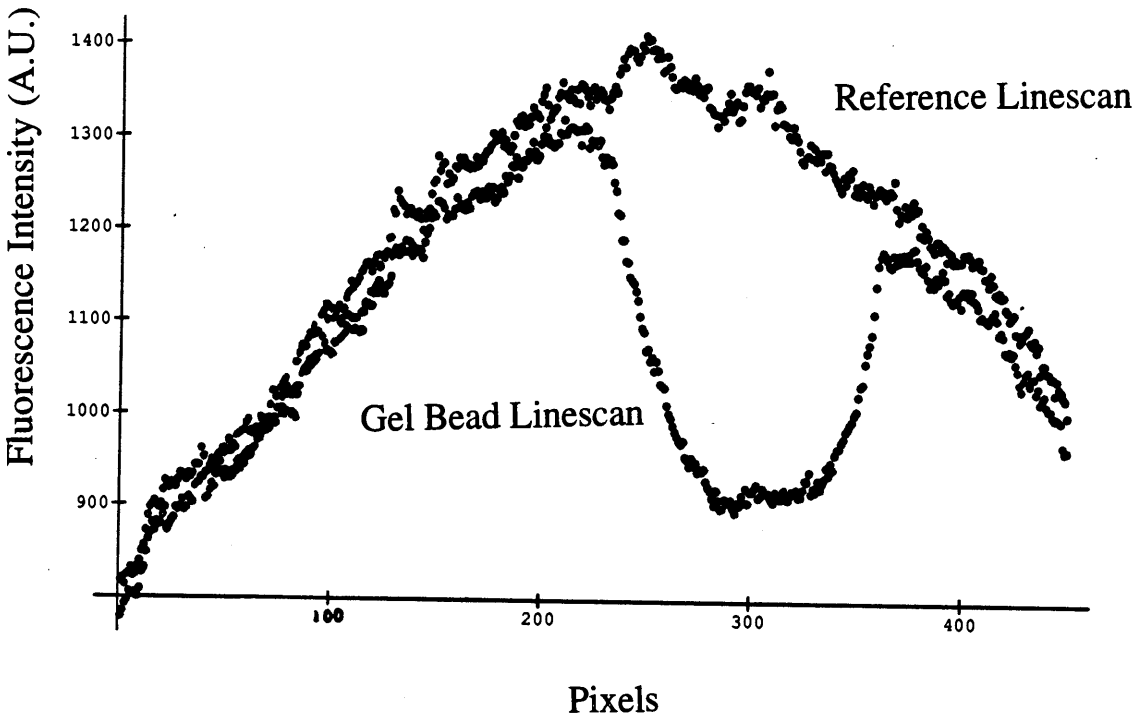

Figure 2.5 A linescan of the fluorescence intensity of dextran - fluorescein (MW 2 million). The reference linescan is the fluorescence intensity across a uniform solution of labeled dextran. There are variations in the measured intensity because of variations in the illumination by the mercury arc lamp. The gel bead linescan is the fluorescence intensity of the exact same pixels as those in the reference linescan but with a gel bead in the center of the field of view.

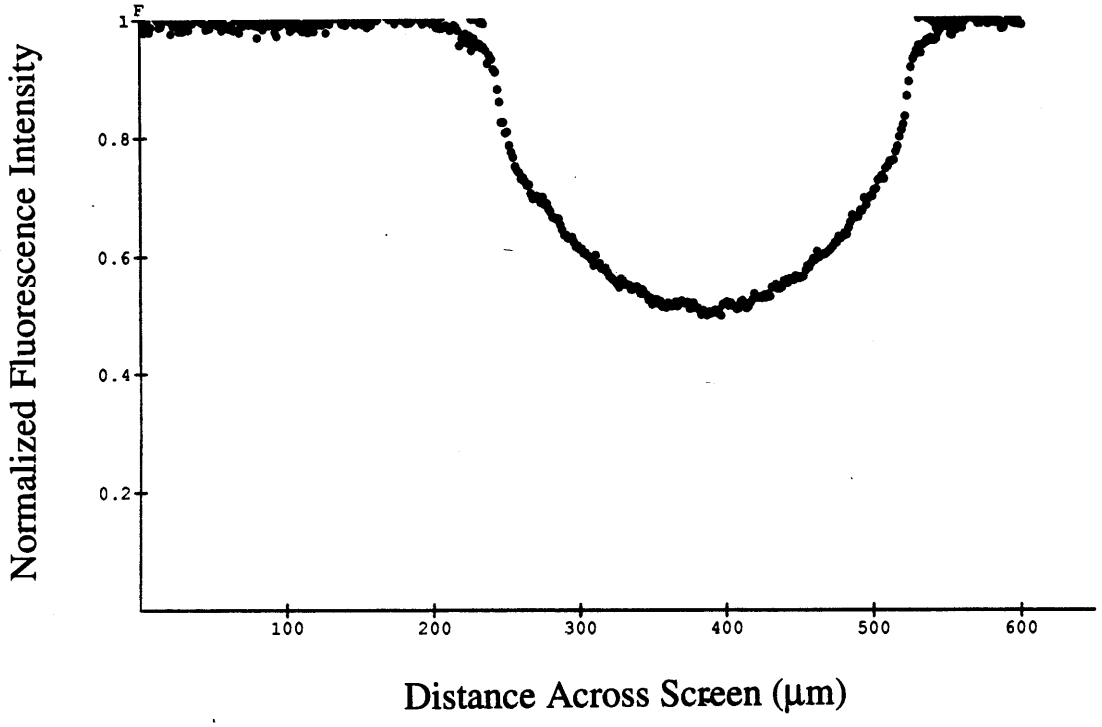

Figure 2.6 The average linescan across a gel bead in equilibrium with dextran - fluorescein (MW 2 million) normalized with the reference linescan. Five sets of linescans were used.

$$\Phi = \frac{I}{BE} - \frac{H}{B} + 1$$
$$B = 2\sqrt{R^2 - (x_n - x_c)^2} \qquad (38)$$

where R is the radius of the gel bead, x_n is the distance from the first pixel to pixel n and x_c is the distance to the pixel at the center of the bead. When we found that the calculated partition coefficient of dextran - fluorescein (2 million Da) was significantly higher than, we concluded that our assumption that the concentration of the macromolecule inside the gel bead was proportional to the measured intensity was erroneous. Since there was significantly more signal inside the bead than we had expected, one suggestion was that there was light being scattered into the bead from the external solution. When we measured the intensity of a small fluorophore, fluorescein, in equilibrium with the gel bead, the intensity of the solution inside the gel bead was higher than in the external solution! This was strong evidence that the gel phase was scattering light in a constructive manner for the microscope.

2.3.4.2 Partition Coefficient Measurement Using Dual Fluorescence

To account for the amount of light scattering into the gel bead from the external solution, a modification of equation 37 was made to include a term for the contribution of light scattered into the gel bead. The intensity at each pixel is then

$$I(n) = H\,E(n) - B(n)\,E(n) + \Phi\,E(n) + Q(n)\,E(n)\,B(n) \qquad (39)$$

where the addition term, Q, is an unknown amount of light scattered to each pixel, n.

To find Q (the amount of light scattered to the pixel point and contributing to that pixels intensity), another fluorophore rhodamine B was used. In contrast to fluorescein which is excited at 488 nm and emits at 515 nm, rhodamine B's excitation wavelength is 555 nm and emits at 579 nm. This allows us to mix the two fluorophores and determine independently their concentrations. To determine the amount of light being scattered from the external solution, the rhodamine B was conjugated to dextran (MW 2 million) which will not penetrate into the gel bead. So a scan of the rhodamine B labeled dextran should give us a direct measurement of Q since $\Phi = 0$.

The assumptions of this analysis include: (1) light from the outside solution is scattered into the gel bead and contributes to the image recorded by the camera; (2) the image recorded by the camera is the linear sum of the intensities in the pathway; (3) the light scattered into the bead from fluorescein in the exterior solution is the same amount of light scattered by rhodamine B; and (4) the illumination is uneven across the field of view and a line scan in the exterior solution only is needed to correct for non-uniform illumination. Each experiment was done using a 10 x 0.3 NA objective. Each point in the line scan was eight pixels wide and the value used for intensity was the average of the eight pixels. Five linescans were taken and averaged to yield a final intensity value for each pixel.

Using a dual scan of the gel bead, one where the intensity of the fluorescein labeled protein is recorded and one where the intensity of the rhodamine B labeled dextran is measured the partition coefficient can be determined. The partition coefficient, Φ, can be solved for using equation 39 to yield

$$\Phi = \left(\frac{I}{HE} - 1 \right) \frac{H}{B} + 1 - Q \qquad (40)$$

where H is the height of the microslide, E is the excitation of the fluorophore by the mercury arc lamp at each pixel, B is the secant length intersecting the gel bead at each pixel and Q is the light scattered to the pixel from the surrounding solution. Each of these parameters must be determined to calculate the partition coefficient.

The height of the microslide, H, is determined by placing the end of the slide under the microscope, recording the image and counting the number of pixels. Knowing the calibration of the pixel distance the height of the microslide can be determined. For the microslides that we used there was typically less than a 3% variation across the width of the microslide. To determine the amount of illumination for each pixel, H E(n), a reference linescan was done in solution away from the gel bead. Since we know that the microslide height, H, was constant, the specific illumination per pixel, E(n), could be determined. A typical example of the lamp variation across the video screen is shown in Figure 2.5. To determine the secant length, B(n), the radius of the bead was measured by taking a video image of the gel bead and counting the number of pixels across the widest portion of the bead. The secant length was calculated from

$$B(n) = 2\sqrt{R^2 - \left[P(n_c - n)\right]^2} \qquad (41)$$

where n_c is the pixel at the center of the bead, n is the pixel number of interest, P is the pixel calibration (typically ~ 0.9 μm)

Taking a linescan of the rhodamine B labeled dextran and using the fact that the partition coefficient is zero, the values for Q(n) could be determined. Then doing a similar

line scan of the fluorescein labeled protein across the same exact pixels (only a filter change was necessary) the partition coefficient, Φ, could be determined. An example of a normalized linescan for both the rhodamine B labeled dextran and BSA-fluorescein in equilibrium with SP-Sepharose at a buffer ionic strength of 1.01 M are shown in Figure 2.7(a) and the partition coefficient calculated for each pixel is shown in Figure 2.7(b). There was no systematic difference between the partition coefficient values calculated for each pixel. The calculated partition coefficient for BSA-fluorescein was 0.43 which is considerably lower than the value measured using the gel chromatography of 0.67 as discussed in section 2.4.1. Since the partition coefficient of fluorescein should be close to unity, a measurement of fluorescein in SP-Sepharose was made in a buffer ionic strength of 1.01 and the results of the linescans and calculations of the partition coefficients are shown in Figure 2.8 (a) and (b). Because the partition coefficient of fluorescein is only 0.53 this leads to some doubt about the validity of this method.

One assumption made in using the dual fluorescence technique is that the scattering properties of the rhodamine B and fluorescein are the same. To test this hypothesis several experiments were performed. In the first set of experiments, dextran (MW 10,000) labeled with fluorescein and tetramethyl rhodamine (Molecular Probes, Eugene, OR) was equilibrated with the gel beads and linescans performed using the appropriate filters. Although the excitation and emission of rhodamine B and tetramethyl rhodamine are slightly different, a dual labeled dextran (MW 10,000) with both rhodamine B and fluorescein was not available. The difference between the linescans was less than 0.05% indicating that the light properties of the fluorescein was identical to that of tetramethyl rhodamine (excitation: 541 nm; emission: 568 nm). Likewise when linescans were performed on a mixture of dextran - fluorescein (MW 2 million) and dextran - rhodamine B (MW 2 million) the difference between the linescans was again less than 0.05%. When BSA - fluorescein was combined with BSA - Texas Red, the difference between their linescans was also less than 0.05%. The excitation and emission wavelengths for Texas

(a)

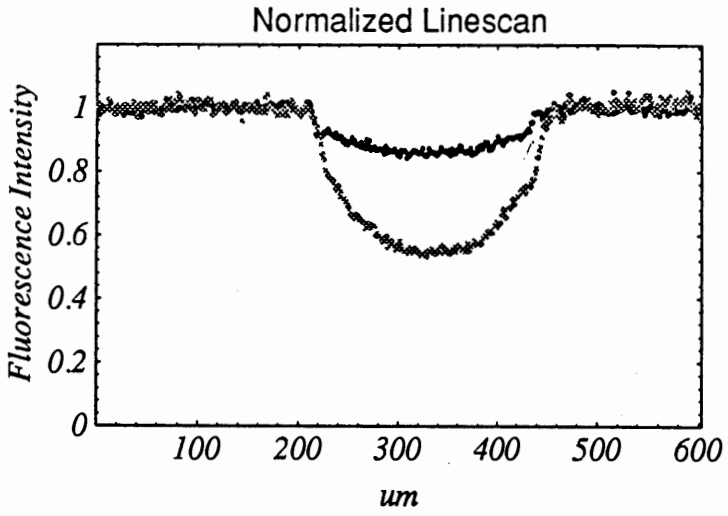

(b)

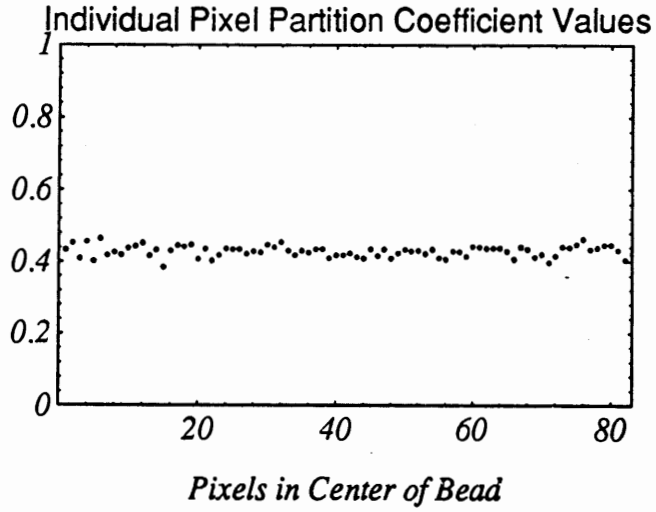

Figure 2.7 Calculation of the equilibrium partition coefficient of BSA in SP-Sepharose at a buffer ionic strength of 1 M. (a) A normalized linescan of BSA - fluorescein and dextran - rhodamine B in equilibrium with a gel bead. (b) The calculation of the partition coefficient for each individual pixel. Note the lack of variation in the partition coefficient as a function of pixel number.

(a)

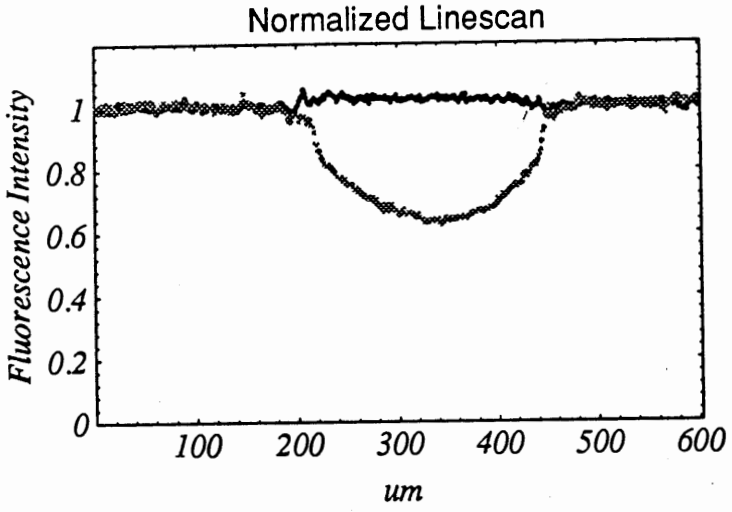

(b)

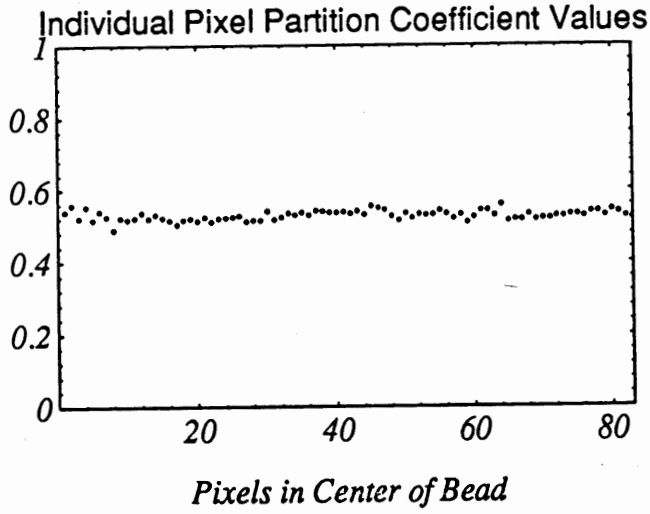

Figure 2.8 Determination of the partition coefficient of fluorescein in SP-Sepharose at ionic strength of 1 M. (a) The normalized linescans of fluorescein and dextran - rhodamine B across a gel bead. (b) The calculation of the individual pixel partition coefficients of which the average is 0.53. Because the partition coefficient of fluorescein should be greater than 0.9 this leads to some doubt about the validity of the dual wavelength method for measuring partition coefficients.

Red were 589 nm and 615 nm, respectively. In the second experiment, the partition coefficient of BSA was measured inside the gel bead for a 0.01 M sodium phosphate, pH 7.8, except this time the fluorescent probes were switched so that BSA was labeled with Texas Red and Dextran (MW 2 million) was labeled with fluorescein. With the BSA - Texas Red the partition coefficient was 0.18 while the BSA - fluorescein was 0.22. The two values were measured on different beads. The bead to bead variation is typically 10%. We concluded that the variation in fluorescent properties was negligible.

The partition coefficients for three proteins were measured for lactalbumin, ovalbumin and BSA in three phosphate buffers, pH 7.1 with potassium chloride added to make a final ionic strength of 0.01 M, 0.1 M and 1.0 M. The experimental values are shown in Table 2.2. When compared to the values obtained using the gel chromatography column method as discussed in section 2.4.1, the partition coefficients obtained using the microfluorescence technique were substantially lower for the higher ionic strengths.

Table 2.2 Comparison of the protein partition coefficients in SP-Sepharose using the microfluorescence technique and the gel chromatography method.

Protein	Ionic Strength (M)	Φ (fluorescence)	Φ (chromatography)
BSA - fluorescein	1.01	0.39 ±0.01	0.67 ±0.03
	0.11	0.38 ±0.01	0.47 ±0.01
	0.01	0.32 ±0.01	0.29 ±0.01
Ovalbumin - fluorescein	1.01	0.44 ±0.01	0.64 ±0.02
	0.11	0.41 ±0.01	0.59 ±0.01
	0.01	0.32 ±0.01	0.29 ±0.02
Lactalbumin - fluorescein	1.01	0.52 ±0.02	0.78 ±0.03
	0.11	0.45 ±0.01	0.75 ±0.04
	0.01	0.38 ±0.01	0.44 ±0.03

While it was very encouraging to find that the calculated partition coefficient did not vary as a function of pixel distance as shown in Figure 2.7(b) for BSA and in Figure 2.8(b) for fluorescein, the value of the partition coefficients place doubt upon the validity of this method. The measured partition coefficient for fluorescein using the microfluorescence technique was 0.53, which is substantially lower than the expected value (> 0.9). In addition the partition coefficients of the three proteins are lower than the values from the gel chromatography method which is calculated from a simple mass balance. It is interesting to note that at the lowest ionic strength where the partition coefficients are the lowest, the two methods come closer to agreeing. It is possible that the microfluorescence technique may be used to measure low values of the partition coefficient. However disappointing, it is concluded that the microfluorescent technique cannot give reliable results for the partition coefficient.

This particular set of experiments does illustrate that the concentration of the fluorescent solution inside the gel bead is not directly proportional to the fluorescence intensity. This is especially important in the diffusion experiments that were discussed in section 2.3.2 making the need for the Fourier transform method all the more necessary for obtaining accurate values of the diffusion coefficient.

2.4 Results

2.4.1 Partition coefficients

The partition coefficients for the proteins at the three ionic strengths are summarized in Table 2.3. For all three proteins there was a marked decrease in Φ with decreasing ionic strength. This is the expected trend for proteins and gels of like charge, because there will be less screening of the repulsive electrostatic interactions at the lower ionic strengths.

Table 2.3 Partitioning and diffusivity of proteins in SP-Sepharose.

Protein	Ionic Strength (M)	D_∞ (10^{-7} cm^2/s)	D (10^{-7} cm^2/s)	D/D_∞	Φ
BSA	1.01	5.7 ± 0.2^a	2.7 ± 0.4^b	0.47 ± 0.07^c	0.67 ± 0.03
	0.11	5.8 ± 0.4^a	2.6 ± 0.2^b	0.45 ± 0.05^c	0.47 ± 0.01
	0.01	5.7 ± 0.2^a	2.6 ± 0.4^b	0.45 ± 0.07^c	0.29 ± 0.01
Ovalbumin	1.01	6.7 ± 0.3	3.1 ± 0.2^e	0.47 ± 0.05^f	0.64 ± 0.02
	0.11	6.8 ± 0.2^d	3.0 ± 0.2^e	0.44 ± 0.04^f	0.59 ± 0.01
	0.01	6.8 ± 0.4^d	2.8 ± 0.5	0.41 ± 0.06	0.29 ± 0.02
Lactalbumin	1.01	9.2 ± 0.5^g	4.9 ± 0.2	0.53 ± 0.09	0.78 ± 0.03
	0.11	9.3 ± 0.8^g	4.5 ± 0.2	0.49 ± 0.05	0.75 ± 0.04
	0.01	9.9 ± 0.6	3.8 ± 0.4	0.38 ± 0.04	0.44 ± 0.03

Diffusivities have been corrected to 20°C using the Stokes-Einstein equation. Values are given as mean ± SD Common superscripts indicate that quantities are not statistically different (95% confidence level).

2.4.2 Diffusivities

The free solution and gel diffusivities for each protein at the three ionic strengths are summarized in Table 2.3. There was no effect of ionic strength on D_∞ for albumin, whereas for ovalbumin and lactalbumin D_∞ exhibited slight (but statistically significant) increases at the lower ionic strengths. The maximum variation in D_∞ with ionic strength was 7%, for lactalbumin. The free solution diffusivities are compared with literature values in Table 2.4. Because the effects of ionic strength on D_∞ were minimal, the "FRAP" values in Table 2.4 were obtained by pooling all of the present data; the Stokes-Einstein radii shown in Table 2.1 were calculated from these average values of D_∞. As seen in Table 2.4, the values of D_∞ obtained here with fluorescein-labeled proteins are about 10% lower than typical values measured for unlabeled proteins using a variety of methods. It is likely that a systematic error of this magnitude could be caused by the propagation of error in the spatial frequencies caused by an error in the measurement of the pixel distance. This should not

affect the diffusivity ratio, D/D_∞, since we used the same frequencies for both the free solution and gel phase diffusion measurements.

Table 2.4 Comparison of free solution diffusivities to literature values (20°C)

Protein	D_∞ (10^{-7} cm^2/s)			
	FRAP	Literature	Literature Method*	Reference
BSA	5.7 ±0.2	5.3	Flow fractionation	Giddings et al., 1976
		5.8 ±0.1	Rayleigh light scattering	Sellen, 1973
		5.9	Hydrodynamic stability	Anderson et al., 1978
		6.0 ±0.1	QELS	Bor Fuh et al., 1993
		6.1 ±0.1	QELS	Raj and Flygare, 1974
		6.2 ±0.4	Flow fractionation	Bor Fuh et al., 1993
		6.3 ±0.1	QELS	Gaigalas et al., 1992
		6.3 ±0.1	Taylor dispersion	Walters et al., 1984
		6.4 ±0.9	FRAP	Jain et al., 1990
Ovalbumin	6.7 ±0.3	7.2 ±0.2	Taylor dispersion	Walters et al., 1984
		7.4	PFG NMR	Gibbs et al., 1991
		7.7 ±0.4	Flow fractionation	Bor Fuh et al., 1993
		7.9 ±0.2	QELS	Bor Fuh et al., 1993
Lactalbumin	9.2 ±0.5	10.6	Sedimentation-diffusion	Gordon and Semmett, 1952

*QELS =quasi-elastic light scattering; PFG = pulsed field gradient

Returning to the results in Table 2.3, for all three proteins the gel diffusion coefficients were substantially lower than the corresponding free solution diffusivities. As with D_∞, the value of D for albumin was not affected by ionic strength. The values of D for ovalbumin and lactalbumin decreased by moderate amounts at low ionic strengths, with maximum changes of 10 % and 23 %, respectively. The diffusivity ratio, D/D_∞, for all three proteins ranged from about 0.4 to 0.5, and exhibited the same trends with ionic strength as did D.

2.5 Discussion

The objective of this study was to compare the effects of electrostatic interactions on the diffusion and equilibrium partitioning of charged macromolecules in gels of like charge. The experimental design allowed both diffusivities and partition coefficients to be measured independently using identical gel beads. We are unaware of any previous data on charge effects in gels where both quantities were measured using the same test macromolecules and gels, under the same conditions. A particular advantage of the FRAP method is that direct comparisons could be made of diffusivities measured in gel beads and in the adjacent bulk solution. For the three anionic proteins (bovine serum albumin, ovalbumin, and lactalbumin) in sulfated agarose gels, there was a much stronger effect of ionic strength on the partition coefficient (Φ) than on the gel diffusivity (D), indicating that electrostatic interactions have a greater effect on partitioning. This suggests that the effects of charge on the effective diffusivity of a globular protein through a gel membrane (Φ D) will result primarily from alterations in Φ.

A consideration of length scales suggests that charge effects on Φ should be important at the lower ionic strengths studied, but probably not at the highest ionic strength. Using the distribution of spacings calculated by Ogston (1958) for a random array of fibers, we estimate that the average distance between agarose fibers in the 6% gels studied was 11 nm (see section 1.6). The Debye length, the characteristic length for electrostatic interactions in electrolyte solutions, ranged from 3 nm at 0.01 M ionic strength to 0.3 nm at 1 M. Thus, at the lowest ionic strength the Debye length was a significant fraction of the interfiber spacing, and a protein molecule located at almost any sterically allowed position in the gel should have experienced some electrostatic repulsion. In contrast, the small ratio of Debye length to interfiber spacing at 1 M should have resulted in minimal electrostatic interactions. A comparison of the measured values of Φ with those

predicted by Ogston's partitioning theory for neutral spheres in random arrays of uncharged fibers suggests that this was in fact the case. As shown in Figure 2.9, the values of Φ measured in the 1 M buffer agree well with those predicted by equation 12. As already mentioned, the Ogston theory generally agrees well with previous measurements of Φ for uncharged macromolecules in neutral agarose gels (see section 1.5.1).

For all three proteins the gel diffusion coefficient, D, was significantly reduced when compared to the free solution diffusivity, D_∞. At the highest ionic strength, the values of D/D_∞ varied little among the proteins, ranging only from 0.47 to 0.53. However, the effects of ionic strength on D or D/D_∞ varied considerably, the magnitude of the changes following the order lactalbumin > ovalbumin > albumin. Thus, the effects of ionic strength on the gel diffusivity seemed to depend inversely on the Stokes-Einstein radius of the protein. This trend may be coincidental, in that other molecular properties (e.g., shape and charge density) may also influence protein mobility within the gel phase. If it is assumed that charge effects were minimal at the highest ionic strength, then it is legitimate to compare the measured values of D/D_∞ with those predicted by equations 13 and 14. The value of κ needed in equation 14 was estimated using a correlation given by Jackson and James (1986) for the hydraulic permeability of three-dimensional arrays of fibers as previously discussed in section 1.4.2.

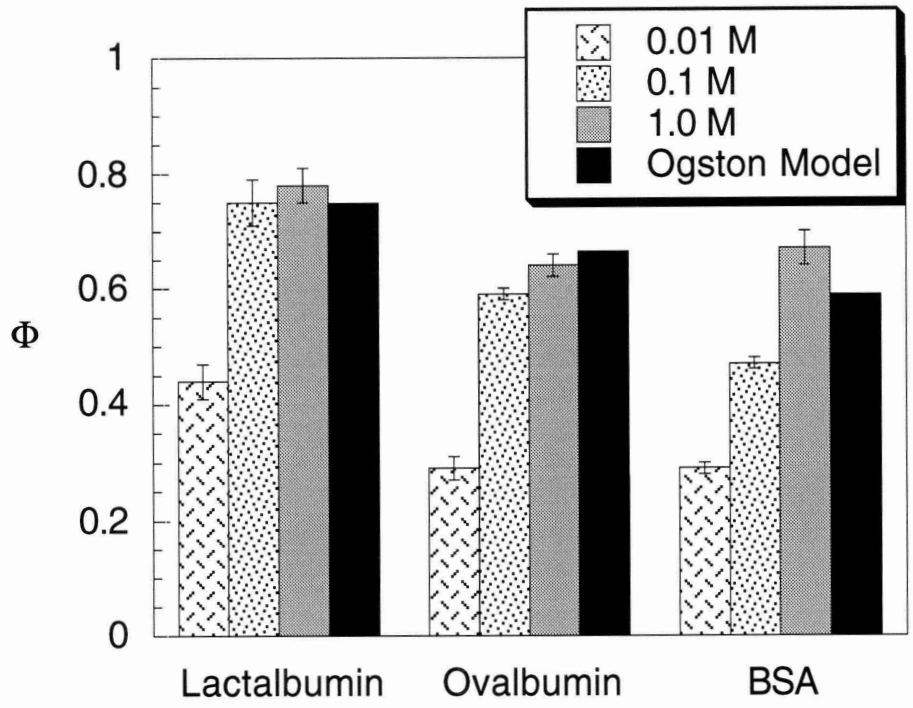

Figure 2.9 Comparison of measured values of the partition coefficient with those predicted using the theory of Ogston (1958), equation 12. The partition coefficients are shown as mean ±SD. The theory (developed for uncharged macromolecules and fibers) agrees well with the data at the highest ionic strength (1 M), where the electrostatic interactions are almost completely screened.

$$\frac{\kappa}{r_f^2} = -\frac{3}{20\phi}(\ln \phi + 0.931) \qquad (42)$$

With r_f = 1.9 nm and ϕ = 0.059 (see section 1.6), equation 42 gives κ = 17.4 nm^2. As shown in Figure 2.10, equation 13 consistently overestimated the value of D/D_∞ at 1 M, and also predicted a larger effect of molecular radius than was observed. Equation 14 gave more accurate values of D/D_∞ for these conditions, but it too predicted a greater sensitivity to molecular radius. It should be noted that the better predictions obtained with the effective medium theory may be fortuitous, in that the values of κ were estimated from equation 42, rather than being measured for our specific gels. While we do not have the Darcy permeabilities for SP-Sepharose, measurements for agarose discussed in Chapter 4 show that equation 42 does underpredict the Darcy permeability by a factor of 2 - 3. A discrepancy of this magnitude will give higher values for D/D_∞.

Equations 12-14 were intended to apply only to uncharged systems, and it is clear that addition theoretical work is needed to describe electrostatic effects on partitioning and diffusion in charged gels or other charged, fibrous media. Our finding that ionic strength tended to have a much more pronounced effect on Φ than on D/D_∞ suggests that it would be especially useful to devote attention to the effects of charge on equilibrium partitioning as is done in Chapter 3. The good agreement between the Ogston partitioning theory and data obtained when charge effects are absent suggest that the geometric model employed, consisting of randomly oriented, cylindrical fibers, may provide a good point of departure in modeling the effects of charge on Φ. Of course, more predictive theories for D/D_∞ of macromolecules in gels, both in neutral and in charged systems, are also needed as well as exact measurements for the Darcy permeability. Measurements for the permeability of agarose are presented in Chapter 4 while a more complete evaluation of equation 4 is given in Chapter 5.

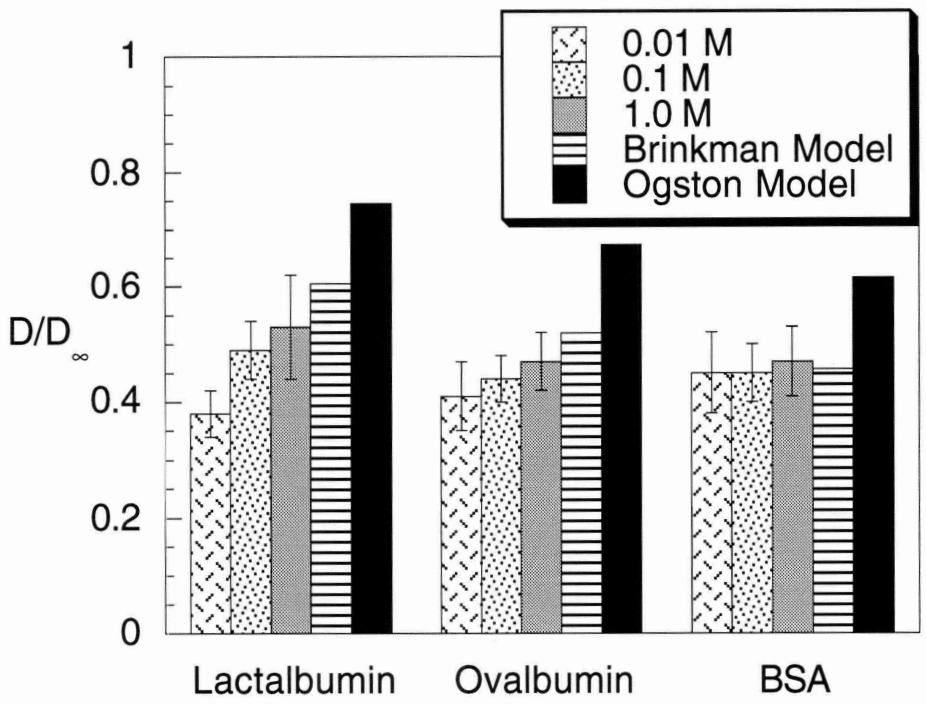

Figure 2.10 Comparison of measured values of reduced diffusivity (D/D_∞) with those predicted using equation 13 (Ogston diffusion model) and equation 14 (Brinkman model). The reduced diffusivities are shown as mean ±SD. The agreement between theory and data at 1 M is better with the Brinkman model, but both theories show greater sensitivity to molecular size than do the experimental results.

Chapter 3

3. Theory for Partitioning of Charged Spheres into Random Fiber Arrays

3.1 Introduction

The partition coefficient (Φ) of a macromolecule between a gel and free solution is the gel-to-free-solution concentration ratio at equilibrium, the concentrations being based on the total volumes of the respective phases. The partition coefficients between gels and dilute solutions are important in chromatographic and membrane separations, as well as for understanding the transport of proteins and other macromolecules through various body tissues. As previously reviewed in section 1.3.1 Ogston (1958) modeled the crosslinked polymer of a gel as a random array of straight fibers, and used geometric arguments to derive an expression for the partition coefficient under conditions where steric exclusion is the dominant factor. The result was

$$\Phi = \exp\left[-\phi\left(1+\frac{r_s}{r_f}\right)^2\right] \qquad (43)$$

where ϕ is the volume fraction of fibers, r_s is the sphere radius, and r_f is the fiber radius. This elegant result was confirmed by Fanti and Glandt (1990), who used statistical mechanical methods to extend the theory to solutions which are not infinitely dilute (i.e., including hard-sphere interactions among solutes).

For neutral agarose gels, and for charged agarose gels where the salt concentration was sufficient to completely screen electrostatic interactions, equation 43 has been found to yield excellent predictions (Laurent, 1967; Boyer and Hsu, 1992; Moussaoui et al., 1992; Johnson et al., 1995) as reviewed in section 1.5.1. However, in many systems the effects of charge on Φ are important. For example, studies using gel beads intended as chromatographic media have shown significant effects of ionic strength on Φ for various proteins (Dubin and Principi, 1989; Dubin et al., 1993; Edwards and Dubin, 1993; Schluter and Zidek, 1993; Johnson et al., 1995). As another example, ultrafiltration of macromolecules across the walls of renal glomerular capillaries has been shown to be highly dependent on molecular charge (Maddox et al., 1992), an effect which is likely to be mediated in large part by values of Φ in the glomerular basement membrane, a charged, gel-like structure.

There has been no theory to predict Φ for charged macromolecules in arrays of charged fibers. To provide an approximate theory for dilute solutions, we have extended the approach of Ogston (1958) to include charge effects. This was done by using a Boltzmann factor, containing an electrostatic free energy, to modify Ogston's expression for the probability of fitting a sphere in a space between fibers. The electrostatic free energy was calculated from solutions to the linearized Poisson-Boltzmann equation for a sphere interacting with a long cylinder, both with specified surface charge densities. Most of the computational effort was devoted to determining the electrostatic potentials, using finite element methods, because no published results were available for sphere-cylinder systems.

3.2 General Formulation for the Partition Coefficient

3.2.1 Partition coefficient

In the fiber-matrix model of Ogston (1958), which considered only steric exclusion, the partition coefficient for a dilute solution was determined from

$$\Phi = \int_0^\infty g(h)\, dh \tag{44}$$

$$g(h) = \frac{2\phi\,(h + r_s + r_f)}{r_f^2} \exp\left[-\frac{\phi\,(h + r_s + r_f)^2}{r_f^2}\right] \tag{45}$$

where the function g(h) is the probability of finding the closest fiber at a surface-to-surface distance h from the sphere. Performing the integration indicated in equation 44 leads to equation 43. As done previously in describing electrostatic effects for spheres in cylindrical pores (Smith and Deen, 1983; Brenner and Gaydos, 1977, Malone and Anderson, 1978), we introduced a Boltzmann factor which describes the relative probabilities of various energy states. Multiplying g(h) by this factor, we obtain

$$\Phi = \int_0^\infty e^{-E(h)}\, g(h)\, dh \tag{46}$$

where E(h) is the electrostatic free energy of the sphere-fiber system divided by kT, where k is Boltzmann's constant and T is absolute temperature. The energy is defined such that

$E(\infty) = 0$; that is, the energy is taken to be zero when the sphere is distant from all cylindrical fibers. It is important to note that the energy term in equation 46 accounts only for interactions between the sphere and the nearest fiber. In an exact theory for dilute solutions, the sphere would interact with multiple fibers, and E would depend on multiple position variables, not just h. The present approach is expected to be most accurate when the Debye length is much smaller than typical interfiber spacings (i.e., for high ionic strengths and/or small ϕ).

3.2.2 Electrical Potential

The first step in calculating E(h) was to solve the linearized Poisson-Boltzmann equation for a sphere-cylinder system for various combinations of parameter values. The electrical potential was scaled by RT/F, where R is the gas constant and F is Faraday's constant, yielding a dimensionless potential denoted by Ψ. The position coordinates were made dimensionless using the sphere radius r_s. Thus, the linearized Poisson-Boltzmann equation was written as

$$\nabla^2\Psi = \tau^2\Psi \tag{47}$$

$$\tau = r_s\kappa = r_s\left(\frac{F}{\varepsilon RT}\sum_i z_i^2 C_{i\infty}\right)^{1/2} \tag{48}$$

The parameter τ is the ratio of the sphere radius to the Debye length (κ^{-1}), $C_{i\infty}$ and z_i are the free solution concentration and valence, respectively, of electrolyte species i, and ε is the dielectric permittivity of the solvent. The dielectric permittivity is the relative dielectric constant multiplied by ε_o, the permittivity of vacuum ($\varepsilon_o = 8.8542 \times 10\text{-}12$ C V^{-1} m^{-1}).

The boundary conditions were written in terms of a dimensionless separation distance (η), fiber radius (β), sphere surface charge density (σ_s), and fiber surface charge density (σ_f). These quantities were defined as

$$\eta = h\kappa, \quad \beta = \frac{r_f}{r_s}, \quad \sigma_s = \frac{r_s F}{\varepsilon RT} q_s, \quad \sigma_f = \frac{r_s F}{\varepsilon RT} q_f, \tag{49}$$

where q_f and q_s are the dimensional surface charge densities. Assuming that the dielectric constant of the solvent greatly exceeds that of the sphere or fiber (a good approximation for most organic materials in water), the constant-charge boundary conditions are

$$\frac{\partial \Psi}{\partial \rho} = \sigma_s \quad \text{at} \quad \rho = 1 \tag{50}$$

$$\frac{\partial \Psi}{\partial r} = \sigma_f \quad \text{at} \quad r = \beta \tag{51}$$

where ρ is radial position in a spherical coordinate system centered at the sphere and r is radial position in a cylindrical coordinate system centered at the fiber. Far from the sphere and the fiber, the potential was taken to be zero. An examination of equations 47 - 51 indicates that the dimensionless potential depends on five parameters, in addition to position; that is, $\Psi = \Psi(\mathbf{x}; \eta, \tau, \beta, \sigma_s, \sigma_f)$, where $\mathbf{x}$ is a dimensionless position vector.

3.2.3 Free Energy and Interaction Potential Energy

The change in free energy due to the interaction between the sphere and fiber is expressed as

$$\Delta G = G_{sf} - G_s - G_f \qquad (52)$$

where the subscripts s, f, and sf refer to the isolated sphere, isolated fiber, and combined sphere-fiber system, respectively. Each of the G terms has been made dimensionless using an electrostatic energy scale, given by $(RT/F)^2 \varepsilon r_s$. As shown by Verwey and Overbeek (1948), the free energy for a system governed by the linear Poisson-Boltzmann equation is evaluated by integrating the potential over the charged surface(s),

$$G = \frac{\sigma}{2} \int_A \Psi(\sigma)\, dA \qquad (53)$$

For the calculation of G_s, G_f, and G_{sf}, the dimensionless area A (scaled by r_s^2) is that of the sphere, the fiber, or the sum of the two, respectively. Thus, the change in free energy is calculated as

$$\Delta G(\eta, \tau, \beta, \sigma_s, \sigma_f) = \frac{\sigma_s}{2} \int_{A_s} (\Psi - \Psi_\infty)\, dA_s + \frac{\sigma_f}{2} \int_{A_f} (\Psi - \Psi_\infty)\, dA_f \qquad (54)$$

where A_s and A_f are the surface areas of the sphere and fiber, respectively. The respective surface potentials evaluated at infinite separation, denoted as Ψ_∞, are given by

$$\Psi_\infty = \frac{\sigma_s}{1+\tau} \quad \text{(sphere)} \tag{55}$$

$$\Psi_\infty = \frac{\sigma_f \, K_0(\tau\beta)}{\tau \, K_1(\tau\beta)} \quad \text{(fiber)} \tag{56}$$

where K_0 and K_1 are modified Bessel functions. The energy needed in equation 46 is obtained by multiplying ΔG by the ratio of the electrostatic and thermal energy scales:

$$E = \frac{(RT/F)^2 \varepsilon \, r_s}{kT} \Delta G \tag{57}$$

For water at 20°C and r_s varying from 1 to 10 nm, $E/\Delta G$ varies from 0.11 to 1.1.

3.3 Numerical Calcuations for the Change in Free Energy

3.3.1 Finite Element Mesh Development

The linearized Poisson-Boltzmann equation was solved using a Galerkin finite element method (FIDAP, Fluid Dynamics, Evanston, IL) on a Cray X-MP supercomputer. The three-dimensional domain was divided into brick-type elements, and quadratic basis functions were used to approximate the potential field. Because there were two planes of symmetry, solutions were obtained for only one-quarter each of the sphere and cylinder.

The half-length of the cylinder was set at 5 times the sphere radius, which was found to be sufficient to give negligible truncation error in evaluating the integral over A_f in equation 54. The mesh was refined close to the cylinder and sphere surfaces, where the potential gradients were highest. A typical mesh is illustrated in Figure 3.1(a), which is a view perpendicular to the axis of the cylindrical fiber. An example of an electrostatic potential field is shown in Figure 3.1(b), which is a similar view containing isopotential lines. To calculate ΔG, the average surface potentials on the cylinder and the sphere were needed. The potentials at the surface nodes were obtained from the FIDAP output file and integrated over the surfaces using Romberg integration (Press et al., 1992) with a fractional tolerance of 1×10^{-6}. The potential field was calculated for two numbers of nodes at each set of conditions, and Richardson extrapolation was used to find ΔG. For this purpose the number of elements was increased uniformly throughout the mesh, from 972 to 2304. The exact free energy calculations for each value of τ, β, η, σ_s, and σ_c are given in Appendix A.1.

3.3.2 Solution Convergence and Error Estimates

For solutions of Laplace's equation with quadratic basis functions on a two-dimensional grid of $N \times N$ elements, the error in the field variable is expected to vary as N^{-3} (Finlayson, 1980). Similar rates of convergence are expected for the present problem, if N is taken to be the cube root of the total number of elements. The error in ΔG should be similar to that in Ψ, so that we expect the error in ΔG to vary as N^{-3}. An example of the actual rate of convergence is shown in Figure 3.2. The "exact" value for ΔG was estimated by extrapolation from the last two points, using the theoretical slope of -3. The actual slope in this representative case, based on all points shown, was calculated to be -3.08. Because the relative sizes of the elements were forced to change as h was varied, the extrapolation was checked at selected values of h by performing calculations at a third

(a)

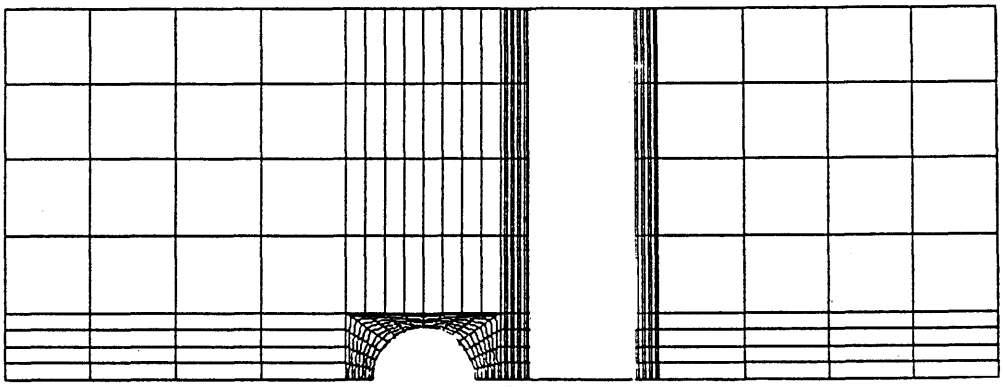

(b)

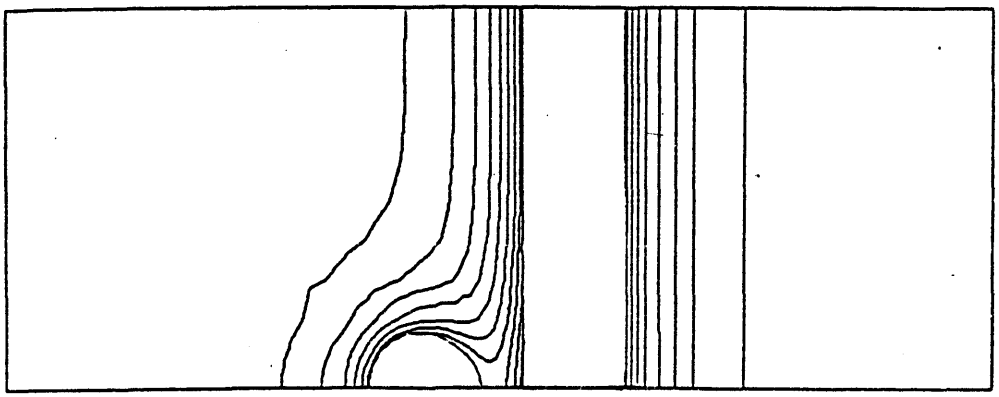

Figure 3.1 (a) The finite element mesh for τ=1, β=1, and η=1 viewed in a plane which includes the center of the sphere and the axis of the fiber. The full three dimensional mesh contains 20,961 nodes. (b) Electrostatic potential field for the same view as shown in (a). Isopotential lines are are evenly spaced between $\Psi = 0$ and 0.87.

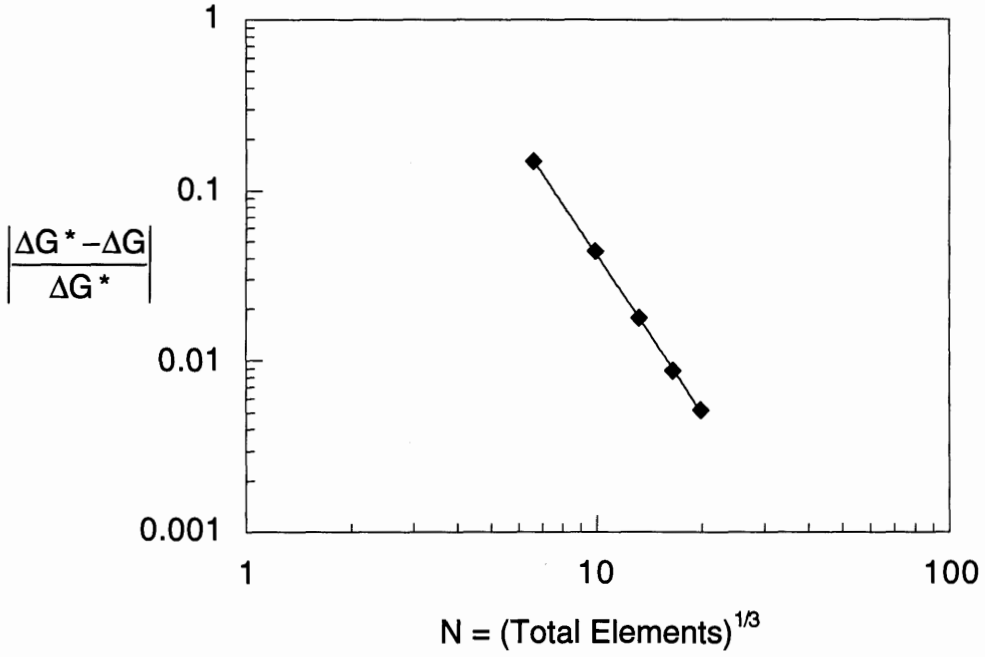

Figure 3.2 Convergence of the electrostatic free energy with increasing numbers of elements. The abscissa (N) is the cube root of the total number of elements and ΔG^* is the best estimate of DG. Richardson extrapolation was used to calculate ΔG^*, based on the theoretical slope of -3 and the results for the two largest numbers of elements. The slope calculated form all of the points was -3.08, in excellent agreement with the theoretical slope. These calculations were for τ=1, β=1, and η=0.5.

(higher) number of elements (4500). The extrapolated value of ΔG differed from these refined values by <2%. The maximum deviations occurred at the largest values of η, where the elements were stretched over the greatest distance and the potentials were the lowest.

3.3.3 Correlation of Interaction Energy Results

The linearity of the governing equations implies that the surface potentials are linear functions of the charge densities. It follows from equation 54 that ΔG has a quadratic dependence on σ_s and σ_f, which we write as

$$\Delta G(\eta,\tau,\beta,\sigma_s,\sigma_f) = A_1(\eta,\tau,\beta)\,\sigma_s\sigma_f + A_2(\eta,\tau,\beta)\,\sigma_s^2 + A_3(\eta,\tau,\beta)\,\sigma_f^2 \quad (58)$$

To evaluate the coefficients $A_i(\eta,\tau,\beta)$ in equation 58, results for ΔG were obtained for 950 sets of parameter values, with $0.125 < \eta < 3.0$, $0.33 < \tau < 10$, $0.25 < \beta < 2.0$, and $0.06 < \sigma_s/\sigma_f < 8.0$. For each set of η, τ, and β the values of A_i were computed by nonlinear regression of $\Delta G/(\sigma_s\,\sigma_f)$ vs. σ_s/σ_f. Each of the A_i coefficients was found to be positive for all conditions. To put the results in a convenient form, these "exact" values for A_i were fitted using empirical correlations, as described below.

To determine suitable functionalities for $A_i(\eta,\tau,\beta)$, we examined an analytical expression for the free energy of two unlike spheres (Ohshima, 1995) and numerical results for the case of a sphere close to a flat plate (Grant and Saville, 1995), both with constant surface charge densities. For two spheres the free energy remains finite at contact ($\eta = 0$), and in the limit of small η (and large τ) the coefficients A_i decrease exponentially with η. The two dominant terms in the free energy expression for a sphere near a charged

plate (eq. 31 in Grant and Saville, 1995) also decay exponentially with η. To see if an exponential decay in η was approximately correct for the present problem, we first fitted the dependence of free energy on η by assuming that

$$A_i(\eta,\tau,\beta) = u_i(\tau,\beta)\exp\left[-v_i(\tau,\beta)\,\eta\right] \qquad (59)$$

For any given combination of τ and β, equation 59 was used to fit the results obtained for each A_i at 38 values of η, thereby yielding a pair of values for u_i and v_i. This was done for each of 25 combinations of τ and β and the values for u_i and v_i are shown in Table 3.1. Three measurements of the error in the curvefit are also shown in Table 3.1; RMS is the root mean square of the fractional residual error (the number of data points used in the mean was decreased by the number of parameters used in the curve fit); <res> is the average absolute fractional residual error and χ^2 is the sum of the square of the fractional residual errors. The fortran program, curvefitter.f, used to determine the curve fit parameters is found in the appendix in section A.4. The average absolute residual (<res>) obtained with equation 59 for any individual case was typically < 5%. Thus, the exponential decay in η was found to be an excellent approximation. One extreme combination of parameter values, $\tau = 10$ and $\beta = 2$, was exceptional in that the average residual was 17%. Because of its relatively poor fit to equation 59, this one combination of τ and β was excluded in developing the overall correlation discussed below. This reduces the number of total data points from 950 to 912. Caution should be used in using the curve fits for this combination of τ and β.

Table 3.1 Constants for equation 59 for each β and τ.

β	$1/\tau$	u_1	v_1	u_2	v_2	u_3	v_3	RMS	<res>	χ^2
0.25	0.1	0.0475	1.1033	0.0141	2.7545	0.0158	3.0499	3.7%	2.6%	0.04
0.25	0.5	0.5813	1.1262	0.0911	3.1007	0.0931	3.1818	1.5%	1.1%	0.01
0.25	1.0	1.2952	1.1876	0.1117	3.7419	0.1428	4.4219	2.5%	1.6%	0.02
0.25	2.0	2.2723	1.2242	0.1875	4.2671	0.2120	5.6344	3.5%	2.6%	0.04
0.25	3.0	2.7326	1.1505	0.2576	3.2565	0.3163	5.7450	8.1%	5.5%	0.21
0.5	0.1	0.0670	1.0447	0.0238	2.8340	0.0244	3.0678	3.6%	2.6%	0.04
0.5	0.5	0.9096	1.1168	0.1866	2.9437	0.1820	3.1940	1.8%	1.4%	0.01
0.5	1	2.1418	1.1735	0.2899	3.3866	0.2948	3.8764	2.0%	1.3%	0.01
0.5	2	3.9683	1.2009	0.4508	3.6326	0.4575	5.1487	3.6%	2.6%	0.04
0.5	3	5.7054	1.2873	0.0743	0.0000	0.5247	6.7399	6.0%	4.3%	0.11
0.75	0.1	0.0780	1.0471	0.0298	2.9066	0.0299	2.9889	3.3%	2.5%	0.04
0.75	0.5	1.1482	1.1153	0.2504	2.8376	0.2386	3.2553	3.3%	2.0%	0.03
0.75	1	2.7325	1.1526	0.4330	3.0478	0.4209	3.7964	1.9%	1.4%	0.01
0.75	2	5.1897	1.1697	0.6178	2.6660	0.6819	4.8106	7.8%	3.8%	0.19
0.75	3	8.2907	1.3253	0.1665	0.0000	1.6716	14.6835	7.3%	4.9%	0.17
1	0.1	0.0873	1.0561	0.0337	2.9894	0.0333	3.0800	3.4%	2.3%	0.04
1	0.5	1.3100	1.1080	0.2926	2.6451	0.2823	3.2916	6.6%	2.8%	0.14
1	1	3.2424	1.1628	0.5519	2.9603	0.4847	3.5949	5.6%	2.5%	0.10
1	2	6.2752	1.1610	0.7819	2.3617	0.8359	4.7056	4.7%	3.2%	0.07
1	3	10.1438	1.3159	0.3451	0.0852	1.6558	12.5736	6.9%	4.7%	0.15
2	0.1	0.1985	2.9622	0.0591	2.7277	0.0428	2.6608	61.3%	16.7%	12.0
2	0.5	1.5893	1.0588	0.4169	2.4463	0.3954	3.2296	3.2%	2.1%	0.03
2	1	4.2636	1.1122	0.8284	2.4341	0.7163	3.5769	2.9%	1.8%	0.03
2	2	8.8758	1.0978	1.0197	1.0850	1.3088	4.5168	7.3%	5.2%	0.17
2	3	15.1468	1.2701	1.6207	0.0957	1.4095	7.5426	5.3%	3.6%	0.09

The aforementioned results for related double-layer problems do not suggest any simple functional forms to use in expressing the dependence of A_i on τ and β. To obtain an overall correlation for the free-energy data, we assumed a power-law dependence for u_i and forced v_i to remain constant. Thus, the coefficients in equation 58 were expressed as

$$A_i(\eta,\tau,\beta) = a_i \tau^{b_i} \beta^{c_i} \exp(-d_i \eta) \qquad \textbf{(60)}$$

The values of the 12 constants (a_i, b_i, c_i, and d_i for i = 1 to 3) obtained from a least-squares fit to a total of 912 data points are shown in Table 3.2. The average absolute residual was 18.5 %. It was found that equation 60 provided a good compromise between accuracy and convenience. Although the 24 individual fits using equation 59 yielded smaller average residuals, those fits involved a total of 144 discrete values of u_i and v_i, and their routine use would require numerical interpolation of u_i and v_i in both τ and β. As will be shown in section 3.4, partition coefficients computed using equation 60 did not differ appreciably from those computed using equation 59.

The "cross" term in equation 58, $A_1\sigma_s\sigma_f$, expresses the major part of the screened repulsion or attraction between a charged sphere and a charged fiber. The terms involving σ_s^2 and σ_f^2 represent the smaller effects which remain when only one of the two objects is charged. Even if one object is uncharged, its low dielectric constant distorts the potential field in the vicinity of the charged object and thereby increases the electrostatic free energy. The relative magnitudes of the three coefficients are illustrated for a typical case in Figure 3.3. It is seen here that A_2 and A_3 are small relative to A_1, declining from a maximum of 17% of A_1 at contact to <5% for $\eta > 0.5$. Thus, although there will be some effects of charge on the partition coefficient when only one object is charged, those effects will tend to be minor compared to those present when the sphere and fiber are both charged.

Table 3.2 Constants for use in free energy correlation (equation 60)

Index (i)	a_i	b_i	c_i	d_i
1	2.3523	0.7599	1.2472	1.0956
2	0.3570	0.5052	0.9512	3.7684
3	0.4473	0.9310	1.1512	2.4987

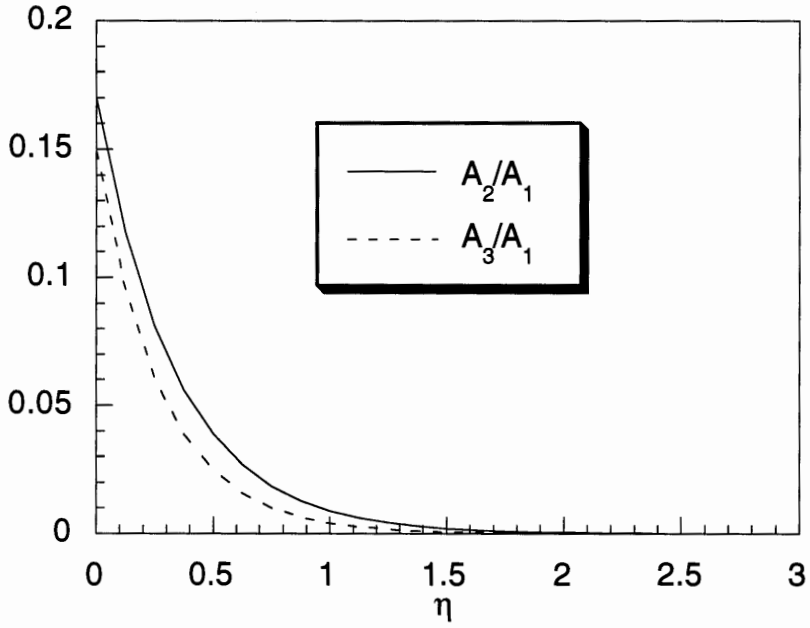

Figure 3.3 Relative magnitudes of the coefficients in the free energy correlation (equation 58), for τ=1 and β=1.

3.4 Partitioning Predictions

Partition coefficients were evaluated by numerical integration of equation 46 using a Fortran routine for Romberg integration (Press et al., 1992). To investigate the errors in Φ which might arise from the empirical correlations used to evaluate ΔG, results obtained using equation 59 and 60 were compared. These comparisons were made for each of the 24 combinations of τ and β, at two ionic strengths and two volume fractions of fibers. As shown in Figure 3.4, the two sets of results were virtually identical, the average difference being $< 2\%$. Because the results obtained with equation 59 should have negligible error, their agreement with those from equation 60 validates the use of the latter, more approximate correlation for this purpose. All other results presented here for Φ are based on equation 60. It should be noted that because values of ΔG were computed only for $0.125 < \eta < 3.0$, evaluation of the integral in equation 46 requires extrapolation of the results to smaller and larger η. However, the nearly exponential decay of A_i with η should make extrapolation errors minimal. Where the percentage errors in ΔG are likely to be greatest, at large η, the absolute values of ΔG are small and the Boltzmann factor in equation 46 is very close to unity.

Figures 3.5-3.8 show a sampling of results for Φ obtained for spheres and fibers of like charge. The results calculated for neutral spheres and fibers using equation 43, the expression derived by Ogston, are included for comparison. As shown in Figure 3.5, repulsive interactions can cause Φ to decline much more rapidly with increasing sphere radius (r_s) than for the uncharged case. The effects of charge are greatest, of course, at the lowest ionic strength. Figure 3.6 shows that the decline in Φ with increasing volume fraction of the fibers (ϕ) is also magnified by repulsive charge interactions. The effects of variations in the surface charge density of the sphere are shown in Figure 3.7. Increasing the sphere charge at a fixed Debye length has the same qualitative effect as increasing the Debye length (decreasing the ionic strength) at a fixed charge density. A plot like

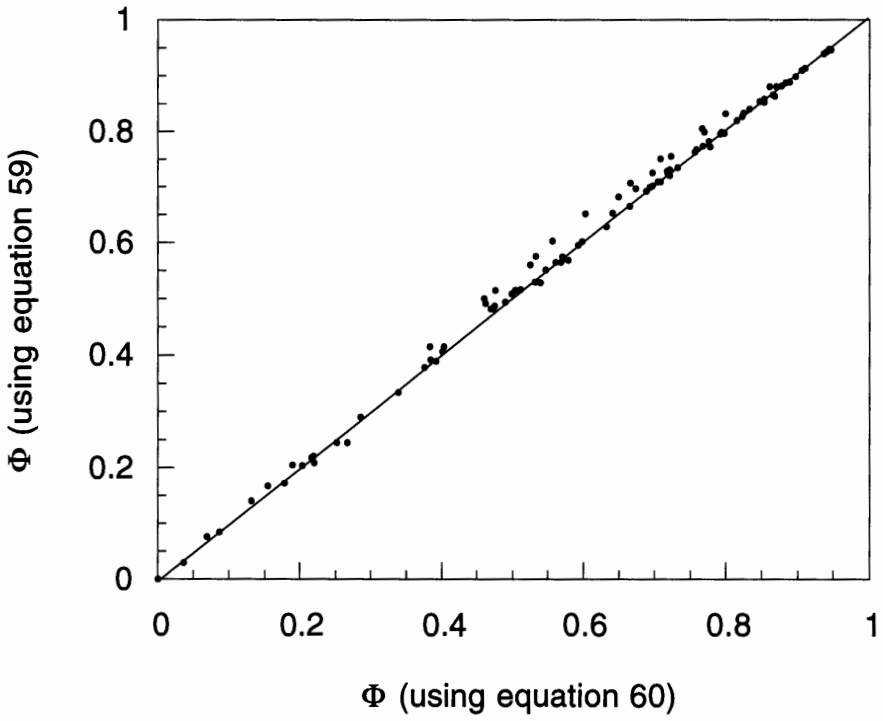

Figure 3.4 Comparison of partition coefficients (Φ) calculated using the free energy correlatins given by equations 59 and 60. The results are for 24 combinations of τ and β, each for ϕ=0.02 and 0.06 and for ionic strengths of 0.01 M and 0.05 M. Because the errors in equation 59 are small (generally < 5%), the corresponding values of Φ should be virtually exact. The agreement between the partition coefficients calculated using the two equations validates the use of the more approximate correlation (equation 60), in computing Φ.

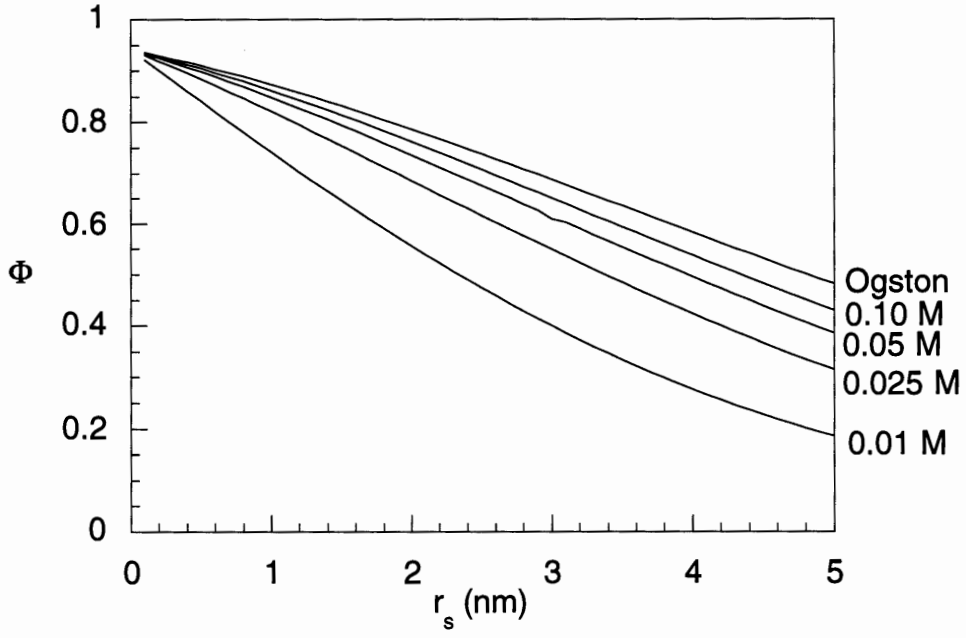

Figure 3.5 Partition coefficient (Φ) as a function of the sphere radius (r_s) and the ionic strength, for spheres and fibers of like charge. The results are for $\phi = 0.06$, $r_f = 2.0$ nm, and $q_s = q_f = -0.01$ C/m^2. Results from the Ogston expression for uncharged systems (equation 43), are also shown. Repulsive charge interactions reduce Φ, and make it more sensitive to r_s.

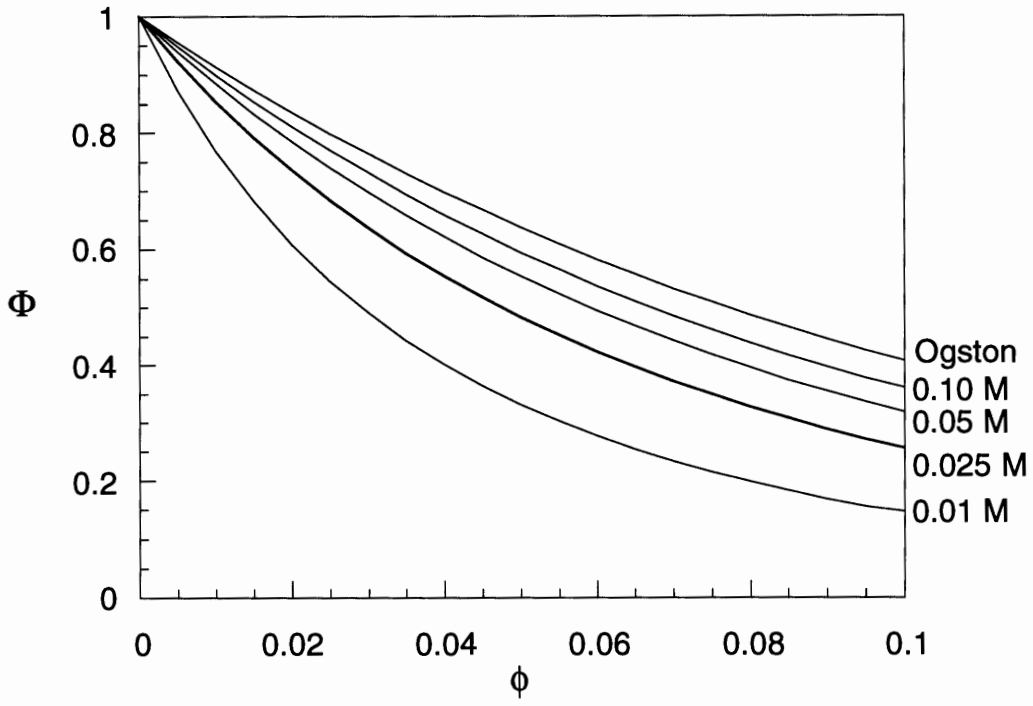

Figure 3.6 Partition coefficient (Φ) as a function of the volume fraction of fibers (ϕ) and the ionic strength, for spheres and fibers of like charge. The results are for r_s = 4.0 nm, r_f = 2.0 nm, and $q_s = q_f$ = -0.01 C/m^2. Results from the Ogston expression for uncharged systems (equation 43), are also shown. Repulsive charge interactions reduce Φ, and make it more sensitive to ϕ.

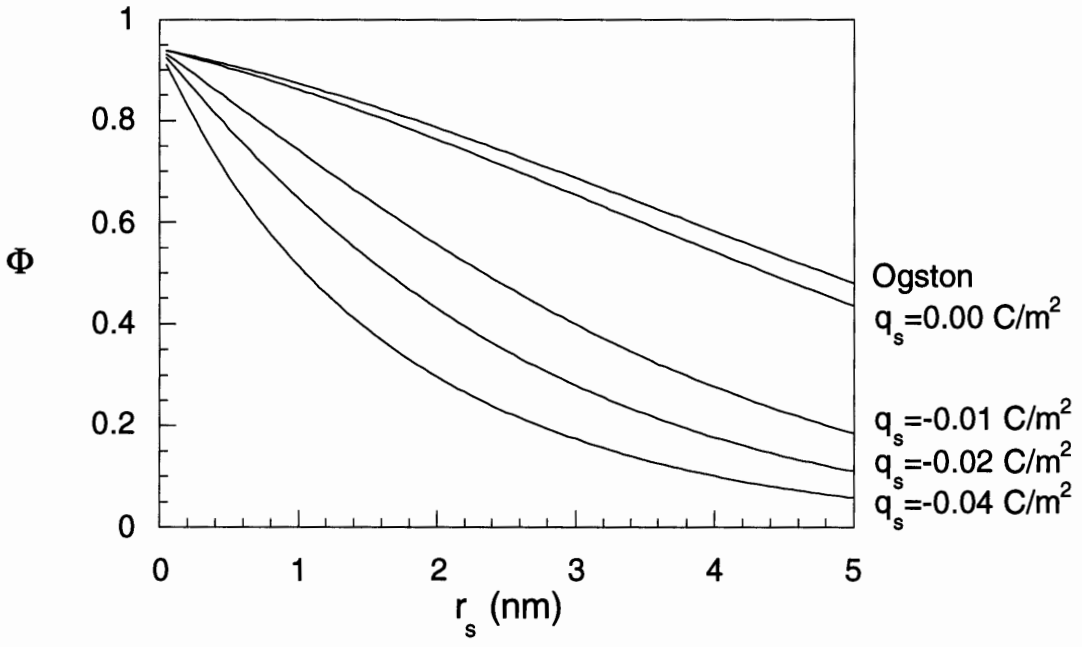

Figure 3.7 Partition coefficient (Φ) as a function of the sphere radius (r_s) and the sphere surface charge density (q_s), for spheres and fibers of like charge. The results are for ϕ = 0.06, r_f = 2.0 nm, ionic strength = 0.01 M, and q_f = -0.01 C/m^2. Results from the Ogston expression for uncharged systems (equation 43), are also shown. Repulsive charge interactions reduce Φ, and make it more sensitive to r_s.

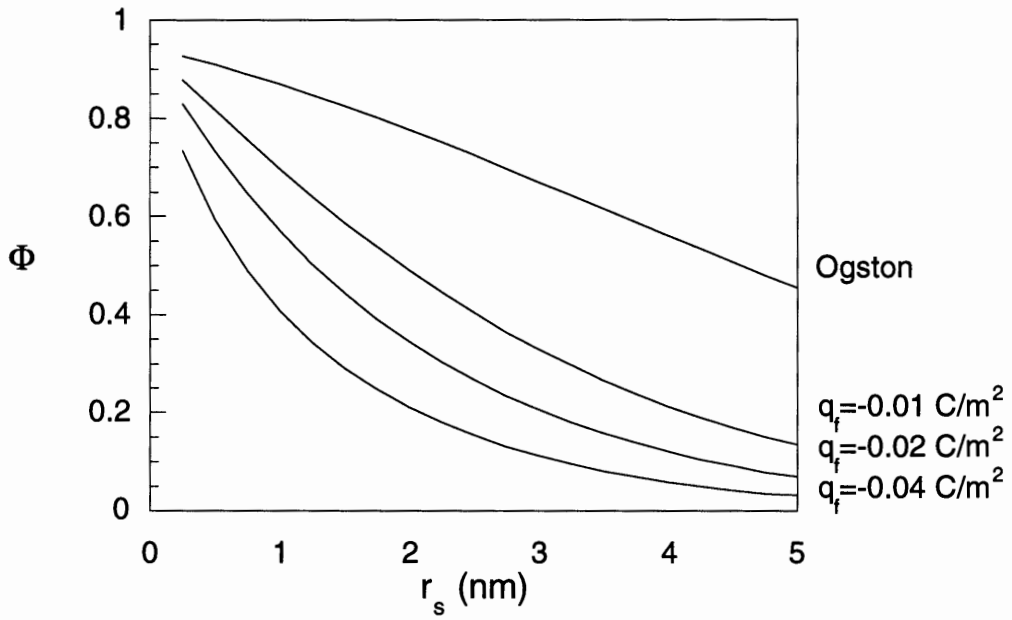

Figure 3.8 Partition coefficient (Φ) as a function of the sphere radius (r_s) and the fiber surface charge density (q_f), for spheres and fibers of like charge. The results are for ϕ = 0.06, r_f = 1.9 nm, ionic strength = 0.01 M, and q_s = -0.01 C/m^2. Results from the Ogston expression for uncharged systems (equation 43), are also shown. Repulsive charge interactions reduce Φ, and make it more sensitive to r_s.

Figure 3.7, but with fiber charge varied as a parameter instead of sphere charge, gives results which are nearly superimposable as shown in Figure 3.8. This is related to the fact that the cross term in equation 58 tends to make the dominant contribution to the electrostatic free energy. Consequently, variations in σ_f have almost the same effect as equivalent variations in σ_s.

Figure 3.9 shows results for spheres and fibers of unlike charge. In this case there is a competition between electrostatic attraction and steric exclusion. For small r_s the charge effects dominate, so that Φ tends to increase with r_s, reaching values greater than unity when the surface charge densities are sufficiently large. There is an initial increase in Φ with r_s because, with surface charge densities held constant, there is an increase in total sphere charge. Eventually, though, Φ declines with increasing r_s as the steric effects become more prominent.

3.5 Discussion

We have presented a theory for predicting the effects of electrostatic interactions on the equilibrium partitioning of spherical macromolecules in random fiber arrays. There has been recent interest in using electrostatic repulsion to enhance the chromatographic separation of molecules of similar size but differing charge densities (Edwards and Dubin, 1993; Garcia et al., 1994). Most or all of the physical parameters in this model can be evaluated independently using light scattering, titration, or other measurements, so that the theory should be useful in identifying advantageous combinations of operating variables such as pH and ionic strength. The model should also provide insight into the charge-selective characteristics of biological barriers, such as the glomerular basement membrane (Maddox et al., 1992).

The theory presented here should be most accurate for low fiber volume fractions, moderate to high ionic strengths, and low surface charge densities. The restrictions on

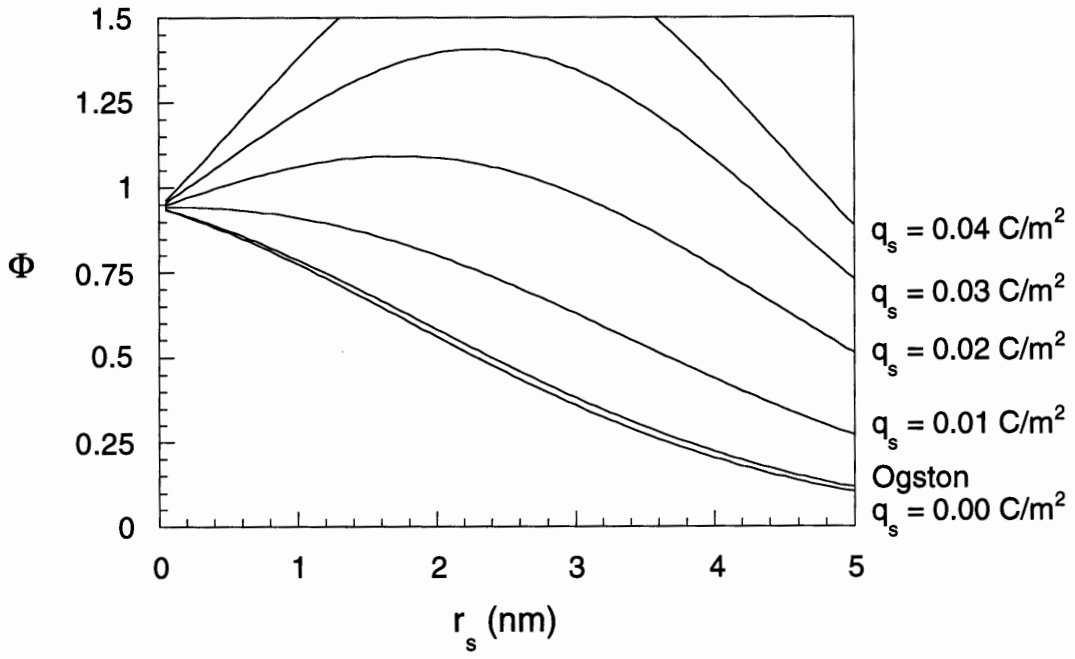

Figure 3.9 Partition coefficient (Φ) as a function of the sphere radius (r_s) and the sphere surface charge density (q_s), for spheres and fibers of unlike charge. The results are for ϕ = 0.06, r_f = 1.0 nm, ionic strength = 0.01 M, and q_f = -0.01 C/m^2. Results from the Ogston expression for uncharged systems (equation 43), are also shown. Attractive charge interactions increase Φ.

fiber volume fraction and ionic strength are due to the fact that the only electrostatic interactions considered are those between the spherical macromolecule and the nearest fiber. At fiber volume fractions and ionic strengths such that the average distance between the fibers is comparable to the Debye length, the electrostatic free energy will be influenced by simultaneous interactions between the sphere and two or more fibers, not just the nearest neighbor. For spheres and fibers of like charge, we expect that interactions with additional fibers will tend to increase the free energy, so that the present model will tend to overestimate Φ (i.e., underestimate the extent to which Φ is reduced below its purely steric value). The restriction to low surface charge densities is due to the well-known limitations of the linearized Poisson-Boltzmann equation. Although derived by assuming that electrostatic potentials are $<<$ RT/F ($\cong$ 25 mV at room temperature), errors in using the linearized Poisson-Boltzmann equation are usually minimal when potentials are $<$ 2-4 RT/F (Hunter, 1986). The corresponding limits for the surface charge densities will depend on the ionic strength; the maximum acceptable values of the sphere and fiber charge densities can be estimated using equations 55 and 56, respectively. Given a high surface charge density (such that potentials exceed 4 RT/F), the linearized Poisson-Boltzmann equation will predict a higher value for the surface potential on a flat plate than will the non-linear form of the equation. Assuming that a similar relationship will hold for the potential field around a proximate sphere and cylinder, at high surface charge densities the linearized Poisson-Boltzmann equation would overestimate the energy of interaction for like charges, and thereby underestimate Φ. In that the effects of multiple-fiber interactions and linearization of the Poisson-Boltzmann equation tend to be in opposite directions, there may be some cancellation of errors in applying the model to real systems.

We have previously reported measurements of Φ for globular proteins in highly sulfated agarose gels (SP-Sepharose), at various ionic strengths (Johnson et al., 1995). Using titration data provided by the manufacturer of these gel beads (Pharmacia), we estimate a fiber surface charge density of 0.42 C/m^2. At an ionic strength of 0.01 M, this

surface charge density gives an electrostatic potential of 38 RT/F for an isolated fiber, which far exceeds the limits for the linearized Poisson-Boltzmann equation. Of course, this isolated cylinder surface potential was calcuated using equation 56, which uses the linearized Poisson-Boltzmann equation to determine the relationship between the surface charge density and the surface potential. At these high potentials, though, the linearized Poisson-Boltzmann equation is invalid so the value of 38 RT/F should not be taken as an exact value but only as an indication that this surface charge density will result in potential fields that are out of range of the linearized Poisson-Boltzmann equation. Thus, we have not attempted to compare the theory with that set of data. However, the conditions employed by Edwards and Dubin (1993) to study the partitioning of bovine serum albumin (BSA) and β-lactoglobulin in a 6% agarose gel (Superose 6) appear to be within the limitations of the theory. Those authors used buffer solutions at pH 7.0 and ionic strengths of 0.02 M and 0.04 M. The average fiber spacing in a 6% agarose gel is approximately 11 nm (Johnson et al., 1995), which greatly exceeds the maximum Debye length of 2.2 nm (at 0.02 M). Moreover, the surface potentials of isolated proteins and fibers calculated from titration data (see below) are < 1.4 RT/F.

To compare the theory with the data of Edwards and Dubin (1993), all of the physical parameters were estimated from independent measurements. As discussed previously in section 1.6 we estimate that for a 6% agarose gel the volume fraction of fibers is 0.059 and the average fiber radius is 1.9 nm. Titration data for Superose 12 (a similar gel with a higher agarose concentration) showed that at pH 7.0 the surface charge density was -0.011 C/m2 (Dubin, personal communication). The net charge on BSA and β-lactoglobulin was determined from titration data to be -21 (Tanford et al., 1955) and -13 (Cannan et al., 1942), respectively. The surface charge densities of BSA and β-lactoglobulin were then calculated to be -0.022 C/m2 and -0.018 C/m2, respectively, assuming the molecular radii to be 3.5 nm (Johnson et al.,1995) and 2.9 nm (Cannan et al., 1942). A comparison between the predicted and measured partition coefficients is

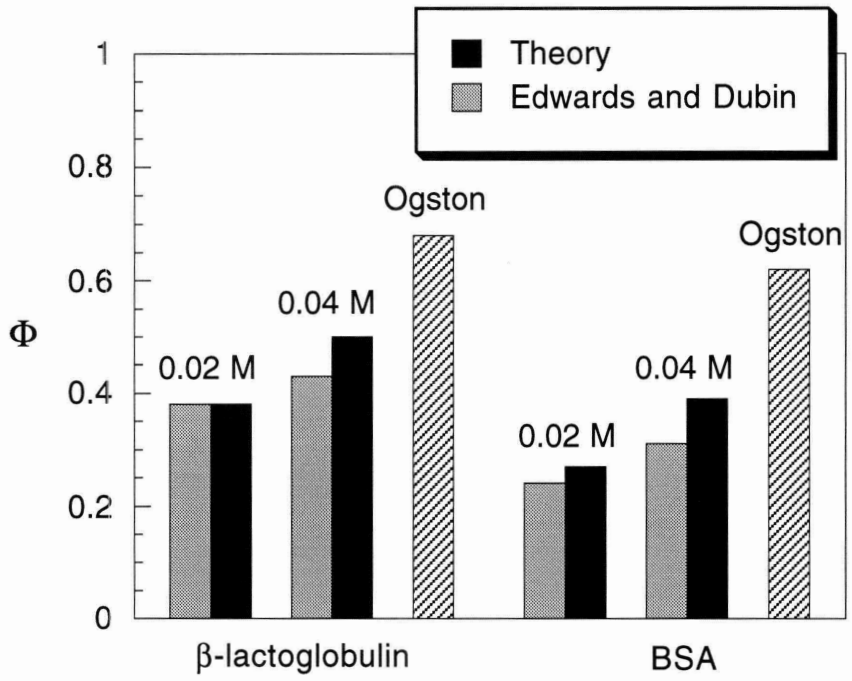

Figure 3.10 Comparison of theoretical predictions for the partition coefficient (Φ) with the experimental data of Edwards and Dubin (1993) for two negatively charged proteins in a negatively charged gel (Superose 6). The predictions and data are in good agreement at both ionic strengths studied, 0.02 M and 0.04 M. Theoretical predictions based on the Ogston expression for uncharged systems (equation 43) are also shown. The values of the various input parameters used in the theories are given in the text.

shown in Figure 3.10. For both proteins there was a clear tendency for Φ to increase with ionic strength, and the model predicted the extent of those increases quite well. The strength of the electrostatic interactions is shown by a comparison with the theoretical predictions shown for uncharged systems.

Two methods which have been proposed to approximate the energy of interaction are a linear superposition of the electrostatic fields, which has been argued to be valid at large separations, and the Deryaguin approximation, which is only valid for short separations and small Debye lengths (Glendinning and Russel, 1983). If it were sufficiently accurate, linear superposition (i.e., adding the potentials obtained for two isolated objects) would be very attractive for the present geometry because it would avoid the need for a finite element (or other numerical) solution for the potential field; however, the integrals in equations 54 and 46 would still need to be evaluated numerically. We tested linear superposition for a number of conditions, and found that for like charges it consistently underestimated the free energy. As shown for a representative case in Figure 3.9, the linear superposition of potentials gave a value for ΔG which was too low at all separation distances. Moreover, the two curves converged very slowly (if at all) at large η, so that extrapolation of our results using equation 60 was preferable to linear superposition even at large separation distances. The Deryaguin approximation has been used with some success for short separation distances between spheres with constant surface potentials, but as Glendinning and Russel (1983) showed it is unlikely to work well for any system with constant surface charge densities.

Although many proteins are compact enough to resemble spheres, their charged groups may not be uniformly distributed over their surface, as assumed here. Calculations by Grant and Saville (1995) for a nonunifomly charged sphere interacting with a charged surface show that charge heterogeneity can have a dramatic effect on the interaction energy. To incorporate a nonuniform sphere charge in the present theory would require an averaging of energies over all possible sphere orientations relative to the fiber. At least as

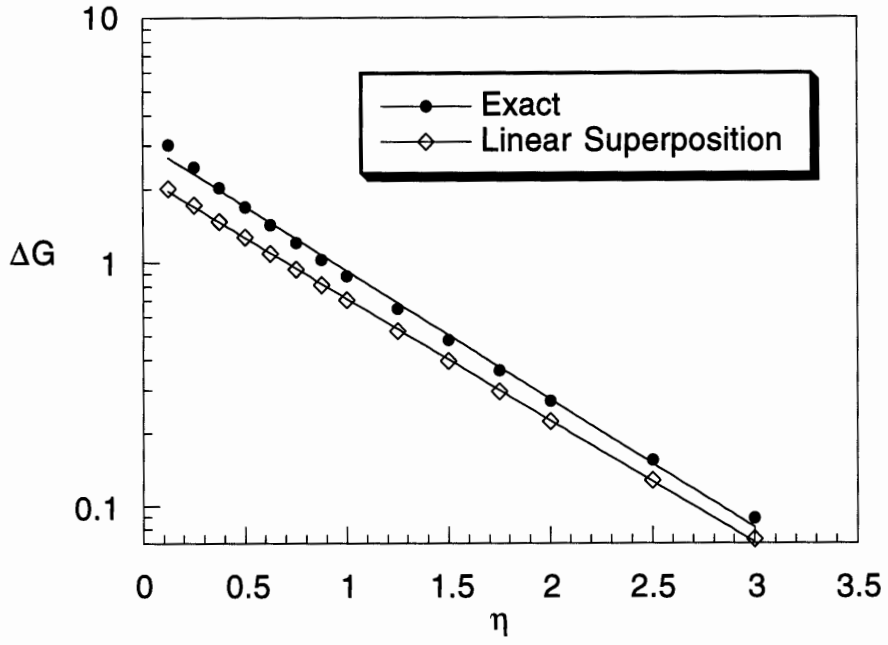

Figure 3.11 Comparison of the "exact" free energy form the finite element solution with that obtained from linear superposition of the potential fields, as a function of the dimensionless separation distance (η). The slopes for the exact and superpositon results are = -1.21 and -1.15, respectively, indicating that the convergence between the two methods is extremely slow. These calculations were for $\tau = 1$, $\beta = 1$ and $\sigma_s = \sigma_f = 1$.

challenging to develop would be a theory for the partitioning of linear polyelectrolytes in gels. One motivation for such a theory derives from interest in separating polyelectrolytes using ion-exclusion chromatography (Dubin and Tecklenburg, 1985, Dubin et al., 1990; Garcia et al., 1994). A relatively simple theory has been proposed to describe the effects of charge on the partitioning of linear polyelectrolytes in straight pores (Lin and Deen, 1990), but accounting for all possible polymer conformations within a fibrous medium presents significant difficulties. Monte Carlo simulations provide one possible approach for modeling linear polyelectrolytes in fibrous media.

Chapter 4

4. Permeability of Agarose Gels

4.1 Introduction

The permeability of agarose gels is important in both describing the microstructure of the gel and in developing predictions for the diffusivity of macromolecules through the gel phase as previously discussed in section 1.5.3. Despite the importance of the permeability, relatively few measurements have been made for gels (as reviewed in section 1.5.3) and none for agarose gels. In addition, because the permeabilities are so low, the methods used for measuring permeabilities required the use of very high pressures and special equipment to measure low flow rates. A novel apparatus has been designed to measure permeabilities with low pressures and high velocities by using ultrathin agarose measurements. In addition, measurements of the permeabilty have been for concentrations ranging between 2 - 7% agarose.

Fluid flow through gels or other porous media is usually modeled using Darcy's law,

$$\mathbf{v} = -\frac{\kappa}{\mu}\nabla\mathbf{P} \qquad (61)$$

where v is the fluid velocity , μ is the viscosity, P is the pressure and κ is the Darcy permeability. For a pressure drop ΔP imposed across a slab of thickness L, the superficial velocity obtained by integrating equation 61 is

$$v = \frac{\kappa \Delta P}{\mu L} \qquad (62)$$

In the membrane literature "hydraulic permeability" usually refers to the proportionality constant relating v to ΔP, namely $\kappa/(\mu L)$, and that is how that phrase is used here.

In an application such as protein separation by electrophoresis, where the main purpose of the gel is to suppress flow, the magnitude of κ is unimportant as long as it is sufficiently small. In other situations, however, the amount of water flow induced by a given applied pressure is of special interest. For example, the rates of fluid flow through renal capillary basement membrane and the extracellular matrix of tumors are critical for maintenance of normal kidney function (Drumond and Deen, 1994) and the delivery of anti-cancer drugs (Jain, 1987), respectively. Even when diffusion is the only mechanism for solute tranport, κ is useful for predicting the hydrodynamic effects of a gel on the mobility of a macromolecular solute (Kosar and Phillips, 1995; Johnson et al., 1995). The value of κ has also been used to infer information on the microstructural characteristics of gels (Tokita and Tanaka, 1991).

Although there are a variety of reasons for measuring the hydraulic permeability (or κ) of hydrogels, limited experimental information is available as was reviewed in section 1.5.3. The hydraulic permeabilities of agar and gelatin have been determined by measuring water flow through a gel column (Pallman and Devel, 1945; Signer and Egli, 1950). Various approaches have been used also to measure κ for cross-linked polyacrylamide (Tokita and Tanaka, 1991; White, 1960; Weiss and Silberberg, 1976). In general,

researchers have employed relatively thick samples (L ranging from ~1 mm to several cm), requiring the use of fairly large applied pressures and/or the measurement of very small water flow rates. The experimental difficulties encountered are not trivial, as evidenced by values of κ for a given concentration of polyacrylamide which span two orders of magnitude (Tokita and Tanaka, 1991; White, 1960; Weiss and Silberberg, 1976).

As previously explained in section 1.6 agarose is a polysaccharide derived from seaweed, and is used extensively in chromatography and electrophoresis. Agarose gels are formed by a reversible, physical association of the polysaccharide chains. At high temperatures (generally > 80 °C, depending on the agarose type) the agarose chains are soluble in water. As the temperature is lowered, the agarose chains join to form α-helical fibrils (Arnott et al., 1974), which aggregate further to form larger fibers. Gelation usually occurs by the time the solution reaches 40 °C. Because the gels are formed by physical linkages among multiple chains, there is a distribution of fiber radii. Electron microscopy (Amsterdam et al., 1975; Spencer, 1982; Waki et al., 1982; Whytock and Finch, 1991) has demonstrated a range of fiber radii of 1-20 nm, without quantifying the distribution of fiber sizes. Light scattering results (Obrink, 1968) suggest an average fiber radius of 1.5-2.0 nm. Data from small angle x-ray scattering (SAXS) (Djabourov et al., 1989) indicate a bimodal distribution, with a radius of 1.5 nm for 87% of the fibers and a radius of 4.5 nm for 13%, yielding a number-average radius of 1.9 nm. Despite its widespread use, there appear to be no previous measurements of κ for agarose.

We report here a simple method for measuring hydraulic permeabilities of gels at low pressures, which we used to obtain values of κ for agarose with concentrations ranging from 2 to 7%. Membranes which were thin but which had sufficient mechanical strength were prepared by casting gels on a woven polyester mesh. Gel thicknessses as small as 70 μm were obtained in this manner.

4.2 Materials and Methods

4.2.1 Preparation of gels.

Gels were made by first adding 10 ml of 0.01 M Phosphate buffer, pH 7 + 0.1 M KCl to a measured amount of agarose powder (Type VI, high gelling; Sigma, St. Louis, MO) in a 20 ml glass vial, and placing the resulting slurry in a 90°C oven for 2-5 hr. The vial, which was sealed to prevent evaporation, was rotated by hand periodically to ensure adequate mixing. Two glass plates were also heated. To cast the membranes, a 2.5 cm diameter piece of woven polyester mesh (Spectrum Medical, Houston, TX) was placed on one of the glass plates. The mesh formed a square pattern with a fiber radius of 20 mm, a center-to-center fiber spacing of 93 mm, and a thickness of 70 mm. The hot agarose was quickly poured onto the mesh and the second plate used to form a sandwich. Care was taken to ensure that air bubbles were not trapped in the gel. The glass plates were then clamped together and allowed to cool to room temperature. Finally, the gel was immersed in 0.01 M phosphate buffer at pH 7.01 containing 0.1 M KCl, and stored (usually overnight) at 4°C.

4.2.2 Hydraulic permeability measurements.

The gel membrane was mounted on a porous frit inside a 3 ml ultrafiltration cell (Model 3, Amicon, Beverly, MA), which was then filled with the phosphate/KCl buffer. The solution was forced through the membrane at a constant pressure using compressed nitrogen. The transmembrane pressure drop was monitored using a pressure transducer (Model DP15, Validyne Engineering, Northridge, CA) while the flow rate was determined by collecting and weighing the filtrate. The height of the water in the ultrafiltration cell was measured during the experiment and a correction was made for the hydrostatic pressure. After the flow measurements were completed (usually 2 repetitions at any given pressure),

the membrane thickness was determined by placing the sample between two microslides and using a micrometer to determine the thickness both with and without the membrane present. The uncertainty in this measurement was estimated as ± 3 μm.

Hydraulic permeability measurements were made for agarose concentrations of 2.0, 3.9, 5.6 and 7.3% (w/v). The volume fraction of fibers was calculated by dividing the weight fraction by 1.025 (section 1.6). To investigate the effects of compression of the membrane, results were obtained at five different pressures: 3, 7, 10, 13, and 20 kPa. The effects of heating and cooling time in gel preparation were also examined.

4.3 Numerical Calculation for Polyester Mesh Obstruction

4.3.1 Correction factor for the effect of the fiber mesh.

Because the open area was reduced considerably by the fiber mesh support, it was necessary to use a correction factor in computing κ. This factor (β) was defined by rewriting equation 62 as

$$v = \beta \frac{\kappa \Delta P}{\mu L} \qquad (63)$$

Thus, in general $0 \leq \beta \leq 1$, with $\beta = 1$ corresponding to the hypothetical case of no mesh. As shown in Figure 4.1, we modeled the mesh structure as a square array of intersecting cylinders. Four independent dimensions are the mesh fiber radius (R), the center-to-center spacing of the fibers (W), the thickness of the gel on the upstream side of the fibers (L_1),

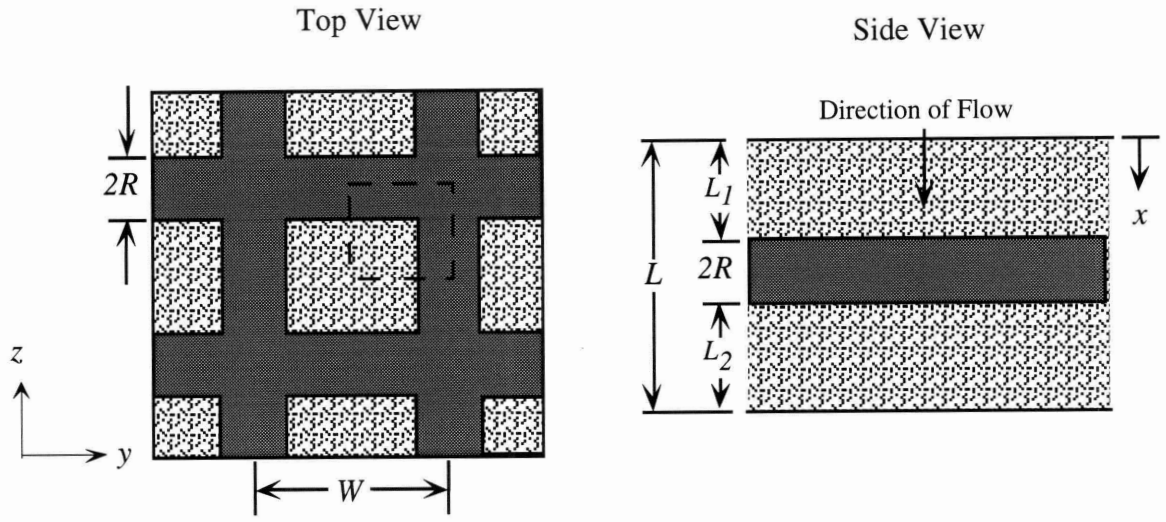

Figure 4.1 Model geometry used for calculating the pressure field and the correction factor for hydraulic permeability for mesh-supported gels. The woven mesh is represented as a coplanar network of intersecting cylinders of radius R, with a center-to-center distance W. The side view shows the total thickness of the membrane, L, and the thicknesses of gel layers upstream and downstream from the fibers, L_1 and L_2, respectively. Because there are two planes of symmetry, the finite-element calculations used only 1/4 of a unit square, as indicated by the dashed box in the top view.

and the total thickness of the membrane (L). With four dimensional lengths, the correction factor β must be a function of three dimensionless groups. These were chosen as

$$\alpha \equiv \left(1 - \frac{2R}{W}\right)^2 \tag{64}$$

$$\lambda \equiv \frac{L}{R} \tag{65}$$

$$\gamma \equiv \frac{L_1}{L_1 + L_2} = \frac{L_1}{L - 2R} \tag{66}$$

Thus, $\beta = \beta(\alpha, \lambda, \gamma)$, where α is the ratio of open area to total area, λ is the ratio of membrane thickness to fiber radius, and γ is the fraction of the "excess" gel which is upstream of the fibers.

The governing equation for the three-dimensional pressure field, P(x,y,z), was obtained by combining the continuity equation with Darcy's law to give

$$\nabla^2 P = 0 \tag{67}$$

Taking x as the direction normal to the membrane surfaces, the square mesh provides symmetry in both y and z. Accordingly, the domain chosen corresponded to only one quarter of a unit cell, as shown by the dashed square in the top view of Figure 4.1. The boundary conditions used were

$$P = \Delta P \quad \text{at } x = 0 \tag{68}$$

$$P = 0 \quad \text{at } x = L \tag{69}$$

$$\mathbf{n} \cdot \nabla P = 0 \quad \text{at fiber surfaces, symmetry planes} \tag{70}$$

where **n** is a unit normal vector. The pressure field and β were computed using a commercial finite element package (FIDAP, Fluid Dynamics International, Evanston, IL) on a Silicon Graphics Indigo workstation. The calculations were based on the Galerkin method with quadratic basis functions. As the number of nodes was increased, the average pressure gradients at the surfaces converged quadratically, as expected. The factor β was calculated as the pressure gradient averaged over the downstream surface,$<-(\partial P/\partial x)|_{x=L}>$, divided by the macroscopic pressure gradient, $\Delta P/L$. Using 5769 nodes in these three-dimensional simulations yielded errors of < 0.1 % in β.

4.4 Results and Discussion

4.4.1 Correction factor for polyester mesh support.

In calculating the correction factor β needed to compute κ from data obtained using mesh-reinforced gels, a simplifying assumption was that the mesh fibers were intersecting cylinders. The actual mesh was woven, so that the fibers were not uniformly coplanar. To estimate the error introduced by this assumption, we varied the parameter γ, which corresponds to the fraction of the excess gel which is on the upstream side of the fibers. For $0.1 \leq \gamma \leq 0.9$ there was less than a 3% change in β. This indicates that the exact location of the cylindrical fibers in the x direction is relatively unimportant. Although it was not practical to calculate β using an exact representation of the woven mesh, the intersecting cylinder model appears to be a reasonable approximation. Having found that $\beta \cong \beta(\alpha, \lambda)$ only, the dependence of β on the remaining two parameters was determined using simulations where $0 \leq \alpha \leq 1$ and $\lambda = 2.50$, 3.75, and 7.50 (with $\gamma = 0.5$). Figure 4.2 shows the results, together with a power-law curve fit for each value of λ, and the

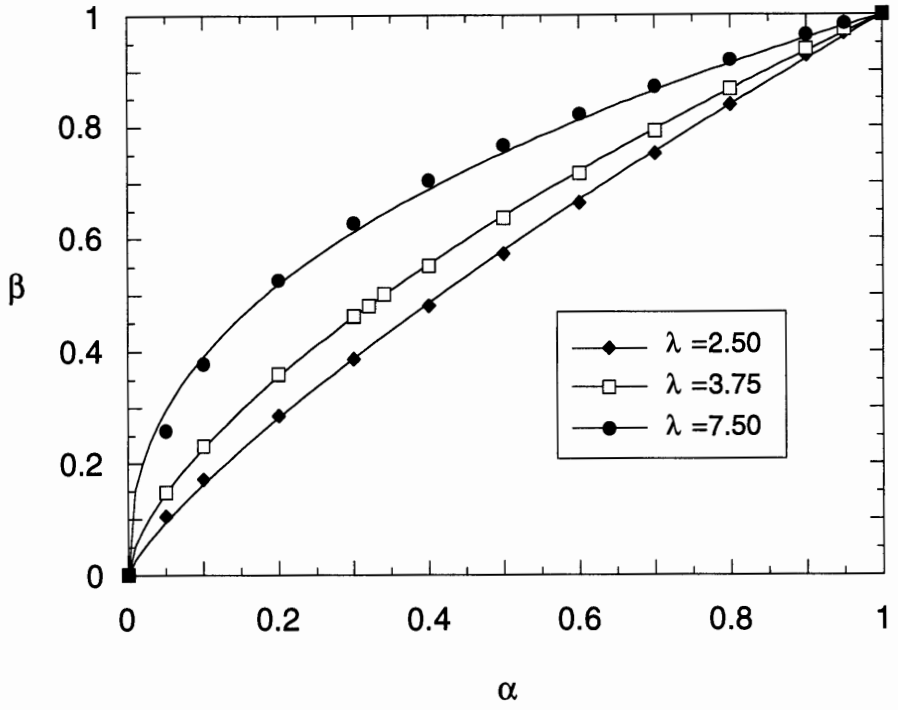

Figure 4.2 Effects of α, the fractional open area, and λ, the ratio of membrane thickness to fiber radius, on the correction factor, β. The symbols show the finite-element results, and the curves are power-law fits of the form $\beta = \alpha^m$. For $\lambda = 2.50$, 3.75, and 7.50 the exponents are $m = 0.787$, 0.642, and 0.409, respectively. All results are for $\gamma = 0.5$.

Table 4.1 Simulations to determine the correction factor, β, for use in the permeability experiments.

Name		Nodes	ΔP	L	R	α	γ	∂P/∂n	β
mesh	001	159	100	75	20	0.34	0.5	0.689872	0.5174
mesh	002	885	100	75	20	0.34	0.5	0.671362	0.5035
mesh	003	2611	100	75	20	0.34	0.5	0.669100	0.5018
mesh	004	5769	100	75	20	0.34	0.5	0.668930	0.5017
mesh	005	10791	100	75	20	0.34	0.5	0.668954	0.5017
mesh	006	18109	100	75	20	0.34	0.5	0.668634	0.5015
mesh	007	5769	100	80	20	0.32	0.5	0.618698	0.4950
mesh	008	5769	100	85	20	0.32	0.5	0.598796	0.5090
mesh	009	5769	100	90	20	0.32	0.5	0.580507	0.5225
mesh	010	5769	100	100	20	0.32	0.5	0.547728	0.5477
mesh	011	5769	100	75	20	0.05	0.5	0.197509	0.1481
mesh	012	5769	100	75	20	0.1	0.5	0.310080	0.2326
mesh	013	5769	100	75	20	0.2	0.5	0.479265	0.3594
mesh	014	5769	100	75	20	0.3	0.5	0.615554	0.4617
mesh	015	5769	100	75	20	0.4	0.5	0.735998	0.5520
mesh	016	5769	100	75	20	0.6	0.5	0.954140	0.7156
mesh	017	5769	100	75	20	0.7	0.5	1.056446	0.7923
mesh	018	5769	100	75	20	0.8	0.5	1.155405	0.8666
mesh	019	5769	100	75	20	0.9	0.5	1.251334	0.9385
mesh	020	5769	100	75	20	0.95	0.5	1.297111	0.9728
mesh	021	5769	100	75	20	0.5	0.5	0.847669	0.6358
mesh	022	5769	100	75	10	0.05	0.5	0.344747	0.2586
mesh	023	5769	100	75	10	0.1	0.5	0.503232	0.3774
mesh	024	5769	100	75	10	0.2	0.5	0.702814	0.5271
mesh	025	5769	100	75	10	0.3	0.5	0.836578	0.6274
mesh	026	5769	100	75	10	0.4	0.5	0.938741	0.7041
mesh	027	5769	100	75	10	0.5	0.5	1.022861	0.7671
mesh	028	5769	100	75	10	0.6	0.5	1.096080	0.8221
mesh	029	5769	100	75	10	0.7	0.5	1.162756	0.8721
mesh	030	5769	100	75	10	0.8	0.5	1.225519	0.9191
mesh	031	5769	100	75	10	0.9	0.5	1.284642	0.9635
mesh	032	5769	100	75	10	0.95	0.5	1.312100	0.9841
mesh	033	5769	100	75	30	0.05	0.5	0.140539	0.1054
mesh	034	5769	100	75	30	0.1	0.5	0.230302	0.1727
mesh	035	5769	100	75	30	0.2	0.5	0.380458	0.2853
mesh	036	5769	100	75	30	0.3	0.5	0.514657	0.3860
mesh	037	5769	100	75	30	0.4	0.5	0.641588	0.4812
mesh	038	5769	100	75	30	0.5	0.5	0.764229	0.5732
mesh	039	5769	100	75	30	0.6	0.5	0.884986	0.6637
mesh	040	5769	100	75	30	0.7	0.5	1.001622	0.7512
mesh	041	5769	100	75	30	0.8	0.5	1.118586	0.8389
mesh	042	5769	100	75	30	0.9	0.5	1.235043	0.9263
mesh	043	5769	100	75	30	0.95	0.5	1.288457	0.9663
mesh	044	5769	100	75	20	0.32	0.5	0.640606	0.4805
mesh	045	5769	100	75	20	0.29	0.5	0.602799	0.4521
mesh	046	5769	100	75	20	0.15	0.5	0.400711	0.3005
mesh	047	5769	100	70	20	0.32	0.5	0.665069	0.4655

exact values are tabulated in Table 4.1. For the actual membranes used R = 20 μm, W = 93 μm, and 70 ≤ L ≤ 100 μm. Thus, $\alpha = 0.32$ and $3.5 \leq \lambda \leq 5.0$. For those particular conditions it was found that β was linear in L, varying from 0.466 at L = 70 μm to 0.548 at L = 100 μm.

4.4.2 Darcy permeabilities.

Duplicate measurements of hydraulic permeability with a given membrane were usually within 1% of one another, and always within 2%. Membrane-to-membrane variations in κ tended to be much larger, so that statistics were calculated on the basis of the number of membranes examined. There was no significant effect of varying the heating time in gel preparation from 2 to 5 hr, or of varying the refrigeration time before study from 1 to 24 hr. We found, however, that if the solution was not carefully mixed during the several hours of heating, inhomogeneities in the gel could cause the permeability to vary by a factor of 2 or 3, especially at the higher gel concentrations. Even with careful attention to mixing, the variation in κ between nominally identical membranes was as much as 27%.

The hydraulic permeabilities were very sensitive to the gel concentration. As shown in Figure 4.3, the Darcy permeability at $\Delta P = 20$ kPa decreased by more than 20-fold as the volume fraction of agarose (ϕ) was increased from 0.019 to 0.072. As indicated by the straight line, there was approximately a power-law relationship between κ and ϕ, with an exponent (slope) of -2.4. This contrasts with the slope of -1.5 which is predicted from scaling theory for semidilute polymer solutions, and which has been observed experimentally for crosslinked polyacrylamide (Tokita and Tanaka, 1991). The difference in these slopes is not surprising, given the very different crosslinking mechanisms (physical association of agarose fibrils vs. chemical crosslinking of polyacrylamide).

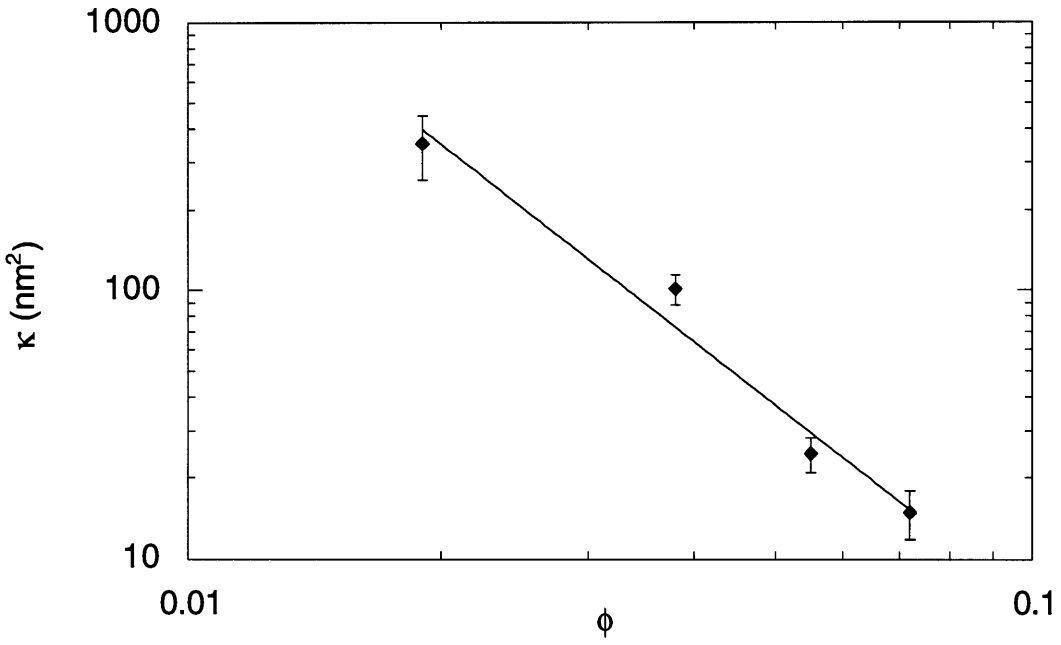

Figure 4.3 The Darcy permeability for agarose gels, κ, as a function of the volume fraction of fibers, ϕ. The symbols show the mean ± SD for n = 5 membranes at each agarose concentration, with ΔP = 20 kPa. The best-fit line is given by $\kappa = 0.0244\ \phi^{-2.45}$.

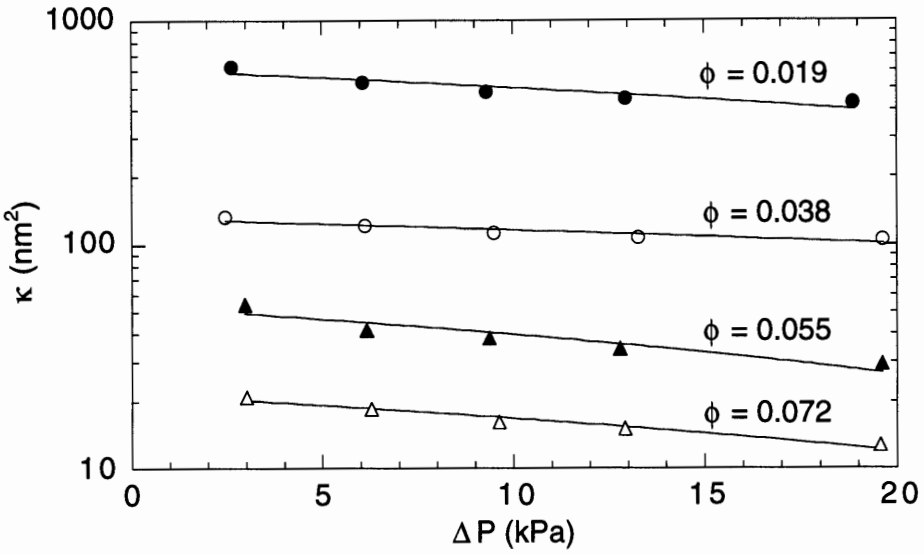

Figure 4.4 Effect of applied pressure, ΔP, on the Darcy permeability, κ, for single membranes at each of four agarose concentrations. The fitted curves are of the form, $\kappa = \kappa_o - c\Delta P$. The intercepts ($\kappa_o$) are given in Table 4.2, and the slopes (in nm^2/kPa) are c = 11.5, 1.59, 1.35, and 0.488 for ϕ = 0.019, 0.038, 0.055, and 0.072, respectively.

There was an effect also of the applied pressure, κ decreasing for any given membrane as ΔP was increased. Figure 4.4 shows κ as a function of ΔP, as determined using one membrane at each agarose concentration. The permeabilities decreased by 14-31% when the pressure drop was increased from 3 to 20 kPa, the relationship between κ and ΔP being approximately linear. Darcy permeabilities extrapolated to zero pressure drop (κ_o) were computed by applying the slopes from the data in Figure 4.4 to the mean values of k measured for all membranes at $\Delta P = 20$ kPa (Figure 4.3). The values of κ and κ_o for the various gel concentrations are shown in Table 4.2. Also shown in Table 4.2 are values of the correlation length, calculated as $\xi = \kappa_o^{1/2}$, which is a measure of interfiber spacing in the gel. Assuming that the average fiber radius is ~2 nm, at the lowest gel concentration the interfiber spacing greatly exceeded the fiber radius, whereas at the highest gel concentration the fibers were only a few radii apart.

Table 4.2 Darcy permeability of agarose gels.

ϕ	κ (nm^2)	κ_o (nm^2)	κ (equation 71) (nm^2)	ξ (nm)
0.019	353±95	616	86	25
0.038	101±13	132	33	12
0.055	25±4	53	19	7
0.072	15±3	22	13	5

Values of κ are mean ± SD for 5 membranes at $\Delta P = 20$ kPa. See text for explanation of other symbols.

As discussed in section 1.4.2 Jackson and James (1986) reviewed theoretical predictions for κ based on hydrodynamic calculations for various arrangements of cylindrical rods, and examined Darcy permeability data obtained from various types of fibrous media. They concluded that κ for random, three-dimensional arrays of fibers could be predicted reasonably well by

$$\frac{\kappa}{r_f^2} = -\frac{3}{20\phi}(\ln\phi + 0.931) \qquad (71)$$

where r_f is the fiber radius and ϕ is the volume fraction of fibers. Using equation 71 with r_f = 1.9 nm, as suggested by the SAXS data cited earlier, we obtain the predicted values of Darcy permeability shown in Table 4.2. The values from equation 71 were smaller than either of the experimental measures of Darcy permeability (κ or κ_0), the discrepancies being greater at the lower gel concentrations. At the three highest gel concentrations, at least, the extent of agreement between equation 71 and the values of either κ or κ_0 (up to four-fold differences) is no worse than what one might expect, given the variablility in the experimental results reviewed by Jackson and James. Nonetheless, the increasing discrepancies at lower gel concentrations might be due to changes in the agarose microstructure. For example, the trend could be explained by a change in average fiber radius with gel concentration, r_f increasing as ϕ decreases, although we are not aware of any structural data which suggest such variations in fiber radius. Another possibility is that the interfiber spacings became more heterogeneous at the lower gel concentrations. The effect of unequal fiber spacings would be to increase κ for given values of r_f and ϕ.

4.4.3 Conclusion

A novel technique was developed to measure the hydraulic permeability of fiber-reinforced gel membranes, allowing calculation of the Darcy permeability for the gel. The method was applied to agarose with concentrations ranging from 2.0-7.3%, providing what appear to be the first measurements of Darcy permeability for this material. A particular advantage in using this methodology is that, because the membranes are very thin (~100 mm), easily measured volumes of filtrate are obtained with modest applied pressures. This simple approach should be adaptable to a variety of other gel materials.

Chapter 5

5. Hindered Diffusion in Neutral Agarose and Evaluation of the Effective Medium Model

5.1 Introduction

The widespread use of hydrogels in areas such as liquid chromatography, drug delivery, and therapeutic implants, and the existence of various body tissues with gel-like characteristics (e.g., connective tissue and basement membranes), makes it important to understand the rates of diffusion of proteins and other macromolecules through these materials. In gels and in other porous media where the pore diameters, interfiber spacing, or other microstructural dimensions are comparable to the size of a diffusing macromolecule, the diffusivity tends to be lower than that in free solution, the percentage of the reduction increasing with molecular size. One approach for interpreting such diffusion data is to assume that the porous material consists of an array of cylindrical (or other regularly shaped pores), and to apply a hydrodynamic theory which extends the Stokes-Einstein equation to account for the effects of the pore walls (Deen, 1987). This theory, which is most completely developed for spherical molecules in long, straight pores, includes two factors which influence the average diffusivity of a neutral macromolecule in a pore. There is an increased hydrodynamic drag on the molecule (and consequent reduction in its mobility) caused by the pore walls, and there are steric restrictions on the positions which can be occupied by a molecule of finite size. Diffusion data obtained in track-etch

membranes (which have straight, uniform pores) are generally consistent with the theory (Deen, 1987), so that the pore model is often a good choice for correlating hindered diffusion results in membranes. However, an array of straight pores bears little resemblance to the microstructure of a crosslinked, polymeric gel as previously discussed in Chapter 1.

A more realistic microstructural model for gels, at least for those with relatively stiff polymer chains, is a randomly oriented array of straight, cylindrical fibers of radius r_f and fiber volume fraction ϕ. This model was proposed by Ogston et al. (1973) to describe diffusion of spherical macromolecules through solutions of linear polymers, as reviewed in section 1.4.1. An expression for the diffusivity in the polymer solution was derived from stochastic arguments, by considering the probability that a molecule of radius rs would encounter spaces of sufficient size to permit its movement. The result, which is equally applicable to a fiber-matrix model for diffusion in gels, was

$$\frac{D}{D_\infty} = \exp\left(-\phi^{1/2}\frac{r_s}{r_f}\right) \qquad (72)$$

where D and D_∞ are the diffusivities in the gel (or polymer solution) and in free solution, respectively. As used in equation 72, D is the macroscopically observable diffusivity defined for solute concentrations based on the *total* gel volume. Macroscopic (or effective) diffusivities in structured media are sometimes defined using concentrations based on the volume of the continuous phase (fluid), and the definition used is not always stated, causing much confusion in the literature. This distinction between these definitions is discussed by Ogston et al. (1973) and by Johansson and Löfroth (1993).

Equation 72 is based on the probability distribution of fiber spacings used by Ogston (1958) to predict equilibrium partition coefficients for macromolecules in fiber

arrays. The fiber-matrix concept is supported by partitioning data for proteins in crosslinked dextran gels (Laurent and Killander, 1964) and agarose gels (Laurent, 1967; Dubin and Principi, 1989; Boyer and Hsu, 1992; Moussaoui et al., 1992; Johnson et al., 1995). Equation 72 successfully correlated diffusion data for macromolecules in various polymer solutions (Ogston et al., 1973), although it was found that the values of r_f needed to fit diffusion data were usually larger than those obtained from partitioning data. This suggests that equation 72 may have a tendency to overestimate D/D_∞ as was discussed in section 1.5.2.

One factor not considered in the derivation of equation 72 is hydrodynamic interactions between the fixed fibers and the diffusing macromolecule, analogous to those seen in pores. Phillips et al. (1989, 1990) addressed this issue by using Stokesian dynamics and generalized Taylor dispersion theory to compute the long-time (macroscopic) diffusivity of a sphere moving through a viscous fluid contained within a periodic array of parallel fibers. It was proposed that the diffusivity could be estimated for other fiber arrangements by treating the fiber array as an effective medium characterized only by its Darcy permeability, κ. The Darcy permeability is the intrinsic conductance of the fiber array for pressure-driven flow of water, and $\kappa^{1/2}$ is a hydrodynamic screening length or correlation length which is of the order of magnitude of the fiber spacing. Using Brinkman's equation (Brinkman, 1947) to compute the drag on a sphere moving through such a medium, it was suggested that $D/D_\infty \cong F$, where

$$F\left(\frac{r_s}{\sqrt{\kappa}}\right) = \left[1 + \left(\frac{r_s}{\sqrt{\kappa}}\right) + \frac{1}{3}\left(\frac{r_s}{\sqrt{\kappa}}\right)^2\right]^{-1} \qquad \textbf{(73)}$$

Kosar and Phillips (1995) have shown that the Brinkman model for describing screened hydrodynamic interactions gives results equivalent to models of the Kirkwood-Riseman type, in which the effects of fixed polymer chains are described using a distribution of immobile point forces. The only structural information in equation 73 is that embedded in κ. Thus, the model implies that macromolecular diffusivities in gels or other fibrous media can be predicted from a single, macroscopic (flow vs. pressure) measurement; the values of r_f and ϕ and the details of fiber spacing and orientation are not needed. Comparisons of equation 73 with the results of rigorous calculations showed fairly good agreement for parallel fibers in square arrays, with $r_s/r_f = 1$ (Phillips et al., 1989). However, subsequent results for smaller or larger values of r_s/r_f and for less uniform fiber arrangements were not as promising (Phillips et al., 1990). Overall, as previously shown in section 1.5.2 equation 73 consistently overestimated D/D_∞.

On the basis of hydrodynamic arguments, Brady (1994) has proposed that the hydrodynamic and steric effects which influence the diffusivity of a macromolecule in a fibrous medium can be separated into two multiplicative factors. According to this approach, the hydrodynamic effect of the fibers can be approximated using the Brinkman result, the function F in equation 73. The other factor is a steric or tortuousity effect, given by a function which we term S. The overall functional dependence is of the form

$$\frac{D}{D_\infty} = F\left(\frac{r_s}{\sqrt{\kappa}}\right) S(f) \qquad \textbf{(74)}$$

$$f = \left(1 + \frac{r_s}{r_f}\right)^2 \phi \qquad \textbf{(75)}$$

The steric factor S is calculated from the effective diffusivity of a point-size molecule in an array of fibers whose centers are positioned as in the actual system, but which have a

radius of $r_f + r_s$. In other words, the volume fraction of fibers is augmented, according to the size of the actual molecule of interest. This adjusted volume fraction of fibers is given in equation 75 as f. Results are available to calculate S(f) for various regular or random arrays of fibers (Perrins et al., 1979; Johansson and Löfroth, 1993; Tomadakis and Sotirchos, 1993). Brady (1994) noted that for diffusion normal to regular arrays of parallel fibers, evaluating S using the results of Perrins et al. (1979) provided excellent agreement between equation 74 and the rigorous calculations of Phillips et al. (1989, 1990). Thus, equation 74 may provide a way to obtain simple and accurate predictions of macromolecular diffusivities in gels.

Various methods have been employed to measure D for proteins and other compact macromolecules in gels and polymer solutions as was reviewed in section 1.5.2. Techniques used in recent years include fluorescence recovery after photobleaching (FRAP) (Hou et al., 1990; Jain et al., 1990; Moussaoui et al., 1991, 1992; Wattenbarger et al., 1992; Berk et al., 1993; Saltzman et al., 1994; Johnson et al., 1995), pulsed-field-gradient NMR (Gibbs et al., 1992), and holographic interferometry (Kosar and Phillips, 1995). Methods involving transient diffusion into a thick slab of gel (Cameron et al., 1994; Leloup et al., 1990) and dispersion in a chromatography column (Boyer and Hsu, 1992) have also been employed; these approaches are somewhat less direct, in that they measure only the product of D and the gel-to-free solution partition coefficient. Despite the amount of experimental activity in this area, there is little data with which to test the hydrodynamic theories for hindered diffusion in gels. In particular, there is a paucity of information on the values of κ in gels where diffusion measurements have been made. The purpose of this study was to provide such data by measuring the diffusion coefficients of several well-characterized macromolecules in agarose gels, varying both r_s and ϕ. The Darcy permeability was determined for each gel sample, and r_f for agarose was obtained independently from the literature, so that all of the parameters needed to apply equations 72 - 74 could be evaluated.

5.2 Methods and Materials

5.2.1 Proteins and narrow fractions of ficoll.

Three fluorescein-labeled proteins, bovine serum albumin (BSA), ovalbumin, and lactalbumin were obtained from Molecular Probes (Eugene, OR). Size-exclusion chromatography indicated that there was no free fluorescein present, so that the proteins were used without further purification. Four narrow fractions of Ficoll were obtained by special order from Pharmacia LKB (Piscataway, NJ) and labeled with fluorescein using a procedure described in the following paragraph. Fresh aqueous samples were prepared by dissolving the fluorescent macromolecule in a buffer consisting of 0.01 M sodium phosphate and 0.1 M potassium chloride at pH 7.0. In each case the macromolecule concentration was 1 mg/mL.

The Ficoll samples were labeled with DTAF (dichlorotryazinyl amino fluorescein, Sigma, St. Louis, MO) using a procedure described by De Belder and Granath (1973). Because the fluorescein is very light sensitive, preparations should be made in minimal light and the reaction container should be covered. For each Ficoll sample, 2 grams was dissolved in 60 mL of distilled water using a magnetic stirrer. A pH probe was inserted to insure that the pH remained above 10. Fifty mgs of DTAF was added to the ficoll solution. At pH values below 10, DTAF is relatively insoluble. The pH was adjusted to be above 10 (but always below 11) by adding 1 N sodium hydroxide. As the reaction proceeds the pH drops, so monitoring is necessary to ensure that the sample is kept above pH 10. The labeling procedure usually occurs over the first 15 minutes but the reaction was always allowed to proceed for at least 2 hours. At the conclusion of the labeling procedure, the pH was adjusted downward to pH ~ 7 using 1 N hydrochloric acid. Samples were purified

from unreacted label using 10 mL desalting chromatography columns (Bio-Rad, Hercules, CA). The desalting columns were rinsed with distilled water before use. Distilled water was used to ensure that when the sample was freeze-dried there was no residual salt. The columns head space was filled with distilled water and 0.3-0.5 mL of the unpurified ficoll solution was layered under the water at the surface of the bed using a disposable glass pipette. As the solution migrated down the column two bands appeared. The ficoll-fluorescein was slightly more orange than the free fluorescein and by the time the first drops of the orange band reached the bottom of the column there were two distinct bands. The first band (the orange ficoll-fluorescein) was collected and pooled. Once all the purified ficoll-fluorescein had been collected the samples were immediately frozen. It is important to minimize the exposure of the fluorescein to any light source and the length of time spent in any solution. Once the purified solution was frozen (usually overnight) the sample was freeze-dried and stored desiccated in the freezer until used.

There are two methods for determining the amount of fluorescein attached to the ficoll solution. The preferred standard is sodium fluorescein, not DTAF which is relatively insoluble in water at pH values below 10. The exact concentration of the standard will depend upon the method used. The fluorescein content can be determined using a spectrofluorimeter (excitation 480 nm; emission 515 nm) which will measure the fluorescence of the sample or by using a spectrophotometer and measuring the UV absorption of the fluorophore at 280 nm. By comparing either the fluorescence or the UV absorption of the ficoll-fluorescein solution to the standard solution the number of fluorophores per ficoll molecule can be determined. The spectrofluorimeter is much more sensitive than the spectrophotometer and more dilute samples can be used. There are two problems with using this method, however. If a significant portion of the fluorophores have been bleached, the spectrofluorimeter will not record the bleached molecules, thus underestimating the true number of fluorescein groups per ficoll. In addition, the excitation and emission characteristics of the fluorophore are highly dependent upon the types of

chemical groups attached so the emission characteristics of the standard fluorescein solution may in fact be different than the attached fluorophore. In addition, the fluorescence of fluorescein is dependent upon the pH of the solution. At low pH the fluorescence is significantly smaller than at higher pH. (Fluorescein in fact has been used as a sensitive pH indicator.) The pK_a of the fluorescein is also dependent upon the type of chemical structure attached via the linker arm. The pK_a of free fluorescein is ~ 6.5 (Haugland, 1992). Presumably, the attachment of other chemical groups do not affect the pK_a drastically, but to ensure the maximum fluorescence the fluorescein determination should be made in buffer solutions that have a pH of at least 8. The second method uses the UV absorption of the fluorescein at 280 nm. While this method requires more sample, the UV absorption is unaffected by bleaching and will therefore provide a more accurate method for determining fluorophore concentration. This is particularly good for ficoll solutions which do not normally adsorb in the UV spectrum.

The characteristics of the seven fluorescein-labeled macromolecules are summarized in Table 5.1. For Ficoll, the weight-average molecular weight (M_w) and polydispersity index (M_w/M_n, where M_n is number-average molecular weight) are values supplied by the manufacturer. The diffusivities and Stokes-Einstein radii were obtained from the diffusion data, as described below.

Table 5.1 Properties of test macromolecules for diffusion experiments in agarose.

Molecule	M_W	M_W/M_N	D_∞ (10^{-7} cm^2/sec)	r_s (nm)
Lactalbumin	14,200		10.10±0.70	2.12
Ovalbumin	45,000		7.15±0.77	3.00
BSA	68,000		5.97±0.44	3.59
Ficoll 21K	21,300	1.22	7.06±0.42	3.03
Ficoll 37K	37,400	1.18	5.63±0.18	3.80
Ficoll 61K	60,700	1.15	4.45±0.18	4.82
Ficoll 105K	105,000	1.13	3.44±0.14	6.23

Diffusion coefficients are given as mean±SD for 5 measurements, corrected to 20 °C.

5.2.2 *Agarose gel Preparation and Characterization*

Gels were made by first adding 10 ml of the phosphate-KCl buffer to a measured amount of agarose powder (Type VI; Sigma, St. Louis, MO) in a 20 ml glass vial, and placing the resulting slurry in a 90°C oven for 3 hr. The vial, which was sealed to prevent evaporation, was rotated by hand periodically to ensure adequate mixing. Two glass plates and several rectangular glass microslide chambers with dimensions of $0.3 \times 3 \times 50$ mm (Vitro Dynamics, Rockaway, NJ) were also heated. To cast membranes for hydraulic permeability measurements, a 2.5 cm diameter piece of woven polyester mesh (Spectrum Medical, Houston, TX) was placed on one of the glass plates. The mesh formed a square pattern with a fiber radius of 20 μm, a center-to-center fiber spacing of 93 μm, and a thickness of 70 μm. The hot agarose was quickly poured onto the mesh and the second plate used to form a sandwich. The glass plates were then clamped together, taking care to ensure that air bubbles were not trapped in the gel. To form a gel for diffusion measurements using the same batch of agarose, the heated solution was drawn into one end of a microslide by capillarity; this was done immediately after casting the membrane. Separate microslide gels were prepared for use with each of the seven test macromolecules. After the gels (in membrane or microslide) cooled to room temperature, they were immersed in the phosphate-KCl buffer and stored overnight at 4°C. Samples were prepared with agarose concentrations ranging from 3.8 to 7.4% (w/v). Weight fractions were converted to volume fractions by dividing by 1.025 (section 1.6).

As discussed in section 1.6 native agarose has very little net charge (the agarose used in the experiments was type VI with a sulfate content of <0.15% and an electro-osmosis reduced migration rate, $-m_r = 0.04$; Sigma, St. Louis, MO) and that the amount of fluorescein label attached (@ 1 fluorescein per Ficoll molecule) was insufficient to give Ficoll a significant charge. Moreover, in highly charged, sulfated agarose gels the

diffusivities of the three proteins have been shown to have little or no dependence on ionic strength at ionic strengths as high as 0.1 M as discussed in section 2.4. Thus, there should be no significant effects of charge in the experiments reported here.

5.2.3 Permeability Experiments

The Darcy permeability of each agarose sample was obtained by measuring the hydraulic permeability of the mesh-reinforced membrane, as described in Chapter 4. Briefly, the gel membrane was mounted on a porous frit inside a 3 mL ultrafiltration cell (Model 3, Amicon, Beverly, MA), and the phosphate-KCl buffer forced through the membrane at a constant pressure drop of 17 kPa using compressed nitrogen. The transmembrane pressure drop was monitored using a pressure transducer (Model DP15, Validyne Engineering, Northridge, CA) and the flow rate was determined by collecting and weighing the filtrate. The thickness of the hydrated membrane was measured using a micrometer, by placing the membrane between two microslides of known dimensions. The Darcy permeability was calculated as

$$\kappa = \frac{\mu Q L}{\beta A \Delta P} \qquad (76)$$

where μ is the viscosity of water, Q is the filtrate volume per unit time, L is the membrane thickness, β (= 0.495) is a correction factor to account for the presence of the polyester mesh support, A (= 1.5 cm^2) is the exposed area of the membrane, and ΔP is the pressure drop.

5.2.4 Diffusion Experiments

Samples for diffusion measurements were prepared by drawing a solution of the fluorescent macromolecule into a microslide containing the agarose gel, using a syringe attached to the microslide by silicon tubing. The gel and solution were allowed to equilibrate for 2 hr, a time which was sufficient to yield diffusional equilibrium at the test locations in the gel (typically centered ~100 mm from the gel-solution interface). Diffusion coefficients were determined using an image-based FRAP technique as discussed in detail in section 2.3.2. The image-based FRAP technique using a spatial Fourier transform has the advantage that the results are insensitive to the actual radius of the bleached spot. This is especially important for measurements in gels which scatter light, such as agarose, because the bleached radius changes as a function of depth in the sample. The consequent uncertainties in the true bleached radius make it difficult to obtain reliable results using a direct photometric analysis. For each test macromolecule, five measurements each were made of the diffusion coefficient in the gel (D) and in free solution (D_∞). To allow for complete recovery of the bleached areas (~20 mm initial radius), the gel measurements were alternated with the free solution measurements. The room temperature was recorded (23 - 29 °C), and all diffusion coefficients were corrected to 20 °C by assuming that $D\mu/T$ (or $D_\infty\mu/T$) is constant, where T is absolute temperature.

5.3 Results

The free-solution diffusivities measured for the three proteins and four Ficoll fractions are given in Table 5.2. Also shown is the corresponding Stokes-Einstein radius (r_s), calculated as

$$r_s = \frac{k_B T}{6\pi\mu D_\infty} \qquad (77)$$

where k_B is Boltzmann's constant. The Stokes-Einstein radii shown for the proteins are very close to those obtained previously using various methods, as summarized in Table 2.4. Likewise, the values of r_s for Ficoll are all within 6% of those measured by quasielastic light scattering using unlabeled samples (Oliver et al., 1992). Overall, the test macromolecules had radii ranging from 2.1 to 6.2 nm.

Table 5.2 Diffusivity ratios (D/D_∞) for individual gel samples.

Molecule	A	B	C	D	E	F
Lactalbumin	0.62±0.04	0.63±0.03	0.47±0.03	0.45±0.05	0.34±0.03	0.30±0.03
Ovalbumin	0.57±0.05	0.55±0.03	0.38±0.02	0.44±0.02	0.25±0.03	0.32±0.03
BSA	0.61±0.07	0.53±0.04	0.40±0.01	0.36±0.03	0.27±0.02	0.28±0.03
Ficoll 21K	0.62±0.03	0.60±0.06	0.46±0.02	0.47±0.02	0.26±0.02	0.39±0.03
Ficoll 37K	0.55±0.04	0.53±0.03	0.42±0.05	0.40±0.02	0.26±0.01	0.30±0.02
Ficoll 61K	0.48±0.03	0.45±0.03	0.37±0.09	0.33±0.02	0.21±0.00	0.23±0.01
Ficoll 105K	0.43±0.03	0.35±0.03	0.28±0.02	0.25±0.01	0.20±0.02	0.23±0.02

All values shown are mean±SD for 5 measurements.

The six agarose samples used, identified as A-F, had the properties summarized in Table 5.3. Two samples each were made with agarose volume fractions (ϕ) of 0.038, 0.055, and ~0.072. The measured Darcy permeability (κ) varied by an order of magnitude over this range of gel concentrations, decreasing as gel concentration was increased. Individual measurements of κ were reproducible to within 1-2%, so that the differences in Table 5.2 between nominally identical gels were evidently due to differences in the gel microstructure. This variability in κ among agarose samples, noted previously in Chapter 4, is the reason care was taken to measure Darcy permeabilities in gels made from the same agarose solutions as the samples used for the diffusion experiments.

Although the gel concentration is the main determinant of the Darcy permeability for agarose, there is a significant effect also of the applied pressure, κ decreasing in an approximately linear manner with increasing ΔP as discussed in section 4.4. Values of the Darcy permeability extrapolated to $\Delta P = 0$ are shown in Table 5.3 as κ_0. The extrapolation of κ to zero applied pressure was done by using values of $\partial\kappa/\partial(\Delta P)$ estimated previously at the respective gel concentrations (section 4.4).

Table 5.3 Characteristics of agarose gels used in diffusion experiments.

Gel	ϕ	κ (data) (nm^2)	κ_0 (nm^2)	κ (equation 78) (nm^2)
A	0.038	103.4	130.4	33.8
B	0.038	85.4	111.2	33.1
C	0.055	29.0	50.3	19.3
D	0.055	16.5	40.6	19.5
E	0.072	5.0	13.6	12.7
F	0.073	7.8	16.2	12.5

Also shown in Table 5.3 are the values of κ predicted from a correlation given by Jackson and James (1986) for fibrous media,

$$\frac{\kappa}{r_f^2} = -\frac{3}{20\phi}(\ln\phi + 0.931) \qquad (78)$$

where r_f is the fiber radius. For these calculations we assumed an average fiber radius for agarose of 1.9 nm, which is the number-average value obtained from small angle x-ray scattering data (Djabourov et al., 1989). (This and other measurements of r_f for agarose are discussed in section 1.4) It is seen that equation 78 is in excellent agreement with the values of κ_0 at the highest gel concentration, but the agreement worsens as gel

concentration is decreased, the correlation underpredicting the (extrapolated) experimental results by a factor of 3-4 at the lowest gel concentration. Previous measurements of Darcy permeability given in Chapter 4 for agarose show similar deviations from equation 78; the reason for these deviations is not clear.

Table 5.2 and Figures 5.1-5.3 show the results for the gel-to-free solution diffusivity ratio, D/D_∞. Values of D and D_∞ measured in succession were paired to compute an individual value for the ratio, and the results averaged over the five repetitions to obtain the mean ± SD values shown in Table 5.3. For each test macromolecule, the diffusivity ratio decreased as the gel concentration increased. For any given gel sample, the diffusivity ratio generally decreased as the probe radius increased. In other words, as one would expect, the hindrances to diffusion were most severe for large macromolecules and/or relatively concentrated gels. The significance of the theoretical curves in Figures 5.1 - 5.3 is discussed in section 5.4.

5.4 Discussion

The present experiments were designed to test the diffusivity predictions given by equations. 5.1-5.3. As mentioned earlier, the function S in equation 74 may be evaluated using available results for various arrangements of cylindrical barriers. Two such arrangements are considered here. Using the result of Perrins et al. (1979) for transport perpendicular to the axis of a square array of cylinders, one gets

$$S(f) = \frac{1}{1-f}\left\{1-2f\left[1+f-\frac{0.35827f^4}{1-1.402958f^8}-0.013362f^8\right]^{-1}\right\} \qquad (79)$$

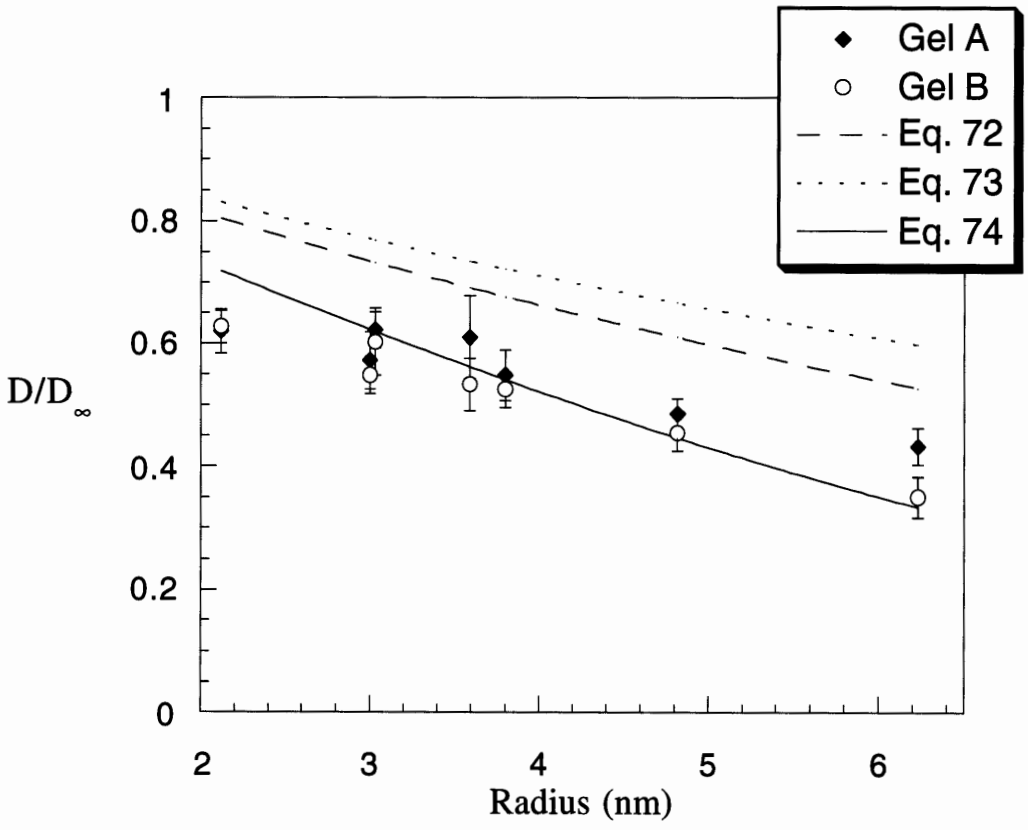

Figure 5.1 The reduced diffusion coefficients D/D_∞ of proteins and ficolls in 3.8% agarose gels. The radius of the proteins is calculated using equation 77 and the error bars are given as ±SD. The three solid lines represent theoretical predictions.

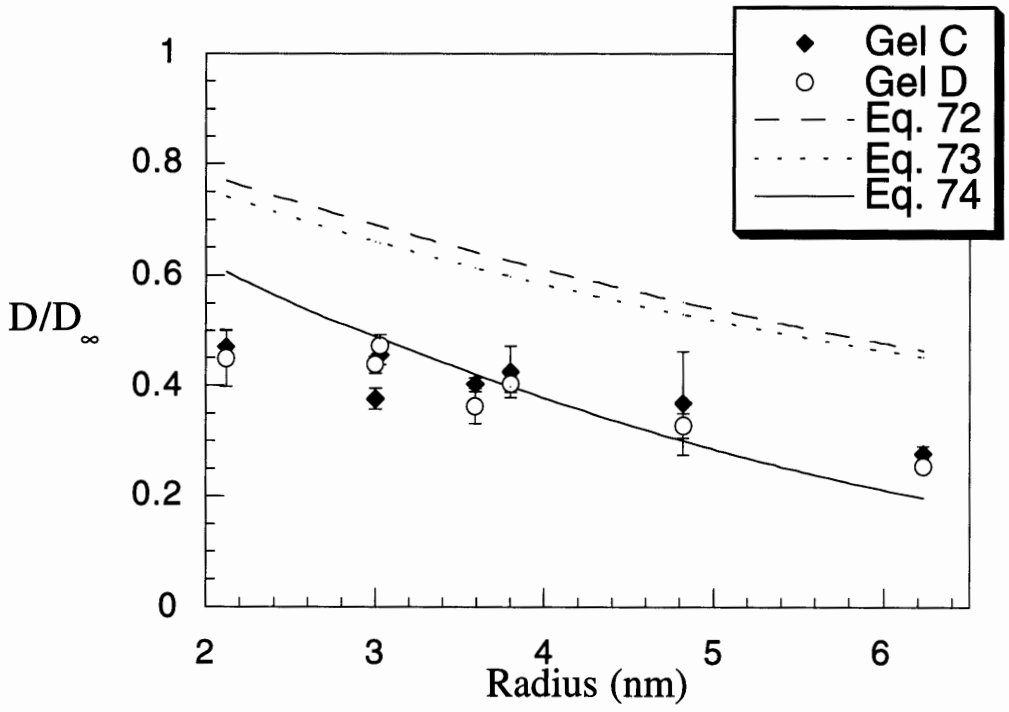

Figure 5.2 The reduced diffusion coefficients D/D_∞ of proteins and ficolls in 5.5% agarose gels. The radius of the proteins is calculated using equation 77 and the error bars are given as ±SD. The three solid lines represent theoretical predictions.

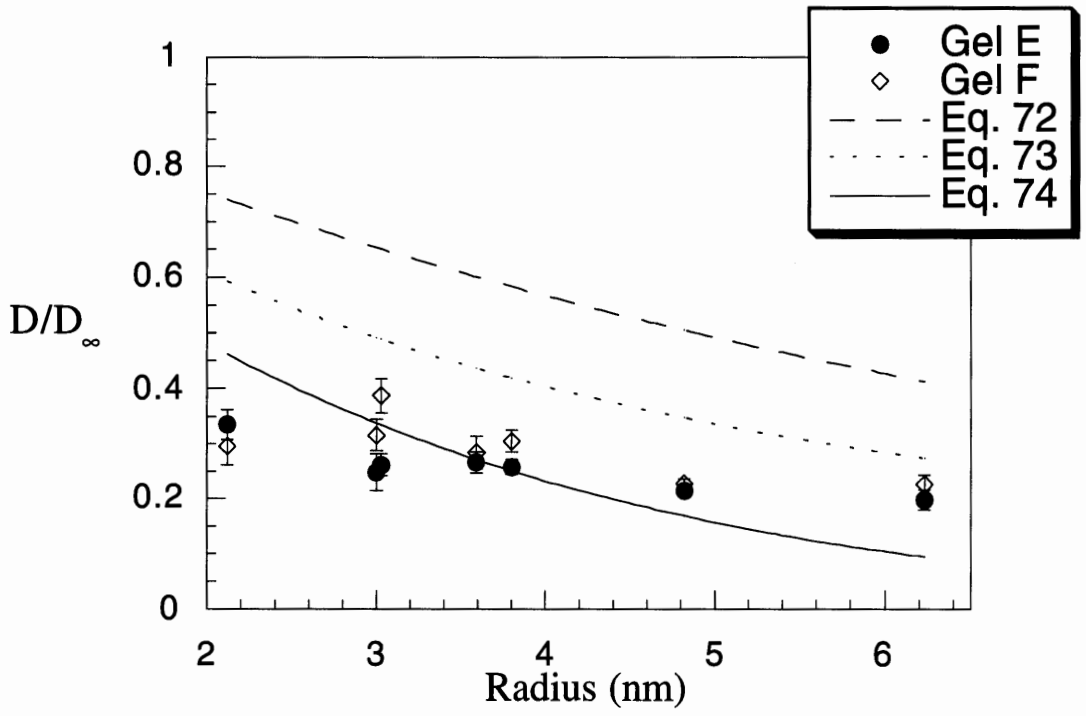

Figure 5.3 The reduced diffusion coefficients D/D_∞ of proteins and ficolls in 7.3% agarose gels. The radius of the proteins is calculated using equation 77 and the error bars are given as ±SD. The three solid lines represent theoretical predictions.

Equation 79 was obtained by dividing eq. 14 of Perrins et al. (1979) by 1 - f. (The result of Perrins et al. is analogous to a transmembrane diffusivity based on external concentrations, so that it must be divided by the partition coefficient, which for a point-size molecule in a fiber array with volume fraction f is 1 - f.) Johansson and Löfroth (1993) used Brownian dynamics simulations to calculate diffusivities for spherical macromolecules moving through random, overlapping arrays of polymer chains. Their calculations were for diffusing molecules of finite r_s, but without hydrodynamic interactions, so that their diffusivity ratios were equivalent to S. Using a curve fit to the simulations for straight polymer chains with $f < 3$, their results are expressed as

$$S(f) = \exp\left(-0.84f^{1.09}\right) \qquad \textbf{(80)}$$

Tomadakis and Sotirchos (1993) review many other results which could be used to evaluate S, including their own Monte Carlo simulations for diffusion of point-size molecules through randomly oriented, overlapping arrays of cylinders. (To obtain S from any of the results summarized by Tomadakis and Sotirchos, one must divide their "inverse formation factor" by 1 - f, as done above for the result of Perrins et al.; f is related to their "matrix volume fraction," ε, by $\varepsilon = 1 - f$.)

Equation 79 implies that $S \to 1 - f$ for $f \to 0$, in agreement with the result for diffusion normal to a dilute array of parallel cylinders (Koch and Brady, 1986). Approximately the same limiting behavior for $f \to 0$ is exhibited by equation 80; the theoretical limit for randomly oriented cylinders is $S \to 1 - (2/3)f$ (Koch and Brady, 1986). The main distinction between regular and random arrays of fibers is in their behavior at large f. This is illustrated in Figure 5.4, which compares the results for S obtained from

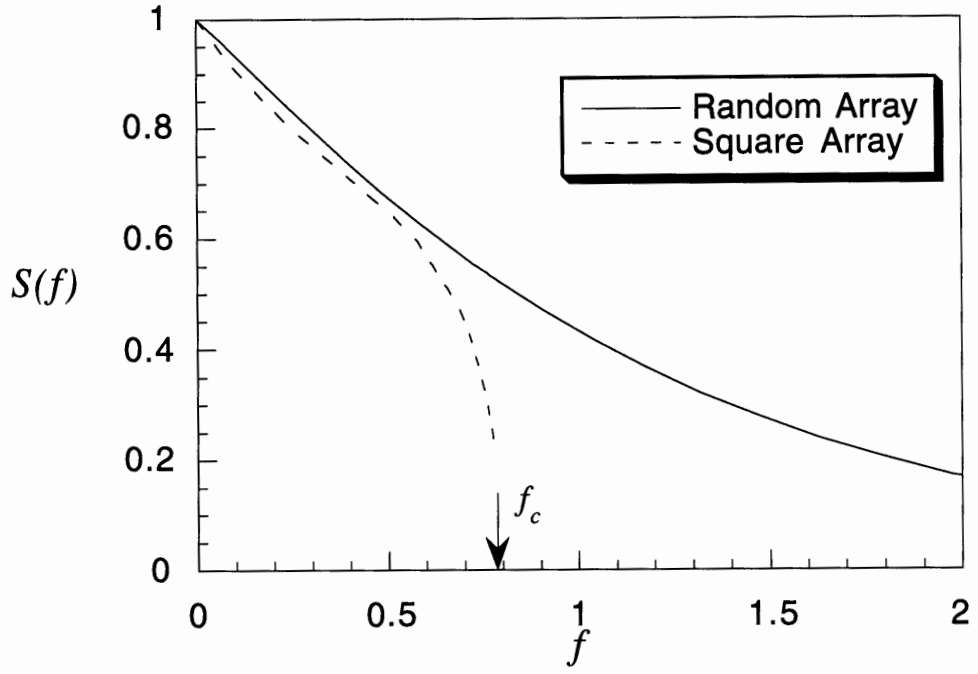

Figure 5.4 The steric factor, S(f), for random (equation 80) and square (equation 79) arrays. The critical value of f for a square array, f_c, is 0.785 and is indicated by an arrow. S(f) asymptotically reaches zero for a square array at f_c.

equations 79 and 80. The results for square and random arrays are very similar for $f < 0.5$, as shown also by Tomadakis and Sotirchos (1993). However, for fibers in a square array there is a critical volume fraction $f_c = \pi/4 = 0.785$ at which all fibers touch, so that for diffusion normal to the fibers $S = 0$ for $f \geq fc$. For random arrays there is no such sharp cutoff in S. The behavior of S(f) for large f is important for the present data, in that $f = 1.33$ for the largest Ficoll in the most concentrated agarose gel. The fact that there were measurable diffusivities for $f > f_c$ strongly suggests a disordered arrangement of the agarose fibers. Accordingly, equation 80 was used for all comparisons with the data.

The measured diffusivity ratios are compared with predictions from equations 72 - 74 in Figures 5.1-5.3. In calculating the hydrodynamic contribution to the diffusional hindrance we used the Darcy permeability extrapolated to zero pressure drop, κ_0, because that value should be most representative of the gel microstructure during the diffusion measurements. In addition, there were small differences in κ_0 for each gel, so the plotted lines for equations 72 - 74 represent the average of the two predictions at each κ_0. Using this method the error in the given predictions is less than 5%. At each gel concentration, the effective medium theory of Brady (1994) yields much better predictions than the other two approaches, which systematically overestimate D/D_∞. Closer inspection reveals that, although the measured values of D/D_∞ for molecules of intermediate size were predicted very accurately by equation 74, the model gives a stronger dependence of D/D_∞ on r_s than was observed. These differences in slope notwithstanding, the agreement between the data and the predictions of equation 74 seems to us very impressive, given that there were no adjustable parameters in the calculations.

It was mentioned earlier that equation 74 gives values of D/D_∞ which agree very closely with the rigorous computational results of Phillips et al. (1989; 1990) for the diffusion of spheres of finite size normal to the axis of parallel arrays of fibers. One of the requirements in applying equation 74 to actual gels is that κ be known. As seen in Table

5.3, the correlation given by equation 78 can be counted on to give only the correct order of magnitude for κ. In Chapter 2 we estimated κ for sulfated agarose beads from equation 78 and, partly because of what seems to have been a cancellation of errors, obtained fairly accurate predictions of protein diffusivities from equation 73. Because κ was measured for each gel sample in the present study, we assume that the discrepancies in slope in Figures 5.1-5.3 have more to due with inaccuracies in the steric factor (S) than in the hydrodynamic factor (F). Although, as already discussed, the diffusion data are inconsistent with a regular, parallel arrangement of agarose fibers, the actual arrangement may differ from the random, overlapping network produced by the simulations leading to equation 80. In other words, at least for gels with relatively stiff polymer chains, the application of equation 74 may be limited more by an inadequate knowledge of the actual microstructure than by any inherent limitations in the effective medium approach.

There are potential effects of polymer structure on the diffusivities of macromolecules in gels. The most successful theory tested here, which uses equations 73 and 80 in equation 74, is based on fibers which are straight and immobile. Agarose fibers are expected to be relatively rigid, because they are aggregates formed from multiple polysaccharide chains. Indeed, there is little motion of agarose chains detectable by dynamic light scattering (Mackie et al., 1978), so that assuming that the fibers are stationary on the time scale of macromolecule diffusion should be an excellent approximation. Fibers in alginate gels have similar characteristics. However, the chains in gels formed from crosslinked polymers, such as polyacrylamide and dextran, may exhibit motions comparable to that of a diffusing solute. For example, Tanaka et al. (1973) reported a collective diffusivity for a 5% polyacrylamide gel, by dynamic light scattering, of 2.4×10^{-7} cm^2/s. An effect of fiber curvature on S is revealed by simulations of Johansson and Lofroth (1993) in which chains were constructed having various persistence lengths; when the persistence length was made sufficiently small, there were significant increases in S. However, those simulations were still based on immobile polymer chains.

A theory capable of describing the effects of local motions in a polymer chain on F and/or S would be of considerable interest.

There are similarities as well as differences between the diffusion of rigid spheres in gels and in semi-dilute (entangled) polymer solutions. In extremely dilute gels or solutions, there is negligible hindrance to diffusion, and the diffusivity is given by the Stokes-Einstein equation (a rearrangement of equation 77). When the system is not quite as dilute, but the diffusing macromolecule is still smaller than the typical separation between polymer chains ($r_s < \kappa^{1/2}$) the steric and hydrodynamic factors governing diffusion should be very similar in the two situations. Kosar and Phillips (1995) discuss theoretical evidence that hydrodynamic screening in a polymer solution is similar to that for an array of fixed obstacles, both conforming to the Brinkman model. For large macromolecules or particles ($r_s >> \kappa^{1/2}$), however, a gel and a polymer solution will behave quite differently. Whereas the crosslinked structure of the gel will eventually prevent translation of the particle, entanglements in a polymer solution can break and reform, so that the particle diffusivity does not fall to zero. Instead, as discussed by Kosar and Phillips (1995), there is a second Stokes-Einstein regime, with the applicable viscosity now being that of the polymer solution, rather than that of the solvent.

Chapter 6

6. Concluding Remarks

6.1 Conclusions

Electrostatic interactions, molecular size, and gel concentration have been examined for their effects on the partition and diffusion of macromolecules in gels. Before this thesis there had been few measurements of and no reliable method to predict the transport properties of macromolecules in charged gel membranes. Previous theoretical predictions for the partition coefficient ignored any colloidal interactions (other than steric) and predictions for the diffusion coefficient of macromolecules in gels had been unsuccessful. The work presented in this thesis both determined the effects of the fundamental molecular parameters on the transport coefficients and provided a method to theoretically predict the partition and diffusion coefficients of macromolecules in charged gels.

Measurements of the two transport coefficients for three proteins, BSA, ovalbumin and lactalbumin, in SP-Sepharose a sulfated agarose gel, demonstrate that the effects of electrostatic interactions are most pronounced in the partition coefficient, with only small contributions to the diffusion coefficient for the smallest protein at the lowest ionic strength. Sulfated agarose gels were chosen because they do not swell or shrink with changing ionic strength, thus keeping the microstructure of the gel constant with changing electrostatic interactions. The experimental methods allowed the direct measurement of both the partitioning and diffusion coefficient. While the partition coefficient was measured using a mass balance on a recirculated gel chromatography column, the diffusivity was

directly measured with fluorescence recovery after photobleaching (FRAP). Most traditional methods of measuring the diffusion coefficient gave values for the effective diffusivity (which is the product of the partition coefficient and the diffusivity) so consequently the diffusivity could not be directly measured, resulting in large errors in reported diffusivities. Using FRAP with a spatial Fourier transform analysis allowed the determination of the diffusivity in light scattering media such as agarose gel. Without this special analysis, there are errors in the measured diffusivity (as discussed in Chapter 2). By determining that the effects of electrostatic interactions were primarily governed by the partition coefficient, this allowed the separation of the theoretical modeling of the transport problem into two areas; the electrostatic effects on the partitioning of macromolecules into charged gels and the prediction of the diffusion coefficient in uncharged gels.

With the theoretical model presented in Chapter 3, predictions for the partition coefficient can be readily made knowing the fundamental molecular parameters, the size of the macromolecule, the volume fraction of fibers in the gel, the radius of the gel fiber, the ionic strength of the buffer and the surface charge densities on the macromolecule and the gel. When comparing the theoretical model predictions to experimental data for the partitioning of two proteins, BSA and β-lactoglobulin in Superose 6 (a 6% agarose gel), there was very good agreement. One of the inherent limitations to the theoretical model is that the electrostatic potentials must be low (because we used the linearized Poisson-Boltzmann equation in determining the energy of interaction) thus restricting the partitioning model to macromolecule / gel systems in which the surface charge densities are low. Application of this model to highly charged gels would result in an underprediction of the partition coefficient. In addition, the theoretical predictions should only be made for relatively dilute gels. By assuming that the energy of interaction is governed primarily by the macromolecule and its nearest fiber, the contributions from the other surrounding fibers were neglected. When the gel becomes more concentrated, the electrostatic contributions from the other fibers may not be negligible. The main benefit of this theoretical model is

that predictions can be made for the effects of electrostatic interactions on the partition coefficient only from the independently measurable molecular parameters.

After determining that the effects of electrostatic interactions were small on the diffusion coefficient, our experimental and theoretical efforts focused on the effects of molecular size, gel concentration, and gel microstructure. While the size of the macromolecules and the gel concentration are readily available, the details of the agarose microstructure had not been completely determined. The average fiber radius of the agarose gel had been measured as reviewed in section 1.6, however, a key parameter, the Darcy permeability had not been determined. A review of the literature (see section 1.5.3) showed that wide discrepancies between permeability measurements for polyacrylamide and gelatin. In addition, special equipment was needed to measure high pressures and/or low flow rates because the gel were cast into thick gels. To eliminate the need for the special equipment, a novel method for casting the gels onto an ultrathin polyester mesh support was developed. A commercially available ultrafiltration cell could then be used to measure the permeabilities. Darcy permeabilities measured for agarose concentrations ranging between 2% and 7.3% showed a power law dependence with the permeability decreasing with increasing gel concentration as described in Chapter 4. After characterizing the gel microstructure with the Darcy permeability, the diffusion coefficient of proteins and ficolls in a range of agarose concentrations was determined. Quantification of the effects of macromolecular size and gel concentration on the diffusivity showed conclusively that as the gel concentration increased and the solute size increased the reduced diffusivity (D/D_∞) decreased as explained in Chapter 5. With this experimental data, an effective medium theory proposed by Brady (1994) that made use of the Brinkman's equation for the hydrodynamic resistance and molecular simulations that predicted the tortuosity through the gel network was evaluated. Comparisons between the effective medium theory and the diffusivity measurements in agarose were remarkably good especially considering that the only parameters needed for the theory were the size of the solute and the gel fiber and the

Darcy permeability of the gel. The effective medium model proved to predict diffusivites very well.

With the theoretical models for the partition and diffusion coefficients, the transport of charged solutes through charged gels can now be predicted using independently measurable parameters.

6.2 Recommendations for future work

While the comparisons between the theoretical models for the partition and diffusion coefficients and the experimental data were very favorable, there are a number of notable restrictions to their use. In particular, the partition coefficient is limited to low surface charge densities, dilute gels and higher ionic strengths. It would be of use to extend the range of this theory. To incorporate higher surface charge densities, the non-linear Poisson-Boltzmann equaiton would need to be solved for the energy of interaction. To look at higher gel concentrations and lower ionic strengths, the incorporation of the electrostatic interactions from the other fibers would be needed. In addition to extending the presented theory, it would also be of interest to further evaluate the model with more experimental data. There was only limited data available to compare the model to. More measurements of proteins in agarose and other slightly charged gels is needed to give a complete evaluation of the validity of the theoretical predictions for the partition coefficient.

The pedictions from the effective medium theory for the proteins and ficolls in agarose gel compared very favorably. however, agarose is a gel that has very rigid fibers and so consequently the microstructure does not change with time or environmental conditions. It would be of interest to determin how well this model works for other polymer gels that have significantly more flexibility and mobility on the microscale. Possible gels to examine could include cross-linked dextran and polyacrylamide. In addition, many biological systems are composed of complex mixtures of polymers.

Measurements of the diffusivity through complex gels may yield a greater understanding of the link between the gel microstructure and the reduction in diffusivity. These experiments could be readily performed using either the FRAP technique described in Chapter 2 or using a standard diffusion cell.

While this thesis has been mostly concerned with the diffusive transport of macromolecules through gels, convective transport is important in many biological and industrial systems. There has been no experimental determination or proposed theories to describe the convective transport of macromolecules through gels. It would be of great interest to determine what effect the gel structure and colloidal interactions have on convective transport. Experimentally, fluorescence recovery after photobleaching can be used effectively to determine the convective transport of fluorescently labeled macromolecules.

Appendix A

A.1 Free Energy Calculations for a Sphere and a Cylinder

The free energy calculations for a sphere near a cylinder calculated using a finite element solver program, FIDAP, as discussed in Chapter 3 are given in Table A.1. In addition the linear superposition approximation was used to approximate the free energy and those values are also listed in Table A.1. For the numerical simulations, the free energy was calculated by solving the linearized Poisson-Boltzmann equation (equation 47) for a sphere near a cylinder. Because there are two planes of symmetry it is only necessary to calculate the energy of interaction for one-quarter sphere near a one-quarter cylinder and multiply ther resulting value by four. This was done for all variations given in Table A.1. To calcualte the change in free energy from the solution to the Poisson-Boltzmann equation, the surface potential values were obtained from the FIDAP output and integrated over the surface of the sphere and cylinder using a Fortran program given in the following section to five the free energy values. The free energy was calculated at two element densities (972) and (2304) and Richardson's extrapolation used to obtain the most accurate value of the free energy as discussed in section 3.3.2.

Table A.1 Summary of sphere / cylinder free energy calculations.

r_s	r_f	$1/\tau$	σ_s	σ_f	h	κh	ΔG	Linear Sup. Approx
1	0.25	0.1	1	1	0.3000	3.000	0.00216984	0.00115500
1	0.25	0.1	1	1	0.2500	2.500	0.00354876	0.00193600
1	0.25	0.1	1	1	0.2000	2.000	0.00594238	0.00324500
1	0.25	0.1	1	1	0.1750	1.750	0.00776984	0.00420200
1	0.25	0.1	1	1	0.1500	1.500	0.01022065	0.00544300
1	0.25	0.1	1	1	0.1250	1.250	0.01355373	0.00705300
1	0.25	0.1	1	1	0.1000	1.000	0.01820259	0.00913700
1	0.25	0.1	1	1	0.0875	0.875	0.02121416	0.01040200
1	0.25	0.1	1	1	0.0750	0.750	0.02486724	0.01184100
1	0.25	0.1	1	1	0.0625	0.625	0.02934108	0.01347900
1	0.25	0.1	1	1	0.0500	0.500	0.03496443	0.01534500
1	0.25	0.1	1	1	0.0375	0.375	0.04221470	0.01747100
1	0.25	0.1	1	1	0.0250	0.250	0.05206757	0.01989100
1	0.25	0.1	1	1	0.0125	0.125	0.06689254	0.02264600
1	0.25	0.1	2	1	0.2000	2.000	0.01186584	0.00649000
1	0.25	0.1	2	1	0.1000	1.000	0.03729297	0.01827300
1	0.25	0.1	2	1	0.0500	0.500	0.07327881	0.03068900
1	0.25	0.1	2	1	0.0125	0.125	0.14355178	0.04529100
1	0.25	0.1	4	1	0.2000	2.000	0.02429849	0.01298000
1	0.25	0.1	4	1	0.1000	1.000	0.08139676	0.03654500
1	0.25	0.1	4	1	0.0500	0.500	0.16951178	0.06137100
1	0.25	0.1	4	1	0.0125	0.125	0.35301362	0.09057500
1	0.25	0.1	8	1	0.2000	2.000	0.05152054	0.02595500
1	0.25	0.1	8	1	0.1000	1.000	0.19326757	0.07308200
1	0.25	0.1	8	1	0.0500	0.500	0.44020238	0.12273800
1	0.25	0.1	8	1	0.0125	0.125	0.99642584	0.18114400
1	0.25	0.1	1	2	0.2000	2.000	0.01223622	0.00649000
1	0.25	0.1	1	2	0.1000	1.000	0.03754378	0.01827300
1	0.25	0.1	1	2	0.0500	0.500	0.07299427	0.03069100
1	0.25	0.1	1	2	0.0125	0.125	0.14233978	0.04529400
1	0.25	0.1	1	4	0.2000	2.000	0.02614854	0.01298200
1	0.25	0.1	1	4	0.1000	1.000	0.08262530	0.03654500
1	0.25	0.1	1	4	0.0500	0.500	0.16809416	0.06137200
1	0.25	0.1	1	4	0.0125	0.125	0.34702616	0.09057800
1	0.25	0.1	1	8	0.2000	2.000	0.05928454	0.02596100
1	0.25	0.1	1	8	0.1000	1.000	0.19834054	0.07308700
1	0.25	0.1	1	8	0.0500	0.500	0.43438670	0.12274400
1	0.25	0.1	1	8	0.0125	0.125	0.97138605	0.18114400

1	0.25	0.5	1	1	1.5000	3.000	0.02023059	0.01613000
1	0.25	0.5	1	1	1.2500	2.500	0.03488800	0.02785000
1	0.25	0.5	1	1	1.0000	2.000	0.06080519	0.04830600
1	0.25	0.5	1	1	0.8750	1.750	0.08065795	0.06374700
1	0.25	0.5	1	1	0.7500	1.500	0.10742832	0.08425700
1	0.25	0.5	1	1	0.6250	1.250	0.14388605	0.11156200
1	0.25	0.5	1	1	0.5000	1.000	0.19414854	0.14801000
1	0.25	0.5	1	1	0.4375	0.875	0.22638184	0.01706250
1	0.25	0.5	1	1	0.3750	0.750	0.26484616	0.19681500
1	0.25	0.5	1	1	0.3125	0.625	0.31119373	0.22716800
1	0.25	0.5	1	1	0.2500	0.500	0.36776659	0.26239200
1	0.25	0.5	1	1	0.1875	0.375	0.43807232	0.30330800
1	0.25	0.5	1	1	0.1250	0.250	0.52808205	0.35090300
1	0.25	0.5	1	1	0.0625	0.125	0.64979016	0.40633300
1	0.25	0.5	2	1	1.0000	2.000	0.12174184	0.09661200
1	0.25	0.5	2	1	0.5000	1.000	0.39304605	0.29601000
1	0.25	0.5	2	1	0.2500	0.500	0.75440638	0.52475300
1	0.25	0.5	2	1	0.0625	0.125	1.35589524	0.81258500
1	0.25	0.5	4	1	1.0000	2.000	0.24585157	0.19322500
1	0.25	0.5	4	1	0.5000	1.000	0.82080184	0.59200100
1	0.25	0.5	4	1	0.2500	0.500	1.64019438	1.04944800
1	0.25	0.5	4	1	0.0625	0.125	3.10500843	1.62508600
1	0.25	0.5	8	1	1.0000	2.000	0.50294022	0.38645100
1	0.25	0.5	8	1	0.5000	1.000	1.79630216	1.18392000
1	0.25	0.5	8	1	0.2500	0.500	3.86160486	2.09879700
1	0.25	0.5	8	1	0.0625	0.125	7.95059351	3.25008800
1	0.25	0.5	1	2	1.0000	2.000	0.12245384	0.09661000
1	0.25	0.5	1	2	0.5000	1.000	0.39375059	0.29601800
1	0.25	0.5	1	2	0.2500	0.500	0.75390778	0.52481300
1	0.25	0.5	1	2	0.0625	0.125	1.35535157	0.81271200
1	0.25	0.5	1	4	1.0000	2.000	0.24940973	0.19321600
1	0.25	0.5	1	4	0.5000	1.000	0.82446757	0.59203200
1	0.25	0.5	1	4	0.2500	0.500	1.63766800	1.04962900
1	0.25	0.5	1	4	0.0625	0.125	3.10231146	1.62548700
1	0.25	0.5	1	8	1.0000	2.000	0.51790854	0.38641100
1	0.25	0.5	1	8	0.5000	1.000	1.81160162	1.18405200
1	0.25	0.5	1	8	0.2500	0.500	3.85055319	2.09921400
1	0.25	0.5	1	8	0.0625	0.125	7.93960292	3.25095900
1	0.25	1.0	1	1	3.0000	3.000	0.03902076	0.03488300
1	0.25	1.0	1	1	2.5000	2.500	0.06780941	0.06106700
1	0.25	1.0	1	1	2.0000	2.000	0.11945168	0.10776400
1	0.25	1.0	1	1	1.7500	1.750	0.15943957	0.14369300
1	0.25	1.0	1	1	1.5000	1.500	0.21383319	0.19218700

1	0.25	1.0	1	1	1.2500	1.250	0.28841200	0.25798100
1	0.25	1.0	1	1	1.0000	1.000	0.39192530	0.34780800
1	0.25	1.0	1	1	0.8750	0.875	0.45816757	0.40459600
1	0.25	1.0	1	1	0.7500	0.750	0.53713492	0.47136000
1	0.25	1.0	1	1	0.6250	0.625	0.63193189	0.55004200
1	0.25	1.0	1	1	0.5000	0.500	0.74710757	0.64305100
1	0.25	1.0	1	1	0.3750	0.375	0.88883892	0.75339800
1	0.25	1.0	1	1	0.2500	0.250	1.06779805	0.88488300
1	0.25	1.0	1	1	0.1250	0.125	1.30613243	1.04227300
1	0.25	1.0	2	1	2.0000	2.000	0.23824065	0.21552800
1	0.25	1.0	2	1	1.0000	1.000	0.78538076	0.69552900
1	0.25	1.0	2	1	0.5000	0.500	1.51043838	1.28590400
1	0.25	1.0	2	1	0.1250	0.125	2.89492357	2.08425200
1	0.25	1.0	4	1	2.0000	2.000	0.47565914	0.43105700
1	0.25	1.0	4	1	1.0000	1.000	1.59140800	1.39081100
1	0.25	1.0	4	1	0.5000	0.500	3.13870649	2.57146000
1	0.25	1.0	4	1	0.1250	0.125	5.84700930	4.16815100
1	0.25	1.0	8	1	2.0000	2.000	0.94975546	0.86211000
1	0.25	1.0	8	1	1.0000	1.000	3.28030984	2.78137300
1	0.25	1.0	8	1	0.5000	0.500	6.80128303	5.14266800
1	0.25	1.0	8	1	0.1250	0.125	13.75350605	8.33598000
1	0.25	1.0	1	2	2.0000	2.000	0.24015903	0.21552600
1	0.25	1.0	1	2	1.0000	1.000	0.79048378	0.69561400
1	0.25	1.0	1	2	0.5000	0.500	1.51216519	1.28629500
1	0.25	1.0	1	2	0.1250	0.125	2.66043827	2.42551300
1	0.25	1.0	1	4	2.0000	2.000	0.48521384	0.43104300
1	0.25	1.0	1	4	1.0000	1.000	1.61683589	1.39121900
1	0.25	1.0	1	4	0.5000	0.500	3.14642746	2.57299800
1	0.25	1.0	1	4	0.1250	0.125	5.71106205	4.17089200
1	0.25	1.0	1	8	2.0000	2.000	0.98995708	0.86205100
1	0.25	1.0	1	8	1.0000	1.000	3.38740465	2.78240400
1	0.25	1.0	1	8	0.5000	0.500	6.83421189	5.14596100
1	0.25	1.0	1	8	0.1250	0.125	13.18192497	8.34367600
1	0.25	2.0	1	1	6.0000	3.000	0.06338973	0.05638500
1	0.25	2.0	1	1	5.0000	2.500	0.10944043	0.10027700
1	0.25	2.0	1	1	4.0000	2.000	0.19332292	0.18029600
1	0.25	2.0	1	1	3.5000	1.750	0.25911211	0.24306500
1	0.25	2.0	1	1	3.0000	1.500	0.34940649	0.32920600
1	0.25	2.0	1	1	2.5000	1.250	0.47476216	0.44844600
1	0.25	2.0	1	1	2.0000	1.000	0.65117146	0.61537300
1	0.25	2.0	1	1	1.7500	0.875	0.76604173	0.72334600
1	0.25	2.0	1	1	1.5000	0.750	0.90456714	0.85264700
1	0.25	2.0	1	1	1.2500	0.625	1.07310876	1.00838700

1	0.25	2.0	1	1	1.0000	0.500	1.28041589	1.19730000
1	0.25	2.0	1	1	0.7500	0.375	1.53827773	1.42836800
1	0.25	2.0	1	1	0.5000	0.250	1.86755395	1.71432100
1	0.25	2.0	1	1	0.2500	0.125	2.30817427	2.07349800
1	0.25	2.0	2	1	4.0000	2.000	0.38516714	0.36059200
1	0.25	2.0	2	1	2.0000	1.000	1.29954627	1.23074600
1	0.25	2.0	2	1	1.0000	0.500	2.56261146	2.39432200
1	0.25	2.0	2	1	0.2500	0.125	4.67355622	4.14652600
1	0.25	2.0	4	1	4.0000	2.000	0.77138022	0.72118400
1	0.25	2.0	4	1	2.0000	1.000	2.60572270	2.46149100
1	0.25	2.0	4	1	1.0000	0.500	5.19270551	4.78817000
1	0.25	2.0	4	1	0.2500	0.125	9.77555351	8.29241100
1	0.25	2.0	8	1	4.0000	2.000	1.55385362	1.44236200
1	0.25	2.0	8	1	2.0000	1.000	5.25471297	4.92271800
1	0.25	2.0	8	1	1.0000	0.500	10.71546973	9.57556000
1	0.25	2.0	8	1	0.2500	0.125	21.46967892	16.58410500
1	0.25	2.0	1	2	4.0000	2.000	0.39084973	0.36058900
1	0.25	2.0	1	2	2.0000	1.000	1.31253124	1.23074300
1	0.25	2.0	1	2	1.0000	0.500	2.59017092	2.39460600
1	0.25	2.0	1	2	0.2500	0.125	4.68836130	4.14773000
1	0.25	2.0	1	4	4.0000	2.000	0.79977535	0.72116800
1	0.25	2.0	1	4	2.0000	1.000	2.67044865	2.46147600
1	0.25	2.0	1	4	1.0000	0.500	5.32908011	4.78920200
1	0.25	2.0	1	4	0.2500	0.125	9.84760443	8.29668900
1	0.25	2.0	1	8	4.0000	2.000	1.67311859	1.44229600
1	0.25	2.0	1	8	2.0000	1.000	5.52706065	4.92291200
1	0.25	2.0	1	8	1.0000	0.500	11.28894595	9.57836300
1	0.25	2.0	1	8	0.2500	0.125	21.76751881	16.59470200
1	0.25	3.0	1	1	9.0000	3.000	0.09950843	0.06603000
1	0.25	3.0	1	1	7.5000	2.500	0.15585503	0.11862700
1	0.25	3.0	1	1	6.0000	2.000	0.25876638	0.21586100
1	0.25	3.0	1	1	5.2500	1.750	0.33977914	0.29303900
1	0.25	3.0	1	1	4.5000	1.500	0.45173232	0.40000800
1	0.25	3.0	1	1	3.7500	1.250	0.60798043	0.54981800
1	0.25	3.0	1	1	3.0000	1.000	0.82954724	0.76260700
1	0.25	3.0	1	1	2.6250	0.875	0.97536000	0.90206500
1	0.25	3.0	1	1	2.2500	0.750	1.15182605	1.07092100
1	0.25	3.0	1	1	1.8750	0.625	1.36836249	1.27702700
1	0.25	3.0	1	1	1.5000	0.500	1.63735721	1.56311830
1	0.25	3.0	1	1	1.1250	0.375	1.97806811	1.84882500
1	0.25	3.0	1	1	0.7500	0.250	2.42019081	2.25317400
1	0.25	3.0	1	1	0.3750	0.125	3.02622151	2.78175300
1	0.25	3.0	2	1	6.0000	2.000	0.50923643	0.43171800

1	0.25	3.0	2	1	3.0000	1.000	1.64831351	1.52521000
1	0.25	3.0	2	1	1.5000	0.500	3.26277978	3.06236200
1	0.25	3.0	2	1	0.3750	0.125	6.08879200	5.56357700
1	0.25	3.0	4	1	6.0000	2.000	1.04112724	0.86313200
1	0.25	3.0	4	1	3.0000	1.000	3.31661265	3.05041200
1	0.25	3.0	4	1	1.5000	0.500	6.57603578	6.12472100
1	0.25	3.0	4	1	0.3750	0.125	12.56528259	11.12729100
1	0.25	3.0	8	1	6.0000	2.000	2.22871308	1.72685600
1	0.25	3.0	8	1	3.0000	1.000	6.77807730	6.10081700
1	0.25	3.0	8	1	1.5000	0.500	13.45469751	12.24945500
1	0.25	3.0	8	1	0.3750	0.125	26.92497773	22.25461000
1	0.25	3.0	1	2	6.0000	2.000	0.54961968	0.43173700
1	0.25	3.0	1	2	3.0000	1.000	1.69760694	1.52523200
1	0.25	3.0	1	2	1.5000	0.500	3.33042627	3.06237700
1	0.25	3.0	1	2	0.3750	0.125	6.15433957	5.55634970
1	0.25	3.0	1	4	6.0000	2.000	1.24275232	0.86346700
1	0.25	3.0	1	4	3.0000	1.000	3.56325200	3.05053200
1	0.25	3.0	1	4	1.5000	0.500	6.91467535	6.12479300
1	0.25	3.0	1	4	0.3750	0.125	12.89142508	11.12701600
1	0.25	3.0	1	8	6.0000	2.000	3.07689297	1.72689200
1	0.25	3.0	1	8	3.0000	1.000	7.81398854	6.10137400
1	0.25	3.0	1	8	1.5000	0.500	14.87618659	12.24986100
1	0.25	3.0	1	8	0.3750	0.125	28.28302724	22.25413600
1	0.50	0.1	1	1	0.3000	3.000	0.00294249	0.00153000
1	0.50	0.1	1	1	0.2500	2.500	0.00486832	0.00255800
1	0.50	0.1	1	1	0.2000	2.000	0.00822962	0.00427900
1	0.50	0.1	1	1	0.1750	1.750	0.01078800	0.00553500
1	0.50	0.1	1	1	0.1500	1.500	0.01424357	0.00715900
1	0.50	0.1	1	1	0.1250	1.250	0.01898108	0.00926400
1	0.50	0.1	1	1	0.1000	1.000	0.02561838	0.01198600
1	0.50	0.1	1	1	0.0875	0.875	0.02997514	0.01363600
1	0.50	0.1	1	1	0.0750	0.750	0.03527741	0.01551100
1	0.50	0.1	1	1	0.0625	0.625	0.04184703	0.01764500
1	0.50	0.1	1	1	0.0500	0.500	0.05016984	0.02007400
1	0.50	0.1	1	1	0.0375	0.375	0.06106184	0.02283600
1	0.50	0.1	1	1	0.0250	0.250	0.07609903	0.02598000
1	0.50	0.1	1	1	0.0125	0.125	0.09914497	0.02955700
1	0.50	0.1	2	1	0.2000	2.000	0.01650324	0.00855800
1	0.50	0.1	2	1	0.1000	1.000	0.05235114	0.02396900
1	0.50	0.1	2	1	0.0500	0.500	0.10499514	0.04014500
1	0.50	0.1	2	1	0.0125	0.125	0.21240778	0.05911900
1	0.50	0.1	4	1	0.2000	2.000	0.03400497	0.01711600
1	0.50	0.1	4	1	0.1000	1.000	0.11537935	0.04793700

1	0.50	0.1	4	1	0.0500	0.500	0.24437395	0.08027700
1	0.50	0.1	4	1	0.0125	0.125	0.52582897	0.11823100
1	0.50	0.1	8	1	0.2000	2.000	0.07280703	0.03422600
1	0.50	0.1	8	1	0.1000	1.000	0.27712984	0.09586600
1	0.50	0.1	8	1	0.0500	0.500	0.64184497	0.16054800
1	0.50	0.1	8	1	0.0125	0.125	1.50049881	0.23642800
1	0.50	0.1	1	2	0.2000	2.000	0.01683135	0.00855900
1	0.50	0.1	1	2	0.1000	1.000	0.05314984	0.02397100
1	0.50	0.1	1	2	0.0500	0.500	0.10589178	0.04014700
1	0.50	0.1	1	2	0.0125	0.125	0.21356173	0.05911900
1	0.50	0.1	1	4	0.2000	2.000	0.03560541	0.01711800
1	0.50	0.1	1	4	0.1000	1.000	0.11840649	0.04793900
1	0.50	0.1	1	4	0.0500	0.500	0.24886130	0.08028100
1	0.50	0.1	1	4	0.0125	0.125	0.53166238	0.11822200
1	0.50	0.1	1	8	0.2000	2.000	0.07950843	0.03423200
1	0.50	0.1	1	8	0.1000	1.000	0.28979135	0.09587600
1	0.50	0.1	1	8	0.0500	0.500	0.66088184	0.16055800
1	0.50	0.1	1	8	0.0125	0.125	1.52493622	0.23644000
1	0.50	0.5	1	1	1.5000	3.000	0.03235189	0.02392300
1	0.50	0.5	1	1	1.2500	2.500	0.05577795	0.04114600
1	0.50	0.5	1	1	1.0000	2.000	0.09712941	0.07103600
1	0.50	0.5	1	1	0.8750	1.750	0.12880259	0.09349200
1	0.50	0.5	1	1	0.7500	1.500	0.17158530	0.12320200
1	0.50	0.5	1	1	0.6250	1.250	0.22997816	0.16258200
1	0.50	0.5	1	1	0.5000	1.000	0.31094789	0.21488400
1	0.50	0.5	1	1	0.4375	0.875	0.36316000	0.24720300
1	0.50	0.5	1	1	0.3750	0.750	0.42584984	0.28451500
1	0.50	0.5	1	1	0.3125	0.625	0.50197578	0.32762200
1	0.50	0.5	1	1	0.2500	0.500	0.59582497	0.37745300
1	0.50	0.5	1	1	0.1875	0.375	0.71404011	0.43511200
1	0.50	0.5	1	1	0.1250	0.250	0.86838951	0.50189000
1	0.50	0.5	1	1	0.0625	0.125	1.08379092	0.57930900
1	0.50	0.5	2	1	1.0000	2.000	0.19453373	0.14207200
1	0.50	0.5	2	1	0.5000	1.000	0.62936865	0.42976900
1	0.50	0.5	2	1	0.2500	0.500	1.22271470	0.75488000
1	0.50	0.5	2	1	0.0625	0.125	2.26866832	1.15853000
1	0.50	0.5	4	1	1.0000	2.000	0.39419373	0.28414500
1	0.50	0.5	4	1	0.5000	1.000	1.32486454	0.85949700
1	0.50	0.5	4	1	0.2500	0.500	2.69284076	1.50963100
1	0.50	0.5	4	1	0.0625	0.125	5.29471178	2.31691200
1	0.50	0.5	8	1	1.0000	2.000	0.81285535	0.56289000
1	0.50	0.5	8	1	0.5000	1.000	2.95119957	1.71887200
1	0.50	0.5	8	1	0.2500	0.500	6.49860086	3.01912400

1	0.50	0.5	8	1	0.0625	0.125	13.97258584	4.63362400
1	0.50	0.5	1	2	1.0000	2.000	0.19613719	0.14207200
1	0.50	0.5	1	2	0.5000	1.000	0.63623773	0.42976900
1	0.50	0.5	1	2	0.2500	0.500	1.23738162	0.75492500
1	0.50	0.5	1	2	0.0625	0.125	2.29339178	1.15870500
1	0.50	0.5	1	4	1.0000	2.000	0.40218259	0.28414400
1	0.50	0.5	1	4	0.5000	1.000	1.35949849	0.82953700
1	0.50	0.5	1	4	0.2500	0.500	2.76608541	1.50986100
1	0.50	0.5	1	4	0.0625	0.125	5.41844076	2.31739100
1	0.50	0.5	1	8	1.0000	2.000	0.84645395	0.56828700
1	0.50	0.5	1	8	0.5000	1.000	3.09630562	1.71907800
1	0.50	0.5	1	8	0.2500	0.500	6.80474195	3.01972700
1	0.50	0.5	1	8	0.0625	0.125	14.49057405	4.63477400
1	0.50	1.0	1	1	3.0000	3.000	0.06685254	0.05746900
1	0.50	1.0	1	1	2.5000	2.500	0.11620216	0.10027200
1	0.50	1.0	1	1	2.0000	2.000	0.20444789	0.17618900
1	0.50	1.0	1	1	1.7500	1.750	0.27265578	0.23431200
1	0.50	1.0	1	1	1.5000	1.500	0.36535589	0.31242800
1	0.50	1.0	1	1	1.2500	1.250	0.49250151	0.41786300
1	0.50	1.0	1	1	1.0000	1.000	0.66932216	0.56090800
1	0.50	1.0	1	1	0.8750	0.875	0.78292919	0.65088900
1	0.50	1.0	1	1	0.7500	0.750	0.91893308	0.75616700
1	0.50	1.0	1	1	0.6250	0.625	1.08306768	0.87964000
1	0.50	1.0	1	1	0.5000	0.500	1.28415589	1.02479500
1	0.50	1.0	1	1	0.3750	0.375	1.53470076	1.19589300
1	0.50	1.0	1	1	0.2500	0.250	1.85695351	1.39814400
1	0.50	1.0	1	1	0.1250	0.125	2.29737968	1.63813000
1	0.50	1.0	2	1	2.0000	2.000	0.40802681	0.35237900
1	0.50	1.0	2	1	1.0000	1.000	1.34259676	1.12173600
1	0.50	1.0	2	1	0.5000	0.500	2.60127459	2.04940300
1	0.50	1.0	2	1	0.1250	0.125	4.74317492	3.27576900
1	0.50	1.0	4	1	2.0000	2.000	0.81782768	0.70475600
1	0.50	1.0	4	1	1.0000	1.000	2.74581568	2.24329800
1	0.50	1.0	4	1	0.5000	0.500	5.49344714	4.09815200
1	0.50	1.0	4	1	0.1250	0.125	10.57461643	6.55067500
1	0.50	1.0	8	1	2.0000	2.000	1.64810486	1.40950500
1	0.50	1.0	8	1	1.0000	1.000	5.77945319	4.48611500
1	0.50	1.0	8	1	0.5000	0.500	12.30985276	8.19544000
1	0.50	1.0	8	1	0.1250	0.125	25.99877070	13.10052500
1	0.50	1.0	1	2	2.0000	2.000	0.41195924	0.35237900
1	0.50	1.0	1	2	1.0000	1.000	1.35903751	1.12181600
1	0.50	1.0	1	2	0.5000	0.500	2.63070822	2.04995700
1	0.50	1.0	1	2	0.1250	0.125	4.76787286	3.27685000

1	0.50	1.0	1	4	2.0000	2.000	0.83745632	0.70475800
1	0.50	1.0	1	4	1.0000	1.000	2.82847838	2.24363200
1	0.50	1.0	1	4	0.5000	0.500	5.63959622	4.09991300
1	0.50	1.0	1	4	0.1250	0.125	10.69846670	6.55475400
1	0.50	1.0	1	8	2.0000	2.000	7.56711449	4.48726300
1	0.50	1.0	1	8	1.0000	1.000	6.12696076	4.48726300
1	0.50	1.0	1	8	0.5000	0.500	12.92638497	8.19982300
1	0.50	1.0	1	8	0.1250	0.125	26.51309319	13.11091900
1	0.50	2.0	1	1	6.0000	3.000	0.11660508	0.10060000
1	0.50	2.0	1	1	5.0000	2.500	0.20047676	0.17848600
1	0.50	2.0	1	1	4.0000	2.000	0.35218865	0.31989500
1	0.50	2.0	1	1	3.5000	1.750	0.47108584	0.43038200
1	0.50	2.0	1	1	3.0000	1.500	0.63384249	0.58146000
1	0.50	2.0	1	1	2.5000	1.250	0.85908778	0.78962300
1	0.50	2.0	1	1	2.0000	1.000	1.17535514	1.07927000
1	0.50	2.0	1	1	1.7500	0.875	1.38104865	1.26556800
1	0.50	2.0	1	1	1.5000	0.750	1.62897103	1.48759200
1	0.50	2.0	1	1	1.2500	0.625	1.93080022	1.75346600
1	0.50	2.0	1	1	1.0000	0.500	2.30248962	2.07370200
1	0.50	2.0	1	1	0.7500	0.375	2.76704097	2.46207200
1	0.50	2.0	1	1	0.5000	0.250	3.36564108	2.93727300
1	0.50	2.0	1	1	0.2500	0.125	4.18284043	3.52587000
1	0.50	2.0	2	1	4.0000	2.000	0.69836908	0.63979500
1	0.50	2.0	2	1	2.0000	1.000	2.34174627	2.15854500
1	0.50	2.0	2	1	1.0000	0.500	4.60690995	4.14723200
1	0.50	2.0	2	1	0.2500	0.125	8.48391730	7.04997300
1	0.50	2.0	4	1	4.0000	2.000	1.39482411	1.27959200
1	0.50	2.0	4	1	2.0000	1.000	4.70994184	4.31709400
1	0.50	2.0	4	1	1.0000	0.500	9.41589351	8.29377500
1	0.50	2.0	4	1	0.2500	0.125	18.07960022	14.09826300
1	0.50	2.0	8	1	4.0000	2.000	2.80407330	2.55918400
1	0.50	2.0	8	1	2.0000	1.000	9.58667254	8.63405600
1	0.50	2.0	8	1	1.0000	0.500	19.83636616	16.58625300
1	0.50	2.0	8	1	0.2500	0.125	41.24633276	28.19467200
1	0.50	2.0	1	2	4.0000	2.000	0.71843189	0.63978000
1	0.50	2.0	1	2	2.0000	1.000	2.38619827	2.15853100
1	0.50	2.0	1	2	1.0000	0.500	4.70149016	4.14739400
1	0.50	2.0	1	2	0.2500	0.125	8.62585189	7.05152400
1	0.50	2.0	1	4	4.0000	2.000	1.49513124	1.27952000
1	0.50	2.0	1	4	2.0000	1.000	4.93197557	4.31702100
1	0.50	2.0	1	4	1.0000	0.500	9.88794259	8.29474900
1	0.50	2.0	1	4	0.2500	0.125	18.78746746	14.10456300
1	0.50	2.0	1	8	4.0000	2.000	3.22534681	2.25588790

1	0.50	2.0	1	8	2.0000	1.000	10.51982216	8.63388100
1	0.50	2.0	1	8	1.0000	0.500	21.81960216	16.58933600
1	0.50	2.0	1	8	0.2500	0.125	44.22277232	28.20896500
1	0.50	3.0	1	1	9.0000	3.000	0.21767697	0.12171200
1	0.50	3.0	1	1	7.5000	2.500	0.32055200	0.21824900
1	0.50	3.0	1	1	6.0000	2.000	0.51101632	0.39613800
1	0.50	3.0	1	1	5.2500	1.750	0.66099492	0.53688000
1	0.50	3.0	1	1	4.5000	1.500	0.86791741	0.73136600
1	0.50	3.0	1	1	3.7500	1.250	1.15643665	1.00269400
1	0.50	3.0	1	1	3.0000	1.000	1.56393946	1.38606500
1	0.50	3.0	1	1	2.6250	0.875	1.83131103	1.63604000
1	0.50	3.0	1	1	2.2500	0.750	2.15446616	1.93736500
1	0.50	3.0	1	1	1.8750	0.625	2.55013795	2.41104100
1	0.50	3.0	1	1	1.5000	0.500	3.04110584	2.75091100
1	0.50	3.0	1	1	1.1250	0.375	3.66226595	3.30533900
1	0.50	3.0	1	1	0.7500	0.250	4.45383157	4.00308600
1	0.50	3.0	1	1	0.3750	0.125	5.58827719	4.89608800
1	0.50	3.0	2	1	6.0000	2.000	0.96309157	0.79226000
1	0.50	3.0	2	1	3.0000	1.000	3.06300032	2.77211300
1	0.50	3.0	2	1	1.5000	0.500	6.01475481	5.50180800
1	0.50	3.0	2	1	0.3750	0.125	11.20630389	9.79218100
1	0.50	3.0	4	1	6.0000	2.000	1.89906519	1.58451300
1	0.50	3.0	4	1	3.0000	1.000	6.10713351	5.54421300
1	0.50	3.0	4	1	1.5000	0.500	12.11863968	11.00359500
1	0.50	3.0	4	1	0.3750	0.125	23.35877589	19.58461600
1	0.50	3.0	8	1	6.0000	2.000	3.89827286	3.16902300
1	0.50	3.0	8	1	3.0000	1.000	12.38292238	11.08839700
1	0.50	3.0	8	1	1.5000	0.500	24.95732022	22.00719200
1	0.50	3.0	8	1	0.3750	0.125	51.32649200	39.16941200
1	0.50	3.0	1	2	6.0000	2.000	1.15582476	0.79228000
1	0.50	3.0	1	2	3.0000	1.000	3.28364681	2.77217100
1	0.50	3.0	1	2	1.5000	0.500	6.29607849	5.50184500
1	0.50	3.0	1	2	0.3750	0.125	11.57243092	9.79218300
1	0.50	3.0	1	4	6.0000	2.000	2.86277308	1.58451500
1	0.50	3.0	1	4	3.0000	1.000	7.21044259	6.06660000
1	0.50	3.0	1	4	1.5000	0.500	13.52661059	11.00382800
1	0.50	3.0	1	4	0.3750	0.125	25.18541189	19.58449000
1	0.50	3.0	1	8	6.0000	2.000	7.94633211	3.16884600
1	0.50	3.0	1	8	3.0000	1.000	17.01710000	11.08972700
1	0.50	3.0	1	8	1.5000	0.500	30.87011027	22.00857000
1	0.50	3.0	1	8	0.3750	0.125	58.99002530	39.16974600
1	0.75	0.1	1	1	0.3000	3.000	0.00338854	0.00176800
1	0.75	0.1	1	1	0.2500	2.500	0.00564205	0.00295000

1	0.75	0.1	1	1	0.2000	2.000	0.00958086	0.00492500
1	0.75	0.1	1	1	0.1750	1.750	0.01257308	0.00636500
1	0.75	0.1	1	1	0.1500	1.500	0.01662432	0.00822600
1	0.75	0.1	1	1	0.1250	1.250	0.02217568	0.01063300
1	0.75	0.1	1	1	0.1000	1.000	0.02999049	0.01374500
1	0.75	0.1	1	1	0.0875	0.875	0.03511524	0.01562900
1	0.75	0.1	1	1	0.0750	0.750	0.04139319	0.01776800
1	0.75	0.1	1	1	0.0625	0.625	0.04918941	0.02020100
1	0.75	0.1	1	1	0.0500	0.500	0.05909989	0.02296900
1	0.75	0.1	1	1	0.0375	0.375	0.07216800	0.02611800
1	0.75	0.1	1	1	0.0250	0.250	0.09036357	0.02969800
1	0.75	0.1	1	1	0.0125	0.125	0.11854346	0.03376900
1	0.75	0.1	2	1	0.2000	2.000	0.01929049	0.00985100
1	0.75	0.1	2	1	0.1000	1.000	0.06161989	0.02748700
1	0.75	0.1	2	1	0.0500	0.500	0.12382238	0.04593800
1	0.75	0.1	2	1	0.0125	0.125	0.25419946	0.06753700
1	0.75	0.1	4	1	0.2000	2.000	0.03987330	0.01970300
1	0.75	0.1	4	1	0.1000	1.000	0.13568854	0.05497100
1	0.75	0.1	4	1	0.0500	0.500	0.28907092	0.09186200
1	0.75	0.1	4	1	0.0125	0.125	0.63156843	0.13506300
1	0.75	0.1	8	1	0.2000	2.000	0.08569568	0.03940100
1	0.75	0.1	8	1	0.1000	1.000	0.32729211	0.10993400
1	0.75	0.1	8	1	0.0500	0.500	0.81039844	0.18371600
1	0.75	0.1	8	1	0.0125	0.125	1.81053351	0.27009300
1	0.75	0.1	1	2	0.2000	2.000	0.01947341	0.00985200
1	0.75	0.1	1	2	0.1000	1.000	0.06217351	0.02748600
1	0.75	0.1	1	2	0.0500	0.500	0.12490724	0.04593800
1	0.75	0.1	1	2	0.0125	0.125	0.25592638	0.06753200
1	0.75	0.1	1	4	0.2000	2.000	0.04077546	0.01970300
1	0.75	0.1	1	4	0.1000	1.000	0.13859341	0.05497000
1	0.75	0.1	1	4	0.0500	0.500	0.29452746	0.09185900
1	0.75	0.1	1	4	0.0125	0.125	0.64019027	0.13505000
1	0.75	0.1	1	8	0.2000	2.000	0.08950400	0.03939900
1	0.75	0.1	1	8	0.1000	1.000	0.33951395	0.13505000
1	0.75	0.1	1	8	0.0500	0.500	0.78570378	0.03939900
1	0.75	0.1	1	8	0.0125	0.125	1.84682454	0.27008900
1	0.75	0.5	1	1	1.5000	3.000	0.04104670	0.02873800
1	0.75	0.5	1	1	1.2500	2.500	0.07060919	0.04926600
1	0.75	0.5	1	1	1.0000	2.000	0.12266865	0.08472900
1	0.75	0.5	1	1	0.8750	1.750	0.16249114	0.11126800
1	0.75	0.5	1	1	0.7500	1.500	0.21624411	0.14627200
1	0.75	0.5	1	1	0.6250	1.250	0.28963632	0.19250700
1	0.75	0.5	1	1	0.5000	1.000	0.39150076	0.25367600

1	0.75	0.5	1	1	0.4375	0.875	0.45728022	0.29135400
1	0.75	0.5	1	1	0.3750	0.750	0.53639903	0.33475200
1	0.75	0.5	1	1	0.3125	0.625	0.63269557	0.38476500
1	0.75	0.5	1	1	0.2500	0.500	0.75179622	0.44243400
1	0.75	0.5	1	1	0.1875	0.375	0.90255395	0.50895300
1	0.75	0.5	1	1	0.1250	0.250	1.10069557	0.58574700
1	0.75	0.5	1	1	0.0625	0.125	1.38026443	0.67447800
1	0.75	0.5	2	1	1.0000	2.000	0.24545449	0.16945900
1	0.75	0.5	2	1	0.5000	1.000	0.79095643	0.50735300
1	0.75	0.5	2	1	0.2500	0.500	1.53988508	0.88479300
1	0.75	0.5	2	1	0.0625	0.125	2.88634605	1.34889000
1	0.75	0.5	4	1	1.0000	2.000	0.49772411	0.33891900
1	0.75	0.5	4	1	0.5000	1.000	1.66827676	1.01463700
1	0.75	0.5	4	1	0.2500	0.500	3.40212108	1.76945600
1	0.75	0.5	4	1	0.0625	0.125	6.77050886	2.69763200
1	0.75	0.5	8	1	1.0000	2.000	1.02890649	0.67783900
1	0.75	0.5	8	1	0.5000	1.000	3.70325503	2.02914900
1	0.75	0.5	8	1	0.2500	0.500	8.27135578	0.88470100
1	0.75	0.5	8	1	0.0625	0.125	18.02770043	5.39504400
1	0.75	0.5	1	2	1.0000	2.000	0.24843038	0.16945600
1	0.75	0.5	1	2	0.5000	1.000	0.80603589	0.50735000
1	0.75	0.5	1	2	0.2500	0.500	1.57401686	0.88486600
1	0.75	0.5	1	2	0.0625	0.125	2.94464876	1.34909700
1	0.75	0.5	1	4	1.0000	2.000	0.51259189	0.33890500
1	0.75	0.5	1	4	0.5000	1.000	1.74370649	1.01469200
1	0.75	0.5	1	4	0.2500	0.500	3.57314022	1.76974100
1	0.75	0.5	1	4	0.0625	0.125	7.06281589	2.69817200
1	0.75	0.5	1	8	1.0000	2.000	1.09143978	0.67778100
1	0.75	0.5	1	8	0.5000	1.000	4.05308530	2.02936000
1	0.75	0.5	1	8	0.2500	0.500	8.98803059	3.53943600
1	0.75	0.5	1	8	0.0625	0.125	19.25290573	5.39631900
1	0.75	1.0	1	1	3.0000	3.000	0.08874627	0.07324900
1	0.75	1.0	1	1	2.5000	2.500	0.15404281	0.12742400
1	0.75	1.0	1	1	2.0000	2.000	0.27035157	0.22305400
1	0.75	1.0	1	1	1.7500	1.750	0.36000930	0.29595900
1	0.75	1.0	1	1	1.5000	1.500	0.48165535	0.39358500
1	0.75	1.0	1	1	1.2500	1.250	0.64826670	0.52479100
1	0.75	1.0	1	1	1.0000	1.000	0.87988584	0.70188400
1	0.75	1.0	1	1	0.8750	0.875	1.02869168	0.81279100
1	0.75	1.0	1	1	0.7500	0.750	1.20746584	0.94215500
1	0.75	1.0	1	1	0.6250	0.625	1.42297049	1.09320100
1	0.75	1.0	1	1	0.5000	0.500	1.68750897	1.27003700
1	0.75	1.0	1	1	0.3750	0.375	2.01878400	1.47748200

1	0.75	1.0	1	1	0.2500	0.250	2.44678422	1.72120300
1	0.75	1.0	1	1	0.1250	0.125	3.03586249	2.00863900
1	0.75	1.0	2	1	2.0000	2.000	0.53886843	0.44610800
1	0.75	1.0	2	1	1.0000	1.000	1.76242303	1.40370600
1	0.75	1.0	2	1	0.5000	0.500	3.41269989	2.53980600
1	0.75	1.0	2	1	0.1250	0.125	6.25927254	4.01671300
1	0.75	1.0	4	1	2.0000	2.000	1.08092703	0.89221500
1	0.75	1.0	4	1	1.0000	1.000	3.62062249	2.80727300
1	0.75	1.0	4	1	0.5000	0.500	7.24283103	5.07897600
1	0.75	1.0	4	1	0.1250	0.125	14.05822735	8.03258100
1	0.75	1.0	8	1	2.0000	2.000	2.18534649	1.78442400
1	0.75	1.0	8	1	1.0000	1.000	7.66710930	5.61385500
1	0.75	1.0	8	1	0.5000	0.500	16.42414411	10.15703900
1	0.75	1.0	8	1	0.1250	0.125	35.07094941	16.06372800
1	0.75	1.0	1	2	2.0000	2.000	0.54690097	0.44610800
1	0.75	1.0	1	2	1.0000	1.000	1.79779038	1.40376800
1	0.75	1.0	1	2	0.5000	0.500	3.48982465	2.54043100
1	0.75	1.0	1	2	0.1250	0.125	6.37437665	4.01786900
1	0.75	1.0	1	4	2.0000	2.000	1.12107405	0.89221200
1	0.75	1.0	1	4	1.0000	1.000	3.79226162	2.80753200
1	0.75	1.0	1	4	0.5000	0.500	7.62774714	5.08085800
1	0.75	1.0	1	4	0.1250	0.125	14.63268108	8.03748200
1	0.75	1.0	1	8	2.0000	2.000	2.35377557	1.78441000
1	0.75	1.0	1	8	1.0000	1.000	8.41484854	5.61505100
1	0.75	1.0	1	8	0.5000	0.500	18.04379265	10.16170200
1	0.75	1.0	1	8	0.1250	0.125	37.48442112	16.07495000
1	0.75	2.0	1	1	6.0000	3.000	0.16248735	0.13617300
1	0.75	2.0	1	1	5.0000	2.500	0.27954032	0.24104700
1	0.75	2.0	1	1	4.0000	2.000	0.48949795	0.43072700
1	0.75	2.0	1	1	3.5000	1.750	0.65241568	0.57839700
1	0.75	2.0	1	1	3.0000	1.500	0.87572541	0.77965700
1	0.75	2.0	1	1	2.5000	1.250	1.18357168	1.05582700
1	0.75	2.0	1	1	2.0000	1.000	1.61418346	1.43807300
1	0.75	2.0	1	1	1.7500	0.875	1.89354465	1.68274100
1	0.75	2.0	1	1	1.5000	0.750	2.22975124	1.97314200
1	0.75	2.0	1	1	1.2500	0.625	2.63846184	2.31922500
1	0.75	2.0	1	1	1.0000	0.500	3.14119459	2.78336580
1	0.75	2.0	1	1	0.7500	0.375	3.76994778	3.23283100
1	0.75	2.0	1	1	0.5000	0.250	4.58071838	3.83807900
1	0.75	2.0	1	1	0.2500	0.125	5.69221557	4.57877200
1	0.75	2.0	2	1	4.0000	2.000	0.96501795	0.86145400
1	0.75	2.0	2	1	2.0000	1.000	3.20613546	2.87614600
1	0.75	2.0	2	1	1.0000	0.500	6.27192800	5.46718300

1	0.75	2.0	2	1	0.2500	0.125	11.52999914	9.15678800
1	0.75	2.0	4	1	4.0000	2.000	1.92184746	1.72290600
1	0.75	2.0	4	1	2.0000	1.000	6.45187135	5.75229100
1	0.75	2.0	4	1	1.0000	0.500	12.86185795	10.93378500
1	0.75	2.0	4	1	0.2500	0.125	24.74865968	18.31192000
1	0.75	2.0	8	1	4.0000	2.000	3.85867038	3.44580600
1	0.75	2.0	8	1	2.0000	1.000	13.18972065	11.50457500
1	0.75	2.0	8	1	1.0000	0.500	27.35891578	21.86606100
1	0.75	2.0	8	1	0.2500	0.125	57.35445222	36.62115600
1	0.75	2.0	1	2	4.0000	2.000	1.00984454	0.86145500
1	0.75	2.0	1	2	2.0000	1.000	3.30361027	2.87614700
1	0.75	2.0	1	2	1.0000	0.500	6.46855989	5.46731600
1	0.75	2.0	1	2	0.2500	0.125	11.86096378	9.15841000
1	0.75	2.0	1	4	4.0000	2.000	2.14598043	1.72290900
1	0.75	2.0	1	4	2.0000	1.000	6.93901189	5.75229400
1	0.75	2.0	1	4	1.0000	0.500	13.84486249	10.93463200
1	0.75	2.0	1	4	0.2500	0.125	26.40483643	18.31827100
1	0.75	2.0	1	8	4.0000	2.000	6.87570638	3.44581900
1	0.75	2.0	1	8	2.0000	1.000	15.23596454	11.50458800
1	0.75	2.0	1	8	1.0000	0.500	31.48971730	21.86926500
1	0.75	2.0	1	8	0.2500	0.125	64.30085881	36.63654300
1	0.75	3.0	1	1	9.0000	3.000	0.35537341	0.16936800
1	0.75	3.0	1	1	7.5000	2.500	0.49936443	0.30313200
1	0.75	3.0	1	1	6.0000	2.000	0.76800259	0.54885500
1	0.75	3.0	1	1	5.2500	1.750	0.97925092	0.74270300
1	0.75	3.0	1	1	4.5000	1.500	1.26886281	1.00983600
1	0.75	3.0	1	1	3.7500	1.250	1.67188508	1.38121100
1	0.75	3.0	1	1	3.0000	1.000	2.23968876	1.90350800
1	0.75	3.0	1	1	2.6250	0.875	2.60983611	2.24258200
1	0.75	3.0	1	1	2.2500	0.750	3.05679232	2.64975000
1	0.75	3.0	1	1	1.8750	0.625	3.60244886	3.14166600
1	0.75	3.0	1	1	1.5000	0.500	4.27751697	3.74044400
1	0.75	3.0	1	1	1.1250	0.375	5.12951530	4.47621900
1	0.75	3.0	1	1	0.7500	0.250	6.23577481	5.39146800
1	0.75	3.0	1	1	0.3750	0.125	7.76424292	6.54837800
1	0.75	3.0	2	1	6.0000	2.000	1.39680897	1.09770900
1	0.75	3.0	2	1	3.0000	1.000	4.32341016	3.80701600
1	0.75	3.0	2	1	1.5000	0.500	8.39117081	7.48088900
1	0.75	3.0	2	1	0.3750	0.125	15.49564151	13.09608800
1	0.75	3.0	4	1	6.0000	2.000	2.68749535	2.19541400
1	0.75	3.0	4	1	3.0000	1.000	8.55601870	
1	0.75	3.0	4	1	1.5000	0.500	16.87733600	14.96161400
1	0.75	3.0	4	1	0.3750	0.125	32.41339730	26.18883700

1	0.75	3.0	8	1	6.0000	2.000	5.40114368	4.39071700
1	0.75	3.0	8	1	3.0000	1.000	17.28206584	15.22789000
1	0.75	3.0	8	1	1.5000	0.500	34.88685276	29.92171500
1	0.75	3.0	8	1	0.3750	0.125	72.06106757	52.37350100
1	0.75	3.0	1	2	6.0000	2.000	1.83091622	1.09768700
1	0.75	3.0	1	2	3.0000	1.000	4.82388541	3.80697600
1	0.75	3.0	1	2	1.5000	0.500	9.01365503	7.48080900
1	0.75	3.0	1	2	0.3750	0.125	16.31802454	13.09781100
1	0.75	3.0	1	4	6.0000	2.000	4.62918476	2.19537400
1	0.75	3.0	1	4	3.0000	1.000	11.05837924	7.61395100
1	0.75	3.0	1	4	1.5000	0.500	19.99155308	14.96161700
1	0.75	3.0	1	4	0.3750	0.125	36.52870141	26.19562200
1	0.75	3.0	1	8	6.0000	2.000	14.51739578	4.39074800
1	0.75	3.0	1	8	3.0000	1.000	27.79176616	15.22790300
1	0.75	3.0	1	8	1.5000	0.500	47.96916951	29.92323500
1	0.75	3.0	1	8	0.3750	0.125	89.32156941	52.39217200
1	1.00	0.1	1	1	0.3000	3.000	0.00368368	0.00193500
1	1.00	0.1	1	1	0.2500	2.500	0.00617838	0.00322500
1	1.00	0.1	1	1	0.2000	2.000	0.01050454	0.00537600
1	1.00	0.1	1	1	0.1750	1.750	0.01380119	0.00694200
1	1.00	0.1	1	1	0.1500	1.500	0.01824411	0.00896500
1	1.00	0.1	1	1	0.1250	1.250	0.02435881	0.01158000
1	1.00	0.1	1	1	0.1000	1.000	0.03295805	0.01495800
1	1.00	0.1	1	1	0.0875	0.875	0.03861632	0.01699800
1	1.00	0.1	1	1	0.0750	0.750	0.04553795	0.01932000
1	1.00	0.1	1	1	0.0625	0.625	0.05414984	0.02195800
1	1.00	0.1	1	1	0.0500	0.500	0.06515935	0.02495500
1	1.00	0.1	1	1	0.0375	0.375	0.07968281	0.02836300
1	1.00	0.1	1	1	0.0250	0.250	0.10001524	0.03223700
1	1.00	0.1	1	1	0.0125	0.125	0.13176919	0.03664200
1	1.00	0.1	2	1	0.2000	2.000	0.02120508	0.01075300
1	1.00	0.1	2	1	0.1000	1.000	0.06778962	0.02991100
1	1.00	0.1	2	1	0.0500	0.500	0.13659384	0.04991200
1	1.00	0.1	2	1	0.0125	0.125	0.28280086	0.07328800
1	1.00	0.1	4	1	0.2000	2.000	0.04391005	0.02150700
1	1.00	0.1	4	1	0.1000	1.000	0.14953319	0.05982300
1	1.00	0.1	4	1	0.0500	0.500	0.31944908	0.09980800
1	1.00	0.1	4	1	0.0125	0.125	0.70402011	0.14654300
1	1.00	0.1	8	1	0.2000	2.000	0.09459427	0.04301300
1	1.00	0.1	8	1	0.1000	1.000	0.36152400	0.11964000
1	1.00	0.1	8	1	0.0500	0.500	0.84516346	0.19960400
1	1.00	0.1	8	1	0.0125	0.125	2.02356757	0.29309100
1	1.00	0.1	1	2	0.2000	2.000	0.02126119	0.01075200

1	1.00	0.1	1	2	0.1000	1.000	0.06829222	0.02991100
1	1.00	0.1	1	2	0.0500	0.500	0.13769654	0.04991100
1	1.00	0.1	1	2	0.0125	0.125	0.28466508	0.07328000
1	1.00	0.1	1	4	0.2000	2.000	0.04421978	0.02150400
1	1.00	0.1	1	4	0.1000	1.000	0.15210335	0.05982000
1	1.00	0.1	1	4	0.0500	0.500	0.32495978	0.09980400
1	1.00	0.1	1	4	0.0125	0.125	0.71344616	0.14654100
1	1.00	0.1	1	8	0.2000	2.000	0.09575438	0.04299900
1	1.00	0.1	1	8	0.1000	1.000	0.37233405	0.11962200
1	1.00	0.1	1	8	0.0500	0.500	0.86855892	0.19959300
1	1.00	0.1	1	8	0.0125	0.125	2.06361589	0.29307400
1	1.00	0.5	1	1	1.5000	3.000	0.04786162	0.03223900
1	1.00	0.5	1	1	1.2500	2.500	0.08208541	0.05511500
1	1.00	0.5	1	1	1.0000	2.000	0.14211178	0.09447800
1	1.00	0.5	1	1	0.8750	1.750	0.18796065	0.12384200
1	1.00	0.5	1	1	0.7500	1.500	0.24983135	0.16247300
1	1.00	0.5	1	1	0.6250	1.250	0.33423416	0.21335800
1	1.00	0.5	1	1	0.5000	1.000	0.45132800	0.28047000
1	1.00	0.5	1	1	0.4375	0.875	0.52698541	0.32170500
1	1.00	0.5	1	1	0.3750	0.750	0.61801146	0.36911400
1	1.00	0.5	1	1	0.3125	0.625	0.72889297	0.42364400
1	1.00	0.5	1	1	0.2500	0.500	0.86622000	0.48639100
1	1.00	0.5	1	1	0.1875	0.375	1.04035524	0.55859800
1	1.00	0.5	1	1	0.1250	0.250	1.26991351	0.64177900
1	1.00	0.5	1	1	0.0625	0.125	1.59574443	0.73764500
1	1.00	0.5	2	1	1.0000	2.000	0.28395373	0.18895600
1	1.00	0.5	2	1	0.5000	1.000	0.91027157	0.56093900
1	1.00	0.5	2	1	0.2500	0.500	1.77084227	0.97268700
1	1.00	0.5	2	1	0.0625	0.125	3.33273557	1.47521000
1	1.00	0.5	4	1	1.0000	2.000	0.57568649	0.37791200
1	1.00	0.5	4	1	0.5000	1.000	1.92074930	1.12178700
1	1.00	0.5	4	1	0.2500	0.500	3.91663351	1.94524600
1	1.00	0.5	4	1	0.0625	0.125	7.83720757	2.95025000
1	1.00	0.5	8	1	1.0000	2.000	1.19135546	0.75581500
1	1.00	0.5	8	1	0.5000	1.000	4.31246714	2.24343000
1	1.00	0.5	8	1	0.2500	0.500	9.55435189	3.89033200
1	1.00	0.5	8	1	0.0625	0.125	20.94445914	5.90032500
1	1.00	0.5	1	2	1.0000	2.000	0.28877362	0.18895600
1	1.00	0.5	1	2	0.5000	1.000	1.46931866	0.56093900
1	1.00	0.5	1	2	0.2500	0.500	1.82349286	0.97278300
1	1.00	0.5	1	2	0.0625	0.125	3.42232562	1.47545400
1	1.00	0.5	1	4	1.0000	2.000	0.59976843	0.37791300
1	1.00	0.5	1	4	0.5000	1.000	2.03766595	1.12187900

1	1.00	0.5	1	4	0.2500	0.500	4.18016735	1.94557100
1	1.00	0.5	1	4	0.0625	0.125	8.28185795	2.95090500
1	1.00	0.5	1	8	1.0000	2.000	1.29243708	0.75582500
1	1.00	0.5	1	8	0.5000	1.000	4.80318195	2.24375800
1	1.00	0.5	1	8	0.2500	0.500	10.65966800	3.89115100
1	1.00	0.5	1	8	0.0625	0.125	22.82352389	5.90179900
1	1.00	1.0	1	1	3.0000	3.000	0.10697211	0.08499900
1	1.00	1.0	1	1	2.5000	2.500	0.18493622	0.14746600
1	1.00	1.0	1	1	2.0000	2.000	0.32397557	0.25727300
1	1.00	1.0	1	1	1.7500	1.750	0.43083741	0.34067600
1	1.00	1.0	1	1	1.5000	1.500	0.57552195	0.45201600
1	1.00	1.0	1	1	1.2500	1.250	0.77328854	0.60110900
1	1.00	1.0	1	1	1.0000	1.000	1.04770454	0.80148400
1	1.00	1.0	1	1	0.8750	0.875	1.22371676	0.92651500
1	1.00	1.0	1	1	0.7500	0.750	1.50010876	1.07196100
1	1.00	1.0	1	1	0.6250	0.625	1.68983114	1.24124100
1	1.00	1.0	1	1	0.5000	0.500	2.00287914	1.43872500
1	1.00	1.0	1	1	0.3750	0.375	2.39483773	1.66947600
1	1.00	1.0	1	1	0.2500	0.250	2.90168519	1.93949500
1	1.00	1.0	1	1	0.1250	0.125	3.60177935	2.25629000
1	1.00	1.0	2	1	2.0000	2.000	0.64449265	0.51454500
1	1.00	1.0	2	1	1.0000	1.000	2.09351946	1.60293000
1	1.00	1.0	2	1	0.5000	0.500	4.04043265	2.87719400
1	1.00	1.0	2	1	0.1250	0.125	7.41160778	4.51192000
1	1.00	1.0	4	1	2.0000	2.000	1.29248735	1.02908800
1	1.00	1.0	4	1	1.0000	1.000	4.29607827	3.20562400
1	1.00	1.0	4	1	0.5000	0.500	8.59002638	5.75361900
1	1.00	1.0	4	1	0.1250	0.125	16.69539405	9.02287700
1	1.00	1.0	8	1	2.0000	2.000	2.61659870	2.05817100
1	1.00	1.0	8	1	1.0000	1.000	9.14545276	6.41049400
1	1.00	1.0	8	1	0.5000	0.500	19.58484649	11.50605800
1	1.00	1.0	8	1	0.1250	0.125	41.91986454	18.04425700
1	1.00	1.0	1	2	2.0000	2.000	0.65837589	0.51454600
1	1.00	1.0	1	2	1.0000	1.000	2.15403189	1.60296800
1	1.00	1.0	1	2	0.5000	0.500	4.17230616	2.87780900
1	1.00	1.0	1	2	0.1250	0.125	7.61914432	4.51313300
1	1.00	1.0	1	4	2.0000	2.000	1.01233656	1.02909100
1	1.00	1.0	1	4	1.0000	1.000	4.59959427	3.20593600
1	1.00	1.0	1	4	0.5000	0.500	9.24602724	5.75561700
1	1.00	1.0	1	4	0.1250	0.125	17.73527005	9.02805700
1	1.00	1.0	1	8	2.0000	2.000	2.90791005	2.05818300
1	1.00	1.0	1	8	1.0000	1.000	10.42082508	6.41187200
1	1.00	1.0	1	8	0.5000	0.500	22.34236811	11.51123500

1	1.00	1.0	1	8	0.1250	0.125	46.27223589	18.05611300
1	1.00	2.0	1	1	6.0000	3.000	0.20103027	0.16536700
1	1.00	2.0	1	1	5.0000	2.500	0.34925319	0.29209500
1	1.00	2.0	1	1	4.0000	2.000	0.61219654	0.52048800
1	1.00	2.0	1	1	3.5000	1.750	0.81398443	0.69770800
1	1.00	2.0	1	1	3.0000	1.500	1.08822832	0.93852800
1	1.00	2.0	1	1	2.5000	1.250	1.46690259	1.26777300
1	1.00	2.0	1	1	2.0000	1.000	1.99399654	1.72136400
1	1.00	2.0	1	1	1.7500	0.875	2.33478443	2.01047700
1	1.00	2.0	1	1	1.5000	0.750	2.74374984	2.35243800
1	1.00	2.0	1	1	1.2500	0.625	3.23957373	2.75831000
1	1.00	2.0	1	1	1.0000	0.500	3.84819178	3.24199800
1	1.00	2.0	1	1	0.7500	0.375	4.60781838	3.82121400
1	1.00	2.0	1	1	0.5000	0.250	5.58657157	4.51860200
1	1.00	2.0	1	1	0.2500	0.125	6.92516054	5.36466800
1	1.00	2.0	2	1	4.0000	2.000	1.19863881	1.04097500
1	1.00	2.0	2	1	2.0000	1.000	3.94327514	3.44272700
1	1.00	2.0	2	1	1.0000	0.500	7.65902357	6.48395400
1	1.00	2.0	2	1	0.2500	0.125	13.99941481	10.72820100
1	1.00	2.0	4	1	4.0000	2.000	2.37894065	2.08194900
1	1.00	2.0	4	1	2.0000	1.000	7.92754638	6.88545300
1	1.00	2.0	4	1	1.0000	0.500	15.72127719	12.96708900
1	1.00	2.0	4	1	0.2500	0.125	30.13888411	21.45503500
1	1.00	2.0	8	1	4.0000	2.000	4.76917859	4.16389100
1	1.00	2.0	8	1	2.0000	1.000	16.23049184	13.77089900
1	1.00	2.0	8	1	1.0000	0.500	33.60587686	25.93283300
1	1.00	2.0	8	1	0.2500	0.125	70.37901211	42.90652800
1	1.00	2.0	1	2	4.0000	2.000	1.27961157	1.04097600
1	1.00	2.0	1	2	2.0000	1.000	4.12015286	3.44272800
1	1.00	2.0	1	2	1.0000	0.500	7.99110065	6.48399700
1	1.00	2.0	1	2	0.2500	0.125	14.54741881	10.73007100
1	1.00	2.0	1	4	4.0000	2.000	2.78379935	2.08195200
1	1.00	2.0	1	4	2.0000	1.000	8.81168368	6.88545600
1	1.00	2.0	1	4	1.0000	0.500	17.38056378	12.96799400
1	1.00	2.0	1	4	0.2500	0.125	32.87023784	21.46129300
1	1.00	2.0	1	8	4.0000	2.000	6.46958724	4.16390300
1	1.00	2.0	1	8	2.0000	1.000	19.95157676	13.77091100
1	1.00	2.0	1	8	1.0000	0.500	40.57915665	25.93598700
1	1.00	2.0	1	8	0.2500	0.125	81.85698216	42.92258500
1	1.00	3.0	1	1	9.0000	3.000	0.51411643	0.21054800
1	1.00	3.0	1	1	7.5000	2.500	0.69494270	0.37615800
1	1.00	3.0	1	1	6.0000	2.000	1.03604292	0.67947500
1	1.00	3.0	1	1	5.2500	1.750	1.30345654	0.91808400

1	1.00	3.0	1	1	4.5000	1.500	1.66826897	1.24605300
1	1.00	3.0	1	1	3.7500	1.250	2.17126595	1.70050800
1	1.00	3.0	1	1	3.0000	1.000	2.87996995	2.33688600
1	1.00	3.0	1	1	2.6250	0.875	3.34006357	2.74834700
1	1.00	3.0	1	1	2.2500	0.750	3.89416400	3.24071900
1	1.00	3.0	1	1	1.8750	0.625	4.56806368	3.83306300
1	1.00	3.0	1	1	1.5000	0.500	5.39832335	4.55032800
1	1.00	3.0	1	1	1.1250	0.375	6.44198659	5.42591200
1	1.00	3.0	1	1	0.7500	0.250	7.79158205	6.50583700
1	1.00	3.0	1	1	0.3750	0.125	9.64823600	7.85534900
1	1.00	3.0	2	1	6.0000	2.000	1.82204541	1.35894800
1	1.00	3.0	2	1	3.0000	1.000	5.47507351	4.67377100
1	1.00	3.0	2	1	1.5000	0.500	10.49017914	9.10065500
1	1.00	3.0	2	1	0.3750	0.125	19.14466303	15.70965800
1	1.00	3.0	4	1	6.0000	2.000	3.42825427	2.71789000
1	1.00	3.0	4	1	3.0000	1.000	10.74851795	9.34754100
1	1.00	3.0	4	1	1.5000	0.500	21.02783038	18.20130900
1	1.00	3.0	4	1	0.3750	0.125	40.05478368	31.41735900
1	1.00	3.0	8	1	6.0000	2.000	6.77748065	5.43575700
1	1.00	3.0	8	1	3.0000	1.000	21.62836616	18.69507600
1	1.00	3.0	8	1	1.5000	0.500	43.52442314	36.40117000
1	1.00	3.0	8	1	0.3750	0.125	89.55110043	62.82961400
1	1.00	3.0	1	2	6.0000	2.000	2.58925589	1.35895000
1	1.00	3.0	1	2	3.0000	1.000	6.37128854	4.67377200
1	1.00	3.0	1	2	1.5000	0.500	11.58835405	9.10065600
1	1.00	3.0	1	2	0.3750	0.125	20.55925957	15.71199200
1	1.00	3.0	1	4	6.0000	2.000	7.26429178	2.71790200
1	1.00	3.0	1	4	3.0000	1.000	15.22959708	9.34754400
1	1.00	3.0	1	4	1.5000	0.500	26.52102584	18.20131200
1	1.00	3.0	1	4	0.3750	0.125	47.12614962	31.42398400
1	1.00	3.0	1	8	6.0000	2.000	22.88882335	5.43580400
1	1.00	3.0	1	8	3.0000	1.000	40.44890573	18.69508800
1	1.00	3.0	1	8	1.5000	0.500	66.59684703	36.40262500
1	1.00	3.0	1	8	0.3750	0.125	119.23001741	62.84796900
1	2.00	0.1	1	1	0.3000	3.000	0.00003330	0.00230100
1	2.00	0.1	1	1	0.2500	2.500	0.00472151	0.00382200
1	2.00	0.1	1	1	0.2000	2.000	0.01142335	0.00635000
1	2.00	0.1	1	1	0.1750	1.750	0.01631189	0.00818200
1	2.00	0.1	1	1	0.1500	1.500	0.02251546	0.01054700
1	2.00	0.1	1	1	0.1250	1.250	0.02418378	0.01359400
1	2.00	0.1	1	1	0.1000	1.000	0.04320508	0.01753200
1	2.00	0.1	1	1	0.0875	0.875	0.04904443	0.01990400
1	2.00	0.1	1	1	0.0750	0.750	0.05737124	0.02259900

1	2.00	0.1	1	1	0.0625	0.625	0.06778476	0.02566200
1	2.00	0.1	1	1	0.0500	0.500	0.08222238	0.02913800
1	2.00	0.1	1	1	0.0375	0.375	0.09973514	0.03309000
1	2.00	0.1	1	1	0.0250	0.250	0.12410822	0.03756900
1	2.00	0.1	1	1	0.0125	0.125	0.16696659	0.04266000
1	2.00	0.1	2	1	0.2000	2.000	0.02554259	0.01269600
1	2.00	0.1	2	1	0.1000	1.000	0.08596281	0.03506700
1	2.00	0.1	2	1	0.0500	0.500	0.16831686	0.05828000
1	2.00	0.1	2	1	0.0125	0.125	0.34989697	0.08532000
1	2.00	0.1	4	1	0.2000	2.000	0.05794616	0.02539300
1	2.00	0.1	4	1	0.1000	1.000	0.18867146	0.07013100
1	2.00	0.1	4	1	0.0500	0.500	0.39409914	0.11655900
1	2.00	0.1	4	1	0.0125	0.125	0.86322054	0.17061900
1	2.00	0.1	8	1	0.2000	2.000	0.13955827	0.05079100
1	2.00	0.1	8	1	0.1000	1.000	0.46297492	0.14025900
1	2.00	0.1	8	1	0.0500	0.500	1.03657470	0.23310900
1	2.00	0.1	8	1	0.0125	0.125	2.47977881	0.34125200
1	2.00	0.1	1	2	0.2000	2.000	0.01960432	0.01269900
1	2.00	0.1	1	2	0.1000	1.000	0.09588108	0.03505700
1	2.00	0.1	1	2	0.0500	0.500	0.18179286	0.05826000
1	2.00	0.1	1	2	0.0125	0.125	0.37570184	0.08530000
1	2.00	0.1	1	4	0.2000	2.000	0.02828022	0.02539700
1	2.00	0.1	1	4	0.1000	1.000	0.23824270	0.07013600
1	2.00	0.1	1	4	0.0500	0.500	0.45842368	0.11651900
1	2.00	0.1	1	4	0.0125	0.125	0.99210670	0.17057600
1	2.00	0.1	1	8	0.2000	2.000		
1	2.00	0.1	1	8	0.1000	1.000	0.67107232	0.14025300
1	2.00	0.1	1	8	0.0500	0.500	1.32008497	0.23310700
1	2.00	0.1	1	8	0.0125	0.125	3.02045319	0.34125100
1	2.00	0.5	1	1	1.5000	3.000	0.06709297	0.04096200
1	2.00	0.5	1	1	1.2500	2.500	0.11245784	0.06946800
1	2.00	0.5	1	1	1.0000	2.000	0.19143514	0.11799700
1	2.00	0.5	1	1	0.8750	1.750	0.25135005	0.15388700
1	2.00	0.5	1	1	0.7500	1.500	0.33190843	0.20078900
1	2.00	0.5	1	1	0.6250	1.250	0.44141816	0.26212000
1	2.00	0.5	1	1	0.5000	1.000	0.59293081	0.34226800
1	2.00	0.5	1	1	0.4375	0.875	0.69067232	0.39137900
1	2.00	0.5	1	1	0.3750	0.750	0.80820335	0.44746500
1	2.00	0.5	1	1	0.3125	0.625	0.95137600	0.51167100
1	2.00	0.5	1	1	0.2500	0.500	1.12878389	0.58518600
1	2.00	0.5	1	1	0.1875	0.375	1.35439632	0.66936900
1	2.00	0.5	1	1	0.1250	0.250	1.65281676	0.76579100
1	2.00	0.5	1	1	0.0625	0.125	2.07750497	0.87626000

1	2.00	0.5	2	1	1.0000	2.000	0.37936043	0.23599600
1	2.00	0.5	2	1	0.5000	1.000	1.18955751	0.68475100
1	2.00	0.5	2	1	0.2500	0.500	2.29771546	1.17031900
1	2.00	0.5	2	1	0.0625	0.125	4.32649611	1.75235900
1	2.00	0.5	4	1	1.0000	2.000	0.76743330	0.47199200
1	2.00	0.5	4	1	0.5000	1.000	2.50975146	1.36387000
1	2.00	0.5	4	1	0.2500	0.500	5.08801643	2.34039700
1	2.00	0.5	4	1	0.0625	0.125	10.19678832	3.50464400
1	2.00	0.5	8	1	1.0000	2.000	1.59173070	0.94398300
1	2.00	0.5	8	1	0.5000	1.000	5.65774043	2.73862100
1	2.00	0.5	8	1	0.2500	0.500	12.47716778	4.68070400
1	2.00	0.5	8	1	0.0625	0.125	27.42683427	7.00904100
1	2.00	0.5	1	2	1.0000	2.000	0.39597286	0.23599100
1	2.00	0.5	1	2	0.5000	1.000	1.24131730	0.68746000
1	2.00	0.5	1	2	0.2500	0.500	2.40336886	1.17036800
1	2.00	0.5	1	2	0.0625	0.125	4.49827286	1.75263700
1	2.00	0.5	1	4	1.0000	2.000	0.85046919	0.47196800
1	2.00	0.5	1	4	0.5000	1.000	2.76804238	1.36947800
1	2.00	0.5	1	4	0.2500	0.500	5.61598324	2.34072200
1	2.00	0.5	1	4	0.0625	0.125	11.05631254	3.50526100
1	2.00	0.5	1	8	1.0000	2.000	1.94107135	0.94387900
1	2.00	0.5	1	8	0.5000	1.000	6.74231611	2.73889900
1	2.00	0.5	1	8	0.2500	0.500	14.69059319	4.68137700
1	2.00	0.5	1	8	0.0625	0.125	31.03397935	7.01046700
1	2.00	1.0	1	1	3.0000	3.000	0.14956854	0.11386100
1	2.00	1.0	1	1	2.5000	2.500	0.27056076	0.19586600
1	2.00	1.0	1	1	2.0000	2.000	0.46808800	0.33819900
1	2.00	1.0	1	1	1.7500	1.750	0.61840854	0.44513600
1	2.00	1.0	1	1	1.5000	1.500	0.82060897	0.58662200
1	2.00	1.0	1	1	1.2500	1.250	1.09527741	0.77415900
1	2.00	1.0	1	1	1.0000	1.000	1.47422605	1.02325200
1	2.00	1.0	1	1	0.8750	0.875	1.71771081	1.17717400
1	2.00	1.0	1	1	0.7500	0.750	2.00886573	1.35488800
1	2.00	1.0	1	1	0.6250	0.625	2.35986854	1.56021400
1	2.00	1.0	1	1	0.5000	0.500	2.78930649	1.79744800
1	2.00	1.0	1	1	0.3750	0.375	3.32597751	2.07205900
1	2.00	1.0	1	1	0.2500	0.250	4.01945092	2.39008500
1	2.00	1.0	1	1	0.1250	0.125	4.97648897	2.75871500
1	2.00	1.0	2	1	2.0000	2.000	0.92569070	0.67640100
1	2.00	1.0	2	1	1.0000	1.000	2.93107168	2.04650900
1	2.00	1.0	2	1	0.5000	0.500	5.58930346	3.59451700
1	2.00	1.0	2	1	0.1250	0.125	10.17256432	5.51670900
1	2.00	1.0	4	1	2.0000	2.000	1.85386530	1.35280600

1	2.00	1.0	4	1	1.0000	1.000	6.01828357	4.09260800
1	2.00	1.0	4	1	0.5000	0.500	11.89660335	7.18815800
1	2.00	1.0	4	1	0.1250	0.125	22.97064973	11.03239800
1	2.00	1.0	8	1	2.0000	2.000	3.76219276	2.70561000
1	2.00	1.0	8	1	1.0000	1.000	12.88731568	8.18267000
1	2.00	1.0	8	1	0.5000	0.500	27.34064454	14.37491100
1	2.00	1.0	8	1	0.1250	0.125	58.18997708	22.06324700
1	2.00	1.0	1	2	2.0000	2.000	0.89458822	0.67388000
1	2.00	1.0	1	2	1.0000	1.000	3.06880151	2.04649500
1	2.00	1.0	1	2	0.5000	0.500	5.91089211	3.59524200
1	2.00	1.0	1	2	0.1250	0.125	10.71798962	5.51814100
1	2.00	1.0	1	4	2.0000	2.000	2.04353286	1.35270800
1	2.00	1.0	1	4	1.0000	1.000	6.70805611	4.09295300
1	2.00	1.0	1	4	0.5000	0.500	13.49833038	7.19044500
1	2.00	1.0	1	4	0.1250	0.125	25.63892854	11.02812200
1	2.00	1.0	1	8	2.0000	2.000	4.55868530	2.70532400
1	2.00	1.0	1	8	1.0000	1.000	15.78480973	8.18575500
1	2.00	1.0	1	8	0.5000	0.500	34.06522973	14.38073900
1	2.00	1.0	1	8	0.1250	0.125	69.61632659	22.07609200
1	2.00	2.0	1	1	6.0000	3.000	0.45473373	0.24407100
1	2.00	2.0	1	1	5.0000	2.500	0.68872930	0.42789200
1	2.00	2.0	1	1	4.0000	2.000	1.09654649	0.75523100
1	2.00	2.0	1	1	3.5000	1.750	1.40694227	1.00648100
1	2.00	2.0	1	1	3.0000	1.500	1.82518714	1.34468200
1	2.00	2.0	1	1	2.5000	1.250	2.39411578	1.80180100
1	2.00	2.0	1	1	2.0000	1.000	3.17923665	2.42273100
1	2.00	2.0	1	1	1.7500	0.875	3.68320811	2.81361600
1	2.00	2.0	1	1	1.5000	0.750	4.28517643	3.27134700
1	2.00	2.0	1	1	1.2500	0.625	5.01109849	3.80843700
1	2.00	2.0	1	1	1.0000	0.500	5.89495492	4.44008800
1	2.00	2.0	1	1	0.7500	0.375	6.98944627	5.18490000
1	2.00	2.0	1	1	0.5000	0.250	8.38421514	6.06563600
1	2.00	2.0	1	1	0.2500	0.125	10.27119427	7.11080000
1	2.00	2.0	2	1	4.0000	2.000	2.01103503	1.51046100
1	2.00	2.0	2	1	2.0000	1.000	6.13593957	4.84563000
1	2.00	2.0	2	1	1.0000	0.500	11.54863405	8.88017700
1	2.00	2.0	2	1	0.2500	0.125	20.53085070	14.22052700
1	2.00	2.0	4	1	4.0000	2.000	3.85588746	3.02091800
1	2.00	2.0	4	1	2.0000	1.000	12.21131816	9.69092600
1	2.00	2.0	4	1	1.0000	0.500	23.60847892	17.75971200
1	2.00	2.0	4	1	0.2500	0.125	44.19114616	28.43855000
1	2.00	2.0	8	1	4.0000	2.000	7.60905362	6.04181400
1	2.00	2.0	8	1	2.0000	1.000	25.00889276	19.38184700

1	2.00	2.0	8	1	1.0000	0.500	50.74136768	35.51674600
1	2.00	2.0	8	1	0.2500	0.125	104.06502195	56.87367000
1	2.00	2.0	1	2	4.0000	2.000	2.56515016	1.51045800
1	2.00	2.0	1	2	2.0000	1.000	6.88439146	4.84545800
1	2.00	2.0	1	2	1.0000	0.500	12.64685935	8.88017200
1	2.00	2.0	1	2	0.2500	0.125	22.13177059	14.22294700
1	2.00	2.0	1	4	4.0000	2.000	6.62643654	3.02090400
1	2.00	2.0	1	4	2.0000	1.000	15.95337514	9.69090300
1	2.00	2.0	1	4	1.0000	0.500	29.09932962	17.76033100
1	2.00	2.0	1	4	0.2500	0.125	52.18893081	28.44588000
1	2.00	2.0	1	8	4.0000	2.000	15.50917622	6.04175300
1	2.00	2.0	1	8	2.0000	1.000	40.72606346	19.38175000
1	2.00	2.0	1	8	1.0000	0.500	73.80276454	35.52060600
1	2.00	2.0	1	8	0.2500	0.125	137.65261005	56.89174000
1	2.00	3.0	1	1	9.0000	3.000	1.66395286	0.33141100
1	2.00	3.0	1	1	7.5000	2.500	1.98420659	0.58822300
1	2.00	3.0	1	1	6.0000	2.000	2.55138108	1.05361000
1	2.00	3.0	1	1	5.2500	1.750	2.98618270	1.41613900
1	2.00	3.0	1	1	4.5000	1.500	3.57332378	1.71007900
1	2.00	3.0	1	1	3.7500	1.250	4.37527632	2.58708600
1	2.00	3.0	1	1	3.0000	1.000	5.48572303	3.52195900
1	2.00	3.0	1	1	2.6250	0.875	6.20056886	4.11876800
1	2.00	3.0	1	1	2.2500	0.750	7.05601611	4.82536800
1	2.00	3.0	1	1	1.8750	0.625	8.09048011	5.66478600
1	2.00	3.0	1	1	1.5000	0.500	9.35206659	6.66596500
1	2.00	3.0	1	1	1.1250	0.375	10.91687427	7.86549000
1	2.00	3.0	1	1	0.7500	0.250	12.90910335	9.31182200
1	2.00	3.0	1	1	0.3750	0.125	15.59156335	11.06667100
1	2.00	3.0	2	1	6.0000	2.000	3.83496876	2.10722100
1	2.00	3.0	2	1	3.0000	1.000	9.62885859	7.04391900
1	2.00	3.0	2	1	1.5000	0.500	17.29022757	13.33193200
1	2.00	3.0	2	1	0.3750	0.125	29.93045038	22.13231200
1	2.00	3.0	4	1	6.0000	2.000	6.44349665	4.21443800
1	2.00	3.0	4	1	3.0000	1.000	18.06600130	14.08783600
1	2.00	3.0	4	1	1.5000	0.500	33.82498811	26.66386400
1	2.00	3.0	4	1	0.3750	0.125	61.78535870	44.26136300
1	2.00	3.0	8	1	6.0000	2.000	11.82593416	8.42885400
1	2.00	3.0	8	1	3.0000	1.000	35.54374205	28.17565800
1	2.00	3.0	8	1	1.5000	0.500	69.52479903	53.32648800
1	2.00	3.0	8	1	0.3750	0.125	138.20893124	88.51733600
1	2.00	3.0	1	2	6.0000	2.000	7.65899427	2.10721700
1	2.00	3.0	1	2	3.0000	1.000	13.73204638	7.04391400
1	2.00	3.0	1	2	1.5000	0.500	21.86280022	13.33192700

1	2.00	3.0	1	2	0.3750	0.125	35.27510811	22.13447900
1	2.00	3.0	1	4	6.0000	2.000	25.56362822	4.21442000
1	2.00	3.0	1	4	3.0000	1.000	38.58194897	14.08781400
1	2.00	3.0	1	4	1.5000	0.500	56.68965492	26.66383800
1	2.00	3.0	1	4	0.3750	0.125	88.50747546	44.26894200
1	2.00	3.0	1	8	6.0000	2.000	92.13053114	8.42877900
1	2.00	3.0	1	8	3.0000	1.000	121.71078065	28.17556600
1	2.00	3.0	1	8	1.5000	0.500	165.56480854	53.32761400
1	2.00	3.0	1	8	0.3750	0.125	250.40053005	88.53782100

A.2 Fortran Programs

The Fortran programs used in the development of the equilibrium partitioning theory are given here.

The program "elec.f" shown in section A.2.1 was used to integrate the Ogston probability distribution times the Boltzmann distribution of energy states. To obtain the energy of interaction between the sphere and the cylinder the general correlation of the free energy results (equation 60) was used.

The program "qcompare.f" given in section A.2.2 was used to read the nodal data points from the FIDAP output file and integrate over the surface of the cylinder and the sphere to give the change in free energy of putting one-quarter sphere near one-quarter cylinder.

The program "curvefitter.f" was used to curvefit the results for the change in free energy and is given in section A.2.3. This program used Powell's method to obtain the best fit to a given form of an equation.

A.2.1 Calculation of the effects of electrostatic interactions on the partition coefficient.

```
******  Numerical Integration of Electrostatic
******  Partition Coefficient using Sphere / Cylinder
******  Linear Superposition Approximation
***************
*  Erin M. Johnson
*  Aug 13, 1992 revised April 20, 1994
*
      REAL DIF,INF,OGSTON,VAL(15),ERROR,BB(10)
      CHARACTER*30 PARAM(15)
      INTEGER I,J
*
       OPEN(13,FILE='results',STATUS='NEW')
*       OPEN(14,FILE='/mit/emmalley/fidap2/robinson',STATUS='NEW')
       OPEN(15,FILE='approx.txt',STATUS='OLD')
*
* read the input parameters from approx.txt
```

```
*
      READ(15,5)J
      DO 99 I = 1,J
       READ(15,4)PARAM(I)
       READ(15,*)VAL(I)
*        WRITE(*,*)PARAM(I),VAL(I)
 99    CONTINUE
      PARAM(8)='Dim Sphere Pot'
      PARAM(9)='Dim Cylinder Pot'
      PARAM(10)='Dim Sphere Charge'
      PARAM(11)='Dim Cylinder Charge'
      PARAM(12)='Kappa * Sphere Rad'
      PARAM(13)='H / Sphere Rad'
      PARAM(14)='Dim y direction'

      BB(1)=0.00
      BB(2)=0.01
      BB(3)=0.02
      BB(4)=0.03
      BB(5)=0.04

 4    FORMAT(A30)
 5    FORMAT(I1)
      INF = 1.0e-7
      DO 54 JI = 1,5
       VAL(4)=BB(JI)
        DO 55 RI = 0.05,5.0,0.05
         VAL(2)=RI*1e-9

*        DO 56 CI = 1,3
*          VAL(3)=CI*1e-9

      CALL QROMB(0.,INF,DIF,VAL)
*
     OGSTON=EXP(-VAL(6)*(1+VAL(2)/VAL(3))*(1+VAL(2)/VAL(3)))
     ERROR = (OGSTON-DIF)/OGSTON*100
*
      WRITE(*,*)
      DO 77 I = 1,15
       WRITE(*,*)PARAM(I),VAL(I)
 77    CONTINUE
      WRITE(*,*)
      WRITE(*,*)'Ogston Partition Coefficient =  ',OGSTON
      WRITE(*,*)'Electrostatic Partition Coeff. =  ',DIF
      WRITE(*,*)'Percent Difference =  ',ERROR
      WRITE(*,*)
*
     AAA=VAL(6)*(1+VAL(2)/VAL(3))**2
     WRITE(13,*)VAL(4),VAL(2)*1e9,DIF,OGSTON,AAA
*
 55    CONTINUE
 56    CONTINUE
 54    CONTINUE
*
```

```
      STOP
      END
*************************************************************
      FUNCTION HFUNC(R,V)
*
      REAL R,V(15),P1,P2,KAPPA,K,TEMP,EO,EPSILON
     $     ,N,DELTAF,SIGMA1,SIGMA2,FAR,RGAS,LAMBDAC
     $     ,RCHARGE,BETA,RRAD,HK
*
      EO = 1.6022E-19
      K = 1.381E-23
      FAR = 9.6486E4
      EPSILON = 80.37 * 8.8542E-12
      TEMP = 293
      RGAS=8.315
      N = 6.022E23
      PI = 3.14159
*
      SIGMA1 = EO/EPSILON/K/TEMP*V(2)*V(4)
      SIGMA2 = EO/EPSILON/K/TEMP*V(2)*V(5)
      KAPPA = SQRT(2000.*N*EO**2/EPSILON/K/TEMP*V(1))
      TAU = V(2)*KAPPA
*       WRITE(*,*)'Sigma1, Sigma2, Kappa,Tau : ',SIGMA1,SIGMA2,
*    +     KAPPA,TAU
*
* P1 is the sphere surface potential
* P2 is the cylinder surface potential
*
      P1=SIGMA1/(1.+V(2)*KAPPA)
      LAMBDAC=TAU*BESSK1(TAU*V(3)/V(2))
      P2=SIGMA2*BESSK0(TAU*V(3)/V(2))/LAMBDAC
*       P2=SIGMA2/V(2)/KAPPA*BESSK0(KAPPA*V(3))/BESSK1(KAPPA*V(3))
      V(8)=P1
      V(9)=P2
      V(10)=SIGMA1
      V(11)=SIGMA2
      V(12)=KAPPA*V(2)
      V(13)=R/V(2)
*       WRITE(*,*)'Tau = Kappa*Sphere Rad :',V(12)
*
*       RCHARGE=SIGMA1/SIGMA2
      BETA=1.0/TAU
      HK=V(12)*V(13)
      RRAD=V(3)/V(2)
      DG=CURVEFIT(SIGMA1,SIGMA2,BETA,HK,RRAD,V)
*       DG=DG
*
      F1 = 2*V(6)*(R+V(3)+V(2))/V(3)/V(3)*EXP(-V(6)*(R+V(3)+V(2))
     $       *(R+V(3)+V(2))/V(3)/V(3))
      DELTAF = EPSILON*(K*TEMP/EO)*(K*TEMP/EO)*V(2)*DG
*
     HFUNC = F1* EXP(-DELTAF/K/TEMP)
      RETURN
      END
```

```
*************************************************************************
      FUNCTION CURVEFIT(s1,s2,DL,HK,RRAD,VV)
*
      REAL s1,s2,DL,HK,RRAD,VV(15)
*
      AA=2.352281094
      AB=.7599117756
      AC=1.247163177
      AD=1.095647335
      BA=.3570383787
      BB=.5052138567
      BC=.9512428045
      BD=3.76839304
      CA=.4472517669
      CB=.9310458899
      CC=1.151174426
      CD=2.498652697
*
      f1=s1*s2*AA*rrad**AB*dl**AC
      f3=exp(-AD*hk)
      f4=s1*s1*BA*rrad**BB*dl**BC
      f5=exp(-BD*hk)
      f6=s2*s2*CA*rrad**CB*dl**CC
      f7=exp(-CD*hk)
      A=f1*f3
      B=f4*f5
      C=f6*f7
*
      CURVEFIT=A+B+C
      RETURN
      END
*************************************************************************
*
* This subroutine integrates using Rhomberg's rule.  It came from
* Numerical Recipes
*
     SUBROUTINE QROMB(A,B,SS,V)
     PARAMETER (EPS=1.E-6, JMAX=300, JMAXP=JMAX+1, K=5, KM=K-1)
     DIMENSION S(JMAXP),H(JMAXP)
     REAL V(15)
     H(1)=1.
     DO 11 J=1,JMAX
       CALL MIDPNT(A,B,S(J),J,V)
*       WRITE(*,*)'QROMB: after trapzd: S and J are : ',S(J),J
       IF (J.GE.K) THEN
         CALL POLINT(H(J-KM),S(J-KM),K,0.,SS,DSS)
        IF (ABS(DSS).LT.EPS*ABS(SS)) RETURN
        IF (ABS(SS).LT.EPS) THEN
          SS=0.0
          RETURN
        ENDIF
       ENDIF
       S(J+1)=S(J)
       H(J+1)=0.25*H(J)
```

```
11   CONTINUE
     PAUSE 'Too many steps.'
     END
*****************************************************************
*
* This is used in integrating a function. (Numerical Recipes)P.120
*
     SUBROUTINE midpnt(a,b,s,n,V)
     INTEGER n
     REAL a,b,s,V(15)
     INTEGER it,j
     REAL ddel,del,sum,tnm,x
     if (n.eq.1) then
       s=(b-a)*hfunc(0.5*(a+b),V)
     else
       it=3**(n-2)
       tnm=it
       del=(b-a)/(3.*tnm)
       ddel=del+del
       x=a+0.5*del
       sum=0.
       do 11 j=1,it
         sum=sum+hfunc(x,V)
         x=x+ddel
         sum=sum+hfunc(x,V)
         x=x+del
11     continue
       s=(s+(b-a)*sum/tnm)/3.
     endif
     return
     END
*****************************************************************
     SUBROUTINE TRAPZD(A,B,S,N,V)
*
*      WRITE(*,*)'Inside trap  N = ',N
     IF (N.EQ.1) THEN
       S=0.5*(B-A)*(HFUNC(A,V)
    $       +HFUNC(B,V))
*        WRITE(*,*)'TRAPZD:  S =   ',S
       IT=1
     ELSE
       IT = (N-1)*2
*        WRITE(*,*) 'IT =  ',IT
       TNM=IT
*        WRITE(*,*)'TNM = ',TNM
       DEL=(B-A)/TNM
*        WRITE(*,*) ' DEL = ',DEL
       X=A+0.5*DEL
*        WRITE(*,*)'Del  = ',DEL,'  X = ',X
       SUM=0.
       DO 11 J=1,IT
*          WRITE(*,*)'TRAP:   J =   ',J,'  IT  =  ',IT, ' DEL = ',DEL
         SUM=SUM+HFUNC(X,V)
*          WRITE(*,*)'TRAP:  Sum   = ',SUM
```

```
      X=X+DEL
11    CONTINUE
*
*     WRITE(13,*) X
*     WRITE(*,*)
      S=0.5*(S+(B-A)*SUM/TNM)
      IT=2*IT
*       WRITE(*,*)'S=  ',S,'  IT  =  ',IT
    ENDIF
*     WRITE(*,*)
    RETURN
    END
*****************************************************************************
*
    SUBROUTINE POLINT(XA,YA,N,X,Y,DY)
    PARAMETER (NMAX=10)
    DIMENSION XA(N),YA(N),C(NMAX),D(NMAX)
    NS=1
    DIF=ABS(X-XA(1))
    DO 11 I=1,N
     DIFT=ABS(X-XA(I))
     IF (DIFT.LT.DIF) THEN
       NS=I
       DIF=DIFT
     ENDIF
     C(I)=YA(I)
     D(I)=YA(I)
11   CONTINUE
    Y=YA(NS)
    NS=NS-1
    DO 13 M=1,N-1
     DO 12 I=1,N-M
       HO=XA(I)-X
       HP=XA(I+M)-X
       W=C(I+1)-D(I)
       DEN=HO-HP
       IF(DEN.EQ.0.)PAUSE
      DEN=W/DEN
       D(I)=HP*DEN
       C(I)=HO*DEN
12     CONTINUE
      IF (2*NS.LT.N-M)THEN
       DY=C(NS+1)
     ELSE
       DY=D(NS)
       NS=NS-1
     ENDIF
     Y=Y+DY
13   CONTINUE
    RETURN
    END
*****************************************************************************
******
    SUBROUTINE LINEAR(SS,V)
```

```
*
      REAL V(15), DGS, DGC, DG
*
      CALL QROMBS(0.,2.,DGS,V)
      CALL QROMBC1(0.,10.,DGC,V)
      DGC=DGC*4.
*
      DG=0.5*(V(10)*DGS+V(11)*DGC)
      SS=DG
*
      RETURN
      END
*************************************************************
       FUNCTION SPHFUNC(X,V)
*
       REAL X,V(15),D,R,PI,LAMBDA
       R=1.0
       PI=3.14159
       CYLRAD=V(3)/V(2)
*
       IF(X.LE.R) THEN
         D=2.*SQRT(R**2-(R-X)**2)
       ELSE
         D=2*SQRT(R**2-(X-R)**2)
       ENDIF
*
       PSI=V(9)
       IF(V(9).GT.4.) THEN
         IF(V(13).GT.V(12)) PSI=4.0
       ENDIF
       LAMBDA=BESSK0(V(12)*CYLRAD)
       F1=PSI/LAMBDA*BESSK0(V(12)*(X+CYLRAD+V(13)))
       SPHFUNC=F1*D*PI
*
       RETURN
       END
*************************************************************
       FUNCTION CYLFUNC1(Y,V)
*
       REAL Y,V(15)
*
       V(14)=Y
       CALL QROMBC2(0.,2*V(3)/V(2),SS,V)
       CYLFUNC1 = SS
       RETURN
       END
*************************************************************
       FUNCTION CYLFUNC2(X,V)
*
       REAL V(15),ETA,ZED,RHO
*
      ETA=SQRT((V(13)+V(2)/V(2)+X)**2+(V(3)/V(2))**2
     $     -(V(3)/V(2)-X)**2)
      ZED=V(14)
```

```
      RHO=SQRT(ETA**2+ZED**2)
*
      F1=V(8)*V(2)/V(2)/RHO*EXP(V(12)*(V(2)/V(2)-RHO))
      CYLFUNC2=F1*2*SQRT((V(3)/V(2)-X)**2)
      RETURN
      END
*****************************************************************
*
* This subroutine integrates using Rhomberg's rule.  It came from
* Numerical Recipes
*
      SUBROUTINE QROMBS(A,B,SS,V)
      PARAMETER (EPS=1.E-3, JMAX=300, JMAXP=JMAX+1, K=3, KM=K-1)
      DIMENSION S(JMAXP),H(JMAXP)
      REAL V(15)
      H(1)=1.
      DO 11 J=1,JMAX
        CALL MIDPNTS(A,B,S(J),J,V)
*       WRITE(*,*)'QROMBS: after trapzd  ',S(J),J
        IF (J.GE.K) THEN
          CALL POLINT(H(J-KM),S(J-KM),K,0.,SS,DSS)
          IF (ABS(DSS).LT.EPS*ABS(SS)) RETURN
          IF (ABS(SS).LT.EPS) THEN
            SS = 0.0
            RETURN
          ENDIF
        ENDIF
        S(J+1)=S(J)
        H(J+1)=0.25*H(J)
11    CONTINUE
      PAUSE 'Too many steps.'
      END
*****************************************************************
*
* This subroutine integrates using Rhomberg's rule.  It came from
* Numerical Recipes
*
      SUBROUTINE QROMBC1(A,B,SS,V)
      PARAMETER (EPS=1.E-3, JMAX=300, JMAXP=JMAX+1, K=3, KM=K-1)
      DIMENSION S(JMAXP),H(JMAXP)
      REAL V(15)
      H(1)=1.
      DO 11 J=1,JMAX
        CALL MIDPNTC1(A,B,S(J),J,V)
*       WRITE(*,*)'QROMBC1: after trapzd  ',S(J),J, V(10)
        IF (J.GE.K) THEN
          CALL POLINT(H(J-KM),S(J-KM),K,0.,SS,DSS)
          IF (ABS(DSS).LT.EPS*ABS(SS)) RETURN
          IF (ABS(SS).LT.EPS) THEN
            SS=0.0
            RETURN
            ENDIF
        ENDIF
        S(J+1)=S(J)
```

```
      H(J+1)=0.25*H(J)
11   CONTINUE
     PAUSE 'Too many steps.'
     END
*****************************************************************
*
* This subroutine integrates using Rhomberg's rule.  It came from
* Numerical Recipes
*
     SUBROUTINE QROMBC2(A,B,SS,V)
     PARAMETER (EPS=1.E-3, JMAX=300, JMAXP=JMAX+1, K=3, KM=K-1)
     DIMENSION S(JMAXP),H(JMAXP)
     REAL V(15)
     H(1)=1.
     DO 11 J=1,JMAX
       CALL MIDPNTC2(A,B,S(J),J,V)
*       WRITE(*,*)'QROMBC2: after trapzd  ', S(J),J
       IF (J.GE.K) THEN
         CALL POLINT(H(J-KM),S(J-KM),K,0.,SS,DSS)
         IF (ABS(DSS).LT.EPS*ABS(SS)) RETURN
         IF (ABS(SS).LT.EPS) THEN
           SS=0.0
           RETURN
         ENDIF
       ENDIF
       S(J+1)=S(J)
       H(J+1)=0.25*H(J)
11   CONTINUE
     PAUSE 'Too many steps.'
     END

*****************************************************************
*
* This is used in integrating a function. (Numerical Recipes)P.120
*
     SUBROUTINE midpnts(a,b,s,n,V)
     INTEGER n
     REAL a,b,s,V(15)
     INTEGER it,j
     REAL ddel,del,sum,tnm,x
     if (n.eq.1) then
       s=(b-a)*sphfunc(0.5*(a+b),V)
     else
       it=3**(n-2)
       tnm=it
       del=(b-a)/(3.*tnm)
       ddel=del+del
       x=a+0.5*del
       sum=0.
       do 11 j=1,it
         sum=sum+sphfunc(x,V)
         x=x+ddel
         sum=sum+sphfunc(x,V)
         x=x+del
```

```
11     continue
       s=(s+(b-a)*sum/tnm)/3.
     endif
     return
     END
*****************************************************************************
*
*
     SUBROUTINE TRAPZDS(A,B,S,N,V)
*
*      WRITE(*,*)'Inside trap  N = ',N
     IF (N.EQ.1) THEN
          S=0.5*(B-A)*(SPHFUNC(A,V)
    $       +SPHFUNC(B,V))
*       WRITE(*,*)'TRAPZD:  S =   ',S
       IT=1
     ELSE
       IT = (N-1)*2
*       WRITE(*,*) 'IT =  ',IT
       TNM=IT
*       WRITE(*,*)'TNM = ',TNM
       DEL=(B-A)/TNM
*       WRITE(*,*) ' DEL = ',DEL
       X=A+0.5*DEL
*       WRITE(*,*)'Del  = ',DEL,'  X = ',X
       SUM=0.
       DO 11 J=1,IT
*         WRITE(*,*)'TRAP:   J =   ',J,'  IT  =  ',IT, ' DEL = ',DEL
           SUM=SUM+SPHFUNC(X,V)
*         WRITE(*,*)'TRAP:  Sum   = ',SUM
        X=X+DEL
11     CONTINUE
*
*      WRITE(13,*) X
*      WRITE(*,*)
       S=0.5*(S+(B-A)*SUM/TNM)
       IT=2*IT
*       WRITE(*,*)'S=  ',S,'  IT  =  ',IT
     ENDIF
*      WRITE(*,*)
     RETURN
     END
*****************************************************************************
*
* This is used in integrating a function. (Numerical Recipes)P.120
*
     SUBROUTINE midpntc1(a,b,s,n,V)
     INTEGER n
     REAL a,b,s,V(15)
     INTEGER it,j
     REAL ddel,del,sum,tnm,x
     if (n.eq.1) then
       s=(b-a)*cylfunc1(0.5*(a+b),V)
     else
```

```
      it=3**(n-2)
      tnm=it
      del=(b-a)/(3.*tnm)
      ddel=del+del
      x=a+0.5*del
      sum=0.
      do 11 j=1,it
        sum=sum+cylfunc1(x,V)
        x=x+ddel
        sum=sum+cylfunc1(x,V)
        x=x+del
11    continue
      s=(s+(b-a)*sum/tnm)/3.
    endif
    return
    END
*****************************************************************************
***
    SUBROUTINE TRAPZDC1(A,B,S,N,V)
*
*     WRITE(*,*)'Inside trap  N = ',N
    IF (N.EQ.1) THEN
        S=0.5*(B-A)*(CYLFUNC1(A,V)+CYLFUNC1(B,V))
*       WRITE(*,*)'TRAPZD:  S =  ',S
      IT=1
    ELSE
      IT = (N-1)*2
*       WRITE(*,*) 'IT =  ',IT
      TNM=IT
*       WRITE(*,*)'TNM = ',TNM
      DEL=(B-A)/TNM
*       WRITE(*,*) ' DEL = ',DEL
      X=A+0.5*DEL
*       WRITE(*,*)'Del  = ',DEL,'  X = ',X
      SUM=0.
      DO 11 J=1,IT
*         WRITE(*,*)'TRAP:   J =   ',J,'  IT  =  ',IT, ' DEL = ',DEL
          SUM=SUM+CYLFUNC1(X,V)
*         WRITE(*,*)'TRAP:  Sum   = ',SUM
        X=X+DEL
11    CONTINUE
*
*       WRITE(13,*) X
*       WRITE(*,*)
      S=0.5*(S+(B-A)*SUM/TNM)
      IT=2*IT
*       WRITE(*,*)'S=  ',S,'  IT  =  ',IT
    ENDIF
*     WRITE(*,*)
    RETURN
    END
*****************************************************************
*
* This is used in integrating a function. (Numerical Recipes)P.120
```

```
*
      SUBROUTINE midpntc2(a,b,s,n,V)
      INTEGER n
      REAL a,b,s,V(15)
      INTEGER it,j
      REAL ddel,del,sum,tnm,x
      if (n.eq.1) then
        s=(b-a)*cylfunc2(0.5*(a+b),V)
      else
        it=3**(n-2)
        tnm=it
        del=(b-a)/(3.*tnm)
        ddel=del+del
        x=a+0.5*del
        sum=0.
        do 11 j=1,it
          sum=sum+cylfunc2(x,V)
          x=x+ddel
          sum=sum+cylfunc2(x,V)
          x=x+del
11      continue
        s=(s+(b-a)*sum/tnm)/3.
      endif
      return
      END
*****************************************************************************
***
      SUBROUTINE TRAPZDC2(A,B,S,N,V)
*
*       WRITE(*,*)'Inside trap  N = ',N
      IF (N.EQ.1) THEN
          S=0.5*(B-A)*(CYLFUNC2(A,V)+CYLFUNC2(B,V))
*       WRITE(*,*)'TRAPZD:  S =   ',S
       IT=1
      ELSE
       IT = (N-1)*2
*       WRITE(*,*) 'IT =  ',IT
       TNM=IT
*       WRITE(*,*)'TNM = ',TNM
       DEL=(B-A)/TNM
*       WRITE(*,*) ' DEL = ',DEL
       X=A+0.5*DEL
*       WRITE(*,*)'Del  = ',DEL,'  X = ',X
       SUM=0.
       DO 11 J=1,IT
*         WRITE(*,*)'TRAP:   J =   ',J,'  IT  =  ',IT, ' DEL = ',DEL
         SUM=SUM+CYLFUNC2(X,V)
*         WRITE(*,*)'TRAP:  Sum   = ',SUM
        X=X+DEL
11     CONTINUE
*
*       WRITE(13,*) X
*       WRITE(*,*)
       S=0.5*(S+(B-A)*SUM/TNM)
```

```
      IT=2*IT
*       WRITE(*,*)'S= ',S,' IT = ',IT
      ENDIF
*     WRITE(*,*)
      RETURN
      END

*********************************************************************
*********************************************************************
      FUNCTION BESSK0(X)
       REAL*8 Y,P1,P2,P3,P4,P5,P6,P7,
     *  Q1,Q2,Q3,Q4,Q5,Q6,Q7
       DATA P1,P2,P3,P4,P5,P6,P7/-0.57721566D0,0.42278420D0,0.23069756D0,
     *  0.3488590D-1,0.262698D-2,0.10750D-3,0.74D-5/
      DATA Q1,Q2,Q3,Q4,Q5,Q6,Q7/1.25331414D0,-0.7832358D-1,0.2189568D-1,
     *  -0.1062446D-1,0.587872D-2,-0.251540D-2,0.53208D-3/
      IF (X.LE.2.0) THEN
       Y=X*X/4.0
       BESSK0=(-LOG(X/2.0)*BESSI0(X))+(P1+Y*(P2+Y*(P3+
     *     Y*(P4+Y*(P5+Y*(P6+Y*P7))))))
      ELSE
       Y=(2.0/X)
       BESSK0=(EXP(-X)/SQRT(X))*(Q1+Y*(Q2+Y*(Q3+
     *     Y*(Q4+Y*(Q5+Y*(Q6+Y*Q7))))))
      ENDIF
      RETURN
      END
*******************************************
*
      FUNCTION BESSI0(X)
       REAL*8 Y,P1,P2,P3,P4,P5,P6,P7,
     *  Q1,Q2,Q3,Q4,Q5,Q6,Q7,Q8,Q9
       DATA P1,P2,P3,P4,P5,P6,P7/1.0D0,3.5156229D0,3.0899424D0,1.2067492D
     *0,
     *  0.2659732D0,0.360768D-1,0.45813D-2/
      DATA Q1,Q2,Q3,Q4,Q5,Q6,Q7,Q8,Q9/0.39894228D0,0.1328592D-1,
     *  0.225319D-2,-0.157565D-2,0.916281D-2,-0.2057706D-1,
     *  0.2635537D-1,-0.1647633D-1,0.392377D-2/
      IF (ABS(X).LT.3.75) THEN
       Y=(X/3.75)**2
       BESSI0=P1+Y*(P2+Y*(P3+Y*(P4+Y*(P5+Y*(P6+Y*P7)))))
      ELSE
       AX=ABS(X)
       Y=3.75/AX
       BESSI0=(EXP(AX)/SQRT(AX))*(Q1+Y*(Q2+Y*(Q3+Y*(Q4
     *   +Y*(Q5+Y*(Q6+Y*(Q7+Y*(Q8+Y*Q9))))))))
      ENDIF
      RETURN
      END
*************************************************
*
      FUNCTION BESSK1(x)
      REAL bessk1,x
CU    USES bessi1
```

```
      REAL bessi1
        DOUBLE PRECISION p1,p2,p3,p4,p5,p6,p7,q1,q2,q3,q4,q5,q6,q7,y
        SAVE p1,p2,p3,p4,p5,p6,p7,q1,q2,q3,q4,q5,q6,q7
       DATA p1,p2,p3,p4,p5,p6,p7/1.0d0,0.15443144d0,-0.67278579d0,
      *-0.18156897d0,-0.1919402d-1,-0.110404d-2,-0.4686d-4/
       DATA q1,q2,q3,q4,q5,q6,q7/1.25331414d0,0.23498619d0,-0.3655620d-1,
      *0.1504268d-1,-0.780353d-2,0.325614d-2,-0.68245d-3/
      if (x.le.2.0) then
        y=x*x/4.0
        bessk1=(log(x/2.0)*bessi1(x))+(1.0/x)*(p1+y*(p2+y*(p3+y*(p4+y*
     *(p5+y*(p6+y*p7))))))
      else
        y=2.0/x
        bessk1=(exp(-x)/sqrt(x))*(q1+y*(q2+y*(q3+y*(q4+y*(q5+y*(q6+y*
     *q7))))))
      endif
      return
      END
C*******************************************************************
C
      FUNCTION BESSI1(X)
       REAL*8 Y,P1,P2,P3,P4,P5,P6,P7,
     *    Q1,Q2,Q3,Q4,Q5,Q6,Q7,Q8,Q9
       DATA P1,P2,P3,P4,P5,P6,P7/0.5D0,0.87890594D0,0.51498869D0,
     *    0.15084934D0,0.2658733D-1,0.301532D-2,0.32411D-3/
      DATA Q1,Q2,Q3,Q4,Q5,Q6,Q7,Q8,Q9/0.39894228D0,-0.3988024D-1,
     *    -0.362018D-2,0.163801D-2,-0.1031555D-1,0.2282967D-1,
     *    -0.2895312D-1,0.1787654D-1,-0.420059D-2/
      IF (ABS(X).LT.3.75) THEN
       Y=(X/3.75)**2
       BESSI1=X*(P1+Y*(P2+Y*(P3+Y*(P4+Y*(P5+Y*(P6+Y*P7))))))
     ELSE
       AX=ABS(X)
       Y=3.75/AX
       BESSI1=(EXP(AX)/SQRT(AX))*(Q1+Y*(Q2+Y*(Q3+Y*(Q4+
     *     Y*(Q5+Y*(Q6+Y*(Q7+Y*(Q8+Y*Q9))))))))
       IF(X.LT.0.)BESSI1=-BESSI1
     ENDIF
     RETURN
     END
C*******************************************************************
C
```

A.2.2 Calculation of the free energy from the FIDAP output

```
********** Comparison of Numerical Values of FIDAP
********** to Analytical Solution
*
*  Erin M Johnson
*  June 25, 1992
*  REVISED: March 4, 1994
*
      CHARACTER*20 XCOORD, YCOORD, ZCOORD, POTENT, LABEL(15),FLUX
      CHARACTER*20 LABT,TLAB
      CHARACTER*6 BCSPH, BCCYL
      CHARACTER*50 HEADING,TEMP
      CHARACTER*14 FILENAME
      CHARACTER*6 FIL
      CHARACTER*10 UL
      DIMENSION X(100000), Y(100000), Z(100000), PHI(100000)
      DIMENSION FLX(100000), EXACT(100000), NONLIN(100000)
      DIMENSION CYLPHI(100000)
      REAL FMAX, FSQUARE, DIFF, PERCENT, PMAX, CONST, FOUR
      REAL VALUE(15),V(10,6),MAG(5),AREA(20),GPOT(20),GFLUX(20)
      REAL EAREA(20,500),EPOT(20,500),EFLUX(20,500),D(4),C(4)
      REAL PSIS, PSIC, LAMBDAC, DELF(20,500), DELG(20), DELTAG(2)
      REAL RAD(5),RADERR, A1,A2,HR,LAM,GAM,ELIN(20,500),EEXT(20,500)
      REAL GEXT(20),GLIN(20),SUPER(2),SUP,SPHFLAT,CON,AUTO,DIFFER
      REAL TX(10,100000),TY(10,100000),TEMPX,A,B,VV(10,6),KAPPA
      REAL CONPHI(10)
      INTEGER NODES,GROUP,NUM(20),EL(20,5000,10),M,KNUM(10)
*
      OPEN(16,FILE='sc.txt',STATUS='OLD')
*
* read in input parameters
      READ(16,94)LABEL(1)
      READ(16,*)VALUE(1)
*     WRITE(*,*)VALUE(1)
      READ(16,94)LABEL(2)
      READ(16,*)VALUE(2)
*     WRITE(*,*)VALUE(2)
      READ(16,94)LABEL(3)
      READ(16,*)VALUE(3)
*     WRITE(*,*)VALUE(3)
      READ(16,94)LABEL(4)
      READ(16,*)VALUE(4)
*     WRITE(*,*)VALUE(4)
      READ(16,94)LABEL(5)
      READ(16,*)VALUE(5)
*     WRITE(*,*)VALUE(5)
      READ(16,94)LABEL(6)
      READ(16,*)VALUE(6)
*     WRITE(*,*)VALUE(6)
```

```
      READ(16,94)LABEL(7)
      READ(16,*)VALUE(7)
*       WRITE(*,*)VALUE(7)
      READ(16,94)LABEL(8)
      READ(16,*)VALUE(8)
*       WRITE(*,*)VALUE(8)
      READ(16,94)LABEL(9)
      READ(16,*)VALUE(9)
*       WRITE(*,*)VALUE(9)
      READ(16,94)LABEL(10)
      READ(16,*)VALUE(10)
*       WRITE(*,*)VALUE(10)
      READ(16,94)LABEL(11)
      READ(16,*)VALUE(11)
*       WRITE(*,*)VALUE(11)
      READ(16,94)LABEL(12)
      READ(16,*)VALUE(12)
*       WRITE(*,*)VALUE(12)
      READ(16,94)LABEL(13)
      READ(16,*)VALUE(13)
*       WRITE(*,*)VALUE(13)
      READ(16,94)LABEL(14)
      READ(16,*)VALUE(14)
* determine what type of boundary conditions we used
       TLAB=LABEL(6)
       BCSPH=TLAB(1:6)
       LABT=LABEL(7)
       BCCYL=LABT(1:6)
*
*read the simulation variables from sc.txt
 90    FORMAT(A20,I10)
 91    FORMAT(5E15.8)
 92     FORMAT(2X,I2,2X,I4)
 93      FORMAT(3X,I3,2X,I4,2X,I4,2X,I4,2X,I4)
 94    FORMAT(A)
*
       FIL='sphcyl'
       IF(VALUE(7).EQ.0) FIL = 'isosph'
       IF(VALUE(6).EQ.0) FIL = 'isocyl'
*
       FILENAME = FIL//'.FPNEUT'
      WRITE(*,*)FILENAME
      OPEN(12,FILE=FILENAME,STATUS='OLD')
*       FILENAME = FIL//'.ELEM  '
*       WRITE(*,*)FILENAME
*       OPEN(14,FILE=FILENAME,STATUS='OLD')
       FILENAME = FIL//'.Zrad  '
      WRITE(*,*)FILENAME
       OPEN(15,FILE=FILENAME,STATUS='NEW')
       FILENAME = FIL//'.Zxyz  '
      WRITE(*,*)FILENAME
       OPEN(19,FILE=FILENAME,STATUS='NEW')
       FILENAME = FIL//'.output'
      WRITE(*,*)FILENAME
```

```
      OPEN(21,FILE=FILENAME,STATUS='NEW')
      FILENAME = FIL//'.Zarea '
      WRITE(*,*)FILENAME
      OPEN(20,FILE=FILENAME,STATUS='NEW')
      FILENAME = FIL//'.Zplane'
      WRITE(*,*)FILENAME
      OPEN(22,FILE=FILENAME,STATUS='NEW')
*
* read the neutral file for the simulation variables
      READ(12,90) XCOORD,NODES
      READ(12,91) (X(I),I=1,NODES)
      WRITE(*,*)'Read X'
      READ(12,90) YCOORD,NODES
      READ(12,91) (Y(I),I=1,NODES)
      WRITE(*,*)'Read Y'
      READ(12,90) ZCOORD,NODES
      READ(12,91) (Z(I),I=1,NODES)
      WRITE(*,*)'Read Z'
      READ(12,90) POTENT,NODES
      READ(12,91) (PHI(I),I=1,NODES)
      WRITE(*,*)'Read Phi'
      READ(12,90) FLUX,NODES
      READ(12,91) (FLX(I),I=1,NODES)
      WRITE(*,*)'Read Flux'
*
* set norm variables to zero
      FMAX = 0.0
      FSQUARE = 0.0
      PMAX = 0.0

* get simulation variables from sc.txt
      RADS = VALUE(2)
      RADC = VALUE(1)
      TAU = 1.0/VALUE(3)
      CC = VALUE(8)+VALUE(1)
      SC = VALUE(8)+VALUE(1)+VALUE(1)+VALUE(4)+VALUE(2)
      WRITE(*,*)'Center of cylinder and sphere: ',CC,SC
* set the constants on the isolated sphere/cylinder potentials
      IF(BCSPH.EQ.'bcflux') THEN
        PSIS = VALUE(6)/(1./RADS+TAU)
        SIGMAS = VALUE(6)
      ELSE
        PSIS = VALUE(6)
        SIGMAS = VALUE(6)*(1./RADS+TAU)
      ENDIF
*
      IF(BCCYL.EQ.'bcflux') THEN
        LAMBDAC = TAU*BESSK1(TAU*RADC)
        PSIC = VALUE(7)*BESSK0(TAU*RADC)/LAMBDAC
        SIGMAC = VALUE(7)
        LAMBDAC = BESSK0(TAU*RADC)
      ELSE
        PSIC = VALUE(7)
        LAMBDAC = BESSK0(TAU*RADC)
```

```
        SIGMAC = VALUE(7)*TAU*BESSK1(TAU*RADC)/LAMBDAC
      ENDIF
      WRITE(*,*)'Calculated psic and psis :  ',PSIC,PSIS
      WRITE(*,*)'Calculated sigmac and sigmas : ',SIGMAC,SIGMAS
*
      FSQUARE=0.0
      CSQR=0.0
      PMAX = 0.0
      CMAX = 0.0
      IN=0
* find the exact potential to compare to simulation results
      DO 11 J = 1, NODES
        DIFF = 0.0
        RS = SQRT((X(J)-SC)*(X(J)-SC)+Y(J)*Y(J)+Z(J)*Z(J))
        RC = SQRT((X(J)-CC)*(X(J)-CC)+Z(J)*Z(J))
        IF(RS.GE.RADS) THEN
          IF(RC.GE.RADC) THEN
           EXACT(J) = PSIS*RADS/RS*EXP(TAU*(RADS-RS))
           EXACT(J) = EXACT(J) + PSIC/LAMBDAC*BESSK0(TAU*(RC))
          ELSE
           EXACT(J) = PSIC+PSIS*RADS/RS*EXP(TAU*(RADS-RS))
          ENDIF
        ELSE
         EXACT(J) = PSIS+PSIC/LAMBDAC*BESSK0(TAU*(RC))
        ENDIF
* calculations for the norm
        DIFF = ABS(EXACT(J) - PHI(J))
        IF(EXACT(J).NE.0) THEN
          P = DIFF/EXACT(J)
        ELSE
          P=0
        ENDIF
        FSQUARE = FSQUARE + DIFF*DIFF
        IF(DIFF.GT.FMAX) THEN
          IF(EXACT(J).NE.0) THEN
           FMAX=DIFF
           MN=J
          ENDIF
        ENDIF
        IF(P.GT.PMAX) PMAX = P
* calculations to see if the box is big enough
        IF(Y(J).EQ.VALUE(9)) THEN
          IN=IN+1
          CYLPHI(J)=PSIC/LAMBDAC*BESSK0(TAU*(RC))
          CDIFF=ABS(CYLPHI(J)-PHI(J))
          CSQR = CSQR + CDIFF*CDIFF
          IF(CDIFF.GT.CMAX) THEN
             CMAX = CDIFF
             JIL = J
             XCYLPHI=CYLPHI(J)
          ENDIF
        ENDIF
*
 11   CONTINUE
```

```
*
      FSQUARE = FSQUARE/REAL(NODES)
      IF(IN.GT.0) THEN
          CSQR = CSQR/REAL(IN)
      ELSE
        WRITE(*,*)'no nodes on cylinder cut'
      ENDIF
      IF(XCYLPHI.GT.0.00001) THEN
         CPER = ABS((XCYLPHI-PHI(JIL))/XCYLPHI)*100.
      ELSE
        WRITE(*,*)'Max diff in cylinder potential is < 0.00001'
        CPER = 0.0
      ENDIF
*
      IF(CPER.GT.5.) WRITE(*,*)'!!!! May not be a good mesh !! ',CPER
      Percent=ABS((EXACT(MN)-PHI(MN))/EXACT(MN))*100.
*
      WRITE(*,*)'NODES = ',NODES
      WRITE(*,*)'L2 NORM = ',FSQUARE
      WRITE(*,*)'MAX NORM = ',FMAX
      WRITE(*,*)
      WRITE(*,*)'Percent max error  = ',PERCENT
      WRITE(*,*)'Node with the maximum error  ',MN
      WRITE(*,*)'X, Y, Z   ',X(MN),Y(MN),Z(MN)
      WRITE(*,*)'PHI AND EXACT   ',PHI(MN),EXACT(MN)
      WRITE(*,*)
      WRITE(*,*)'The cylinder L2 norm is : ',CSQR
      WRITE(*,*)'The cylinder max norm is : ',CMAX
      WRITE(*,*)'The % cylinder max err is : ',CPER
*
 120  FORMAT(A)
 121  FORMAT(A,1X,F7.1)
      WRITE(19,120)'X coordinate'
      WRITE(19,120)'Potential'
      WRITE(19,121)'xmin',0.0
      WRITE(19,121)'xmax',2*VALUE(1)+2*VALUE(2)+VALUE(4)+2*VALUE(8)
      WRITE(19,121)'ymin',0.0
      WRITE(19,121)'ymax',PSIC+PSIS
      WRITE(19,121)'end'
      WRITE(19,120)'1.0e32  1 1 1'
*
      DO 99 J = 1,NODES
        IF(Y(J).EQ.0.0) THEN
          IF(Z(J).EQ.0.) WRITE(19,91) X(J),PHI(J)
        ENDIF
 99   CONTINUE
      WRITE(19,120)'1.0e32  4 9 5 '
*
      DO 66 J = 1,NODES
        IF(Y(J).EQ.0.0) THEN
          IF(Z(J).EQ.0.) WRITE(19,91) X(J),EXACT(J)
        ENDIF
 66   CONTINUE
*
```

```
      WRITE(22,120)'X coordinate'
      WRITE(22,120)'Y coordinate'
      WRITE(22,120)'horz'
       WRITE(22,121)'xorg',1.25
       WRITE(22,121)'yorg',2.0
      WRITE(22,120)'labl 1'
       WRITE(22,120)' 4.5 5.0 -0.2'
      WRITE(22,120)'Two Dimensional Potential Profile'
      XMAX=2*VALUE(1)+2*VALUE(2)+VALUE(4)+2*VALUE(8)
      YMAX=5*VALUE(2)
       WRITE(22,121)'xlen',9.0
      WRITE(22,121)'ylen',YMAX*9.0/XMAX
       WRITE(22,121)'xmin',0.0
       WRITE(22,121)'xmax',XMAX
       WRITE(22,121)'ymin',0.0
      WRITE(22,121)'ymax',5*VALUE(2)
       WRITE(22,121)'end'
       WRITE(22,120)'1.0e32  110'
*
       IF(PSIS.GE.PSIC) THEN
         CON = PSIS
      ELSE
         CON = PSIC
      ENDIF
      AUTO=CON/10.
      CON=CON+AUTO

      DO 202 L=1,10
        CON=CON-AUTO
        K=0
       DO 201 J= NODES,1,-1
         IF(Z(J).EQ.0.) THEN
           DIFFER=ABS(PHI(J)-CON)
           IF(DIFFER.LT.0.01) THEN
             K=K+1
             TX(L,K)=X(J)
             TY(L,K)=Y(J)
             CONPHI(L)=CON
             KNUM(L)=K
           ENDIF
         ENDIF
 201   CONTINUE
* write values to file
       DO 206 I=1,K
         WRITE(22,91)TX(L,I),TY(L,I)
 206   CONTINUE
        IF(K.GT.0) WRITE(22,120)'1.0e32 110 '
 202    CONTINUE
************************************************
* read the node numbers for each element from *.ELEM
*
      FILENAME = FIL//'.ELEM  '
      OPEN(14,FILE=FILENAME,STATUS='OLD')
*
```

```
      DO 89 K=10,18
        READ(14,*,END=89)GROUP,NUM(K)
       DO 87 I = 1,NUM(K)
        READ(14,301) (EL(GROUP,I,J),J=1,10)
 87     CONTINUE
 89    CONTINUE
 301     FORMAT(2X,I4,1X,I5,1X,I5,1X,I5,1X,I5,1X,I5,1X,I5,1X,I5,1X,I5,
    +       1X,I5,1X,I5)
 4     FORMAT(A20)
*
*****************************************************************
* calculation of the average surface potentials, surface fluxes
* and the area of the sphere and the cylinder
*
* K is the group number:  10-12 are cylinder 13-16 are sphere
*
      DO 50 K = 10,18
* I is a surface element in each group
       AREA(K)=0.0
       GPOT(K)=0.0
       GFLUX(K)=0.0
       GEXT(K)=0.0
       GLIN(K)=0.0
       DELG(K)=0.0
       DO 51 I=1,NUM(K)
* define one node as the origin and vectors to the other 3 nodes
* mag is the magnitude of the vector from the element origin.
         WRITE(20,*)'Area calcs for group ',K
         WRITE(20,*)'Element : ',I
           WRITE(20,*)'Node','X','Y','Z'
         DO 52 J=1,9
*           WRITE(*,*)'Node number is : ',EL(K,I,J+1)
           VV(J,1)=X(EL(K,I,J+1))-X(EL(K,I,2))
           VV(J,2)=Y(EL(K,I,J+1))-Y(EL(K,I,2))
           VV(J,3)=Z(EL(K,I,J+1))-Z(EL(K,I,2))
           VV(J,4)=PHI(EL(K,I,J+1))
           VV(J,5)=FLX(EL(K,I,J+1))
           VV(J,6)=EXACT(EL(K,I,J+1))
*            WRITE(*,*)'Node : ',J,' for element: ',I,' = ',
*    +     'X = ',V(J,1),' Y = ',V(J,2),' Z = ',V(J,3)
 52      CONTINUE
* get the node values in the correct format *
        DO 302 J=1,6
          V(1,J)=VV(1,J)
          V(2,J)=VV(7,J)
          V(3,J)=VV(5,J)
          V(4,J)=VV(3,J)
          V(5,J)=VV(8,J)
          V(6,J)=VV(6,J)
          V(7,J)=VV(4,J)
          V(8,J)=VV(2,J)
          V(9,J)=VV(9,J)
 302     CONTINUE
        DO 303 J=1,9
```

```
          WRITE(20,*)I,(V(J,KK),KK=1,6)
 303      CONTINUE
**********************
* calculate the areas
**********************
*         WRITE(*,*)'Before Calling Qromb ',K,I
         V(10,2)=0.
         CALL QROMB(-1.,1.,EA,V)
*
         EAREA(K,I)=EA
*         WRITE(*,*)'The element area is : ',K,I,EA
*         WRITE(20,*)'The element area is : ',EAREA(K,I)
         WRITE(20,*)
         AREA(K)=AREA(K)+EAREA(K,I)
**********************************
* calcuate the accuracy of the nodes
**********************************
         WRITE(15,*)'The nodal radius for group: element: ', K, I
         WRITE(15,32)'Element Number','Calculated Radius',
     +         'Actual Radius','Percent Error'
 32       FORMAT(A14,1X,A20,1X,A14,1X,A14,1X,A14)
 33        FORMAT(4X,I5,8X,F16.13,6X,F6.2,7X,F10.7)
         DO 69 L=2,10
          RY=Y(EL(K,I,L))**2
          RZ=Z(EL(K,I,L))**2
          IF (K.GE.10) THEN
            RX=(X(EL(K,I,L))-SC)**2
           RAD(L)=SQRT(RX+RY+RZ)
           RADTEMP=VALUE(2)
           RADERR=(VALUE(2)-RAD(L))/VALUE(2)*100.
          ELSE
            RX=(X(EL(K,I,L))-CC)**2
           RAD(L)=SQRT(RX+RZ)
           RADTEMP=VALUE(1)
           RADERR=(VALUE(1)-RAD(L))/VALUE(1)*100.
          ENDIF
          WRITE(15,33)EL(K,I,L),RAD(L),RADTEMP,RADERR
 69       CONTINUE
*
************************************************
* calculate the average element potential and flux
************************************************
         EPOT(K,I)=0.0
         EFLUX(K,I)=0.0
         EEXT(K,I)=0.0
         ELIN(K,I)=0.0
         DELF(K,I)=0.0
*
         V(10,2)=4.0
         CALL QROMB(-1.,1.,EPOT(K,I),V)
         V(10,2)=5.0
         CALL QROMB(-1.,1.,EFLUX(K,I),V)
         V(10,2)=6.0
         CALL QROMB(-1.,1.,EEXT(K,I),V)
```

```
*
        WRITE(20,*)
        WRITE(20,*)'The average potential on this element is:'
        WRITE(20,*)EPOT(K,I)/EAREA(K,I)
        WRITE(20,*)'The average flux on this element is:'
        WRITE(20,*)EFLUX(K,I)/EAREA(K,I)
        WRITE(20,*)'The average linear superposition potential is:'
        WRITE(20,*)EEXT(K,I)/EAREA(K,I)
*
       GPOT(K)=GPOT(K)+EPOT(K,I)
        GFLUX(K)=GFLUX(K)+EFLUX(K,I)
       GEXT(K)=GEXT(K)+EEXT(K,I)
       WRITE(20,*)
       WRITE(20,*)'The group potential average is'
       WRITE(20,*)K,GPOT(K)/AREA(K)
       WRITE(20,*)'The group flux average is: '
       WRITE(20,*)K,GFLUX(K)/AREA(K)
       WRITE(20,*)'The group linear superposition is'
       WRITE(20,*)K,GEXT(K)/AREA(K)
       WRITE(20,*)
* do delta g calculations
        IF(K.GE.13) THEN
          IF (BCSPH.EQ.'bcflux')  THEN
           DELF(K,I)=EPOT(K,I)-PSIS*EAREA(K,I)
         ELSE
           DELF(K,I)=EFLUX(K,I)+SIGMAS*EAREA(K,I)
         ENDIF
         ELIN(K,I)=EEXT(K,I)-PSIS*EAREA(K,I)
       ELSE
          IF(BCCYL.EQ.'bcflux') THEN
            DELF(K,I)=EPOT(K,I)-PSIC*EAREA(K,I)
         ELSE
            DELF(K,I)=EFLUX(K,I)+SIGMAC*EAREA(K,I)
         ENDIF
         ELIN(K,I)=EEXT(K,I)-PSIC*EAREA(K,I)
       ENDIF
*
       DELG(K) = DELG(K)+DELF(K,I)
        GLIN(K) = GLIN(K)+ELIN(K,I)
*
 51    CONTINUE
 50   CONTINUE
*
     DO 59 I=10,18
       IF(AREA(I).GT.0) THEN
         WRITE(*,*)'THE AREA OF GROUP : ',I,'  is : ',AREA(I)
        GPOT(I)=GPOT(I)/AREA(I)
        WRITE(*,*)'The average potential is :  ',GPOT(I)
        GFLUX(I)=GFLUX(I)/AREA(I)
        WRITE(*,*)'The average flux is :  ',GFLUX(I)
        WRITE(*,*)'The delta g is :  ',DELG(I)
        WRITE(*,*)'The linear g is :  ',GLIN(I)
       ELSE
          WRITE(*,*)'The area of group ',I,' is zero'
```

```
      ENDIF
 59   CONTINUE
*
      IF(BCSPH.EQ.'bcflux') THEN
        DELTAG(1) = SIGMAS/2.*(DELG(13)+DELG(14)+DELG(15)+DELG(16)+
     +      DELG(17)+DELG(18))
      ELSE
        DELTAG(1) = PSIS/2.*(DELG(13)+DELG(14)+DELG(15)+DELG(16)+
     +      DELG(17)+DELG(18))
      ENDIF
      IF(BCCYL.EQ.'bcflux') THEN
        DELTAG(2) = SIGMAC/2.*(DELG(10)+DELG(11)+DELG(12))
      ELSE
        DELTAG(2) = PSIC/2.*(DELG(10)+DELG(11)+DELG(12))
      ENDIF
      WRITE(*,*)'The change is free energy is : ',DELTAG(1)+DELTAG(2)
      SUPER(1)=SIGMAS/2.*(GLIN(13)+GLIN(14)+GLIN(15)+GLIN(16)+
     +      GLIN(17)+GLIN(18))
      SUPER(2)=SIGMAC/2.*(GLIN(10)+GLIN(11)+GLIN(12))
      SUP=SUPER(1)+SUPER(2)
      WRITE(*,*)'The linear sup free energy is : ',SUP
*
**********************************************************************
* Output for each simulation
**********************************************************************
      WRITE(*,*)'The boundary condition is : ',BCSPH
      IF(BCSPH.EQ.'bcflux') THEN
        HEADING = 'Constant Surface Charge Density'
      ELSE
        HEADING = 'Constant Surface Potential'
      ENDIF
      WRITE(*,*)'The heading is : ',HEADING
*
      UL = '__________'
 20   FORMAT(A,/)
 21   FORMAT(A)
 110  FORMAT(T10,A,T55,A,/)
      WRITE(21,*)
      WRITE(21,110)HEADING,'Erin M. Johnson'
      WRITE(21,131)UL,UL,UL,UL,UL,UL
      WRITE(21,*)
      WRITE(21,20)'Constants'
 101  FORMAT(2X,A20,1X,F6.3,5X,A20,1X,F6.3)
      WRITE(21,101)'Cylinder Radius',VALUE(1),'Sphere Radius'
     +      ,VALUE(2)
      WRITE(21,101)'Inverse Debye Length',VALUE(3),'Surface Distance',
     +   VALUE(4)
      WRITE(21,*)
      WRITE(21,20)'Boundary Conditions'
      WRITE(21,101)LABEL(6),VALUE(6),LABEL(7),VALUE(7)
      IF(BCSPH.EQ.'bcflux') THEN
        WRITE(21,101)'Isolated Sph Pot',PSIS,'Isolated Cyl Pot',PSIC
      ELSE
        WRITE(21,101)'Isolated Sph Flux',SIGMAS,'Isolated Cyl Flux'
```

```
     +     ,SIGMAC
           ENDIF
           WRITE(21,*)
           WRITE(21,131)UL,UL,UL,UL,UL,UL
           WRITE(21,*)
           WRITE(21,20)'Nodal Data'
 103       FORMAT(2X,A20,2X,I6)
           WRITE(21,103)'Nodes',NODES
           WRITE(21,101)'L2 Norm',FSQUARE,'Max Norm',FMAX
           WRITE(21,*)
 104       FORMAT(2X,A20,1X,F7.3,5X,A20,2X,I6)
           WRITE(21,104)'% Max error',PERCENT,
     +     'Maximum error node',MN
 107       FORMAT(2X,A20,1X,F7.3,2X,F7.3,2X,F7.3)
           WRITE(21,101)'Numerical Potential',PHI(MN),
     +     'Linear Sup Potential',EXACT(MN)
           WRITE(21,107)'Max err node X, Y, Z',X(MN),Y(MN),Z(MN)
           WRITE(21,*)
 105       FORMAT(2X,A20,1X,F6.3)
           WRITE(21,105)'Length of x-axis',2*VALUE(8)+2*VALUE(1)
     +     +VALUE(4)+2*VALUE(2)
           WRITE(21,101)'Box height (Y)',VALUE(9),'Box width (Z)',
     +     VALUE(10)
*          WRITE(21,101)'Cyl detail length',VALUE(11),
*    +     'Sph detail length',VALUE(12)
*          WRITE(21,101)'Ratio of detail',VALUE(14)
           WRITE(21,*)
 131       FORMAT(5A10,A4,/)
           WRITE(21,131)UL,UL,UL,UL,UL,UL
           WRITE(21,20)'Nodal Group Information'
*
 102       FORMAT(A,2X,I2)
           DO 41 J=10,18
              WRITE(21,102)'Group',J
              WRITE(21,106)'Area',AREA(J)
              WRITE(21,106)'Ave Potential',GPOT(J),'Average Flux'
     +        ,-1.*GFLUX(J)
              WRITE(21,106)'Delta G',DELG(J)
              WRITE(21,*)
 41        CONTINUE
           WRITE(21,*)
           WRITE(21,131)UL,UL,UL,UL,UL,UL
           WRITE(21,*)
*
           WRITE(21,20)'Cylinder Summary : Groups 10-12 '
           CYLAREA=AREA(10)+AREA(11)+AREA(12)
           CYLEXACT=3.14159*VALUE(1)*VALUE(9)
 106       FORMAT(2X,A20,1X,F11.6,5X,A20,1X,F11.6)
           WRITE(21,106)'Area',CYLAREA,'Exact area',CYLEXACT
           CYLERR=(CYLEXACT-CYLAREA)/CYLEXACT
           WRITE(21,106)'% Error in Area',CYLERR
           CYLPOT=(GPOT(10)*AREA(10)+GPOT(11)*AREA(11)+
     +     GPOT(12)*AREA(12))/CYLAREA
           CYLFLUX=(GFLUX(10)*AREA(10)+GFLUX(11)*AREA(11)
```

```
     +    +GFLUX(12)*AREA(12))/CYLAREA
          WRITE(21,106)'Ave Potential',CYLPOT,'Average Flux',-1.0*CYLFLUX
          WRITE(21,*)
          WRITE(21,20)'Sphere Summary : Groups 13-18 '
          SPHAREA=AREA(13)+AREA(14)+AREA(15)+AREA(16)+AREA(17)+
     +     AREA(18)
          SPHEXACT=3.14159*VALUE(2)**2
          WRITE(21,106)'Area',SPHAREA,'Exact Area',SPHEXACT
          SPHERR = (SPHEXACT-SPHAREA)/SPHEXACT*100
          WRITE(21,106)'% Error in Area',SPHERR
          SPHPOT=(GPOT(13)*AREA(13)+GPOT(14)*AREA(14)+GPOT(15)*AREA(15)+
     +    GPOT(16)*AREA(16)+GPOT(17)*AREA(17)+GPOT(18)*AREA(18)
     +    )/SPHAREA
          SPHFLUX=(GFLUX(13)*AREA(13)+GFLUX(14)*AREA(14)+
     +    GFLUX(15)*AREA(15)+GFLUX(16)*AREA(16)+GFLUX(17)*AREA(17)+
     +    GFLUX(18)*AREA(18))/SPHAREA
          WRITE(21,106)'Ave Potential',SPHPOT,'Average Flux',-1.0*SPHFLUX
          WRITE(21,*)
          WRITE(21,131)UL,UL,UL,UL,UL,UL
          WRITE(21,*)
          WRITE(21,21)'Simulation Change in Free Energy Summary'
          WRITE(21,*)
          WRITE(21,106)'Sph part delta F',DELTAG(1),
     +    'Cyl part delta F',DELTAG(2)
          WRITE(21,*)
  108     FORMAT(2X,A30,2X,F11.6)
          WRITE(21,108)'Sphere and Cylinder delta F',
     +    (DELTAG(1)+DELTAG(2))
          WRITE(21,*)
          WRITE(21,108)'Linear Sup Cyl/Sph delta F',SUP
          WRITE(21,*)
          WRITE(21,131)UL,UL,UL,UL,UL,UL
          WRITE(21,*)
          WRITE(21,21)'Comparison of Free Energy to Approximations'
          WRITE(21,*)
          WRITE(21,108)'Simulation delta F',
     +    4.*(DELTAG(1)+DELTAG(2))
          WRITE(21,108)'Linear Superposition delta F',4*SUP
          WRITE(21,*)
          SPHSUP=4.*3.14159*VALUE(1)*VALUE(2)/
     +    (VALUE(4)+VALUE(1)+VALUE(2))*PSIC*PSIS
     +     *EXP(-TAU*VALUE(4))
          WRITE(21,108)'Linear Sup Sph/Sph delta F',SPHSUP
          A1=VALUE(1)
          A2=VALUE(2)
          HR=VALUE(4)
          LAM=SQRT((A2*(HR+A1)/A1/(HR+A2)))+SQRT(A1*(HR+A2)/A2/(HR+A1))
          GAM=SQRT(A1*A2/(HR+A1)/(HR+A2))*EXP(TAU*(A1+A2))
          BELLF=2.*3.14159/TAU
     +    *A1*A2*(HR+A1)*(HR+A2)/(HR+A1+A2)/((A1+A1)*(HR+A1+A2)
     +    -A1*A1-A2*A2)*((PSIC**2+PSIS**2+LAM*PSIC*PSIS)*
     +    LOG(1+GAM*EXP(-TAU*(HR+A1+A2)))
     +    + (PSIC**2+PSIS**2-LAM*PSIC*PSIS)*
     +    LOG(1-GAM*EXP(-TAU*(HR+A1+A2))))
```

```
      WRITE(21,108)'Bell/Deryaguin Approx delta F',BELLF
      LAM=SQRT((A2+HR)/A2)+SQRT(A2/(A2+HR))
      SPHFLAT=2.*3.14159/TAU*A2*(A2+HR)/(2.*A2+HR)*
     +   ((PSIC**2+PSIS**2+LAM*PSIC*PSIS)*
     +   LOG(1.+SQRT(A2/(A2+HR))*EXP(-TAU*HR))+
     +   (PSIC**2+PSIS**2-LAM*PSIS*PSIC)*
     +   LOG(1.-SQRT(A2/(A2+HR))*EXP(-TAU*HR)))
*     WRITE(21,108)'Bell Sphere/Flat Plate delta F',SPHFLAT
      SPHFLAT=4.*3.14159*PSIC*PSIS*
     +      EXP(-TAU*HR)+0.25*PSIS*PSIS*A2/(HR+A2)*
     +      EXP(-2.*TAU*HR)
      WRITE(21,108)'2nd Sphere/Flat Plate delta F',SPHFLAT
      WRITE(21,400)
  400 FORMAT(1X,/////////)
      WRITE(21,110)'Comparison of Simulation to Superposition'
  401  FORMAT(T5,A,T10,A,T25,A,T50,A,/)
  402   FORMAT(2X,F6.2,3X,F8.4,T28,F8.4,T50,F6.2)
       WRITE(21,401)'X','Simulation','Superposition','% Diff'
      DO 403 J=1,NODES
        IF((Y(J).EQ.0.).AND.(Z(J).EQ.0.)) THEN
         PERDIF=ABS((PHI(J)-EXACT(J))/EXACT(J))*100.
          WRITE(21,402)X(J),PHI(J),EXACT(J),PERDIF
        ENDIF
  403  CONTINUE
      WRITE(21,131)UL,UL,UL,UL,UL,UL
      WRITE(21,110)'Comparison of Simulation to Isolated Cylinder'
       WRITE(21,401)'X','Simulation','Iso. Cylinder','% Diff'
      DO 405 J=1,NODES
        IF((Y(J).EQ.VALUE(9)).AND.(Z(J).EQ.0.)) THEN
         PERDIF=ABS((CYLPHI(J)-EXACT(J))/EXACT(J))*100.
          WRITE(21,402)X(J),CYLPHI(J),EXACT(J),PERDIF
        ENDIF
  405  CONTINUE
      WRITE(21,131)UL,UL,UL,UL,UL,UL
      WRITE(21,110)'Isopotential Lines For X - Y Surface'
      WRITE(21,*)
  406  FORMAT(1X,A,T15,A,T23,A,T31,A,T39,A,T47,A,T55,A)
  407   FORMAT(2X,F6.3,T12,F6.3,T20,F6.3,T28,F6.3,T36,F6.3,
    +    T44,F6.3,T52,F6.3)
        WRITE(21,406)'Potential','X','Y','X','Y','X','Y'
      DO 408 L=1,10
        DO 409 K = 1,KNUM(L),3
          IF (K+2.LE.KNUM(L)) THEN
            WRITE(21,407)CONPHI(L),TX(L,K),TY(L,K),TX(L,K+1),
    +       TY(L,K+1),TX(L,K+2),TY(L,K+2)
          ELSEIF (K+1.LE.KNUM(L)) THEN
            WRITE(21,407)CONPHI(L),TX(L,K),TY(L,K),TX(L,K+1),
    +       TY(L,K+1)
          ELSE
            WRITE(21,407)CONPHI(L),TX(L,K),TY(L,K)
          ENDIF
  409     CONTINUE
  408  CONTINUE
*
```

```
*
*
      Stop
      END
**************************************
*
      FUNCTION BESSK0(X)
       REAL*8 Y,P1,P2,P3,P4,P5,P6,P7,
     *   Q1,Q2,Q3,Q4,Q5,Q6,Q7
       DATA P1,P2,P3,P4,P5,P6,P7/-0.57721566D0,0.42278420D0,0.23069756D0,
     *   0.3488590D-1,0.262698D-2,0.10750D-3,0.74D-5/
       DATA Q1,Q2,Q3,Q4,Q5,Q6,Q7/1.25331414D0,-0.7832358D-1,0.2189568D-1,
     *   -0.1062446D-1,0.587872D-2,-0.251540D-2,0.53208D-3/
       IF (X.LE.2.0) THEN
        Y=X*X/4.0
        BESSK0=(-LOG(X/2.0)*BESSI0(X))+(P1+Y*(P2+Y*(P3+
     *      Y*(P4+Y*(P5+Y*(P6+Y*P7))))))
       ELSE
        Y=(2.0/X)
        BESSK0=(EXP(-X)/SQRT(X))*(Q1+Y*(Q2+Y*(Q3+
     *      Y*(Q4+Y*(Q5+Y*(Q6+Y*Q7))))))
       ENDIF
       RETURN
       END
******************************************
*
      FUNCTION BESSI0(X)
       REAL*8 Y,P1,P2,P3,P4,P5,P6,P7,
     *   Q1,Q2,Q3,Q4,Q5,Q6,Q7,Q8,Q9
       DATA P1,P2,P3,P4,P5,P6,P7/1.0D0,3.5156229D0,3.0899424D0,1.2067492D
     *0,
     *   0.2659732D0,0.360768D-1,0.45813D-2/
       DATA Q1,Q2,Q3,Q4,Q5,Q6,Q7,Q8,Q9/0.39894228D0,0.1328592D-1,
     *   0.225319D-2,-0.157565D-2,0.916281D-2,-0.2057706D-1,
     *   0.2635537D-1,-0.1647633D-1,0.392377D-2/
       IF (ABS(X).LT.3.75) THEN
        Y=(X/3.75)**2
        BESSI0=P1+Y*(P2+Y*(P3+Y*(P4+Y*(P5+Y*(P6+Y*P7)))))
       ELSE
        AX=ABS(X)
        Y=3.75/AX
        BESSI0=(EXP(AX)/SQRT(AX))*(Q1+Y*(Q2+Y*(Q3+Y*(Q4
     *     +Y*(Q5+Y*(Q6+Y*(Q7+Y*(Q8+Y*Q9))))))))
       ENDIF
       RETURN
       END
**************************************************
*
      FUNCTION BESSK1(x)
      REAL bessk1,x
CU    USES bessi1
      REAL bessi1
       DOUBLE PRECISION p1,p2,p3,p4,p5,p6,p7,q1,q2,q3,q4,q5,q6,q7,y
       SAVE p1,p2,p3,p4,p5,p6,p7,q1,q2,q3,q4,q5,q6,q7
```

```
      DATA p1,p2,p3,p4,p5,p6,p7/1.0d0,0.15443144d0,-0.67278579d0,
     *-0.18156897d0,-0.1919402d-1,-0.110404d-2,-0.4686d-4/
      DATA q1,q2,q3,q4,q5,q6,q7/1.25331414d0,0.23498619d0,-0.3655620d-1,
     *0.1504268d-1,-0.780353d-2,0.325614d-2,-0.68245d-3/
     if (x.le.2.0) then
       y=x*x/4.0
       bessk1=(log(x/2.0)*bessi1(x))+(1.0/x)*(p1+y*(p2+y*(p3+y*(p4+y*
     *(p5+y*(p6+y*p7))))))
     else
       y=2.0/x
       bessk1=(exp(-x)/sqrt(x))*(q1+y*(q2+y*(q3+y*(q4+y*(q5+y*(q6+y*
     *q7))))))
     endif
     return
     END
C*********************************************************
C
      FUNCTION BESSI1(X)
       REAL*8 Y,P1,P2,P3,P4,P5,P6,P7,
     *   Q1,Q2,Q3,Q4,Q5,Q6,Q7,Q8,Q9
       DATA P1,P2,P3,P4,P5,P6,P7/0.5D0,0.87890594D0,0.51498869D0,
     *   0.15084934D0,0.2658733D-1,0.301532D-2,0.32411D-3/
      DATA Q1,Q2,Q3,Q4,Q5,Q6,Q7,Q8,Q9/0.39894228D0,-0.3988024D-1,
     *   -0.362018D-2,0.163801D-2,-0.1031555D-1,0.2282967D-1,
     *   -0.2895312D-1,0.1787654D-1,-0.420059D-2/
      IF (ABS(X).LT.3.75) THEN
       Y=(X/3.75)**2
       BESSI1=X*(P1+Y*(P2+Y*(P3+Y*(P4+Y*(P5+Y*(P6+Y*P7))))))
     ELSE
       AX=ABS(X)
       Y=3.75/AX
       BESSI1=(EXP(AX)/SQRT(AX))*(Q1+Y*(Q2+Y*(Q3+Y*(Q4+
     *    Y*(Q5+Y*(Q6+Y*(Q7+Y*(Q8+Y*Q9))))))))
       IF(X.LT.0.)BESSI1=-BESSI1
     ENDIF
     RETURN
     END
C*********************************************************************
C
C This subroutine integrates using Rhomberg's rule.  It came from
C Numerical Recipes
C
      SUBROUTINE QROMB(A,B,SS,V)
      PARAMETER (EPS=1.E-6, JMAX=300, JMAXP=JMAX+1, K=5, KM=K-1)
      DIMENSION S(JMAXP),H(JMAXP)
      REAL V(10,6)
      H(1)=1.
      DO 11 J=1,JMAX
       CALL TRAPZDT(A,B,S(J),J,V)
*       WRITE(*,*)'QROMB: after trapzd  ',S(J),J, V(10,1)
       IF (J.GE.K) THEN
         CALL POLINT(H(J-KM),S(J-KM),K,0.,SS,DSS)
        IF (ABS(DSS).LT.EPS*ABS(SS)) RETURN
       ENDIF
```

```
      S(J+1)=S(J)
      H(J+1)=0.25*H(J)
11    CONTINUE
     PAUSE 'Too many steps.'
     END
*****************************************************************************
*
* This subroutine integrates using Rhomberg's rule.  It came from
* Numerical Recipes
*
     SUBROUTINE QROMB2(A,B,SS,V)
     PARAMETER (EPS=1.E-6, JMAX=300, JMAXP=JMAX+1, K=5, KM=K-1)
     DIMENSION S(JMAXP),H(JMAXP)
     REAL V(10,6)
     H(1)=1.
     DO 11 J=1,JMAX
       CALL TRAPZDS(A,B,S(J),J,V)
*       WRITE(*,*)'QROMB2: after trapzd  ', S(J),J
       IF (J.GE.K) THEN
         CALL POLINT(H(J-KM),S(J-KM),K,0.,SS,DSS)
        IF (ABS(DSS).LT.EPS*ABS(SS)) RETURN
       ENDIF
       S(J+1)=S(J)
       H(J+1)=0.25*H(J)
11    CONTINUE
     PAUSE 'Too many steps.'
     END
*****************************************************************************

     SUBROUTINE TRAPZDT(A,B,S,N,V)
*
*      WRITE(*,*)'Inside trap  N = ',N
     IF (N.EQ.1) THEN
         S=0.5*(B-A)*(TOVERT(A,V)
    $       +TOVERT(B,V))
*       WRITE(*,*)'TRAPZD:  S =   ',S
      IT=1
     ELSE
      IT = (N-1)*2
*       WRITE(*,*) 'IT =  ',IT
      TNM=IT
*       WRITE(*,*)'TNM = ',TNM
      DEL=(B-A)/TNM
*       WRITE(*,*) ' DEL = ',DEL
      X=A+0.5*DEL
*       WRITE(*,*)'Del  = ',DEL,'  X = ',X
      SUM=0.
      DO 11 J=1,IT
*         WRITE(*,*)'TRAP:   J =   ',J,'  IT  =  ',IT, ' DEL = ',DEL
          SUM=SUM+TOVERT(X,V)
*         WRITE(*,*)'TRAP:  Sum   = ',SUM
        X=X+DEL
11     CONTINUE
*
```

```
*      WRITE(13,*) X
*      WRITE(*,*)
       S=0.5*(S+(B-A)*SUM/TNM)
       IT=2*IT
*        WRITE(*,*)'S=  ',S,'  IT  =  ',IT
      ENDIF
*      WRITE(*,*)
      RETURN
      END
*****************************************************************
      SUBROUTINE TRAPZDS(A,B,S,N,V)
*
*     WRITE(*,*)'Inside trap s  N = ',N
      IF (N.EQ.1) THEN
          S=0.5*(B-A)*(SOVERS(A,V)+SOVERS(B,V))
*       WRITE(*,*)'TRAPZD:  S =   ',S
       IT=1
      ELSE
       IT = (N-1)*2
*       WRITE(*,*) 'IT =  ',IT
       TNM=IT
*       WRITE(*,*)'TNM = ',TNM
       DEL=(B-A)/TNM
*       WRITE(*,*) ' DEL = ',DEL
       X=A+0.5*DEL
*        WRITE(*,*)'Del  = ',DEL,'  X = ',X
       SUM=0.
       DO 11 J=1,IT
*          WRITE(*,*)'TRAP:   J =   ',J,'  IT  =  ',IT, ' DEL = ',DEL
           SUM=SUM+SOVERS(X,V)
*         WRITE(*,*)'TRAP:  Sum   = ',SUM
        X=X+DEL
11     CONTINUE
*
*      WRITE(13,*) X
*      WRITE(*,*)
       S=0.5*(S+(B-A)*SUM/TNM)
       IT=2*IT
*        WRITE(*,*)'S=  ',S,'  IT  =  ',IT
      ENDIF
*      WRITE(*,*)
      RETURN
      END
************************************************
      FUNCTION TOVERT(S,V)
*
      REAL S,V(10,6)
*
      V(10,1)=S
      CALL QROMB2(-1.,1.,SS,V)
      TOVERT = SS
       RETURN
       END
************************************************************
```

```
*
      FUNCTION SOVERS(T,V)
*
       REAL V(10,6),JACOB,S,G11,G22,G12,X(9),Y(9),Z(9),T
      REAL FIELD(9)
*
      S=V(10,1)
*       WRITE(*,*)' Inside Sovers; S and T are : ',S,T
      DO 101 I=1,9
        X(I)=V(I,1)
        Y(I)=V(I,2)
        Z(I)=V(I,3)
        IF(V(10,2).EQ.4.) FIELD(I)=V(I,4)
        IF(V(10,2).EQ.5.) FIELD(I)=V(I,5)
        IF(V(10,2).EQ.6.) FIELD(I)=V(I,6)
 101    CONTINUE
*
      G11=DNDS(S,T,X)**2+DNDS(S,T,Y)**2+DNDS(S,T,Z)**2
      G22=DNDT(S,T,X)**2+DNDT(S,T,Y)**2+DNDT(S,T,Z)**2
      G12=DNDS(S,T,X)*DNDT(S,T,X)+DNDS(S,T,Y)*DNDT(S,T,Y)+
     +     DNDS(S,T,Z)*DNDT(S,T,Z)
      JACOB=ABS(G11*G22-G12*G12)
      IF(V(10,2).GE.0.5) THEN
        F1 = QUAD(S,T,FIELD)
      ELSE
        F1= 1.0
      ENDIF
      SOVERS=F1*SQRT(JACOB)
      RETURN
      END
*************************************************************************
      FUNCTION QUAD(S,T,W)
*
      REAL S,T,W(9),TEMP,R(9)
*
      TEMP=0.0
*
      R(1)= 0.25*T*S*(1.-S)*(1.-T)
      R(2)=-0.25*T*S*(1.+S)*(1.-T)
      R(3)= 0.25*T*S*(1.+S)*(1.+T)
      R(4)=-0.25*T*S*(1.-S)*(1.+T)
      R(5)=-0.5*T*(1.-T)*(1.-S*S)
      R(6)= 0.5*S*(1.+S)*(1.-T*T)
      R(7)= 0.5*T*(1.+T)*(1.-S*S)
      R(8)=- 0.5*S*(1.-S)*(1.-T*T)
      R(9)= (1.-T*T)*(1.-S*S)
*
      DO 101 I=1,9
        TEMP = TEMP+R(I)*W(I)
 101    CONTINUE
*
      QUAD=TEMP
      RETURN
      END
```

```
*************************************************************************
      FUNCTION DNDS(S,T,W)
*
      REAL S,T,R(9),W(9),TEMP
*
      TEMP=0.0
*
       R(1)= 0.25*T*(1.-T)*(1.-2.*S)
       R(2)=-0.25*T*(1.-T)*(1.+2.*S)
       R(3)= 0.25*T*(1.+T)*(1.+2.*S)
       R(4)=-0.25*T*(1.+T)*(1.-2.*S)
       R(5)=-0.5*T*(1.-T)*(-2.*S)
       R(6)= 0.5*(1.-T*T)*(1.+2.*S)
       R(7)= 0.5*T*(1.+T)*(-2.*S)
       R(8)=-0.5*(1.-T*T)*(1.-2.*S)
      R(9)=  (-2.*S)*(1.-T*T)
*
      DO 101 I=1,9
        TEMP=TEMP+R(I)*W(I)
 101   CONTINUE
*
     DNDS=TEMP
     RETURN
     END
*************************************************************************
      FUNCTION DNDT(S,T,W)
*
      REAL S,T,R(9),W(9),TEMP
*
      TEMP=0.0
*
       R(1)=  0.25*S*(1.-S)*(1.-2.*T)
       R(2)= -0.25*S*(1.+S)*(1.-2.*T)
       R(3)=  0.25*S*(1.+S)*(1.+2.*T)
       R(4)= -0.25*S*(1.-S)*(1.+2.*T)
       R(5)= -0.5*(1.-S*S)*(1.-2.*T)
       R(6)=  0.5*S*(1.+S)*(-2.*T)
       R(7)=  0.5*(1.-S*S)*(1.+2.*T)
       R(8)= -0.5*S*(1.-S)*(-2.*T)
      R(9)=   (-2.*T)*(1.-S*S)
*
      DO 101 I=1,9
        TEMP=TEMP+R(I)*W(I)
 101   CONTINUE
*
     DNDT=TEMP
     RETURN
     END
*************************************************************************
*
    SUBROUTINE POLINT(XA,YA,N,X,Y,DY)
    PARAMETER (NMAX=10)
    DIMENSION XA(N),YA(N),C(NMAX),D(NMAX)
    NS=1
```

```
      DIF=ABS(X-XA(1))
      DO 11 I=1,N
        DIFT=ABS(X-XA(I))
        IF (DIFT.LT.DIF) THEN
          NS=I
          DIF=DIFT
        ENDIF
        C(I)=YA(I)
        D(I)=YA(I)
11    CONTINUE
      Y=YA(NS)
      NS=NS-1
      DO 13 M=1,N-1
        DO 12 I=1,N-M
          HO=XA(I)-X
          HP=XA(I+M)-X
          W=C(I+1)-D(I)
          DEN=HO-HP
          IF(DEN.EQ.0.)PAUSE
          DEN=W/DEN
          D(I)=HP*DEN
          C(I)=HO*DEN
12      CONTINUE
        IF (2*NS.LT.N-M)THEN
          DY=C(NS+1)
        ELSE
          DY=D(NS)
          NS=NS-1
        ENDIF
        Y=Y+DY
13    CONTINUE
      RETURN
      END
*****************************************************************************
```

A.2.3 Curve fit routine used to determine coefficients for equation (59) and (60)

```
**********************************************************************

      program curvefitter
      implicit real*4(a-h,o-z), integer(i-n)
      common/ data1/ tetbm(50000),phi(50000),tetslit(50000),pe(50000)
      common/ data2/ hh(50000),delg(50000),es(50000),ef(50000)
      common/ data3/ ndata,nparamsfit
      common/ array/ params(15),lista(15)
      common/ results/ res(50000),avres,rms,tetabmth(50000)
       dimension p(15),xi(15,15),stnderr2(15),covar(15,15)
      dimension fjv(5000),fji(5000),ci(5000)

C     INPUT PARAMETERS

      nparamsmax = 15
      print*,'number of parameters to be fitted ?'
      read*, nparamsfit
c     nparamsfit = 3
      if (nparamsfit .gt. 15) then
        print*,'which should be fitted ? # 1, 2 or 3 ? '
        do 03 i=1,nparamsfit
          read*,lista(i)
03      continue
        v=1
        do 05 i=nparamsfit+1,nparamsmax
          do 07 k=1,nparamsfit
            if (lista(k) .eq. v) v=v+1
07        continue
          lista(i) = v
          v=v+1
05      continue
      else
        do 09 i=1,nparamsfit
          lista(i) = i
09      continue
      endif
      ftol = 1.0e-5
      print*,'initial value for param 1 (A) ?'
      read*, a
      print*,'initial value for param 2 (B) ?'
      read *, b
      print*,'initial value for param 3 (C) ?'
      read *, c
      print*,'initial value for param 4 (D) ?'
      read *, d
      print*,'initial value for param 5 (E) ?'
      read *, e
      print*,'initial value for param 6 (F) ?'
```

```
      read*, f
      print*,'initial value for param 7 (G) ?'
      read*, g
      print*,'initial value for param 8 (H) ?'
      read*, h
      print*,'initial value for param 9 (Q) ?'
      read *, q
      print*,'initial value for param 10 (R) ?'
      read *, r
      print*,'initial value for param 11 (S) ?'
      read *, s
      print*,'initial value for param 12 (T) ?'
      read*, t
      print*,'initial value for param 13 (U) ?'
      read*, u
      print*,'initial value for param 14 (V) ?'
      read*, v
      print*,'initial value for param 15 (W) ?'
      read*, w

C     READ DATA
************************************************
       open(unit=1,file='delg.txt',status='old')
      read(1,*)ndata1
      ndata = ndata1
      do 100 i=1,ndata1
        read(1,*)pe(i),phi(i),hh(i),es(i),ef(i),delg(i)
 100  continue
*       close(1,status='keep')
************************************************
C     DEPOSIT ALL PARAMETERS (TO BE FIXED AND TO BE FIT) IN PARAMS(I)
      params(1) = a
      params(2) = b
      params(3) = c
      params(4) = d
      params(5) = e
      params(6) = f
      params(7) = g
      params(8) = h
      params(9) = q
      params(10) = r
      params(11) = s
      params(12) = t
      params(13) = u
      params(14) = v
      params(15) = w

      do 240 i=1,nparamsmax
        p(i) = params(lista(i))
        do 230 j=1,nparamsfit
          xi(i,j) = 0.0
          if (i.eq.j) xi(i,j) = p(i)*0.1
 230    continue
 240  continue
```

```
C    OBTAIN BEST FIT OF P VECTOR TO DATA

     print *, 'Beginning powell fitting . . .'
     call powell(p,xi,nparamsfit,nparamsmax,ftol,iter,fret)
     print *, 'Done.'


C    RESET FIT PARAMETERS IN PARAMS TO VALUES IN P
     do 260 i=1,nparamsmax
       params(i)=p(i)
 260  continue

C    FINAL VALUES
     a = params(1)
     b = params(2)
     c = params(3)
     d = params(4)
     e = params(5)
     f = params(6)
     g = params(7)
     h = params(8)
     q = params(9)
     r = params(10)
     s = params(11)
     t = params(12)
     u = params(13)
     v = params(14)
     w = params(15)

 111   format(f7.3,2x,f7.3,2x,f7.3,2x,f7.3,2x,f7.3,2x
    +       ,f7.3,2x,f7.3,2x,f7.3)
     do 280 i=1,ndata
       if (res(i). gt. 0.05) then
         write(*,111)res(i),delg(i),tetabmth(i)
    +     ,hh(i),phi(i),pe(i),es(i),ef(i)
      endif
 280  continue
      do 281 i=1,nparamsfit
         print*,'parameter ',i,' is : ',params(i)
         write(2,*)'parameter ',i,' is :',params(i)
 281  continue
      print*,' '
     print*,'value of chi2',fret
     write(2,*)'value of chi2',fret
     print*,'root mean-square error in %',rms*100.0
     write(2,*)'root mean-square error in %',rms*100.0
     print*,'average residual in %',avres*100.0
     write(2,*)'average residual in %',avres*100.0
 555  continue
     end
*****************************************************************
C    FUNCTION TO CALCULATE CHI-SQUARE VALUES FOR A GIVEN
*    PARAMETER VECTOR
```

```
      function chisq(pms)
      implicit real*4(a-h,o-z), integer(i-n)
      common/ data1/ tetbm(50000),phi(50000),tetslit(50000),pe(50000)
      common/ data2/ hh(50000),delg(50000),es(50000),ef(50000)
      common/ data3/ ndata,nparamsfit
      common/ array/ params(15),lista(15)
      common/ results/ res(50000),avres,rms,tetabmth(50000)
      dimension pms(15)

C     ASSIGN CURRENT VALUE OF FITTED PARAMETERS

      chisq = 0.0
      ntotal = ndata

      do 10 i=1,nparamsfit
        params(lista(i))=pms(i)
        if (pms(i) .lt. 0.0) chisq = 1.0e30
 10   continue

C     THIS SECTION NOT GENERAL:  MAKE ASSIGNMENTS FROM PARAMS
      A=params(1)
      B=params(2)
      C=params(3)
      D=params(4)
      E=params(5)
      F=params(6)
      G=params(7)
      H=params(8)
      Q=params(9)
      R=params(10)
      S=params(11)
      T=params(12)
      U=params(13)
      V=params(14)
      W=params(15)

      avres = 0
      do 100 i=1,ndata
        f1=A*es(i)*ef(i)*pe(i)**B*phi(i)**C
        f2=exp(-D*hh(i))
        f3=E*es(i)**2*pe(i)**F*phi(i)**G
        f4=exp(-H*hh(i))
        f5=Q*ef(i)**2*pe(i)**R*phi(i)**S
        f6=exp(-T*hh(i))
        tetabmth(i)=f1*f2+f3*f4+f5*f6

        res(i) = abs(tetabmth(i)/delg(i)-1)
c       if (es(i) .le. 0.025) then
c         res(i)=0.0
c         ntotal = ntotal - 1
c       endif
        avres = avres + res(i)
        chisq = chisq + res(i)**2
```

```
100  continue
     avres = avres/ntotal
     rms = sqrt(chisq/(ntotal-nparamsfit))
     return

     end

*****************************************************************************
***


C    POWELL'S ROUTINE

* subroutine powell *

      SUBROUTINE POWELL(P,XI,N,NP,FTOL,ITER,FRET)
     PARAMETER (NMAX=40,ITMAX=400)
      DIMENSION P(15),XI(15,15),PT(nmax),PTT(nmax),XIT(nmax)

     FRET = chisq(P)
     DO 11 J=1,N
       PT(J)=P(J)
11    CONTINUE
     ITER=0
1     ITER=ITER+1
     FP=FRET
     IBIG=0
     DEL=0.
     DO 13 I=1,N
       DO 12 J=1,N
         XIT(J)=XI(J,I)
12     CONTINUE
       FPTT=FRET
       CALL LINMIN(P,XIT,N,FRET)
       IF(ABS(FPTT-FRET).GT.DEL)THEN
         DEL=ABS(FPTT-FRET)
         IBIG=I
       ENDIF
13    CONTINUE
     IF(2.*ABS(FP-FRET).LE.FTOL*(ABS(FP)+ABS(FRET)))RETURN
     IF(ITER.EQ.ITMAX) then
        print*, 'Powell exceeding maximum iterations.'
        return
     endif
     DO 14 J=1,N
       PTT(J)=2.*P(J)-PT(J)
       XIT(J)=P(J)-PT(J)
       PT(J)=P(J)
14    CONTINUE
     FPTT =chisq(PTT)
     IF(FPTT.GE.FP)GO TO 1
     T=2.*(FP-2.*FRET+FPTT)*(FP-FRET-DEL)**2-DEL*(FP-FPTT)**2
     IF(T.GE.0.)GO TO 1
     CALL LINMIN(P,XIT,N,FRET)
```

```
      DO 15 J=1,N
        XI(J,IBIG)=XIT(J)
15    CONTINUE
      GO TO 1
      END

* subroutine linmin *

      SUBROUTINE LINMIN(P,XI,N,FRET)
      PARAMETER (NMAX=80,TOL=1.E-4)
      EXTERNAL F1DIM
      DIMENSION P(n),XI(n)
      COMMON /F1COM/ NCOM,PCOM(NMAX),XICOM(NMAX)
      NCOM=N
      DO 11 J=1,N
        PCOM(J)=P(J)
        XICOM(J)=XI(J)
11    CONTINUE
      AX=0.
      XX=1.
      CALL MNBRAK(AX,XX,BX,FA,FX,FB)
      FRET=BRENT(AX,XX,BX,TOL,XMIN)
      DO 12 J=1,N
        XI(J)=XMIN*XI(J)
        P(J)=P(J)+XI(J)
12    CONTINUE
      RETURN
      END

* subroutine mnbrak

      SUBROUTINE MNBRAK(AX,BX,CX,FA,FB,FC)
      PARAMETER (GOLD=1.618034, GLIMIT=100., TINY=1.E-20)

      FA=f1dim(AX)
      FB=f1dim(BX)
      IF(FB.GT.FA)THEN
        DUM=AX
        AX=BX
        BX=DUM
        DUM=FB
        FB=FA
        FA=DUM
      ENDIF
      CX=BX+GOLD*(BX-AX)
      FC=f1dim(CX)
1     IF(FB.GE.FC)THEN
        R=(BX-AX)*(FB-FC)
        Q=(BX-CX)*(FB-FA)
        U=BX-((BX-CX)*Q-(BX-AX)*R)/(2.*SIGN(MAX(ABS(Q-R),TINY),Q-R))
        ULIM=BX+GLIMIT*(CX-BX)
        IF((BX-U)*(U-CX).GT.0.)THEN
          FU=f1dim(U)
          IF(FU.LT.FC)THEN
```

```
          AX=BX
          FA=FB
          BX=U
          FB=FU
          RETURN
         ELSE IF(FU.GT.FB)THEN
          CX=U
          FC=FU
          RETURN
         ENDIF
         U=CX+GOLD*(CX-BX)
         FU=f1dim(U)
        ELSE IF((CX-U)*(U-ULIM).GT.0.)THEN
         FU=f1dim(U)
         IF(FU.LT.FC)THEN
          BX=CX
          CX=U
          U=CX+GOLD*(CX-BX)
          FB=FC
          FC=FU
          FU=f1dim(U)
         ENDIF
        ELSE IF((U-ULIM)*(ULIM-CX).GE.0.)THEN
         U=ULIM
         FU=f1dim(U)
        ELSE
         U=CX+GOLD*(CX-BX)
         FU=f1dim(U)
        ENDIF
        AX=BX
        BX=CX
        CX=U
        FA=FB
        FB=FC
        FC=FU
        GO TO 1
      ENDIF
      RETURN
      END

* function brent *

      FUNCTION BRENT(AX,BX,CX,TOL,XMIN)
      PARAMETER (ITMAX=1000,CGOLD=.3819660,ZEPS=1.0E-10)

      A=MIN(AX,CX)
      B=MAX(AX,CX)
      V=BX
      W=V
      X=V
      E=0.
      FX=f1dim(X)
      FV=FX
      FW=FX
```

```
      DO 11 ITER=1,ITMAX
        XM=0.5*(A+B)
        TOL1=TOL*ABS(X)+ZEPS
        TOL2=2.*TOL1
        IF(ABS(X-XM).LE.(TOL2-.5*(B-A))) GOTO 3
        IF(ABS(E).GT.TOL1) THEN
          R=(X-W)*(FX-FV)
          Q=(X-V)*(FX-FW)
          P=(X-V)*Q-(X-W)*R
          Q=2.*(Q-R)
          IF(Q.GT.0.) P=-P
          Q=ABS(Q)
          ETEMP=E
          E=D
          IF(ABS(P).GE.ABS(.5*Q*ETEMP).OR.P.LE.Q*(A-X).OR.
     *       P.GE.Q*(B-X)) GOTO 1
          D=P/Q
          U=X+D
          IF(U-A.LT.TOL2 .OR. B-U.LT.TOL2) D=SIGN(TOL1,XM-X)
          GOTO 2
        ENDIF
1       IF(X.GE.XM) THEN
          E=A-X
        ELSE
          E=B-X
        ENDIF
        D=CGOLD*E
2       IF(ABS(D).GE.TOL1) THEN
          U=X+D
        ELSE
          U=X+SIGN(TOL1,D)
        ENDIF
        FU= f1dim(U)
        IF(FU.LE.FX) THEN
          IF(U.GE.X) THEN
            A=X
          ELSE
            B=X
          ENDIF
          V=W
          FV=FW
          W=X
          FW=FX
          X=U
          FX=FU
        ELSE
          IF(U.LT.X) THEN
            A=U
          ELSE
            B=U
          ENDIF
          IF(FU.LE.FW .OR. W.EQ.X) THEN
            V=W
            FV=FW
```

```
        W=U
       ELSE IF(FU.LE.FV .OR. V.EQ.X .OR. V.EQ.W) THEN
        V=U
        FV=FU
       ENDIF
      ENDIF
11   CONTINUE
     PAUSE 'Brent exceed maximum iterations.'
3     XMIN=X
     BRENT=FX
     RETURN
     END

* function f1dim *

     FUNCTION F1DIM(X)
     PARAMETER (NMAX=80)
     COMMON /F1COM/ NCOM,PCOM(NMAX),XICOM(NMAX)
     DIMENSION XT(nmax)
     DO 11 J=1,NCOM
       XT(J)=PCOM(J)+X*XICOM(J)
11   CONTINUE
     F1DIM = chisq(XT)
     RETURN
     END
```

Bibliography

Amsterdam, A., Z. Er-El, and S. Shaltiel. 1975. Ultrastructure of beaded agarose. *Arch. Biochem. Biophys.* 171:673-677.

Anderson, J.L., F. Rauh, and A. Morales. 1978. Particle diffusion as a function of concentration and ionic strength. *J. Phys. Chem.* 82:608-616.

Arnott, S., A. Fulmer, W.E. Scott, I.C.M Dea, R. Moorhouse, and D.A. Rees. 1974. The agarose double helix and its function in agarose gel structure. *J. Mol. Biol.* 90: 269-284.

Berk, D.A., F. Yuan, M. Leunig, and R.K. Jain. 1993. Fluorescence photobleaching with spatial Fourier analysis: Measurement of diffusion in light-scattering media. *Biophys. J.* 65:2428 -2436.

Bor Fuh, C., S. Levin, and J.C. Giddings. 1993. Rapid diffusion coefficient measurements using analytical SPLITT fractionation: application to proteins. *Anal. Biochem.* 208:80-87.

Boyer, P. M. and J. T. Hsu. 1992. Experimental studies of restricted protein diffusion in an agarose matrix. *AIChE J.* 38(2):259-272.

Brady, J. (1994). Hindered diffusion. AIChE Annual Meeting, November 13-18, San Francisco, CA, American Institute of Chemical Engineers.

Brenner, H. and L. J. Gaydos. 1977. The constrained brownian movement of spherical particles in cylindrical pores of comparable radius. *J. Coll. Inter. Sci.* 58:312.

Brigham, E.O. 1974. The Fast Fourier Transform. Prentice-Hall, Englewood Cliffs, NJ. pp. 140-147.

Brinkman, H. C. 1947. A calculation of the viscous force exerted by a flowing fluid in a dense swarm of particles. *Appl. Sci. Res. A.* 1:27-34.

Cameron, R. E., M. A. Jalil and A. M. Donald. 1994. Diffusion of bovine serum albumin in amylopectin gels measured usng fourier transform infrared microspectroscopy. *Macromol.* 27:2708-2713.

Cannan, R. K., A. H. Palmer and A. C. Kibrick. 1942. The hydrogen ion dissociation curve of β-lactoglobulin. *J. Biol. Chem.* 142:803-822.

Crone, H.D. 1974. Ion-exclusion effects on the chromatography of acetyl-cholinesterase and other protens on agarose columns at low ionic strengths. *J. Chrom.* 92:127-135.

De Belder, A. N. and K. Granath. 1973. Preparation and properties of fluorescein-labelled dextrans. *Carb. Res.* 30:375-378.

Deen, W. M. 1987. Hindered transport of large molecules in liquid-filled pores. *AIChE J.* 33(9):1409-1425.

Djabourov, M., A. H. Clark, D. W. Rowlands and S. B. Ross-Murphy. 1989. Small-Angle X-ray scattering characterization of agarose sols and gels. *Macromolecules* 22:180-188.

Drumond, M. C. and W. M. Deen. 1994. Structural determinants of glomerular hydraulic permeability. *Am J. Physiol.* 266:F1-F12.

Dubin, P. L. (1994). *Personal communication.* Titration curve of Superose 12.

Dubin, P. L. and J. M. Principi. 1989. Optimization of size-exclusion separation of proteins on a Superose column. *J. Chromat.* 479:159-164.

Dubin, P. L. and M. M. Tecklenburg. 1985. Size-exclusion chromatography of strong polyelectrolytes on porous glass columns. *Anal. Chem.* 57:275-279.

Dubin, P. L., R. M. Larter, C. J. Wu and J. I. Kaplan. 1990. Size-exclusion chromatography of polyelectrolytes: comparison with theory. *J. Phys. Chem.* 94:7243-7250.

Dubin, P. L., S. L. Edwards, M. S. Mehta and D. Tomalia. 1993. Quantitation of non-ideal behavior in protein size-exclusion chromatography. *J. Chromat.* 635:51-60.

Dubin, P.L. and J.M. Principi. 1989. Optimization of size-exclusion separation of proteins on a Superose column. *J. Chrom..* 479:159-164.

Edwards, S. L. and P. L. Dubin. 1993. pH effects on non-ideal protein size-exclusion chromatography on Superose 6. *J. Chromat.* 648:3-7.

Fanti, L. A. and E. D. Glandt. 1990. Partitioning of spherical particles into fibrous matrices. *J. Coll. Inter. Sci.* 135(2):385-395.

Finlayson. 1980. Nonlinear analysis in chemical engineering. New York, McGraw-Hill.

FMC BioProducts Source Book. 1988. FMC Bioproducts, Rockland, Maine.

Gaigalas, A.K., J.B. Hubbard, M. McCurley, and S. Woo. 1992. Diffusion of bovine serum albumin in aqueous solutions. *J. Phys. Chem.* 96:2355-2359.

Garcia, R., I. Porcar, A. Campos, V. Soria and J. E. Figueruelo. 1994. Solution properties of polyelectrolytes: X. Influence of ionic strength on the electrostatic secondary effects in aqueous size-exclusion chromatography. *J. Chromat.* 662:61-69.

Gibbs, S., J., E. N. Lightfoot and T. W. Root. 1992. Protein diffusion in porous gel filtration chromatography media studied by pulsed field gradient NMR sepctroscopy. *J. Phys. Chem.* 96:7458-7462.

Gibbs, S.J., A.S. Chu, E.N. Lightfoot, and T.W. Root. 1991. Ovalbumin diffusion at low ionic strength. *J. Phys. Chem.* 95:467-471

.

Giddings, J.C., F.J.F. Yang, and M.N. Myers. 1976. Flow field-flow fractionation: a versatile new separation method. *Science.* 193:1244-1245.

Glendinning, A. B. and W. B. Russel. 1983. The electrostatic repulsion between charged spheres from exact solutions to the linearized Poisson-Boltzmann equation. *J. Coll. Interf. Sci.* 93(1):95-104.

Gordon, W.G. and W.F. Semmett. 1953. Isolation of crystalline a-lactalbumin from milk. *J. Am. Chem. Soc.* 75:328-330.

Grant, M. L. and D. A. Savil. 1995. Electrostatic interactions between a nonuniformly charged sphere and a charged surface. *Journal of Colloid and Interfacial Science.* 171:35-45.

Haugland, R. 1992-1994. Molecular Probes: Handbook of Fluorescent Probes and Research Chemicals. 5th Edition. Molecular Probes, Eugene, OR.

Hou, L., F. Lanni and K. Luby-Phelps. 1990. Tracer diffusion in F-actin and ficoll mixtures: toward a model for cytoplasm. *Biophys. J.* 58:31-43.

Hunter, R. J. 1986. Foundation of Colloid Science: Volume I. Oxford, Clarendon Press.

Jackson, G. W. and D. F. James. 1986. The permeability of fibrous porous media. *Can. J. Chem. Eng.* 64:364-374.

Jain, R. K. 1987. Transport of molecules in the tumor interstitium. *Cancer Res.* 47:3039-3051.

Jain, R.K., R.J. Stock, S.R. Chary, and M. Rueter. 1990. Convection and diffusion measurements using fluorescence recovery after photobleaching and video image analysis: in vitro calibration and assessment. *Microvasc. Res.* 39:77-93.

Johansson, L. and J.-E. Löfroth. 1993. Diffusion and interactionin gels and solutions. 4. Hard sphere Brownian dynamics simulations. *J. Chem. Phys.* 98(9):7471-7479.

Johnson, E. M., D. A. Berk, R. K. Jain and D. W. M. 1995. Diffusion and partitioning of proteins in charged agarose gels. *Biophys. J.* 68:1561-1568.

Johnson, K.A., G.B. Westermann-Clark, and D.O. Shah. 1989, Diffusion of charged micelles through charged microporous membranes. *Langmuir* 5:932-938.

Kanwar, Y. S. and M.A. Venkatachalam. 1992. "Ultrastructure of glomerulus and juxtaglomerular apparatus", in Handbook of Physiology: Renal Physiology, section 8, volume 1, (ed.) E.E. Windhager. Oxford University Press, New York.

Koch, D. L. and J. F. Brady. 1986. The effective diffusivity of fibrous media. *AIChE J.* 32(4):575-591.

Kosar, T. F. and R. J. Phillips. 1995. Measurement of protein diffusion in dextran solutions by holographic interferometry. *AIChE J.* 41(3):701-711.

Lacey, P.E., O.D. Hegre, A. Gerasimidi-Vazeou, F.T. Gentile, and K.T. Dionne. 1991. Maintenance of normoglycemia in diabetic mice by subcutaneous xenografts of encapsulated islets. *Science* 254:1728-1784.

Larson, R.J. and M.L. Marx. 1986. An Introduction to Mathematical Statistics and Its Applications. Second Edition. Prentice-Hall, Englewood Cliffs, New Jersey.

Laurent, T. C. 1967. Determination of the structure of agarose gels by gel chromatography. *Biochim. Biophys. Acta.* 136:199-205.

Laurent, T. C. and J. Killander. 1964. A theory of gel filtration and its experimental verification. *J. Chromat.* 14:317-330.

Leloup, V. M., P. Colonna and S. G. Ring. 1990. Studies on probe diffuison and accessiblity in amylose gels. *Macromol.* 23:862-866.

Lin, N.P. and W.M. Deen. 1992. Charge effects on the diffusion of polystyrene sulfonate through porous membranes. *J. Colloid Interface Sci.* 153:483-492.

Mackie, W., D. B. Sellen and J. Sutcliffe. 1978. Spectral broadening of light scattered from polysaccharide gels. *Polymer.* 19:9-16.

Maddox, D.A., Deen, W.M., and Brenner, B.M. 1992. *in* "Handbook of Physiology, Section 8, Renal Physiology, Vol.1" (E.E. Windhager, Ed.), p. 545. Oxford University Press, New York.

Malone, D. M. and J. L. Anderson. 1978. Hindered diffusion of particles through small pores. *Chem. Eng. Sci.* 33:1429.

Moussaoui, M., M. Benlyas, and P. Wahl. 1992. Diffusion of proteins in Sepharose Cl-B gels. *J. Chromat.* 591:115-120.

Obrink, B. 1968. Characterization of fiber parameters in agarose gels by light scattering. *J. Chromatogr.* 37:329-330.

Ogston, A. G. 1958. The spaces in a uniform random suspension of fibers. *Trans. Faraday. Soc.* 54:1754-1757.

Ogston, A. G., B. N. Preston and J. D. Wells. 1973. On the transport of compact particles through solutions of chain polymers. *Proc. R. Soc. Lond. A.* 333:297-316..

Ohshima, H. 1995. Electrostatic Interaction between two dissimilar spheres with constant surface charge density. *Journal of Colloid and Interfacial Science.* 170:432-439.

Oliver, J. D., S. Anderson, J. L. Troy, B. M. Brenner and W. M. Deen. 1992. Determination of glomerular size-selectivity in the normal rat with ficoll. *J. Am. Soc. Nephrol.* 3:214-228.

Overbeek, J. Th. G. 1950. Quantitative interpretation of the electrophoretic velocity of colloids. In Advances in Colloid Science. Vol. III. Ed. H. Mark, J.W. Verwey. Interscience Publishers, New York. pp. 97-133.

Pallmann, H. and H. Deval. 1945. Über die Wasserdurchlässigkeit von Hydrogelen. *Experientia* 1:325-326.

Peppas, N.A. (ed.). 1987. Hydrogels in Medicine and Pharmacy. Volume III. Properties and Applications. CRC Press, Boca Raton, FL.

Perrins, W. T., D. R. McKenzie and R. C. McPhedran. 1979. Transport properties of regular arrays of cylinders. *Proc. R. Soc. Lond. A.* 369:207-225.

Phillies, G.D.J., C. Malone, K. Ullmann, G.S. Ullmann, J. Rollings, and L. Yu. 1987. Probe diffusion in solutions of long-chain polyelectrolytes. *Macromol.* 20:2280-2289.

Phillies, G.D.J., T. Pirnat, M. Kiss, N. Teasdale, D. Maclung, H. Inglefield, C. Malone, A. Rau, L. Yu, and J. Rollings, 1989. Probe diffusion in solutions of low molecular weight polyelectrolytes. *Macromol.* 22:4068-4075.

Phillips, R. J., W. M. Deen and J. F. Brady. 1989. Hindered transport of spherical macromolecules in fibrous membranes and gels. *AIChE J.* 35(11):1761-1769.

Phillips, R. J., W. M. Deen and J. F. Brady. 1990. Hindered transport in fibrous membranes and gels: effect of solute size and fiber configuration. *J. Coll. Inter. Sci.* 139(2):363-373.

Press, W. H., B. P. Flannery, S. A. Teukolsky and W. T. Vetterling. 1992. Numerical Recipes: The Art of Scientific Computing (Fortran Version). New York, NY USA, Cambridge University Press.

Raj, T. and W.H. Flygare. 1974. Diffusion studies of bovine serum albumin by quasi-elastic light scattering. *Biochem.* 13:3336-3340.

Righetti, P.G. and T. Caravaggio. 1976. Isoelectric points and molecular weights of proteins: A table. *J. Chromatogr.* 127:1-28.

Roden, L., M. Roden, H. Yu, J. Jin and J. Greenshields. 1993. Separation of sugars by ion-exclusion chromatography on a cation-exchange resin. *J. Chrom.* 638:29-34.

Saltzman, W. M., M. L. Radomsky, K. J. Whaley and R. Cone A. 1994. Antibody diffusion in human cervical mucus. *Biophys. J.* 66:508-515.

Schlüter, H. and W. Zidek. 1993. Applicaton of non-size-related separation effects to the purification of biologically active substances with a size-exclusion gel. *J. Chrom.* 639:17-22.

Sellen, D.B. 1973. Light scattering Rayleigh linewidth measurements on some globular protein solutions. *Polymer.* 14:359-364.

Sellen, D.B. 1985. Quasi-elastic light scattering studies of the diffusion of compact macromolecules through gels. In Physical Optics of Dynamic Phenomena and Processes in Macromolecular Systems. pp. 177-190.

Shukla, T.P. 1973. Chemistry and biological function of α-lactalbumin. *CRC Crit. Rev. Food Tech.* 3:241-312.

Signer, R. and H. Egli. 1950. Sedimentation von Makromolekülen und Durchströmung von Gelen. *Rec. Trav. Chim.* 69:45-58.

Smith, F. G. and W. M. Deen. 1980. Electrostatic double-layer interactions for spherical colloids in cylindrical pores. *J. Colloid Interf. Sci.* 78(2):444-465.

Smith, F. G. and W. M. Deen. 1983. Electrostatic effects on the partitioning of spherical colloids between dilute bulk solution and cylindrical pores. *J. Coll. Inter. Sci.* 91(2):571-590.

Spencer, M. 1982. Reverse salt gradient chromatography of tRNA on unsubstituted agarose: III. Physical and chemical properties of different batches of sepharose 4B. *J. Chromatogr.* 238:317-325.

Tanaka, T., L. O. Hocker and G. B. Benedek. 1973. Spectrum of light scattered from a viscoelastic gel. *J. Chem. Phys.* 59(9):5151-5159.

Tanford, C., S. A. Swanson and W. S. Shore. 1955. Hydrogen ion equilibria of bovine serum albumin. *J. Am. Chem. Soc.* 77:6414-6421.

Tokita, M. and T. Tanaka. 1991. Friction coefficient of polymer networks of gels. *J. Chem. Phys.* 95:4613-4619.

Tomadakis, M. M. and S. V. Sotirchos. 1993. Transport properties of random arrays of freely overlapping cylinders with various orientation distributions. *J. Chem. Phys.* 98(1):616-626.

Tsay, T.T. and K. A. Jacobson. 1991. Spatial Fourier analysis of video photobleaching measurements: Principles and optimization. *Biophys. J.* 60:360-368.

Verwey, E. J. W. and J. T. G. Overbeek. 1948. Theory of the stability of lyophobic colloids. Amsterdam, Elsevier.

Waki, S., J. D. Harvey and A. R. Bellamy. 1982. Study of agarose gels by electron microscopy of freeze-fractured surfaces. *Biopolymers* 21:1909-1926.

Walters, R.R., J.F. Graham, R.M., Moore, and D.J. Anderson. 1984. Protein diffusion coefficient measurements by laminar flow analysis: method and applications. Anal. *Biochem.* 140:190-195.

Wattenbarger, M. R., V. A. Bloomfield, Z. Bu and P. S. Russo. 1992. Tracer diffusion of proteins in DNA solutions. *Macromol.* 25(20):5263-5265.

Weast, R.C. and M.J. Astle (eds.). 1980. CRC Handbook of Chemistry and Physics, 61st Edition. CRC Press Inc., Boca Raton, FL, p. F-51.

Weiss, N. and A. Silberberg. 1976. Permeability as a means to study the structure of gels. In Hydrogels for Medical and Related Applications, J. D. Andrade (Ed.). ACS Symposium Series, American Chemical Society, Washington, DC. p. 69-79.

White, M. L. 1960. The permeability of an acrylamide polymer gel. *J. Phys. Chem.* 64:1563-1565.

Whytock, S. and J. Finch. 1991. The substructure of agarose gels as prepared for electrophoresis. *Biopolymers* 31:1025-1028.